Developing a Multiphysics Solver in APOLLO3 and Applications to Cross Section Homogenization

Kevin Dugan

NNT : 2016SACLS309

Thèse de Doctorat

de

l'Université Paris-Saclay

preparée à

l'Université Paris Sud XI

École Doctorale N° 576
Particules, Hadrons, Énergie, Noyau, Instrumentation, Imagerie, Cosmos et Simulation

Spécialité de doctorat : Énergie Nucléaire

par

Kevin James Dugan

Développement d'un solveur multiphysique dans le code APOLLO3® et applications à l'homogénéisation des sections efficaces

Thèse présentée et soutenue à Saclay, le 21 octobre 2016:

Composition du Jury :

Président du Jury,	Bertrand Mercier,	Institute National des Sciences & Techniques Nucléaires
Rapporteur,	Jean C. Ragusa,	Texas A&M University
	Piero Ravetto,	Politecnico di Torino
Examinateur,	Jean C. Ragusa,	Texas A&M University
	Piero Ravetto,	Politecnico di Torino
	Bertrand Mercier,	Institute National des Sciences & Techniques Nucléaires
	Ernest Mund,	Université Libre de Bruxelles
Directeur de thèse,	Richard Sanchez,	Université Paris-Saclay
Invité,	Igor Zmijarevic,	CEA Saclay

Résumé

Le couplage multiphysique devient important dans les domaines de l'ingénierie nucléaire et de l'informatique. La capacité d'obtenir des solutions précises pour des modèles réalistes est essentielle à la conception et l'autorisation des conceptions nouvelles de réacteurs nucléaires, surtout dans des situations d'accidents graves. Les modèles physiques qui décrivent le comportement des réacteurs nucléaires dans des conditions accidentelles sont : le transport des neutrons, la conduction/convection thermique, la thermomécanique du combustible et des structures de support, la stœchiométrie du combustible, et d'autres encore. Cependant cette thèse se concentre sur le couplage entre deux modèles, le transport des neutrons et la conduction/convection thermique.

Le but de cette thèse est de développer un solveur multiphysique pour la simulation des accidents de réacteurs nucléaires. Le travail s'est focalisé à la fois sur l'environnement de simulation et sur le traitement des données pour de telles simulations.

Ces travaux discutent le développement d'un solveur multiphysique basé sur la méthode Newton-Krylov sans la jacobienne (JFNK). Ce solveur inclut des solveurs linéaires et non-linéaires, accompagné des interfaces par le calcul des résidus aux codes existantes pour le transport des neutrons et la thermo hydraulique (APOLLO3 et MCTH respectivement). Une nouvelle formulation pour le résidu du transport de neutrons est explorée, qui réduit la taille de la solution et l'espace de recherche par un facteur important ; le résidu, au lieu d'être basé sur le flux angulaire, est basé sur la source de fission.

La question de savoir si l'utilisation d'un flux fondamental pour l'homogénéisation des sections efficaces est suffisamment précise pendant les simulations transitoires rapides est aussi explorée. Il est montré que, dans le cas d'un milieu infini et homogène, l'utilisation des sections efficaces fabriquées avec un flux fondamental est significativement différente d'une solution de référence. Cette erreur est diminuée en utilisant un flux de pondération alternatif qui vient d'un calcul à dépendance temporelle ; soit avec un flux intégré en temps soit avec une solution asymptotique. Le flux intégré en temps vient d'une solution multiphysique sur un sous-domaine de l'accident et intégrée en temps. L'intégration en temps peut être réalisée sur plusieurs « morceaux » qui ont le même comportement temporel. La solution asymptotique vient d'un calcul de valeur propre alpha et emploie un ou plusieurs modes alpha comme flux de pondération. Entre les deux méthodes, la méthode avec un flux intégré en temps est plus précise, mais prend plus de temps.

Le domaine d'application de ces nouvelles méthodes est étendu en étudiant les effets d'hétérogénéités spatiales et la discrétisation des macro-intervalles en temps. Premièrement, un cas avec des hétérogénéités spatiales et une perturbation locale est utilisé pour montrer que ces méthodes peuvent être utilisées pour l'homogénéisation au niveau des assemblages. Ces nouvelles méthodes fonctionnent mieux que la méthode traditionnelle avec un flux fondamental. Deuxièmement, une estimation a priori pour une discrétisation optimale est obtenue pour la méthode avec le flux intégré en temps. Il est montré que d'autres divisions du

domaine en temps réduisent l'erreur sur plusieurs métriques jusqu'au moment où les erreurs numériques deviennent dominantes.

Pour montrer que le solveur multiphysique fonctionne bien pour des calculs de grande taille, un calcul sur un cœur REB réduit est effectué. Cette simulation est basée sur un accident de chute de grappe dans un REB au démarrage. Des sections efficaces en deux groupes d'énergie homogénéisées sur des assemblages sont utilisées, et montrent que le solveur multiphysique peut produire des solutions multiphsyiques.

Mots clés: multi-physique, homogénéisation, transport des neutrons, thermo-hydraulique

Abstract

Multiphysics coupling is becoming of large interest in the nuclear engineering and computational science fields. The ability to obtain accurate solutions to realistic models is important to the design and licensing of novel reactor designs, especially in design basis accident situations. The physical models involved in calculating accident behavior in nuclear reactors includes neutron transport, thermal conduction/convection, thermo-mechanics in fuel and support structure, and fuel stoichiometry, among others. However, this dissertation focuses on the coupling between two models, neutron transport and thermal conduction/convection.

The goal of this dissertation is to develop a multiphysics solver for simulating accidents in nuclear reactors. The focus is both on the simulation environment and the data treatment used in such simulations.

This work discusses the development of a multiphysics framework based on the Jacobian-Free Newton-Krylov (JFNK) method. The framework includes linear and nonlinear solvers, along with interfaces to existing numerical codes that solve individually neutron transport and thermal hydraulics models (APOLLO3 and MCTH respectively) through the computation of residuals. A new formulation for the neutron transport residual is explored, which reduces the solution size and search space by a large factor; instead of the residual being based on the angular flux, it is based on the fission source.

The question of whether using a fundamental mode distribution of the neutron flux for cross section homogenization is sufficiently accurate during fast transients is also explored. It is shown that, in an infinite homogeneous medium, using homogenized cross sections produced with a fundamental mode flux differ significantly when comparing the homogeneous solution to a reference solution. The error is remedied by using an alternative weighting flux taken from a time dependent calculation; either a time-integrated flux or an asymptotic solution. The time-integrated flux comes from the multiphysics solution of the accident on a subdomain and an integration in time. The integration can be broken into several "chunks" that capture similar time-dependent behavior. The asymptotic solution comes from an alpha-eigenvalue calculation and uses one or several alpha modes as the weighting flux. Between the two methods, the time-integrated flux is more accurate, but takes longer to obtain a solution.

The usability of these new homogenization methods is further developed by studying the effects of spatial heterogeneities and of the discretization of the time-"chunks". First, a case with spatial heterogeneities and a localized perturbation is used to show that these methods can be applied to heterogeneous lattice homogenization. The new methods are shown to perform well with spatial heterogeneities when compared to using a traditional, fundamental mode, homogenization method. Second, an a priori estimate for an optimal time discretization is obtained for the time-integrated flux method. It is shown that further divisions of the time domain reduce the error for several metrics until numerical errors become dominant.

To show that the multiphysics framework works well for industrial sized calculations, a reduced size BWR core calculation is performed. This simulation

is based on a rod-drop accident in the core during startup. Two energy group assembly homogenized cross sections are used, which show that the framework is capable of producing coupled physics solutions.

Keywords: multiphysics, homogenization, neutron transport, thermal hydraulics

Acknowledgments

I would first like to thank my advisors Drs. Richard Sanchez and Igor Zmijarevic for the time, effort, and guidance they provided during my Ph.D. study. Their dedication and knowledge have proven invaluable in preparing this work. Thank you to the manuscript reviewers, Drs. Jean Ragusa and Piero Ravetto, for their thorough reviews and helpful critiques. Thank you to the examiners Drs. Bertrand Mercier and Ernest Mund for their detailed questions and critiques of this work leading to a higher quality dissertation.

I would like to thank my family, who has been a constant source of support and encouragement since the beginning of my studies. My grandparents have said that I have always been a curious spirit, and have encouraged me to explore. My parents have always been behind me supporting me and giving me a little nudge up the mountain when I am starting to slow. Thank you for teaching me to explore and being my base of support. Merci à ma belle-famille de m'avoir accueilli et de m'avoir donné une sensation de « chez moi » en France.

Thank you to Dr. Marc-Oliver Delchini for your comments and suggestions while writing this manuscript. Finally, I would like to thank my fiancée Annabelle for supporting my dream to pursue a Ph.D. in France. Thank you for coming with me on this adventure, your support and love has kept me sane the last five years. I look forward to the many happy years we will share together.

Nomenclature

I/O	Input/Output
PDE	Partial Differential Equation
JFNK	Jacobian-Free Newton-Krylov
GMRes	Generalized Minimum Residual Method
MINRes	Minimum Residual Method
CG	Conjugate Gradient
KBA	Koch-Baker-Alouffe
PBJ	Parallel Block Jacobi
NEAMS	Nuclear Engineering Advanced Modeling and Simulation
CASL	Consortium for Advanced Simulation of Light water reactors
MoC	Method of Characteristics
HZP	Hot Zero Power
HFP	Hot Full Power
CZP	Cold Zero Power
LWR	Light Water Reactor
PWR	Pressurized Water Reactor
BWR	Boiling Water Reactor
REB	Réacteur à Eau Bouillante
DBA	Design Basis Accident
MCCI	Molten Corium Concrete Interaction
CFD	Computational Fluid Dynamics
DNS	Direct Numerical Simulation
LES	Large Eddy Simulation
RANS	Reynolds Averaged Navier Stokes
MCTH	Multi-Channel Thermal Hydraulics

Table of Contents

Page

List of Figures

Figure **Page**

List of Tables

Table **Page**

Chapter 1

Introduction

The nuclear engineering domain encompasses a vast array of subjects such as the transport of particles through media, the transfer of heat within a nuclear power plant, and the formation of hydrogen gas during a severe accident. The accurate solution to such physical models allows scientists and engineers to build more efficient power generation stations [1], as well as predict the effects of radiation exposure [2], study the effectiveness of using magnetic confinement for fusion reactors [3], and understand the process of collapsing supernovae [4, 5], among others.

Often the physical processes being studied by nuclear engineers and scientists are composed of many separate but coupled physical processes. The focus of this work is on the development of simulation strategies which can be used to produce high fidelity solutions to coupled physics problems encountered in nuclear engineering. The objective of this Ph.D. work is to show how physics component codes may be adapted to work within a multiphysics framework based on a Jacobian-Free Newton-Krylov (JFNK) method, and to develop homogenization procedures which reduce errors when applied to transient simulations. This work began with the intention of studying multiphysics coupling strategies applicable to industrial calculations in nuclear engineering, but as is often the case in research, it was discovered that the treatment of cross section homogenization for transient calculations was lacking in development. The focus of this work was then shifted to exploring cross section homogenization methods which were applicable to multiphysics transient simulations. The current chapter introduces the domain of study for this work, discusses the current state of this domain, and specifies which improvements to this domain are considered in this work.

1.1 Behavior of Nuclear Reactors

Nuclear reactor power plants are characterized by their primary heat source coming from a nuclear process; presently this is limited to fission events in commercial power plants. Depending on the design, a nuclear power plant consists of a primary coolant loop and possibly several secondary coolant loops. The primary

coolant is heated by passing directly through the reactor core, which generates its heat from nuclear processes. In boiling water reactors (BWRs) the coolant in the primary loop passes forthwith through the turbine generator, resulting in a Rankine power cycle [6]. In pressurized water reactors (PWRs), the pressure in the primary coolant loop is high enough to maintain the coolant below the saturation temperature. The thermal energy of the primary coolant is transferred to a secondary loop at a lower pressure, which then passes through a turbine generator.

The interior of a reactor core is a rich environment for physics simulations because of the complexities of high turbulence flows, fluid structure interactions, and material behavior under irradiation, among others. In addition to this rich environment of physical phenomena, many of these physical phenomena interact with one another. As an example, the power of the nuclear reactor is directly related to the way in which neutrons are distributed throughout the core. The distribution of neutrons can be determined based on the geometry of the core, the material composition within the core, and the temperature distribution in the core. However, the temperature distribution in the core can be determined by the power distribution within the core, the core geometry, and the entering coolant conditions. Furthermore, the geometry of the core is determined by the temperature distribution (from thermal expansion), vibrations caused by the interaction of the fluid and structure material, and others. This interaction of physical components can be treated as a multiphysics system, of which much effort has been devoted to its study recently [7–10].

1.2 Multiphysics Simulations

Obtaining solutions to coupled physics problems is becoming a large interest in many scientific domains. The United States Department of Energy started the Nuclear Engineering Advanced Modeling and Simulation (NEAMS) program, an international collaboration to produce a toolkit for modeling the multiphysics and multiscale behavior in nuclear reactors [11]. This program supports the Consortium for Advanced Simulation of Light Water Reactors (CASL) research hub focused on developing advanced simulation tools for understanding phenomena which limit the performance of Light Water Reactors (LWRs). The European based NUclear REactor SAFEty simulation platform (NURESAFE) aims to deliver reliable software for the analysis of design basis accidents. The NURESAFE program extends the advances made by the NUREISP and NURESIM programs in the simulation of multiscale and multiphysics phenomena during light water reactor accidents [12]. Such recent interest in resolving coupled physics problems has produced several software frameworks available for special purposes: MOOSE [8], LIME [13], and SALOME [14] to name a few.

Depending on the constraints of obtaining a coupled solution from several physics components, numerous choices are available, but three will be discussed: Operator Splitting, Multiphysics Toolkits, and JFNK. If the primary constraint is code reuse, an operator splitting technique can be used [10]. This technique leverages the many years of experience that went into the development of each

physics component code. Presently, multiphysics solutions are sought in the application domain where heavy modification to component codes becomes risky and error prone. This consideration creates a large focus on producing stable operator splitting methods. Additionally, the component codes are generally written without extensibility in mind and extending such codes to operate in a multiphysics environment can be problematic. It is reasonable that the easiest path to a multiphysics solution is to use a driver program with file Input/Output (I/O) between physics component codes. The driver program should be based on an operator splitting method which controls the input and output between component codes; this design maximizes code reuse and minimizes the modifications needed in component codes.

In the commercial simulation community, multiphysics toolkits are becoming prominent where the focus is on ease of use at the application level. These toolkits provide a framework in which multiphysics simulations can be performed. Typically these frameworks provide interfaces to existing codes which then manipulate the existing code, based on the desired computational scheme. These interfaces can either be provided by the toolkit, making only supported component codes usable within the framework, or be generated by the toolkit based on the existing code, as is the case for SALOME [15]. The calculation schemes will specify the flow of data between physics components during the simulation, and will generally only treat weak coupling between physics components. Higher order time discretizations are possible, but are prone to instabilities [16]. These types of frameworks are excellent choices for scoping studies to determine the general behavior of a coupled system, but fall short when applied to strongly coupled physics components and situations which require higher order time discretizations.

Several recent projects are based on a JFNK method, where each physics component is required to return a solution residual [8, 13, 17]. These methods treat physics components as strongly coupled and support high order time discretization methods. However, existing physics codes are generally not equipped to return a solution residual without heavy modification. The frameworks that provide coupling through a JFNK method will generally either provide separate physics component codes designed to work within the coupling framework, or users can build their own physics component codes from base libraries provided within the framework. Adapting existing codes to operate within a JFNK multiphysics environment is generally a difficult task, and will be a large focus of this work.

1.3 Severe Accidents

In the design of nuclear reactors, special attention is paid to how reactors will perform in unlikely but largely detrimental situations. These situations form the class of Design Basis Accidents (DBA) for which reactors must be shown to survive without loss of integrity to systems, structures, and components necessary to ensure public health and safety [18]. These accidents include large power excursions induced by neutronic control failure or loss of primary coolant, large earthquakes, flooding, and other possible scenarios.

A failure of the neutronic control or some other perturbation of the state of the reactor has the possibility to induce a large power excursion. A neutronic control failure may come from the mechanical failure of a control rod drive during the start-up phase, or through insufficient mixing of the soluble neutron absorber present in PWRs. Additional perturbations can come through the state of the coolant entering a core; a turbine trip in a BWR will cause a large pressure increase and induce a large power excursion. A large increase in power can weaken the cladding in the fuel, which is the first containment barrier. There are three main levels of containment designed into reactor facilities to protect the public from undue radiation exposure; these levels are listed from interior to exterior: the fuel cladding, the primary system loop, and the containment building. The more severe accidents involve the second and third levels of containment.

During such accidents, various physical phenomena can appear at different stages of the accident. A prolonged loss of primary coolant accident can eventually lead to risks of hydrogen gas formation due to a chemical reaction between zirconium cladding with an elevated temperature and a water based coolant [19]. The modeling of the distribution and combustion of hydrogen gas is an important area of research because of the possibility for a hydrogen deflagration event, which can compromise the integrity of the containment structure [20]. The process of reactor design involves treating how to safely vent or convert hydrogen-rich air to be far from an ignition concentration.

If a severe accident progresses far enough, the structural integrity of the core will be compromised and the formation of molten core material (Corium) will begin to interact with the pressure vessel and eventually the concrete structure of the containment floor [21]. The modeling of the progression of the Molten Corium Concrete Interaction (MCCI) involves many physical and chemical processes [22]. The design consideration of such an accident is to ensure that the molten Corium will be sufficiently cooled before melting through the containment floor. The MCCI phase of a severe accident can be modeled by a multiphysics system with strong coupling between physics components [23].

The computational methods reviewed in this work will be applied to design basis accidents involving large power excursions that can impact the integrity of nuclear fuel because of their effect on the first level of containment. This choice is based on the availability of component codes which solve the underlying physics of the problem and on the importance of ensuring the integrity of the first and arguably most important level of containment. However, these computational methods can also be used to explore the behavior of more serious accidents such as the formation of hydrogen gas in the containment vessel or the interaction between molten core material and the concrete of the containment floor.

1.4 State of the Art in Nuclear Engineering

The current state of the methods available to the simulation community will be reviewed in this section. The state of the art will focus on main areas of development in the resolution of coupled physics problems in nuclear engineering. First the active research in neutronics and thermal hydraulics is reviewed

with an emphasis on time dependent problems. Next, two ways of treating coupled physics problems are reviewed. This section finishes with the application of parallel methods and how data is treated in time dependent problems.

1.4.1 Time Dependent Neutronics

Without taking into account the thermal feedback effects which affect a nuclear system during a transient, there has been much work devoted to resolving the time dependent neutron transport equation. Time dependent methods typically depend on expanding the time dependent flux onto an orthogonal basis [24], or decomposing the time dependent flux into a product of two functions [25]. The difficulty in expanding onto an orthogonal basis is in finding appropriate orthogonal functions which accurately capture the features of a transport solution. Usually a reduced model in 0-D is required to find an appropriate basis on which to expand; the solutions to the α-eigenvalue problem provide such a basis [26, 27]. This basis has been used to show how the energy spectrum is shifted from the fundamental mode distribution during a transient [28]. Decomposing the flux into the product of a shape and amplitude function has been applied to the solution of space-time kinetics; this method is commonly referred to as the *quasi-static* method [25]. The amplitude function depends only on time, and changes rapidly with time. This function dictates the global behavior of the time dependent transport solution. The shape function depends on all variables, but is slowly varying in time. The shape function is updated on longer time scales and is used to update parameters which drive the evolution of the amplitude function.

1.4.2 Thermal Hydraulics

The development of accurate thermal hydraulic models is important to the continued progression of advanced reactor design. Thermal hydraulic phenomena in a nuclear reactor system operate on disparate time and space scales, which make the solution process difficult. The trend in thermal hydraulic research is to produce ever finer solutions on these time and space scales.

Thermal hydraulic phenomena which occur outside the reactor core are typically treated with a 1-D lumped parameter model [29]. This treatment gives an integral perspective of the thermal hydraulic phenomena which occur excore. The interior of the core contains more complex thermal hydraulic phenomena, which require more elaborate modeling techniques to resolve their detail. The thermal hydraulics of an entire reactor core is typically modeled by a set of coupled 1-D channels which resolve the 3-D spatial dependence. Turbulence and mixing within the channels is handled by Reynolds Averaged Navier Stokes (RANS) models such as the k-ε model [30]. On ever smaller spatial scales, more detail may be modeled in the heat transfer and fluid flow. However, for the general behavior of a reactor core, such detailed models become prohibitively expensive and lower order models are needed [31].

Thermal hydraulic modeling aims to predict the behavior of fluid flows and heat transfer in novel reactor designs. There is a large demand on advanced ther-

mal hydraulic models to predict the behavior of novel generation-IV reactors [32]. The complex flow around fuel in pebble bed reactors for example, requires robust methods able to treat the conduction, convection, and radiative heat transfer within such environments.

1.4.3 Operator Splitting

Once a time dependent model is produced, an effective way to acquire coupled physics solutions, with minimal modifications to the existing physics component codes, is to use an operator splitting technique. In this approach, each physics component interacts with other physics components through I/O channels. This is typically the first method used for scoping studies in the behavior of coupled systems [33, 34]. These methods usually do not accurately treat the nonlinear coupling terms of the multiphysics problems, requiring smaller time steps during the simulation to maintain accurate solutions [35]. This can lead to expensive simulations because of the increased number of steps which must be taken to produce a time dependent solution. Some of the errors encountered through operator splitting may be reduced by using higher order time integration methods, but will also not completely converge nonlinear terms between physics components [9]. To remove more errors from a coupled physics simulation, a strongly coupled method is needed. An additional concern for operator splitting methods has been the appearance of instabilities when applied to certain propagation problems [16].

Operator splitting methods have been applied to a variety of problems in the nuclear engineering field. The time dependent radiation-diffusion equations present phenomena which are difficult to resolve without special attention to time step size control [33]. The efficacy of using operator splitting methods in nuclear reactor applications was applied to reduced dimensional problems [35]. Several operator splitting variations were applied to couple thermal hydraulics and neutronics in both 0-D and 1-D. It was shown that to reduce errors due to the stiffness of the coupled system, higher order time integration methods need to be used. Also, to converge nonlinearities between physics components, an iteration among physics components is needed. However, when analyzing accidents of nuclear reactors, it is customary to use a 3-D neutron diffusion model coupled to a 3-D thermal hydraulic model to accurately capture spatial effects important to the transient [36]. The focus on using high order operator splitting methods is not yet pursued in application level computations.

1.4.4 Jacobian-Free Newton-Krylov Method

As was stated earlier, an efficient way to resolve strong coupling between physics components is to use a JFNK method, with all relevant physics components combined in a single numerical system. While there has been much work on producing computational frameworks based on a JFNK method, the physics components used within these frameworks are limited to those which are provided by the framework and those which are built inside the framework.

A significant portion of the work in developing an efficient simulation of a multiphysics system is in the acceleration techniques used to converge to a solution faster. In JFNK methods, this acceleration is realized through preconditioners on the linear system. It has been shown that using preconditioners, which are based on the physics of the underlying components, work very well [37]. This type of preconditioner will generally solve an uncoupled (or weakly coupled) version of the multiphysics system.

Other considerations when building a multiphysics framework can focus on the design of software within the framework. The complexity of multiphysics problems requires many pieces of software to work together seamlessly. This type of complexity demands a modular architecture for the framework. A modular design contains well defined interfaces at boundaries of individual modules. Well defined interfaces also allow modular components to be easily exchanged. For example, a linear solver module could contain several linear solver algorithms from which to choose. Furthermore, well defined interfaces allow for the use of external numerical libraries such as PETSc [17] or Trilinos [38].

1.4.5 Parallel Computing

With increased demand placed on the ever detailed solution in nuclear reactors, parallel solution methods are becoming necessary and viable options. The first level of parallel computing consists of processes which are nearly independent of each other, such processes are referred to as *embarrassingly* parallel processes [39]. An example of such processes is the transport sweeps along given directions in a medium. The scalability of such parallelization is limited by the number of independent processes available. In the example of transport sweeps, scalability is limited to the number of directions used to discretize the angular flux. Additional levels of parallelization may be implemented, each with more complex requirements on communication between parallel processes. It is becoming evident with the increased demand placed on detailed solutions of neutron transport and thermal hydraulics within nuclear reactors, more levels of parallelism will be sought [40, 41].

There are many numerical linear algebra libraries available to harness the power of parallel computing [17, 38]. These libraries may be used in developing multiphysics simulations, however the bottleneck in such simulations often comes from underlying serial physics codes. To harness the power of parallel computing in multiphysics simulations, the underlying physics component codes must also be parallel. The work presented in this dissertation only touches on the use of parallel algorithms because the underlying physics component codes used in this work are implemented as serial processes. The parallelization of such codes falls outside the scope of this subject. However, the use of parallel methods in multiphysics simulations is of great importance and should be investigated in the continuation of this work.

1.4.6 Cross Section Homogenization

In reactor analysis, the cost of computing a detailed solution is typically prohibitive. Cross section homogenization provides a means to pretreat the data before a simulation to reduce the number of unknowns. In many cases, cross section homogenization involves producing an approximate solution which can be used to attain average cross section values, typically over the space and energy domains. This approximate solution will generally come from steady state calculations for various configurations of temperature and material composition, which are interpolated during the larger reactor calculation.

Cross section homogenization is optimized for static calculations, which represent the majority of operation time for commercial reactors. To be computationally advantageous, cross section homogenization is performed at the assembly level in 2-D. Early work in homogenization focuses on how to conserve reaction rates when transitioning between transport calculations on assemblies to diffusion calculations on the core. Reaction rates can be better conserved by introducing discontinuities of the flux at homogenized region boundaries [42] or through a procedure which iteratively adjusts cross sections [43].

Much of the recent work in homogenization methods involves producing homogenized cross sections where the global solution can be largely different from the solution produced by an isolated assembly [44]. This situation arises when neighboring assemblies are very different in material composition; this case occurs in MOX fuel assemblies. In such a case, the approximate solution is far from what the global solution is, and cross sections homogenized with the approximate solution will poorly represent reality. Methods which take into account the neighboring assemblies should be used, such as the *color-set* method.

Cross section homogenization techniques may be applied to time dependent problems by using on-the-fly homogenization techniques. Such methods update homogenized cross sections at certain times in the transient when the cross sections are deemed in error [45]. On-the-fly calculations can take into account the effects of a time dependent flux when it remains close to the fundamental mode flux.

1.5 Improvements to the State of the Art

The goal of this work is to extend the current state of methods used in the numerical simulation community. These improvements to the state of the art will be introduced presently. Two large themes for these improvements in current simulation methods will be explored within this work. The first is on coupling methods which treat physics components. The second theme focuses on how data is treated during the simulation of transients.

1.5.1 Jacobian-Free Newton-Krylov Methods

The JFNK method has been successfully applied to couple physics components with physics solvers that are built within a robust JFNK based framework.

However, it is desirable to include computer codes which are highly optimized for specific physics models; it is desired to reuse the substantial effort that has been put into developing smaller domain specific codes. This work will focus on how an existing numerical code can be adapted to work within a JFNK framework when this feature was not in the original intent of the code.

The existing codes will be connected to a JFNK framework through the residual computation, which will be specific to each physics component. The residual computation will provide a transparent interface with which physics components may interact. Once a residual for a physics component is defined, the physics component can be used in a simulation. Additional physics components can be added to the simulation by defining a residual computation module for the physics component.

Special attention will be devoted to a new formulation for the residual for neutron transport. The neutron transport solution size can be prohibitively large, and the new residual formulation aims to reduce the size of this solution. The new formulation of the neutron transport residual will be shown to be correctly implemented and reduces the size of the sought solution. The reduction in size provides more benefits than just reducing memory consumption. A vector of a smaller size resides in a smaller search space; any Krylov solver which builds successive subspaces will converge faster if the subspace can accurately approximate the full search space.

A physics-based preconditioner which is truly matrix-free is explored. Generally physics-based preconditioners require direct manipulation of the underlying physics code. The desire to operate in a modular framework and only interact with physics codes through residual computation requires modified preconditioners which only manipulate the solution residual. Both a Block Jacobi and a Block Gauss-Seidel preconditioner are developed from manipulations of the solution residual.

1.5.2 Cross Section Homogenization

As was mentioned earlier, cross section homogenization provides a way to reduce the number of unknowns of the numerical system in reactor analysis. Many of the advancements in cross section homogenization methods are oriented towards homogenization in steady state calculations. The majority of a reactor's operation history is performed at steady state, with rare excursions which last a short time compared to normal operation. The study of the impact of applying such homogenization methods during transient calculations has not largely appeared in the literature surrounding reactor analysis. Only a single report was found which mentions using different eigenvalue problems during homogenization for different configurations [46].

A question that arose during this work was, "Will homogenized cross section intended for steady state calculations perform adequately during transient simulations?" It was soon discovered that during very rapid transients, where the reactor is far from critical, these cross sections can introduce large errors in the time dependent power. This realization prompted the author to explore ways to

reduce the error introduced by homogenized cross sections.

Two methods, which are designed to reduce the error introduced when using cross sections intended for steady state calculations, are developed and tested. One method is based on an expansion of the time dependent flux over a basis that comes from an eigenvalue problem which accounts for time dependent behavior. The expansion method has the freedom to choose how large the expansion basis is and the relative weight between vectors in the expansion basis. These weights can be determined through a minimization over the expansion subspace and some chosen solution, typically the initial condition. The other method is based on a time integrated flux over large time intervals of the transient simulation. The time intervals are free to be chosen and should generally coincide with important changes of the solution: time of perturbation, maximum power, delayed neutron decay, etc. This method, in addition to capturing the time dependent behavior of the solution, captures thermal feedback effects from changes in temperature during the simulation. These two methods are tested against reference solutions for a variety of available transients.

1.6 Organization

The remainder of this dissertation is organized thusly. Chapter 2 discusses the models used to describe each physics component treated in simulations for this work. The focus is on the physical aspects of the models which are coupled together, and how this coupling manifests in the models. The models discussed are Neutron Transport, which describes how neutrons are expected to distribute within a medium, and Thermal Hydraulics, which describes how heat is transferred within a nuclear reactor core. Many of the approximations made when solving the neutron transport equation are developed and discussed. The problems in this work are treated by transport, and hence other models often used in neutronics such as diffusion or simplified P_N are not discussed. Two thermal hydraulics models are discussed. One largely simplified 1 point model is used in simplified geometries. The other is a more complicated subchannel model which involves multiple coupled 1-D channels. This model is applied to heterogeneous spatial geometries. The physical manifestation of coupling between these models through temperature dependent macroscopic cross sections is also discussed.

Chapter 3 discusses the numerical methods used to resolve the coupling between the models discussed in Chapter 2. The numerical methods include operator splitting methods along with JFNK methods. All the linear and nonlinear solvers included within the JFNK framework are discussed. Special attention is devoted to building effective preconditioners which are manipulated from within the JFNK framework; meaning a preconditioner is sought which does not require knowledge of the underlying physical behavior of the solution residual. Two physics-based preconditioners (Block Jacobi and Block Gauss-Seidel) are discussed, which rely only on manipulations of the solution residual. These preconditioners are tested on a spatially heterogeneous problem against an identitiy preconditioner. The physics-based preconditioners are shown to reduce the average ratio of linear iterations per nonlinear iteration when compared to the identity

preconditioner. While these preconditioners may not be the optimum choice for acceleration, they perform well and are an acceptable starting point. A novel neutron transport residual formulation is developed based on the fission source. This new formulation is verified to be correctly implemented by comparing the rate of temporal convergence to the analytic solution of a 1 point, 1 energy group solution with 2 delayed neutron precursor groups.

Chapter 4 details the new homogenization methods developed to treat cross section homogenization during transient simulations. The eigenvalue spectrum of the α-eigenvalue problem is studied and used to develop various versions of the Alpha homogenization method. Several combinations of α-eigenvectors are used in the Alpha method with varying levels of success depending on characteristics of the transient simulated. The two methods, described in Section 1.5.2, are tested on a variety of transients. The first tests are in an infinite homogeneous medium with 281 energy groups. The effect of suppressing and activating delayed neutron precursors is investigated. It is found that when suppressing delayed neutron precursors in this geometry, a single dominant α-eigenvector is adequate in producing homogenized cross sections. Both the Fluence and Alpha methods perform well when compared to a classical homogenization method in reproducing a reference power transient. It is also shown that the new methods perform well for a variety of reactivity insertions and homogenized group structures when delayed neutron precursors are suppressed. Activating delayed neutron precursors reveals that multiple α-eigenvectors must be taken to produce homogenized cross sections which will reproduce the time dependent power of a reference solution. A spatially heterogeneous domain with 26 energy groups is also used to study a heterogeneous reactivity insertion and whether the Fluence method will perform better than a classical homogenization method. The optimal discretization of time intervals is studied with this geometry and reveals that refining the time discretization reduces the errors in the transient power up to a point, whereafter interpolation errors begin to become dominant.

Chapter 5 explores using the multiphysics framework on a more realistic problem of a reduced BWR core during a startup accident. The reduced core demonstration problem is meant to show how the multiphysics framework is capable of producing accurate multiphysics solutions to industrial sized applications. Several simplifying assumptions are made to the physics models based on the accident starting from Cold Zero Power. The framework is able to produce coupled physics solutions on larger simulations, however the computation time becomes prohibitive even when using 2 group assembly homogenized cross sections. The continued expansion of using such a multiphysics solver will need to incorporate improvements in computational efficiency, including parallelization of the underlying physics component models. Further improvements can be achieved through parallelization of the residual computations and inversion of the preconditioning matrix.

Chapter 6 finishes this dissertation with a few conclusions on modeling multiphysics phenomena with strong nonlinear coupling and on the applicability of the new transient homogenization methods. The possibility to couple existing physics component codes in a JFNK framework is discussed, along with the use-

fulness of the new homogenization method in industrial applications. As with any amount of research, there are many more crevasses which remain to be explored. Several directions for the further study of multiphysics modeling and transient homogenization techniques are outlined at the end of this work.

Chapter 2

Physical Models

Describing the behavior of nuclear reactors involves modeling the interchanges between several physical processes (neutron transport, heat transfer, solid mechanics, etc). These interchanges between physical processes manifest as couplings between models. For example, heat transfer models are coupled to neutron transport through the fission rate in the fuel, which serves as a heat source. Likewise, the neutron transport model is coupled to heat transfer models through the temperature dependence of material cross sections, which change how likely a neutron is to interact with the nucleus of the background material. This coupling between physics components produces systems of equations that are difficult to solve with current tools and require special attention.

The present chapter details the physical models used throughout this dissertation (neutron transport and heat transfer). There are many models that could be applied to describe the behavior of a nuclear reactor. The following is a non-exhaustive list of physical phenomena that can affect reactor behavior. The ballooning of fuel under irradiation and strong temperature gradients change both the shape and density of fuel [1]. In PWRs, the soluble boron in the coolant can deposit on the cladding of fuel elements and affect the behavior of neutrons in that part of the core [47]. Under irradiation, the stoichiometry of fuel changes, which can account for changes in thermal properties [48]. Additionally, the state of a reactor is dependent on the incoming coolant, which can be affected by how much heat is extracted from the coolant on the system side [49]. The state of the coolant can also be altered if the soluble boron is not homogeneously mixed at the entrance, producing fluctuations in the neutron density [50].

The objective of this work is to improve the methods used to solve multiphysics systems. In this light, only the most prominent physical models that impact the behavior of a nuclear reactor under a reactivity initiated accident will be taken: the time dependent transport of neutrons in a medium, and the heat transfer between solid fuel and liquid coolant. These models are important in the simulation of the behavior of LWRs during transients.

2.1 Neutron Transport

The distribution of neutral particles in a medium is governed by a transport model in which the density of particles is low enough that the possibility of two particles interacting is negligible. The low density assumption allows a linear transport model to be used; otherwise, a nonlinear interaction term would need to be included. The probability of particles interacting with the background medium is captured by macroscopic cross sections. These macroscopic cross sections are given in units of interactions per neutron path length, so that when multiplied by the scalar flux in units of neutron path length per phase space volume, the product is an interaction density. The integro-differential form of the described transport model, called the linear Boltzmann equation, is shown in Equation 2.1. The linear Boltzmann equation is derived as a particle density balance equation over a differential control volume [51]. The derivation consists of describing each type of interaction a neutron can have within an arbitrary volume of phase space.

$$\begin{aligned}\frac{1}{v(E)}\frac{\partial\psi(\vec{r},E,\vec{\Omega},t)}{\partial t}+\vec{\Omega}\cdot\vec{\nabla}\psi(\vec{r},E,\vec{\Omega},t)+\Sigma_t(\vec{r},E,t)\psi(\vec{r},E,\vec{\Omega},t)=\\ \int_0^\infty\int_{4\pi}\mathrm{d}\Omega'\,\mathrm{d}E'\,\Sigma_s(\vec{r},E'\to E,\vec{\Omega}'\cdot\vec{\Omega},t)\psi(\vec{r},E',\vec{\Omega}',t)+\\ \frac{\chi(E)}{4\pi}(1-\beta)\int_0^\infty\mathrm{d}E'\,\nu\Sigma_f(\vec{r},E',t)\phi(\vec{r},E',t)+\\ \frac{1}{4\pi}\sum_{j=1}^{N_d}\chi_D^j(E)\lambda_jC_j(\vec{r},t)+S_{ext}(\vec{r},E,\vec{\Omega},t)\end{aligned}\tag{2.1}$$

$$\phi(\vec{r},E,t)=\int_{4\pi}\mathrm{d}\Omega\,\psi(\vec{r},E,\vec{\Omega},t)\tag{2.2}$$

$$\frac{\partial C_j(\vec{r},t)}{\partial t}=\beta_j\int_0^\infty\mathrm{d}E\,\nu\Sigma_f(\vec{r},E,t)\phi(\vec{r},E,t)-\lambda_jC_j(\vec{r},t)\qquad j=1,2,\ldots,N_d\tag{2.3}$$

The first term of Equation 2.1 accounts for the change in time of the neutron density, where the neutron density is the angular flux divided by the neutron speed. The second term ($\vec{\Omega}\cdot\vec{\nabla}\psi$) accounts for the streaming of particles from a differential phase space volume to other points in the phase space. The last term on the left side of the equality accounts for the total interaction between neutrons and the material they are streaming through.

The right side of Equation 2.1 contains the scattering term, which accounts for particles being transferred from a phase space volume in energy and direction to other phase space volumes. The scattering cross section (Σ_s) describes a double differential probability in energy and angle, meaning the cross section depends on the incoming and outgoing angle and energy. For the cases relevant to nuclear reactor analysis, there are enough small and randomly oriented single crystals

in polycrystalline material, giving no preferential direction for streaming in such a medium [52]. In these cases, cross sections will not depend on the incident neutron direction. Additionally, the scattering cross section only depends on the angle formed between incident and outgoing directions; this is reflected in the scattering cross section shown in Equation 2.1. The second term accounts for prompt fission, which occurs shortly after interaction ($\sim 10^{-15}s$). This prompt fission term in general depends on the specific isotope undergoing fission, and the total prompt fission source is a summation of all fissile isotopes undergoing fission. Rigorously written, this term should include a sum over fissile isotopes with χ, $\nu\Sigma_f$, and β being isotope dependent. The third term accounts for the decay of delayed neutron precursors, which emit neutrons on a longer time scale than prompt fission (from tens of milliseconds to seconds). Again, the rigorous definition of this term involves a sum over isotope with χ_D, λ, and C also being dependent on isotope. The last term accounts for any fixed source of neutrons which are independent on the state of the nuclear system.

The dependent variable in Equation 2.1 is the angular flux, ψ, which occupies the six dimensional phase space volume {space($\vec{r}$), energy(E), and direction($\vec{\Omega}$)} and is a function of time t. The scalar flux ϕ, defined in Equation 2.2 and appearing in the prompt fission term (containing $\nu\Sigma_f$), is the integration of the angular flux over all directions. While the linear Boltzmann equation seeks to model every type of interaction a neutron can experience while traveling through a medium, several simplifying assumptions are made. Namely the linear transport model of Equation 2.1 makes the following assumptions:

- Influence of gravity ignored (Straight paths of travel between interactions)
- No neutron-neutron collisions
- Point particle neutrons
- Instantaneous and local interactions
- Population of neutrons and nuclei large enough so that deviations from expected value is small

2.1.1 Delayed Neutron Precursors

Fission events release neutrons on two time scales. Prompt neutrons are those that are released within femtoseconds of the fission event. These neutrons allow nuclear systems to respond quickly to changes in material composition and the system geometry. Delayed neutrons are those neutrons that are released milliseconds to seconds after the fission event. They are released after several beta decays of the fission products produced from the fission event. The isotope in the chain of beta decays which is just before the release of a neutron is called a *delayed neutron precursor*. The concentration of these delayed neutron precursors is modeled in Equation 2.3 by a balance equation of the sources and sinks for radioactive elements. The delayed neutron concentration (C_j) for the j-th delayed neutron

group depends on space and time, β_j is the delayed neutron fraction giving the fraction of neutrons produced that will appear in the j-th delayed neutron group, and λ_j is the probability of decay for the j-th delayed neutron group. The fission cross section and β_j being dependent on isotope makes the delayed neutron precursor concentration also dependent on isotope. Consequently, for the models described in this work, the delayed neutron precursor concentration will be defined with the sum over isotopes included for each delayed precursor group.

There are approximately 100 fission products, produced from the thermal fission of ^{235}U, that can potentially release a neutron after a series of β decays [53]. Tracking all of these 100 fission product concentrations would be needlessly expensive; instead delayed neutron precursors are sorted into groups that have a similar decay constant. Generally six or eight groups are needed to accurately model the behavior of delayed neutron emission [54, 55]. The β_j for a delayed neutron group are given by an average over energy of the ratio between the delayed neutron emission (ν_d) and the total neutron emission (ν) for isotopes in delayed group j. The β that appears in Equation 2.1 is the sum of β_j over all delayed neutron groups.

Because delayed neutron precursors are released at a later time, their presence gives a stabilizing effect to nuclear systems. The absence of delayed neutrons would make any small positive reactivity insertion to the system result in a very fast transient, uncontrollable by human reactions. In a critical configuration, the combination of prompt and delayed neutrons work together to maintain a constant neutron population. The nuclear system can be in a supercritical state but still need delayed neutrons to maintain its critical state. However, if the nuclear system is far enough from the critical state such that delayed neutrons are not needed to maintain criticality, the system is said to be in a *super-prompt-critical* state. A nuclear system in this state behaves as if delayed neutrons were not present, and the neutron population increases rapidly. These different states are depicted in Figure 2.1.

The conditions in Figure 2.1 show the limits for the super-prompt-critical cutoff. An additional parameter is introduced in the figure: ρ. This parameter is known as the reactivity and measures the departure from criticality. There are several ways to define the reactivity of the system, depending on which eigenvalue problem is used to describe the nuclear system. To illustrate the effect of the presence of delayed neutron precursors, a relation to the k-eigenvalue is chosen $\left(\rho = \frac{k-1}{k}\right)$ [56]. In reactor kinetics, transients are initiated by inserting or removing reactivity from the system; this corresponds to changing the system in some way which affects the value of k_{eff}.

Determining the delayed neutron parameters is generally performed through pulsed or saturated neutron irradiation experiments, where group constants are determined from the neutron flux decay after irradiation [57]. These experiments treat the aggregate behavior of a sample of a given fissile isotope; this is referred to as a macroscopic treatment of delayed neutron precursor data generation. More recently, a microscopic treatment of generating delayed neutron precursor data has been explored, where the group constants are generated based on the physics of the individual precursor isotope [58, 59]. More accurate representations

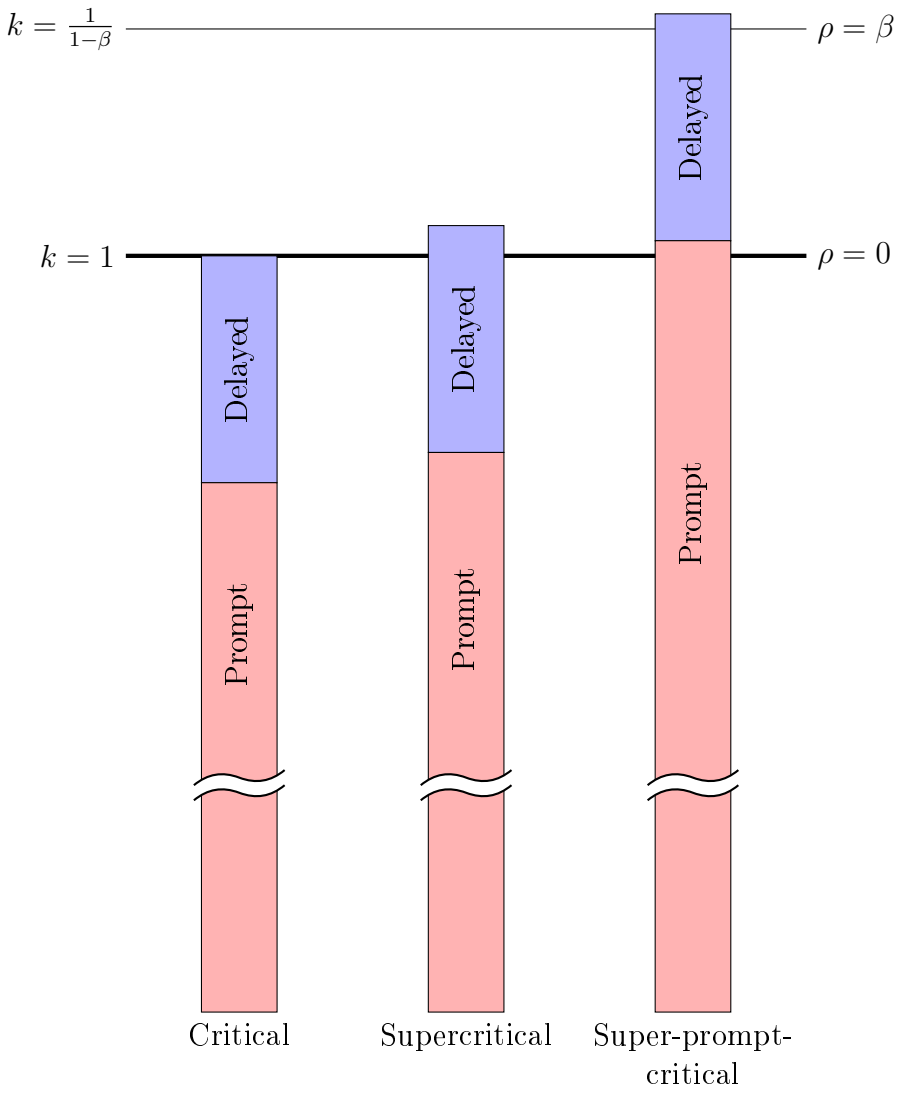

Figure 2.1. Pictorial of the Relationship Between Nuclear System States: Critical, Supercritical, and Super-prompt-critical

have been produced based on a synergistic method using both a macroscopic and microscopic treatment to produce group constants [60]. In the general case, since $\frac{\nu_d}{\nu}$ is energy dependent, the delayed neutron group constants depend on the incident neutron energy [61]. However, this dependence on incident energy is weak and the implementation of this dependence greatly complicates the use of the time dependent neutron transport model. For this work, the delayed neutron data is assumed to be independent of incident neutron energy.

2.1.2 Boundary & Initial Conditions

Equation 2.1 is accompanied by boundary conditions which define the angular flux incident on the spatial region being modeled, and an initial condition which specifies the initial angular flux distribution within the modeled region. Equation 2.3 contains a single first order derivative in time which requires a single

initial condition for the distribution of delayed neutron precursors. The initial condition for the coupled Equations 2.1 & 2.3 is composed of a given distribution for the angular flux and precursor concentration at a specific time, corresponding to the beginning of the simulation. The initial angular flux depends on space, energy, and angle, while the initial delayed neutron precursor concentration only depends on space. A time independent form of Equation 2.1 is

$$\vec{\Omega}\cdot\vec{\nabla}\psi(\vec{r},E,\vec{\Omega})+\Sigma_t(\vec{r},E)\psi(\vec{r},E,\vec{\Omega})= \int_0^\infty\int_{4\pi}\mathrm{d}\Omega'\,\mathrm{d}E'\,\Sigma_s(\vec{r},E'\to E,\vec{\Omega}'\cdot\vec{\Omega})\psi(\vec{r},E',\vec{\Omega}')+ \frac{1}{k}\frac{1}{4\pi}\left[(1-\beta)\chi(E)+\sum_{j=1}^{N_d}\chi_D^j(E)\beta_j\right]\int_0^\infty\mathrm{d}E'\,\nu\Sigma_f(\vec{r},E')\phi(\vec{r},E'), \quad (2.4)$$

known as the criticality equation and has the same boundary conditions as Equation 2.1. The term within square brackets is the average fission emission spectrum from both prompt and delayed neutrons. A parameter, k, is added to the neutron production term to permit a solution for any physically valid material composition. There are infinitely many solutions which satisfy Equation 2.4, where a solution consists of a pair between a value k and a function ψ. There may be more than one function ψ which corresponds to a value k, in which case the value k is said to be *degenerate*. The largest k-eigenvalue corresponds to a function which is positive everywhere, and given the symbol k_{eff}. For a value of $k_{\text{eff}}<1$, the system is said to be *subcritical* and any neutron population present will eventually be extinguished. For $k_{\text{eff}}=1$, the nuclear system is said to be *critical* and will sustain a constant average neutron population in time. For a value of $k_{\text{eff}}>1$, the system is said to be *supercritical* and the average neutron population will increase to infinity. The eigenfunction ψ of Equation 2.4 is determined up to a multiplicative constant; this suggests that the criticality of a system is not dependent on the neutron population present, but only on the configuration of the system itself. The magnitude of the eigenfunction must be determined by other information, such as the power or other reaction rates.

Notice that there is no fixed source present in Equation 2.4. The criticality equation is used to obtain information about the nuclear system itself, in the absence of external sources. Inserting a fixed source into Equation 2.4 will only produce solutions when the nuclear system is subcritical, where the asymptotic flux tends to $\psi\sim\frac{Q}{1-k_{\text{eff}}}$. For the two other states, the flux does not have an asymptotic limit and must be studied using the time dependent transport equation, Equation 2.1. For example, adding a constant source to a critical nuclear system will cause the average flux to increase linearly in time.

The boundary conditions for the transport equation specify the incoming flux for the spatial domain being modeled, i.e. on all outer boundaries. There are two main types of boundary conditions for the transport equation: Dirichlet and Reflecting [62]. The boundary may be composed of surfaces, each with a different

boundary condition. Dirichlet boundary conditions impose an incoming angular flux over the boundary and are defined as

$$\text{Dirichlet}: \quad \psi(\vec{r}, E, \vec{\Omega}) = \psi_{\text{inc}}(\vec{r}, E, \vec{\Omega}) \quad \begin{cases} \forall \vec{r} \in \partial V \\ \\ \forall \vec{\Omega} \mid \vec{\Omega} \cdot \vec{n} < 0 \end{cases}, \tag{2.5}$$

where ∂V is the boundary of the spatial region, and $\vec{n}$ is the outward normal vector for the spatial region. Vacuum boundaries are a special case of Dirichlet conditions where $\psi_{\text{inc}} = 0$. Vacuum boundary conditions specify that the particles exiting the boundary are lost and cannot reenter the problem; care must be taken for reentrant geometries where particles have the possibility to exit a geometry and reenter at a different location.

Reflecting boundary conditions specify the incoming flux at the boundary as a function of the exiting flux. Reflecting boundary conditions can be defined as

$$\text{Refl}: \quad \psi(\vec{r}, E, \vec{\Omega}) = \int\limits_{\vec{\Omega}' \cdot \vec{n} > 0} \mathrm{d}\Omega' \, A(\vec{\Omega}' \to \vec{\Omega}) \psi(\vec{r}, E, \vec{\Omega}') \quad \begin{cases} \forall \vec{r} \in \partial V \\ \\ \forall \vec{\Omega} \mid \vec{\Omega} \cdot \vec{n} < 0 \end{cases}, \tag{2.6}$$

where $A(\vec{\Omega}' \to \vec{\Omega})$ is a special case of an albedo function that relates the outgoing to the incoming directions. In its general form, the albedo function would be defined with spatial and energy dependence to account for particles entering the volume at a different location, and with a different energy than the exiting particles; that is $A(\vec{r}\,' \to \vec{r}, E' \to E, \vec{\Omega}' \to \vec{\Omega})$. The albedo function can describe many different types of reflections. Specular reflection corresponds to the exiting direction being reflected about the surface normal. The albedo function representing specular reflection can be described by a Placzek delta [63], defined as

$$\begin{aligned} \delta_2(\vec{\Omega}' \cdot \vec{\Omega}) = 0 \qquad \vec{\Omega}' \neq \vec{\Omega} \\ \int_{4\pi} \mathrm{d}\vec{\Omega}' \; \delta_2(\vec{\Omega}' \cdot \vec{\Omega}) f(\vec{\Omega}') = f(\vec{\Omega}), \end{aligned} \tag{2.7}$$

where $f(\vec{\Omega})$ is some function of angle. The albedo function of Equation 2.6 is then written as

$$A(\vec{\Omega}' \to \vec{\Omega}) = \delta_2(\vec{\Omega}' \cdot \vec{\Omega}_r), \tag{2.8}$$

where

$$\vec{\Omega}_r = \vec{\Omega} - 2\vec{n}(\vec{n} \cdot \vec{\Omega}). \tag{2.9}$$

The specular reflection boundary condition works well in Cartesian fuel cells where a circular fuel pin is surrounded by a rectangular moderator boundary.

This geometry models an infinite lattice of rectangular pin cells. However, if the square pin cell is transformed to an equivalent circular pin cell, through the Wigner-Seitz approximation for example, a specular reflection boundary can produce travel directions which do not behave the same. A travel direction, chosen in the square pin cell, which intersects the fuel after a number of reflections on the boundary may not intersect the fuel at all in the circular pin cell. To improve such behavior in circular pin cells, a *white boundary* can be used [64]. The white boundary states that the incoming flux is isotropically distributed. Thus, the albedo function in Equation 2.6 is defined as

$$A(\vec{\Omega}' \to \vec{\Omega}) = \frac{b}{\pi}|\vec{\Omega}' \cdot \vec{n}|, \tag{2.10}$$

where b is a constant between zero and one to account for any losses outside the region of interest.

2.1.3 Cross Section Data

Microscopic cross sections represent the probability of a neutron with a specific energy interacting with a given nucleus. Microscopic cross sections depend strongly on energy with the general trend of increasing for lower energy, decreasing for higher energy, and having large resonances in the mid energy range. Lower energies experience the cross section varying with a $\frac{1}{\sqrt{E}}$ relation. The resonances in the mid energy range can experience a large increase or decrease in probability, sometimes by several orders of magnitude, for very small variations in energy. Figure 2.2 gives example plots of the total interaction cross section as a function of energy for ^{238}U, ^{90}Zr, and ^{1}H. We see the large variations for the ^{238}U and ^{90}Zr in the mid energy range; the hydrogen cross section is one exception to the general rule on resonances. The cross sections shown in Figure 2.2 were produced by the JANIS application through the OECD [65].

The cross sections used in Equation 2.1 are not the microscopic cross sections shown in Figure 2.2, but macroscopic cross sections defined as

$$\Sigma_x = \sum_{i \in I} N_i \sigma_x^i, \tag{2.11}$$

where Σ_x is the macroscopic cross section for reaction x, N_i is the atom density for isotope i, σ_x^i is the microscopic cross section for reaction x of isotope i, and I is the set of isotopes in the background material.

In addition to the large variations in energy, the macroscopic cross sections are affected by the temperature of the background medium. This temperature dependence is the result of both the change in atom density, and of thermal vibrations of the medium nuclei. When a nucleus vibrates, the relative velocity between the neutron and nucleus is changed. This change in relative velocity manifests as a broadening of the resonance peaks, which will absorb more neutrons because of the larger energy band covered.

If we zoom in on the lowest energy resonance of ^{238}U in Figure 2.2 for illustration, the temperature dependence can be more precisely seen as in Figure 2.3.

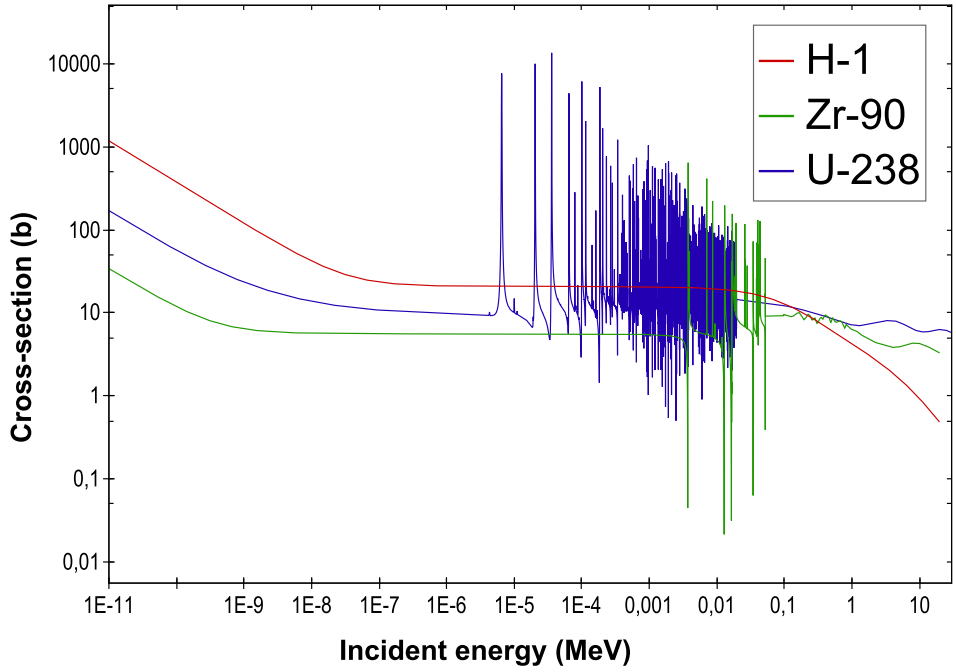

Figure 2.2. Energy Dependent Total Interaction Microscopic Cross Sections

This specific resonance was taken to illustrate the behavior of resonances when the material temperature changes, but this behavior is present in all isotopes containing resonances. This temperature dependence is strongly observed for isotopes that have large resonances of the cross section. As the temperature increases, the resonances are broadened due to the increased thermal vibrations of the nucleus.

The probability of interaction is plotted against the incident neutron energy in Figure 2.3. As a material is heated from absolute zero, the atoms begin to vibrate introducing a distribution of the relative velocity. As the temperature is increased, the resonance in Figure 2.3 shows two behaviors: the width of the resonance is increased, and the height is decreased. The temperature dependent cross section can be defined as a convolution of a temperature dependent velocity distribution (typically Maxwellian) and the energy dependent microscopic cross section times the relative velocity. The resonant peak decreases because for any relative velocity, the convolution will produce a cross section which is less than the maximum. Conversely at energies further from the peak energy, the convolution will produce a cross section which is larger than the value at absolute zero. This behavior results in the broadened resonances depicted in Figure 2.3. The increased width of resonances leads to a larger probability that a neutron will be scattered into the resonance.

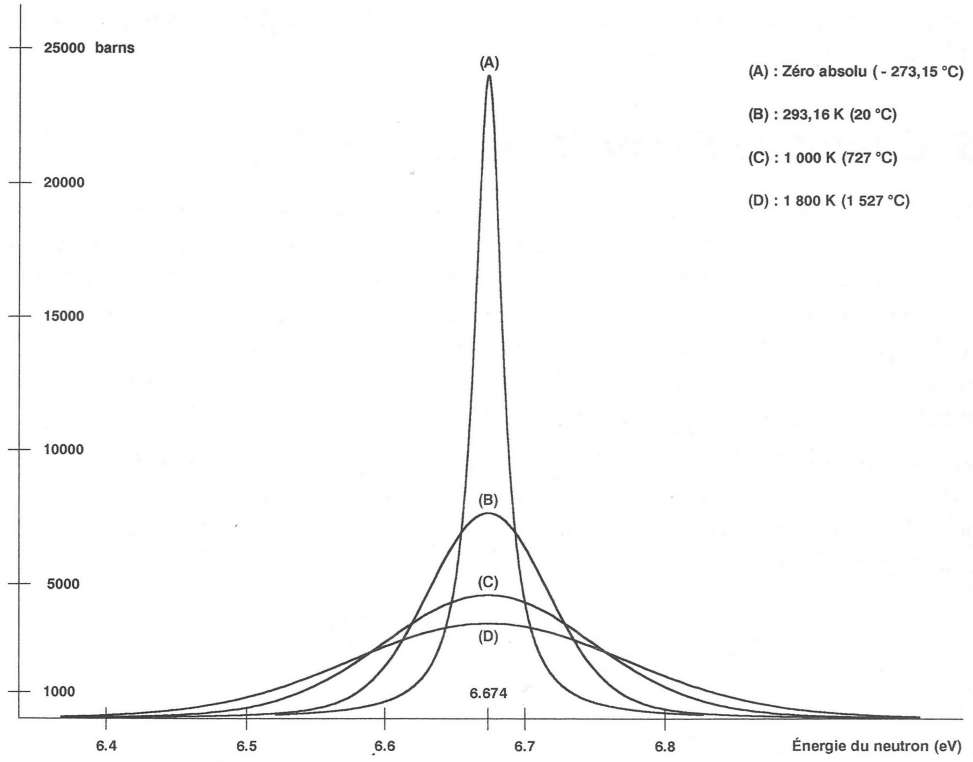

Figure 2.3. Doppler Broadening for ^{238}U [66].

2.1.4 Integro-Differential Transport Approximations

The integro-differential form of the neutron transport equation discussed in Section 2.1 is not in a form that is readily solvable for realistic scenarios. Equation 2.1 must be discretized into a form that is readily solvable on numerical computers. Some common approximations and discretizations of independent variables will be discussed in the present section.

Multigroup Approximation

The first approximation involves a discretization of the energy domain by use of discrete energy groups. The energy domain is partitioned between E_0, the highest possible energy, and E_G, the lowest possible energy; this partition is shown in Figure 2.4. The partitioning of the energy domain seeks to optimize the energy structure to reduce the error in computed reaction rates. For example, the energy mesh for use in fast spectrum reactors will have many groups in the high energy range, while thermal reactors will require many groups in the thermal and lower resonance range.

Starting from the criticality equation (Equation 2.4), the multigroup angular flux for group g can be defined as the total flux within the energy interval $[E_g, E_{g-1}]$

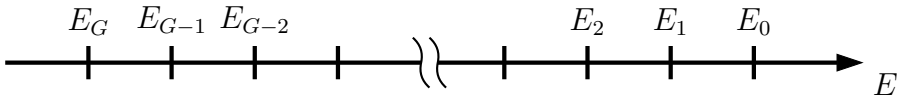

Figure 2.4. Multigroup Energy Mesh

$$\psi_g(\vec{r},\vec{\Omega}) = \int_{E_g}^{E_{g-1}} \mathrm{d}E\, \psi(\vec{r},E,\vec{\Omega}) \qquad g = 1,2,\ldots,G, \tag{2.12}$$

with the scalar flux sharing a similar definition. Multigroup cross sections are defined in a way that will preserve reaction rates within a given energy interval in the transport equation. For example, a multigroup cross section for reaction x is defined by

$$\Sigma_{x,g}(\vec{r}) = \frac{\int_{E_g}^{E_{g-1}} \mathrm{d}E\, \Sigma_x(\vec{r},E)\phi(\vec{r},E)}{\int_{E_g}^{E_{g-1}} \mathrm{d}E\, \phi(\vec{r},E)} \qquad g = 1,2,\ldots,G, \tag{2.13}$$

or a weighted average taking the weight function to be the scalar flux. The inverse velocity of Equation 2.1 can be treated as a cross section of type x. The scattering cross section is defined in a similar manner, but because of the integration over the energy domain for exiting energies, the scattering cross section includes an integration over these energies as well

$$\Sigma_{s,g'\to g}(\vec{r},\vec{\Omega}'\cdot\vec{\Omega}) = \int_{E_g}^{E_{g-1}} \mathrm{d}E\, \frac{\int_{E_{g'}}^{E_{g'-1}} \mathrm{d}E'\, \Sigma_s(\vec{r},E'\to E,\vec{\Omega}'\cdot\vec{\Omega})\phi(\vec{r},E')}{\int_{E_{g'}}^{E_{g'-1}} \mathrm{d}E'\, \phi(\vec{r},E')}$$
$$g,g' = 1,2,\ldots,G. \tag{2.14}$$

Using these definitions and integrating over the energy domain between E_g and E_{g-1}, the continuous energy integro-differential transport equation (Equation 2.4) can be written in its multigroup formulation

$$\vec{\Omega}\cdot\vec{\nabla}\psi_g(\vec{r},\vec{\Omega}) + \Sigma_{t,g}(\vec{r})\psi_g(\vec{r},\vec{\Omega}) = \sum_{g'=1}^{G}\int_{4\pi}\mathrm{d}\Omega'\,\Sigma_{s,g'\to g}(\vec{r},\vec{\Omega}'\cdot\vec{\Omega})\psi_{g'}(\vec{r},\vec{\Omega}') +$$
$$\frac{1}{k}\frac{1}{4\pi}\left[(1-\beta)\chi_g + \sum_{j=1}^{N_d}\chi_{D,g}^{j}\beta_j\right]\sum_{g'=1}^{G}\nu\Sigma_{f,g'}(\vec{r})\phi_{g'}(\vec{r}). \tag{2.15}$$

In a rigorous sense, the multigroup cross sections will depend on direction because Equations 2.13 & 2.14 should be defined with the angular flux [64]. There has been work on treating anisotropy for multigroup cross sections. This work showed that

using the angular flux to produce anisotropic multigroup cross sections is better at recovering the local reconstructed flux distribution, where using a scalar flux experienced convergence difficulties [67–69]. The inclusion of these anisotropic cross sections could be implemented through a modification of the anisotropic scattering cross section, but for the problems studied in this work the gain is expected to be small. For this work, it is assumed that the anisotropic term from using an angular flux in the multigroup cross section definition is small, and the scalar flux can be used to define multigroup cross sections. This is a common practice in LWR analysis to retain the independence of cross sections on incident angle [54].

The multigroup transport equation (Equation 2.15) represents a system of G coupled equations, coupled through the scattering and fission terms. A way to solve for the multigroup flux is to repeatedly invert the left hand side of Equation 2.15 for each group g while updating the right hand side with the new value of ψ_g. This process is known as *source iteration*, and is used in current deterministic transport methods. For these methods, the scattering source is split into three contributions

$$\sum_{g'=1}^{G} S_{g'\to g}(\vec{r},\vec{\Omega}) = \underbrace{\sum_{g'=1}^{g-1} S_{g'\to g}(\vec{r},\vec{\Omega})}_{\text{known source}} + \underbrace{S_{g\to g}(\vec{r},\vec{\Omega})}_{\text{current group}} + \underbrace{\sum_{g'=g+1}^{G} S_{g'\to g}(\vec{r},\vec{\Omega})}_{\text{upscattering}} \tag{2.16}$$

$$S_{g'\to g}(\vec{r},\vec{\Omega}) = \int_{4\pi} \mathrm{d}\Omega'\, \Sigma_{s,g'\to g}(\vec{r},\vec{\Omega}'\cdot\vec{\Omega})\psi_{g'}(\vec{r},\vec{\Omega}'). \tag{2.17}$$

The contribution labeled "known source" is known from previous inversions of the left hand side for groups with energies higher than the current group. The contribution labeled "current group" contains the current group solution which can be combined with the total interaction cross section during the inversion. The last term labeled "upscattering" is responsible for scattering from groups of lower energy to higher energy. If there is no upscattering, this term is zero, otherwise the upscattering source needs to be resolved simultaneously for the upscattering group range or through an iterative process within each iteration over the fission source.

The iterations through the energy domain require a large computational effort and involve many transport sweeps through the spatial geometry. Acceleration methods have been studied which reduce the number of iterations required to converge the scattering source; two of these methods are thermal group rebalancing, and multigrid in energy.

Rebalancing is a method, where during thermal iterations the resultant flux is normalized to ensure neutron conservation [70]. The process involves finding scaling factors for the groupwise flux which force neutron conservation for a given thermal iteration. The balance equation is obtained by integrating the multigroup equation (Equation 2.15) over volume

$$\left[(J_g^+ - J_g^-) + \langle \Sigma_{t,g}\psi_g \rangle\right] f_g = \sum_{g' \in \text{thermal}} \langle \Sigma_{s,g'\to g}\psi_{g'} \rangle f_{g'} + \langle Q_g \rangle \quad g \in \text{thermal}$$
$$\langle \Sigma_{x,g}\psi_g \rangle = \sum_r \Sigma_{x,g,r}\psi_{g,r}V_r, \tag{2.18}$$

where $J_g^{\pm}$ are the partial currents through the surface, V_r is the volume of the region r, and $\langle Q_g \rangle$ is a source from fission and energy groups where no upscattering is present. The factors f_g are the rebalance factors which ensure neutron conservation. Equation 2.18 forms a system of equations the size of the number of thermal groups and can be inverted to find the rebalance factors after each pass through the thermal groups. As the solution converges, the rebalance factors should approach unity [71].

A novel multigrid in energy acceleration technique was applied to the Krylov solvers in the Denovo code [72]. Multigrid methods work by successively projecting an error vector of the solution to coarser grids. At the coarsest level, the solution is computed quickly because of the small number of discretized points; the solution is then successively prolongated to the original fine grid. Multigrid methods use a stationary iterative solver which is effective at reducing the error in high frequency modes but is ineffective at reducing the error in low frequency modes; this ineffectiveness at reducing the error in low frequency modes causes the convergence of stationary iterative solvers to drastically slow after several iterations. Projecting errors to a coarser mesh causes low frequency modes to have a high frequency. On this coarse mesh, the stationary iterative solver is again effective at reducing the error in the now high frequency modes. This process is repeated through several levels, then the error is prolongated back to the finest mesh; this process is referred to as a V-cycle [73]. Multigrid methods have been shown to be of $\mathcal{O}(N)$ computational complexity, which is optimal [74]. Their optimal complexity makes multigrid methods ideal preconditioners. Additionally when used as a preconditioner for Krylov subspace methods, multigrid methods have been shown to keep the number of Krylov iterations constant while the computational problem domain is refined.

Angular Discretization

The discretization of the angular variable is conducted in two principal ways: P_N or S_N. The P_N method involves constructing the angular flux as an expansion of spherical harmonics in the angular variable. Truncating this expansion yields a finite set of coupled equations for which the expansion coefficients can be solved. Whereas the S_N, or discrete ordinates, method chooses a set of quadrature directions to solve the transport equation along. The integrals over direction are then approximated with quadrature sums over the chosen directions [51].

The P_N method is used in industrial applications, but may require significant storage for highly heterogeneous problems [75]. The numerical system which

results from the P_N approximation produces $(N+1)^2$ coupled equations for an anisotropy order of N. Hence the numerical system size will grow as N^2 for each order added to the P_N method.

One of the largest problems with the S_N method is ray effects, but these are more prominent when concentrated sources are present, like in shielding calculations [76, 77]. In reactor analysis, where the neutron sources are distributed, ray effects are not significant. Another disadvantage of the S_N method is in the quadrature used to discretize the angular domain. For a level-symmetric quadrature set, the order is limited due to the apparition of negative quadrature weights. Increasing to higher orders requires using a different quadrature set. However, the S_N method has many redeeming qualities over the P_N method. First, the discrete directions chosen in the S_N method can be swept independently of the others, lending well to parallelization. Second, as the method order increases, the system size will grow linearly compared to quadratically for the P_N method. These benefits make the S_N method the most widely used method in the transport community and the method used in this work. The multigroup transport equation, discretized by the S_N method, is

$$\vec{\Omega}_d \cdot \vec{\nabla}\psi_{g,d}(\vec{r}) + \Sigma_{t,g}(\vec{r})\psi_{g,d}(\vec{r}) = S_{\text{scatt},g,d}(\vec{r}) + \frac{1}{k}\frac{1}{4\pi}\left[(1-\beta)\chi_g + \sum_{j=1}^{N_d}\chi_{D,g}^{j}\beta_j\right]\sum_{g'=1}^{G}\nu\Sigma_{f,g'}(\vec{r})\phi_{g'}(\vec{r}), \quad (2.19)$$

where S_{scatt} is the scattering source. The scattering source is formulated using spherical harmonics in the angular domain. The assumption that the medium is invariant under rotation allows for an expansion of the scattering cross section over Legendre polynomials

$$\Sigma_{s,g'\to g}(\vec{r}, \vec{\Omega}' \cdot \vec{\Omega}) \approx \sum_{l=0}^{L}\left(\frac{2l+1}{4\pi}\right)\sigma_{s,l}^{g'\to g}(\vec{r})P_l(\vec{\Omega}' \cdot \vec{\Omega}) \quad (2.20)$$

$$\sigma_{s,l}^{g'\to g}(\vec{r}) = 2\pi\int_{-1}^{1}\mathrm{d}\mu_0\,\Sigma_{s,g'\to g}(\vec{r},\mu_0)P_l(\mu_0), \quad (2.21)$$

where P_l are Legendre polynomials, and $\mu_0 = \vec{\Omega}' \cdot \vec{\Omega}$. Using the addition theorem for spherical harmonics [51], the Legendre polynomials may be written as

$$P_l(\vec{\Omega}' \cdot \vec{\Omega}) = \left(\frac{4\pi}{2l+1}\right)\sum_{m=-l}^{l}Y_{lm}^{*}(\vec{\Omega}')Y_{lm}(\vec{\Omega}) \quad (2.22)$$

$$Y_{lm}(\vec{\Omega}) = Y_{lm}(\theta,\eta) = \sqrt{\left(\frac{2l+1}{4\pi}\right)\frac{(l-|m|)!}{(l+|m|)!}}P_{lm}(\cos\theta)e^{im\eta}, \quad (2.23)$$

where the associated Legendre functions (P_{lm}) are defined in terms of the m-th derivative of the Legendre polynomial P_l. Using the Legendre expansion for the scattering cross section, the scattering source becomes

$$S_{\text{scatt},g,d}(\vec{r}) = \sum_{g'=1}^{G} \int_{4\pi} \mathrm{d}\vec{\Omega}' \sum_{l=0}^{L} \left(\frac{2l+1}{4\pi} \right) \sigma_{s,l}^{g' \to g}(\vec{r}) P_l(\vec{\Omega}' \cdot \vec{\Omega}_d) \psi_g(\vec{r}, \vec{\Omega}'). \tag{2.24}$$

The angular flux is also expanded in terms of spherical harmonics as

$$\psi_g(\vec{r}, \vec{\Omega}) \approx \sum_{l=0}^{L} \sum_{m=-l}^{l} Y_{lm}(\vec{\Omega}) \phi_{lm}^{g}(\vec{r}) \tag{2.25}$$

$$\phi_{lm}^{g}(\vec{r}) = \int_{4\pi} \mathrm{d}\vec{\Omega}\ Y_{lm}^{*}(\vec{\Omega}) \psi_g(\vec{r}, \vec{\Omega}) \approx \sum_{d} w_d Y_{lm}^{*}(\vec{\Omega}_d) \psi_{g,d}(\vec{r}), \tag{2.26}$$

where the expansion coefficients are used to evaluate the angular dependence of the flux in calculations. Through this definition, the scalar flux is equivalent to the first flux moment $\phi_{00}^{g}(\vec{r})$. The formulation in Equation 2.24 allows an arbitrary level of anisotropy to be contained in the anisotropic scattering cross sections, however it has been shown that using a P_2 scattering anisotropy approximation is sufficient for LWR analysis. A higher anisotropy order of P_3 can be used as a reference and is comparable to results obtained from Monte Carlo calculations [78].

Ultimately, the spatially continuous transport equation for a single energy group can be written as

$$\vec{\Omega}_d \cdot \vec{\nabla} \psi_{g,d}^{i}(\vec{r}) + \Sigma_{t,g}(\vec{r}) \psi_{g,d}^{i} = \sum_{l=0}^{L} \sigma_{s,l}^{g \to g}(\vec{r}) \sum_{m=-l}^{l} Y_{lm}(\vec{\Omega}_d) \phi_{lm}^{g,i-1}(\vec{r}) + Q_{g,d}(\vec{r}), \tag{2.27}$$

where the within group scattering term is evaluated using flux moments $\phi_{lm}^{g,i-1}(\vec{r})$ from the previous inner iteration. Equation 2.27 defines an iterative scheme to resolve the self scattering term by repeatedly inverting the streaming and total interaction operators, a process which will be discussed in the next section.

Spatial Discretization

The spatially continuous, one group $\mathrm{S_N}$ transport equation for a given iteration over the self scattering source can be formulated as

$$\vec{\Omega}_d \cdot \vec{\nabla} \psi_d(\vec{r}) + \Sigma_t(\vec{r}) \psi_d(\vec{r}) = Q_d(\vec{r}), \tag{2.28}$$

where Q combines the contribution from the scattering and fission sources. The spatial discretization of Equation 2.28 begins with a partition of the spatial domain with non-overlapping cells. Each cell is assumed to have a spatially uniform material composition.

A balance equation can be produced by integrating Equation 2.28 over each cell of the partitioned domain. The resulting balance equation in Cartesian coordinates, after applying the divergence theorem, is

$$\frac{\psi_x^+ - \psi_x^-}{\Delta x}\Omega_x + \frac{\psi_y^+ - \psi_y^-}{\Delta y}\Omega_y + \frac{\psi_z^+ - \psi_z^-}{\Delta z}\Omega_z + \Sigma_t\bar{\psi} = \bar{Q}, \tag{2.29}$$

where the direction dependence and cell index have been suppressed for clarity. The $(\psi_u^{\pm},\ u = x, y, z)$ are angular fluxes averaged on cell boundaries for the outgoing $(+)$ and incoming $(-)$ directions. The total interaction is taken to be constant within a spatial cell. In solving the balance equation (Equation 2.29), the incoming flux (ψ_u^-) and the volume-averaged source $(\bar{Q})$ are known; the source and incoming flux depend on the volume-averaged flux $(\bar{\psi})$, but this dependence is resolved through iterations on the balance equation. The outgoing and volume-averaged fluxes are sought by solving Equation 2.29. A standard way to evaluate the spatial dependence of the angular flux is to start at the boundary and, given a direction, traverse the geometry in that direction. This method is known as a *transport sweep*. When all sweeps are completed, the angular flux can be used to update the source $\bar{Q}$ and incoming flux.

The balance equation contains too many unknowns, and closure relations must be used to relate the volume-averaged flux to boundary fluxes. A straight forward closure relation states that the flux varies linearly across the cell; this closure relation is named the *Diamond Difference* method. While this closure relation works well in 1-D problems, it suffers from stability issues in multidimensional cases [79].

An improvement over using closure relations and a balance equation is through the use of the finite element method. The finite element method consists of multiplying Equation 2.28 by a trial function and integrating over all cells of the partitioned domain. This operation produces the weak form of the equation, which only satisfies projections of Equation 2.28 onto a function space. The solution is then approximated as a projection onto a basis of functions spanning the finite dimensional approximation space. The solution approximation can then be inserted into the weak form, which produces a sparse matrix system. It is desirable to have trial and basis functions which have only local support and cause spatial points to only be coupled locally. The local support of these functions is what results in a sparse matrix system. In Galerkin finite element methods, the trial and basis functions span the same space [80]. Continuous finite element schemes force the continuity of the solution at cell interfaces. While a continuous solution may be appealing, the forcing of continuity at interfaces reduces the degrees of freedom available to specify the solution. Discontinuous methods however do not force the solution to be continuous at cell interfaces, leaving more degrees of freedom to specify the solution. Some discontinuous methods have been shown to be unstable in multidimensional, optically thick

problems unless certain geometrical and function space criteria are met [81].

A more stable and accurate method for spatial discretization accounts for particle transport within cells. Equation 2.28 can be analytically integrated along the path of neutron travel $\vec{\Omega}_d$, or *characteristic*, to obtain

$$\psi_{g,d}(\vec{r}) = \psi_{g,d}(\vec{r}')\mathcal{F}(\vec{r},\vec{r}';\vec{\Omega}_d) + \int_0^{|\vec{r}-\vec{r}'|} \mathrm{d}s\; Q_{g,d}(\vec{r}-s\vec{\Omega}_d)\mathcal{F}(\vec{r},\vec{r}-s\vec{\Omega}_d;\vec{\Omega}_d) \quad (2.30)$$

$$\mathcal{F}(\vec{r},\vec{r}';\vec{\Omega}_d) = e^{-\int_0^{|\vec{r}-\vec{r}'|}\mathrm{d}s\;\Sigma_{t,g}(\vec{r}-s\vec{\Omega}_d)}, \quad (2.31)$$

where the flux at $\vec{r}'$ and the source distribution are presumed to be known. Equation 2.30 makes no assumption about the partitioned domain with constant cross sections within cells, which allows the total cross section in Equation 2.31 to vary piecewise continuously. The integrals in Equation 2.30 may be numerically integrated in two principal ways, leading to two versions of the same numerical method: the *Method of Short/Long Characteristics*. In the Method of Short Characteristics, Equation 2.30 is evaluated within each spatial cell given some expansion of the volumetric source and incoming boundary flux. Given these expansions, and assuming some expansion for the spatially dependent flux and outgoing boundary flux, the integrals may be analytically evaluated [40, 82]. Alternatively for the Method of Long Characteristics, given a direction and a spacing between trajectories, the flux for the given direction is evaluated along trajectories throughout the domain. The spatially dependent flux within cells may then be computed by using the flux along trajectories within a cell. Additionally, the currents on cell faces may be calculated given the flux on cell boundaries by numerical integration [83, 84]. Collectively these versions can be referred to as the Method of Characteristics (MoC). Because of the explicit treatment of the streaming term in the transport equation, the method of characteristics performs especially well in deep penetration problems where scattering is less dominant [85]. Also because of the exponential attenuation provided within spatial cells, errors are damped when sweeping through the domain; this makes for a robust transport sweep.

A straight forward parallelization of transport sweeps will perform sweeps in each direction independently and collect all fluxes when updating sources. A more complex effort at parallelization of transport sweeps can be accomplished by also splitting the spatial domain into subdomains. The transport sweeps can then be performed in a traveling wave algorithm. Two such parallel algorithms are the Koch-Baker-Alcouffe (KBA) algorithm [86] and the Parallel-Block-Jacobi (PBJ) method [87]. The Denovo code [40] uses the KBA method and the approximations discussed earlier in this section. This code has been applied to large transport problems and exhibits high parallel performance on a large number of parallel cores $\mathcal{O}(10^5)$ [88].

Time Discretization

A straight forward way to discretize the time variable is to approximate the time derivative as a finite difference. Taking an implicit form of this discretization applied to Equation 2.1, with the previously discussed approximations, produces

$$\frac{1}{v_g}\frac{\psi_{g,d}^{n+1}(\vec{r}) - \psi_{g,d}^{n}(\vec{r})}{\Delta t} + \vec{\Omega}_d \cdot \vec{\nabla}\psi_{g,d}^{n+1}(\vec{r}) + \Sigma_{t,g}^{n+1}(\vec{r})\psi_{g,d}^{n+1}(\vec{r}) = Q_{g,d}^{n+1}(\vec{r}), \tag{2.32}$$

where the solution at the current time step ($\psi_{g,d}^{n}(\vec{r})$) is known either from an initial condition or the previous evaluation of the angular flux. All other time dependent parameters are evaluated at the next time step. This produces a method that is unconditionally stable in terms of the time step size. Equation 2.32 can be rearranged by combining the solution at the previous time step with the fixed source and combining the $\frac{1}{\Delta t v_g}$ term with the total cross section [89].

Many different methods exist to increase the convergence order of temporal discretization; one such method class is Runge-Kutta methods [90]. Runge-Kutta methods take ordinary differential equations of the form

$$\frac{\partial u}{\partial t} = F(u,t), \tag{2.33}$$

where $F(u,t)$ is some function which describes the rate of change of the solution. For neutron transport, $F(u,t)$ would be formulated by moving the streaming and total reaction terms to the right hand side and multiplying by v_g. Once in the form of Equation 2.33, the Y-formulation of a general s-stage Runge-Kutta method is defined as

$$\begin{aligned} Y_i &= u^n + \Delta t \sum_{j=1}^{s} a_{ij} F(Y_j, t_n + c_j \Delta t) \quad i = 1, 2, \ldots, s \\ u^{n+1} &= u^n + \Delta t \sum_{i=1}^{s} b_i F(Y_i, t_n + c_i \Delta t), \end{aligned} \tag{2.34}$$

where the $\{a, b, c\}$ are values dependent on the specific Runge-Kutta method used. The coefficients $\{a, b, c\}$ appearing in Equation 2.34 are chosen to optimize the Runge-Kutta method. The coefficients are subject to order conditions based on the structure of the method and the convergence order sought. The order conditions will, in general, not completely specify the coefficients of the system, and other constraints must be imposed to determine these coefficients. Additional constraints could be based on ensuring linear or absolute stability, or on the minimization of higher order terms in a Taylor expansion [91]. These values can be stored in a Butcher Tableau with the general form

c	A
	b^T

where b and c are vectors of size s, and A is a matrix of size $s \times s$. For example, the time discretization in Equation 2.32, discussed previously, would have the following Butcher Tableau.

1.0	1.0
	1.0

There has been an effort to parallelize the time domain through an iterative process [92]. The effort was mildly successful because of the difficulty to parallelize a physically serial process.

2.1.5 Solution Method

The approximations and discretizations discussed previously can be implemented and brought together in a deterministic transport code. Industrial deterministic transport codes have a nested algorithm, which consists of several levels of iteration to produce a converged solution. The innermost level is one of a *transport sweep* that, given a source distribution, produces the corresponding angular flux by solving Equation 2.28, after an appropriate spatial discretization, throughout the computation domain and for every direction in the quadrature set.

The level above transport sweeps and inner iterations involves iterations over the energy domain and scattering source. At this level, the angular source for each energy group is computed using the previous iteration's solution. Iterations over the energy domain only occur if there is upscattering present, or $\Sigma_{s,g' \to g} \neq 0$ for $g' > g$. Otherwise the multigroup flux can be computed with a single sweep through the energy domain.

The last and exterior level is either an iteration on the eigenvalue/eigenvector of the nuclear system, or a loop over the discretized time domain. The dominant eigenvalue/eigenvector pair can be computed through a power iteration algorithm. This embedded solution scheme is depicted in Figure 2.5.

The methods to solve the neutron transport equation, developed over the past and well into the current century, have produced solution processes optimized for the solution of the linear transport equation. In addition to the numerical approximations discussed in this section, there are many more details to the timely solution of the transport model. These details include accelerations, material data processing, and cross section homogenization, among others.

2.2 Heat Transfer

The transfer of heat in a nuclear reactor is important in determining the spatial dependent temperatures in the core. Such temperatures are used to determine whether the materials within the reactor core will be below certain limits

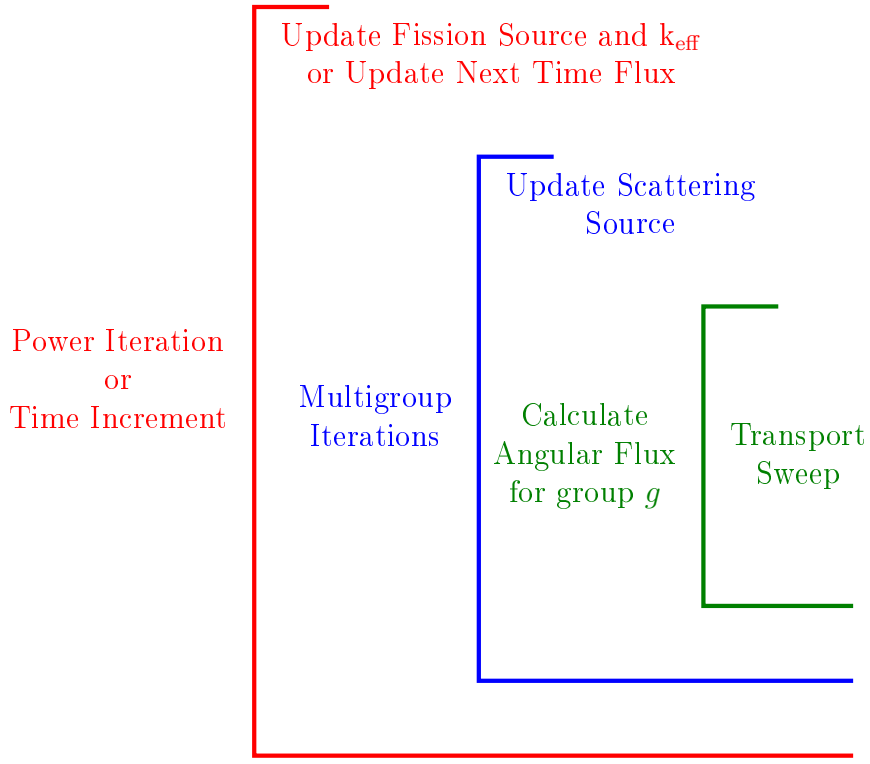

Figure 2.5. Embedded Solution Algorithm for S_N Transport Solvers

which guarantee the structural integrity of the fuel. Given the spatial temperature distribution, the location of the maximum cladding temperature, which is the likely failure location in LWRs during reactivity initiated accidents, can be found [93, 94]. Additionally the spatial temperatures can be used to compute effective cross sections, and temperature coefficients for the fuel and moderator, among others.

This section will discuss the two heat transfer models used for simulations in this work. The first model is a simple lumped capacitance model [95]. The second model is a more complex two phase subchannel model that accounts for boiling in the coolant and exchanges between neighboring coolant channels [96].

2.2.1 Lumped Capacitance Model

A lumped capacitance model is used here to describe the heat transfer in an infinite homogeneous medium. A lumped capacitance model simply assumes that the temperature gradient within a region is negligible [95]; thus there is no conduction within the material. Consequently a full energy balance is performed on the system which yields

$$\frac{\partial T}{\partial t} = \kappa P(t) - \dot{Q}(t), \tag{2.35}$$

where κ is a heat generation constant, P is the time dependent power, and $\dot{Q}$ is some time dependent heat sink. The heat sink is added to allow for an equilibrium

condition when the power is non-zero. In the cases discussed in Chapter 4, the heat sink will be equal to the heat generation constant times the initial power. This condition produces a temperature which is initially stable until the power changes. For this setup, the value of the heat generation constant will significantly affect the behavior of the time dependent temperature. A small value of κ will cause a small change in temperature for a large deviation in power. Likewise a large value of κ will result in a large change in temperature for a small deviation in power. In the context of large positive reactivity insertions, for a small value of κ, the power will increase largely before the temperature has risen high enough to counteract the reactivity insertion. Conversely for a large value of κ, a small increase in power will be enough to increase the temperature to a point which counteracts the reactivity insertion.

2.2.2 Subchannel Model

Computational Fluid Dynamics (CFD) is the study of physical models which describe the details of fluid flow through regions of space. Often these regions include complex geometries and cause intricate flow patterns. One such type of complex region is that of a fuel assembly from a nuclear reactor. In addition to all of the intricate paths through the fuel assembly from the array of parallel fuel rods, fuel assemblies contain spacer grids over the length of the fuel assembly. These spacer grids serve two purposes: first is to provide structural support to fuel rods, and second is to introduce turbulence to the fluid flowing through the assembly which consequently increases the efficacy of the coolant to remove heat from the fuel assembly. Resolving the details of these types of flow patterns can be achieved at several levels. In addition to complex flow patterns induced by structural material, the presence of boiling will alter the way heat is removed from the system. The thermal hydraulics of forced convection systems will change for different flow regimes. Within a reactor core, there are four principle flow regimes as pictured in Figure 2.6.

Bubbly flow is a flow regime characterized by free bubbles of vapor dispersed in the bulk flow; the bubbles can be of various sizes. With an increasing heat flux, the Slug flow regime is reached. This flow regime is characterized by large irregular bubbles which combine with smaller bubbles. With a still increasing heat flux, the Churn flow regime is reached. This flow regime is more chaotic than the Slug flow regime. The annular flow regime is reached when the large irregular bubbles of the Churn flow combine to form a central column of vapor. If the vapor flow rate is large enough, the vapor can entrain liquid droplets. Each of these flow regimes requires special attention to the dominant physics appearing in thermal hydraulics models.

The physics of two-phase thermal hydraulics happens over many length scales. The physics range from the level of 10s of microns to the size of pipes in the cooling circuit. This vast range of length scales warrants a multiscale approach to modeling thermal hydraulic behavior. There are four large categories which address these length scales: Direct Numerical Simulation (DNS), Large Eddy Simulation (LES), Reynolds Averaged Navier Stokes (RANS), and Porous Medium [98]. DNS

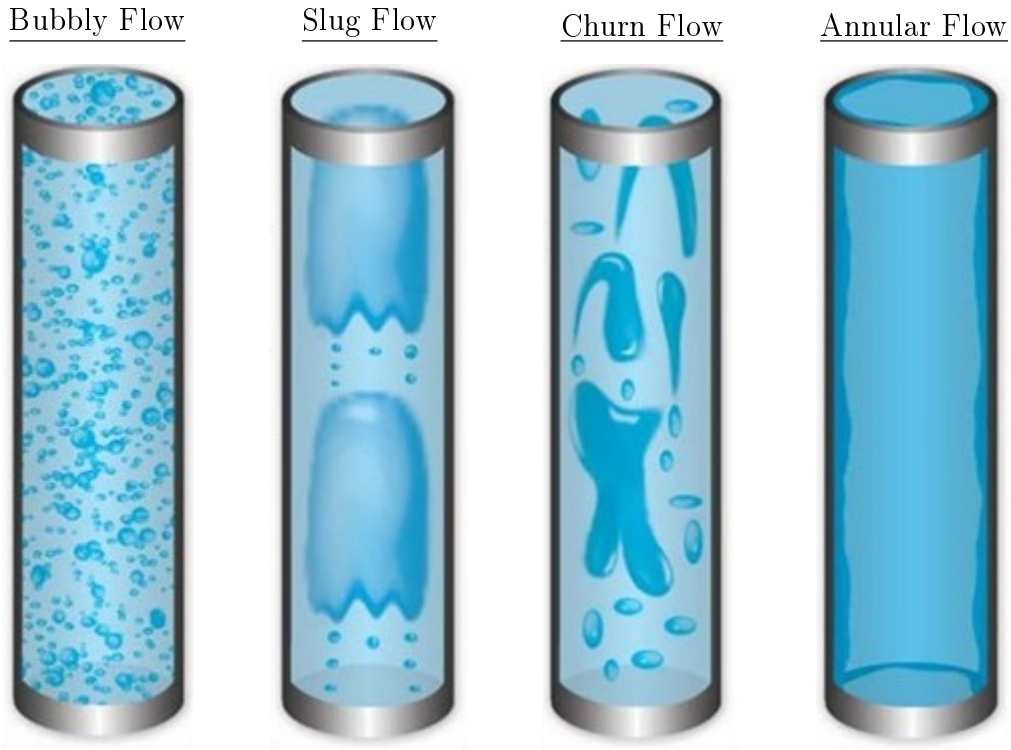

Figure 2.6. Flow Regimes in Vertical Channel [97]

is focused on the level of several single bubbles, or in single-phase modeling very small turbulent eddies. In two-phase conditions, extra models are required to simulate the formation of bubble interfaces. Currently this type of simulation is too expensive to be applied to a macroscale simulation. DNS is currently used to derive correlations which are used in other simulation methods. The next length scale up can be treated by LES, where small eddies are filtered out while large eddies are simulated. LES can be used to model some dispersion flows and flows with free surfaces. Like DNS, LESs are still expensive and are not generally applied to macroscale problems. Again LES, like DNS, is used to produce correlations used in less expensive simulation methods. RANS simulations filter out even larger eddies than LES, and average over interfaces between phases. This large averaging removes the ability for RANS to distinguish intermittency of bubble formation in the flows. RANS can be applied to length scales which are of engineering scale (flow between assembly). This is the type of model used to simulate turbulent flows by many computer codes [99–101]. The largest length scale used for modeling thermal hydraulic phenomena is of the size of system components. At this level, a porous medium model is used with several spatial averages yielding appropriately dimensioned models. This type of model is used to model the behavior of system components such as turbines, heat exchangers, and main steam lines [102]. The thermal hydraulic model discussed in this section is a coupled 1-D porous medium model. Each subchannel is averaged over the cross sectional area and coupled to neighboring subchannels through interfaces.

The following discusses the area and time averaged mass, momentum, and

energy balances. These three balance equations and experimental correlations are used to produce the two-phase thermal hydraulic model used in this work. In models designed for use in BWR cores, generally two species of coolant are taken because of the large amount of vapor present in the core. Additional species can be defined to give more fidelity to the physical models. For example, balance relations can be written for the continuous liquid, dispersed gas, continuous gas, and dispersed liquid phases. The latter two phases are only prevalent when the flow is beyond the Bubbly flow regime.

The mass balance for species x is

$$\frac{\partial}{\partial t}\int_V \rho_x \mathrm{d}V + \int_{\partial V} \rho_x \vec{V}_x \cdot \mathrm{d}\vec{A} = -\sum_{x'} \Gamma_{x\to x'}, \tag{2.36}$$

where ρ_x is the density of species x, V is the control volume, and $\vec{V}_x$ is the velocity for species x. $\Gamma_{x\to x'}$ is the net rate at which species x transforms into species x' in control volume V. This transformation rate depends on the flow conditions and on the rate at which heat is added to the control volume. For the case of treating two species (liquid water and steam) the relation $\Gamma_{x\to x'} = -\Gamma_{x'\to x}$ comes from mass conservation. Equation 2.36 simply says that the rate of change of mass is equal to the net mass flux coming into the control volume; the entrance can be from a physical boundary or the boundary between species [103].

The gamma function appearing in Equation 2.36 can be approximated from a thermodynamic relation involving the heat addition rate and the latent heat of vaporization of water. This relation gives the rate at which liquid water turns to steam at saturation conditions.

The momentum balance equation is given by

$$\frac{\partial}{\partial t}\int_V \rho_x \vec{V}_x \mathrm{d}V + \int_{\partial V} \vec{V}_x \rho_x \vec{V}_x \cdot \mathrm{d}\vec{A} = \vec{F}_S + \vec{F}_B, \tag{2.37}$$

where $\vec{F}_S$ and $\vec{F}_B$ are the resultant surface and body forces on the control volume. Equation 2.37 is a vector equation and would have three components in a 3-D Cartesian geometry. In an LWR, friction between the fluid and structural material, as well as the forces due to pressure on the surface, manifest as surface forces while gravity is the only body force.

Equation 2.37 is written for a species x, but in the treatment of thermal hydraulics in this work, we will simplify the momentum equation to be that of the mixture (liquid water and steam). Hence the density ρ_x becomes $\rho_m = \alpha\rho_v + (1-\alpha)\rho_l$, and the species velocity becomes the mixture velocity [6]. The void fraction α is defined as the volume fraction of vapor in a fixed volume. However unequal velocities of the liquid water and steam can be introduced through a drift flux model where the velocity of the vapor is given by the sum of the mixture velocity and a drift velocity. The drift velocity can be determined by correlations depending on the characteristics of the two-phase flow regime

$$\vec{V}_v = \vec{V}_m + \vec{V}_{vd}. \tag{2.38}$$

The surface forces can be split into contributions from the pressure and frictional forces. The pressure can be expressed as the integral over the surface of the control volume,

$$\vec{F}_s^{\text{pressure}} = -\int_{\partial V} P \mathrm{d}\vec{A}. \tag{2.39}$$

This formulation states that the pressure P is always applying a force toward the interior of the control volume. The friction force due to the interaction between the mixture and the structural material is given by

$$\vec{F}_s^{\text{friction}} = -\int_{\partial V} \vec{\tau}_w |\mathrm{d}\vec{A} \cdot \vec{n}|. \tag{2.40}$$

The factor $\vec{\tau}_w$ is given by correlations depending on the velocity, mixture density, the contact surface, and others [6]; the formulation used in this work is given in Equation 2.41. The direction of the vector quantity $\vec{\tau}_w$ is in the same direction as the velocity.

$$\vec{\tau}_w = \frac{f_{tp}}{4}\left[\frac{G_m^2}{2\rho_m^+}\right]\left(\frac{\vec{V}_m}{\|\vec{V}_m\|}\right) = \frac{f_{tp}}{4}\left[\frac{1}{2}\left(\rho_v \alpha V_v^2 + \rho_l(1-\alpha)V_l^2\right)\right]\left(\frac{\vec{V}_m}{\|\vec{V}_m\|}\right) \tag{2.41}$$

Here f_{tp} is a parameter depending on an empirical correlation of the product between a single-phase friction factor and a two-phase flow multiplier. The single-phase flow friction factor is a function of the Reynolds number; the subchannel code used in this work uses a relation from Marinelli and Pastori [104]. The two-phase flow multiplier is drawn from assumptions about the two-phase flow regime. The thermal hydraulic model from this work uses the Jones correlation [6, 105].

The energy balance equation is given by

$$\begin{gathered}\frac{\partial}{\partial t}\int_V e_x \rho_x \mathrm{d}V + \int_{\partial V} e_x \rho_x \vec{V}_x \cdot \mathrm{d}\vec{A} = \dot{Q}_x - \dot{W}_x \\ e_x = u + \frac{\vec{V}^2}{2} + g\Delta z,\end{gathered} \tag{2.42}$$

where e_x is the total energy, $\dot{Q}$ is the heat input to the system, and $\dot{W}$ is the work done by the system. The work done by the system can be broken into the work done by normal stress on the control volume, and other work ($\dot{W} = \dot{W}_n + \dot{W}_{\text{other}}$). The rate of normal work is produced by a normal stress on the surface of the control volume moving with a velocity

$$\dot{W}_n = -\int_{\partial V} \sigma_n \vec{V} \cdot \mathrm{d}\vec{A}, \tag{2.43}$$

where σ_n is the normal stress on the control surface. Rearranging the terms in Equation 2.42 gives

$$\frac{\partial}{\partial t}\int_V e_x\rho_x \mathrm{d}V + \int_{\partial V}\left(\underbrace{u_x+\sigma_n\nu_x}_{h_x}+\frac{\vec{V}_x^2}{2}+g\Delta z\right)\rho_x\vec{V}_x\cdot\mathrm{d}\vec{A} = \dot{Q}-\dot{W}_{\text{other}} \quad (2.44)$$

where $\nu = \frac{1}{\rho}$ is the specific volume, and $h_x \equiv u_x + \sigma_n\nu_x$ is defined to be the enthalpy of species x.

As with the momentum balance, species x is taken to be the mixture of liquid water and steam. This statement requires that the two species be in thermal equilibrium. A four equation model (2 mass, 1 momentum, and 1 energy balance) is often applied to nearly steady state transients. These slow transients allow the steam and liquid to remain near thermal equilibrium. For fast transients, a two fluid model would be needed to allow for thermal non-equilibrium between the two species. This description of a six equation model reduces the modeling errors of the four equation model applied to fast transients. However in this work a six equation model is not available in the thermal hydraulic code chosen for this work. Only a four equation model is available to be applied to fast transients. Consequently, the accidents simulated in Chapters 4 & 5 are all from startup conditions. Startup conditions are such that the fluid and fuel are at low temperatures, and the liquid and steam are likely to not move far from thermal equilibrium even in prompt critical transients. In the transients studied in this work, the power increases quickly which increases the fuel temperature quickly. The effect of Doppler broadening in the fuel causes the power to eventually decrease at a modest rate. All this change in fuel temperature happens before the fluid can react to the perturbation in power. This type of transient is near adiabatic and hence the four equation model presented earlier will introduce minimal model error.

Equations 2.36, 2.37, and 2.44 describe the heat exchange between the fluid and walls of the fuel, but are not suited for describing the heat transfer in the fuel. Heat transfer within the fuel is governed by conduction as in

$$\frac{1}{\rho C_p}\frac{\partial T}{\partial t} - \nabla k\nabla T = q''', \quad (2.45)$$

where ρ is the fuel density, C_p is the fuel heat capacity, k is the conductivity, and q''' is the volumetric heat generation rate. Equation 2.45 can be coupled to the fluid equations by the rate at which heat crosses the exterior surface of the fuel. The remaining boundary condition for cylindrical fuel rods can be taken as a vanishing temperature gradient at the center of the fuel rod. This means that a cylinder in r-z geometry is simulated with azimuthal symmetry.

The CFD models described at the beginning of this section are generally expensive in both computation time and storage when applied to assembly or core level calculations. Many improvements over the years focus on the parallelization of such CFD models. Simulations using RANS or porous medium models exploit parallelization through domain decomposition methods, which split the spatial

domain into subdomains that are controlled by a single processor [106]. Communication between processors happens at the boundaries of these subdomains. The thermal hydraulic model used in this work does not exploit any parallelization and thus is limited to smaller sized domains.

This section presented two heat transfer models which can be applied in either a homogeneous or heterogeneous case. The first lumped capacitance model is used in a homogeneous problem where conduction cannot occur because of the lack of a temperature gradient. The second model of a coupled set of subchannels can be applied to heterogeneous problems. The accidents treated in this work are rapid and occur during startup conditions where the fuel and coolant temperatures are low. These accidents produce near adiabatic conditions for heat transfer, and the two models discussed are expected to have similar behavior.

2.3 Feedback Mechanisms

The safe operation of nuclear power plants relies heavily on how the reactor will respond to perturbations in its operating state. For example, a higher electrical demand from the power grid will draw more energy from the steam turbine, causing the coolant which enters the reactor core to be cooler than nominal conditions. These types of small perturbations will cause the reactor system to respond; nuclear engineers strive to design stable systems which will respond slowly to perturbations in operating state.

Understanding and modeling these physical mechanisms which cause changes in reactor behavior is important for the design of safe nuclear power plants. This section discusses several mechanisms which can cause changes in reactor behavior and focuses on the accurate modeling of these mechanisms.

The most predominant feedback mechanism in uranium fueled reactors is the thermal absorption of ^{238}U. This isotope of uranium has a large resonance at 6.67 eV, which occurs just at the upper bound of the thermal range where the fission cross section for ^{235}U begins to increase with lower energies. Doppler broadening of resonances was discussed earlier in this chapter and it was shown that as the temperature increases, the probability of a neutron being absorbed by a resonance increases. The low energy resonance of ^{238}U creates a barrier neutrons need to surpass to cause a fission reaction in ^{235}U.

Since thermal neutrons do not have a high probability to cause fission in ^{238}U, this increased absorption removes neutrons that would have otherwise created a fission event; this type of feedback is negative. Negative feedback is generally what reactor designers are seeking because of its stabilizing effects; it will oppose any perturbations to the system. As an example, an increase in power causes an increase in temperature. This temperature increase causes more thermal absorption in ^{238}U, which removes neutrons from the system and the reactor can eventually reach a new equilibrium. Conversely, if an increase in temperature caused less thermal absorption in ^{238}U, there would be more fission events because more neutrons would be available to be absorbed by ^{235}U. More fission events would increase the power and fuel temperature, and the reactor could not reach a new equilibrium.

Doppler broadening is not the only form of feedback present in nuclear reactors, but it does respond very quickly to perturbations in operating state. Some of the fission products from the fission events will produce isotopes which have enormous absorption cross sections. Two such isotopes are ^{135}Xe and ^{149}Sm. Given a constant power, these isotopes will naturally build up to an equilibrium concentration over the operating time of a reactor. However perturbations in the power can lead to these concentrations being off equilibrium and can invoke oscillations in the power over medium sized time intervals. The longer time intervals over which the power changes will require more accurate thermal hydraulics models because of the possibility of the coolant species to be out of thermal equilibrium.

As mentioned in the introduction of this section, perturbations of the coolant entering the reactor core can drive changes in reactor behavior. These perturbations can be from the temperature of the coolant, which will affect the moderation power of the coolant. In LWR cores, a higher coolant temperature leads to less moderation which causes the power to decrease. Conversely a decrease in coolant temperature, like the scenario presented with an increased electrical demand, will cause more moderation and increase the power. Like Doppler broadening of resonances, this is a negative feedback mechanism which introduces stability in the reactor. In addition to the temperature of the coolant, in PWR designs a neutron absorber is dissolved in the coolant to control the reactor during operation. A perturbation of the concentration of this absorber would cause changes in the reactor behavior.

The feedback mechanisms presented thus far can be modeled with coupled neutron transport and thermal hydraulic modes. The reactor poisons presented can be modeled by introducing rate equations for the concentration of each isotope which can be produced from fission and lost from neutron absorption; additionally ^{135}Xe can be lost through radioactive decay. The accurate simulation of the behavior of nuclear reactors is essential to the design process which produces inherently safe reactors. The accurate simulation of such behavior includes resolving the nonlinear feedback present during reactor transients, both operational and accident.

Beyond operational and accident transients, severe accidents involve long term damage to the reactor core and are generally difficult to model. These accidents (Three Mile Island, Chernobyl, and Fukushima) occur rarely, and last for long times on the order of days to months. The characteristic common in severe accidents is the irreparable damage to the reactor core, usually in the form of fuel melting. When core melt occurs, physio-chemical interactions between the core material and structural material become important and must be accounted for [21]. These types of accidents result in complicated models which require special attention to produce accurate results.

This work will focus on operational and accident transients because of their more common occurrence and lower severity. These transients affect the integrity of the first level of containment, and should be thoroughly investigated. The physical models to describe such transients are readily available in the form of computer codes and can be modified to work together to produce a high fidelity multiphysics solution.

Chapter 3

Numerical Methods

The physical manifestation of coupling was discussed in the previous chapter. This chapter discusses two numerical methods available for resolving multiphysics systems: simultaneous and sequential coupling methods. Sequential coupling methods are ones in which each physics component is solved independently and coupled to other physics components through data transfers of the physics components' solutions. Simultaneous coupling methods treat the multiphysics system as a single system and obtain a solution to all physics components through nonlinear iterations. Each method has its drawbacks and strengths which will be discussed in the present chapter.

3.1 Sequential System

The most readily available method for coupling stand alone physics models is through a sequential coupling manner; which may also be referred to as *Operator Splitting*. This method involves solving each physics component separately with the other physics components' solutions as input. There are variations of this method based on which input solution is used from other physics components: either at the previous time step, or the most recent solution. This method is advantageous when there are separate physics models for each physics component that are optimized to treat the length and time scales characteristic to that physics component. There are generally several years of combined experience that manifest in a computer code to solve a given physics component; this method builds directly on that experience.

Operator Splitting is generally a noniterative process, meaning that at each time step, only a single pass through the physics models is performed. This does not converge the nonlinearities between physics components, and can be at best a first order in time method [35]. However several modifications, such as predictor-corrector steps, to the noniterative operator split technique can be made to improve the convergence of nonlinearities and stability of this explicit scheme [9, 35, 107]. This method is depicted in Figure 3.1, where the neutronics model takes the temperature from the previous time step as input. The power

produced from the neutronics method is fed into the thermal hydraulic model, which produces an updated temperature distribution. Often this lagged method will not accurately capture the nonlinearities produced from the temperature dependent cross sections at each time step. The convergence of such a method can come into question, especially if the physics components operate on significantly different time scales [108]. Additionally, because of the explicit nature of this numerical scheme, oscillations can be observed in certain cases [109, 110].

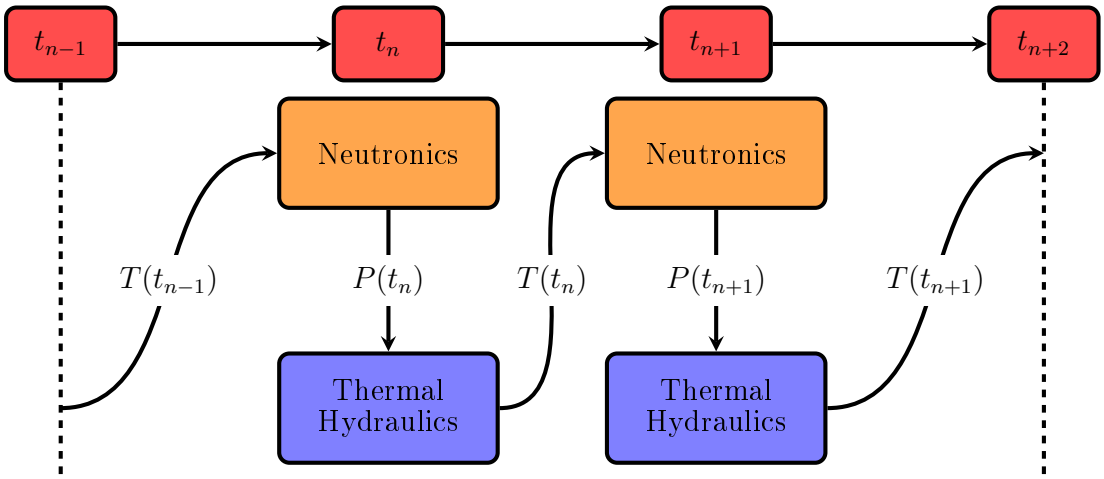

Figure 3.1. Operator Splitting Schematic with Updated Solution (Gauss-Seidel) Showing Two Coupled Physics Components: Neutronics and Thermal Hydraulics

The operator splitting method can be iterated upon until the nonlinearities between physics components are fully converged. This process is depicted in Figure 3.2 where at each time step, the most recent solution to the neutronics model is input to the thermal hydraulics model. After which the most recent solution for the thermal hydraulics model is input to the neutronics model. The process is repeated until a sufficient level of convergence between the two models is achieved. While this process does converge the nonlinearities between each physics component, the rate of convergence is linear and can become computationally expensive. It is generally necessary to accelerate this type of method to have an acceptable computation time [107]. The iterative process between physics components produces an unconditionally stable numerical method, which removes the oscillations observed from the lagged version of operator splitting [109, 110].

Sequential coupling methods are common methods used to couple existing codes because of the low overhead involved in implementing these methods [89, 111, 112]. The real challenge presented from these methods is in how to transfer solutions to other physics component models accurately. The solution transfer can be accomplished through some type of interpolation or projection onto another physics component's mesh [113].

While the Operator Splitting method may have its drawbacks in obtaining a multiphysics solution, it is useful as a preconditioner to simultaneous methods. The use of *Block* or *Physics Based* preconditioners have been shown to be essential

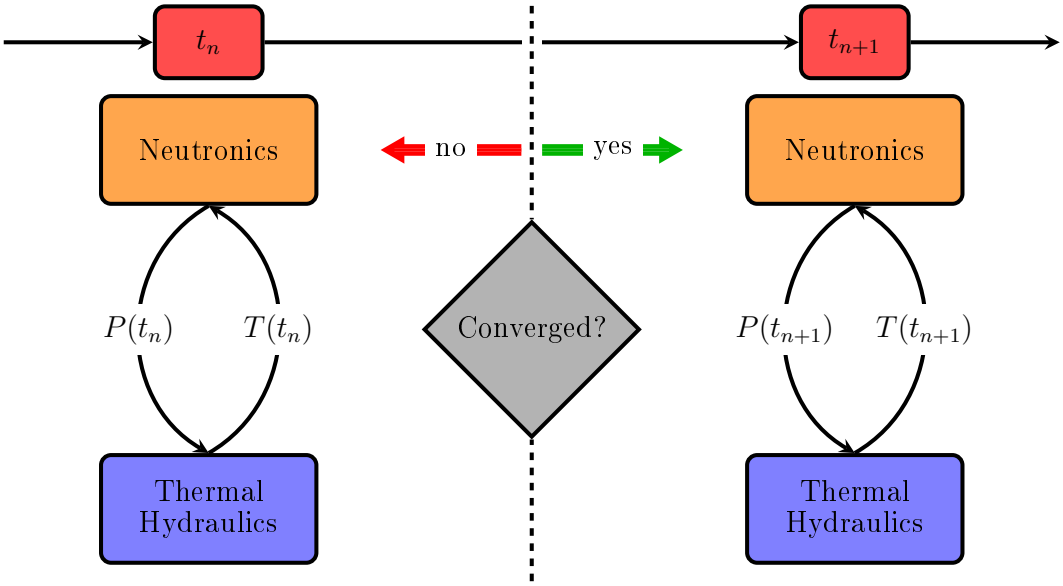

Figure 3.2. Operator Splitting Schematic with Iteration Between Two Coupled Physics Components

in solving simultaneous multiphysics problems [37, 114]. Preconditioners will be discussed in Section 3.2.2.

3.2 Simultaneous System

A large body of recent work has been devoted to studying the numerics of a simultaneous system approach [8, 9, 115, 116]. The simultaneous system is constructed by forming a nonlinear residual for each physics component and placing each residual component in a global residual for the coupled system. This global residual has the form

$$\vec{F}(\vec{U}) = \begin{bmatrix} f_1(u_1, u_2, \ldots, u_n) \\ f_2(u_1, u_2, \ldots, u_n) \\ \vdots \\ f_n(u_1, u_2, \ldots, u_n) \end{bmatrix}, \tag{3.1}$$

where each f_i is the residual and u_i is the solution from the i-th physics component in the system. The nonlinear coupled physics problem can then be stated as

$$\text{given } \vec{F}(\vec{U}) : \mathbb{R}^n \to \mathbb{R}^n, \text{ find } \vec{U}^* \in \mathbb{R}^n \text{ such that } \vec{F}(\vec{U}^*) = 0, \tag{3.2}$$

which can be described as a zero search method of which there are many algorithms to choose from: fixed point iteration, Picard, Broyden, Newton, among others.

In this work Newton's method is used exclusively to find the solution of Equation 3.2, which consists of a linearization of the nonlinear residual and an iterative process to find a solution which makes the linearization of the residual zero. Newton's method is derived from the multivariate Taylor expansion of the residual $\vec{F}$

$$\vec{F}(\vec{U}+\delta\vec{U}) = \vec{F}(\vec{U}) + \mathbf{J}(\vec{U})\delta\vec{U} + \frac{1}{2}\underline{\underline{\underline{\mathbf{T}}}}(\vec{U})\delta\vec{U}\delta\vec{U} + \ldots, \tag{3.3}$$

where $\underline{\underline{\underline{\mathbf{T}}}}$ is a rank-3 tensor of second derivative terms, and $\mathbf{J}$ is a matrix of first derivative terms, called the Jacobian matrix, and defined as

$$\mathbf{J} = \begin{bmatrix} \frac{\partial f_1}{\partial u_1} & \frac{\partial f_1}{\partial u_2} & \cdots & \frac{\partial f_1}{\partial u_n} \\ \frac{\partial f_2}{\partial u_1} & \frac{\partial f_2}{\partial u_2} & \cdots & \frac{\partial f_2}{\partial u_n} \\ \vdots & \vdots & \ddots & \vdots \\ \frac{\partial f_n}{\partial u_1} & \frac{\partial f_n}{\partial u_2} & \cdots & \frac{\partial f_n}{\partial u_n} \end{bmatrix}. \tag{3.4}$$

Newton's method is constructed from the truncation of Equation 3.3 after the linear term and solving for the update $\delta\vec{U}$ that will make the residual approximation zero. Newton's method consists of computing the Jacobian and residual for the current iterate $\vec{U}$ and inverting the Jacobian matrix to find the appropriate update vector $\delta\vec{U}$ which is added to the current solution; the method is expressed in Equation 3.5.

$$\begin{aligned} \delta\vec{U} &= -\mathbf{J}(\vec{U}^n)^{-1}\vec{F}(\vec{U}^n) \\ \vec{U}^{n+1} &= \vec{U}^n + \delta\vec{U} \end{aligned} \tag{3.5}$$

This process is repeated until the residual or the update vector is *sufficiently small*. A commonly used definition of *sufficiently small* is some absolute tolerance plus a fraction of the original residual size [117]. This definition of the nonlinear tolerance allows Newton's method to converge even if the original residual is large; in such a case, a significant reduction in the residual size is sought.

The second order tensor term in Equation 3.3 can be used if the Jacobian matrix is singular, resulting in a local quadratic model for the residual [118]. However the Jacobians found in reactor accident analysis are generally nonsingular and well behaved at the solution, thus only a first order linearization will be used for the problems encountered in this work.

Newton's method is locally q-quadratic convergent, meaning if the initial iterate for the method is sufficiently close to the solution, the method will converge quadratically. The requirement for the initial iterate to be sufficiently close to the converged solution is not as constraining as might be expected. In the application of Newton's method for solving implicitly integrated PDEs, the initial iterate is taken as the solution from the previous time step [119, 120]. If the time step is made small enough, the solution will be close to the solution at the previous time

step.

To ensure Newton's method converges to the correct solution, even when the initial iterate is far from the solution, a globalization technique must be used [119]. There are two main globalization techniques used for Newton's method: trust region and line search. The trust region method builds a local quadratic model around the current iterate and solves the quadratic model within a trusted region of a certain radius. The trust region requires significant modifications in the Newton algorithm to incorporate this globalization [121]. The line search globalization however, only requires small modifications if the Newton algorithm is already locally convergent; hence the line search method will be preferred in this work.

The line search method assumes that the solution update is oriented in the correct direction (meaning a descent direction) but may overshoot the target solution. The goal of the line search method is to reduce the magnitude of the solution update until the residual norm is sufficiently reduced. The reduction factor for the solution update can be obtained through the Armijo rule [122]. Thus the update relation of Equation 3.5 is transformed to

$$\vec{U}^{n+1} = \vec{U}^n + \lambda \delta \vec{U}, \tag{3.6}$$

where $\lambda = 2^{-j}$ for some $j \geq 0$ until the residual satisfies the sufficient decrease condition

$$\|\vec{F}(\vec{U} + \lambda \delta \vec{U})\| < (1 - \alpha\lambda)\|\vec{F}(\vec{U})\|. \tag{3.7}$$

For the methods used in this work, α is taken to be 10^{-4} as suggested by [123]. Additionally the index j is limited to 15 iterations, but experience shows that five reductions is sufficient for the problems in this work. The small number of reductions required supports the idea that for time dependent problems, the solution from the previous time step is reasonably close to the converged solution.

3.2.1 Linear System Inversion

Newton's method is built on repeatedly solving the linear system $\mathbf{J}\delta\vec{U} = -\vec{F}$, which will be written as $\mathbf{A}\vec{x} = \vec{b}$ in this section. The linear system $\mathbf{A}\vec{x} = \vec{b}$ can be solved in a multitude of ways. Direct inversion using a variant of Gaussian Elimination can be applied if one has access to the matrix elements and the matrix $\mathbf{A}$ is not prohibitively large. Gaussian Elimination requires $\mathcal{O}(n^3)$ operations to invert matrix $\mathbf{A}$, where n is the size of $\mathbf{A}$ [124].

Conversely an iterative method can be used to invert $\mathbf{A}$, of which there are two categories: stationary and nonstationary. Stationary linear solvers are ones for which the next solution iterate does not depend on the history of solution iterates. This category includes methods like Jacobi and Gauss-Seidel, where these methods are generally based on a decomposition of the system matrix. For example the Jacobi method uses the decomposition

$$\mathbf{A} = \mathbf{D} + \mathbf{L} + \mathbf{U}, \tag{3.8}$$

where $\mathbf{D}$ is the diagonal of the matrix while $\mathbf{L}$ and $\mathbf{U}$ are the lower and upper triangular portions respectively. Jacobi iteration can then be applied as

$$\vec{x}^{n+1} = -\mathbf{D}^{-1}\left(\mathbf{U} + \mathbf{L}\right)\vec{x}^{n} + \mathbf{D}^{-1}\vec{b}. \tag{3.9}$$

This method will converge if the matrix $\mathbf{A}$ is diagonally dominant and requires $\mathcal{O}(n^2)$ operations [124]. Jacobi iteration is normally the slowest converging stationary iterative method, with the convergence rate diminishing as the size of $\mathbf{A}$ increases.

The second category of iterative linear methods, nonstationary methods, have some dependence on previous iterates. The current iterate is given as some linear combination of previous iterates.

A popular class of nonstationary linear solvers are the Krylov subspace solvers, which build approximations to the current iterate over a Krylov subspace defined as

$$\mathcal{K}_k(\mathbf{A}, \vec{b}) = \text{span}\left\{\vec{r}_0, \mathbf{A}\vec{r}_0, \mathbf{A}^2\vec{r}_0, \ldots, \mathbf{A}^{k-1}\vec{r}_0\right\}, \tag{3.10}$$

where $\mathbf{A}$ is the system matrix to be inverted, $\vec{b}$ is the right hand side, and $\vec{r}_0 = \vec{b} - \mathbf{A}\vec{x}_0$ is the initial linear residual for a given initial guess $\vec{x}_0$. The most recent approximation to the solution is then a linear combination of the basis vectors for the current subspace $\mathcal{K}_k$,

$$\vec{x}_k = \vec{x}_0 + \sum_{j=0}^{k-1} \gamma_j \vec{v}_j, \tag{3.11}$$

where the $\vec{v}_j$ are basis vectors for the current subspace, and the coefficients γ_j are determined in different ways for different Krylov subspace methods.

The Generalized Minimum Residual (GMRes) method will be the linear solver of choice for inverting Jacobian matrices for the problems studied in this work [125, 126]. The GMRes method produces a sequence of solution iterates that minimize the linear residual over the current Krylov subspace, and does not have the constraint of needing a symmetric system matrix like MINimum Residual (MINRes) method or positive definiteness like the Conjugate Gradient (CG) method [127]. Unfortunately the freedom to solve nonsymmetric matrices requires GMRes to store all basis vectors of the subspace since no recurrence relations exist between the basis vectors. This means that the storage requirements for GMRes grow as the iteration process progresses. To reduce the storage requirements of GMRes, a restarted version can be used where, after a set number of iterations, the iteration process is restarted with the most recent iterate as the new initial guess. The price to pay for reducing the storage in this way is to possibly have a slower convergence rate, which may stagnate [125, 128]. Where possible, a full GMRes method will be used to minimize the effect of linear convergence stagnation. GMRes involves minimizing the linear residual over the current Krylov subspace

$$\min_{\vec{x}_k \in \vec{x}_0 + \mathcal{K}_k} \|\vec{b} - \mathbf{A}\vec{x}_k\|. \tag{3.12}$$

In GMRes, the basis vectors for the Krylov subspace are computed using a Gram-Schmidt process adapted to Krylov subspaces called the *Arnoldi* process [129]. The orthonormal basis vectors are stored as columns of a matrix $\mathbf{V}_k$ of size $n \times k$, with n being the size of the square system matrix $\mathbf{A}$. The coefficients from the Arnoldi process are stored in an upper Hessenberg matrix $\mathbf{H}_k$ of size $(k+1) \times k$. The Arnoldi process gives the relation

$$\mathbf{A}\mathbf{V}_k = \mathbf{V}_{k+1}\mathbf{H}_k, \tag{3.13}$$

which means that if $\vec{x}_k \in \vec{x}_0 + \mathcal{K}_k$, then $\vec{x}_k = \mathbf{V}_k\vec{y} + \vec{x}_0$ for some coefficient vector $\vec{y}$. The minimization problem Equation 3.12 can be transformed using the relation in Equation 3.13

$$\mathbf{A}\vec{x}_k = \mathbf{A}\mathbf{V}_k\vec{y} + \mathbf{A}\vec{x}_0 = \mathbf{V}_{k+1}\mathbf{H}_k\vec{y} + \mathbf{A}\vec{x}_0. \tag{3.14}$$

The first basis vector of the Krylov subspace is constructed from the original linear residual $\vec{r}_0$, thus

$$\vec{r}_0 = \beta\mathbf{V}_{k+1}\vec{e}_1, \tag{3.15}$$

where $\beta = \|\vec{r}_0\|$ is the norm of the initial linear residual, and $\vec{e}_1$ is the first vector from the canonical basis. Equation 3.14 and Equation 3.15 can be used to reduce the size of the minimization problem in Equation 3.12 as

$$\min_{\vec{x}_k \in \vec{x}_0 + \mathcal{K}_k} \|\vec{b} - \mathbf{A}\vec{x}_k\| = \min_{\vec{y} \in R^k} \|\beta\vec{e}_1 - \mathbf{H}_k\vec{y}\|. \tag{3.16}$$

This transformation reduces the size of the minimization problem from size n to size k, which can be significant if n is large. Additionally, the QR algorithm for finding the linear least squares solution to Equation 3.16, with an upper Hessenberg matrix $\mathbf{H}_k$, can be done with a single Given's rotation, or a single Householder reflector per column vector.

The transformation of the linear least squares problem in Equation 3.16 depends on the matrix $\mathbf{V}_{k+1}$ being unitary, or the columns of $\mathbf{V}_{k+1}$ need to be orthonormal. However the Gram-Schmidt process, used to compute the columns of $\mathbf{V}_{k+1}$, suffers from numerical errors that lead to a loss of orthogonality. Two methods exist to reduce the loss of orthogonality: Modified Gram-Schmidt and re-orthogonalization [130, 131]. The modified Gram-Schmidt algorithm reorders the classical Gram-Schmidt algorithm to reduce the introduction of round-off errors, while re-orthogonalization repeats the orthogonalization process once to reduce the round-off errors. The cost of re-orthogonalization is then twice as much as the modified Gram-Schmidt, however the re-orthogonalization procedure allows the algorithm to more adequately exploit parallel computer architectures [131]. Because of the added expense incurred by re-orthogonalization, methods have been studied to check for the loss of orthogonality and only re-orthogonalize when a

loss of orthogonality is suspected [132].

3.2.2 Linear System Preconditioning

The convergence of the solution to the linear system $\mathbf{A}\vec{x} = \vec{b}$ is dependent on the condition number of $\mathbf{A}$ [117, 133]. If $\|\mathbf{I} - \mathbf{A}\|_2 < 1$, then the convergence rate can be expressed as

$$\frac{\|\vec{e}_k\|_2}{\|\vec{e}_0\|_2} \leq \kappa_2(\mathbf{A}) \frac{\|\vec{r}_k\|_2}{\|\vec{r}_0\|_2}, \tag{3.17}$$

where $\vec{e}_k = \vec{x}_k - \vec{x}^*$ is the solution error, $\vec{r}_k = \vec{b} - \mathbf{A}\vec{x}_k$ is the linear residual, and a zero subscript denotes the initial iterate. The relative condition number with respect to inversion, $\kappa(\mathbf{A})$ is defined as

$$\kappa_p(\mathbf{A}) = \|\mathbf{A}\|_p \|\mathbf{A}^{-1}\|_p, \tag{3.18}$$

where a condition number close to unity corresponds to a well-conditioned system. Preconditioning provides a way to reduce the condition number of the linear system, hence increasing the convergence rate of the linear solver. There are three versions of preconditioning available to linear systems:

- *Left Preconditioning*
$$\mathbf{M}_L^{-1}\mathbf{A}\vec{x} = \mathbf{M}_L^{-1}\vec{b}, \tag{3.19}$$
- Right Preconditioning
$$\mathbf{A}\mathbf{M}_R^{-1}\left(\mathbf{M}_R\vec{x}\right) = \vec{b}, \tag{3.20}$$
- Split Preconditioning
$$\mathbf{M}_L^{-1}\mathbf{A}\mathbf{M}_R^{-1}\left(\mathbf{M}_R\vec{x}\right) = \mathbf{M}_L^{-1}\vec{b}. \tag{3.21}$$

Split preconditioning will be discussed presently as it is a generalization of both Left and Right preconditioning; both methods can be recovered by setting $\mathbf{M}_R$ and $\mathbf{M}_L$ to the identity respectively. Effective preconditioners are ones for which $\|\mathbf{I} - \mathbf{M}_L^{-1}\mathbf{A}\mathbf{M}_R^{-1}\|_2 < 1$ and for which the condition number of $\mathbf{M}_L^{-1}\mathbf{A}\mathbf{M}_R^{-1}$ is significantly smaller than $\mathbf{A}$. Additionally, the preconditioner should be easy to invert. Left preconditioning changes the residual vector, which will affect the estimation of convergence for the linear system. A preconditioned GMRes algorithm is presented in Algorithm 1. Notice that the cost is the same to apply a left or right preconditioner.

In all cases of preconditioning, the matrix $\mathbf{M}_{L,R}$ is an approximation to the matrix $\mathbf{A}$. With preconditioning there is always a trade-off between obtaining a good approximation of $\mathbf{A}$ and the cost of obtaining such an approximation. The most effective preconditioner is the matrix itself, however the cost to invert this

Algorithm 1: Right Preconditioned GMRes with Reorthogonalization in Arnoldi

Input : Linear System Matrix $\mathbf{A}$, right-hand side $\vec{b}$, initial iterate $\vec{x}_0$
Output: Converged Solution $\vec{x}$

$\vec{r}_0 = \mathbf{M}_L^{-1}\left(\vec{b} - \mathbf{A}\vec{x}_0\right), \quad \beta = \|\vec{r}_0\|, \quad \vec{v}_1 = \frac{\vec{r}_0}{\beta}, \quad \mathbf{V}_1 = \vec{v}_1$ // Init first basis vector
for $k = 1, 2, \ldots$ **do**
  $\vec{z} = \mathbf{M}_R^{-1}\vec{v}_k$ // Apply Preconditioner
  $\vec{w} = \mathbf{M}_L^{-1}\mathbf{A}\vec{z}$ // Action of matrix
  $\vec{h}' = \mathbf{V}_k^{\mathrm{T}}\vec{w}$ // Calculate projection coefficients
  $\vec{v}\,' = \vec{w} - \mathbf{V}_k\vec{h}'$ // First orthogonalization
  $\vec{h}'' = \mathbf{V}_k^{\mathrm{T}}\vec{v}\,'$ // Recalculate projection coefficients
  $\vec{h} = \vec{h}' + \vec{h}''$ // Combine projection coefficients
  $\hat{v}_{k+1} = \vec{v}\,' - \mathbf{V}_k\vec{h}''$ // Reorthogonalization
  $\vec{v}_{k+1} = \frac{\hat{v}_{k+1}}{\|\hat{v}_{k+1}\|}$ // Normalization of basis vector
  $\mathbf{H}_k = \begin{bmatrix} \mathbf{H}_{k-1} & \vec{h} \\ 0 & \|\hat{v}_{k+1}\| \end{bmatrix}$ // Augmentation of Hessenberg Matrix
  $\min_y \|\beta\vec{e}_1 - \mathbf{H}_k\vec{y}_k\|$ // Solve minimization problem
  if $\|\beta\vec{e}_1 - \mathbf{H}_k\vec{y}_k\| <$ tolerance **then**
    exit // If converged, exit "for" loop
  else
    $\mathbf{V}_{k+1} = \left[\mathbf{V}_k \mid \vec{v}_{k+1}\right]$ // otherwise, augment basis matrix
  end
end
$\vec{x} = \vec{x}_0 + \mathbf{M}_R^{-1}\mathbf{V}_k\vec{y}$ // Return converged solution

preconditioner is much too expensive; likewise the most cost-effective preconditioner is the identity matrix, but may be a terrible approximation for $\mathbf{A}$. Many methods have been proposed to precondition the linear system: (Block)Jacobi, (Block)Gauss-Seidel, ILU, Multigrid, etc.

Since the present work is focused on multiphysics solutions, the preconditioner will be based on the physics of the components of the system. This type of preconditioner manifests as a Block Jacobi or Block Gauss-Seidel preconditioner. The Block Jacobi preconditioner involves partitioning the matrix $\mathbf{A}$ into blocks and inverting each block diagonal. For example a 3×3 block matrix is inverted by repeatedly applying the relation

$$\begin{bmatrix} \vec{x}_1 \\ \vec{x}_2 \\ \vec{x}_3 \end{bmatrix}^{n+1} = \begin{bmatrix} \mathbf{A}_{11}^{-1} & & \\ & \mathbf{A}_{22}^{-1} & \\ & & \mathbf{A}_{33}^{-1} \end{bmatrix} \left(\begin{bmatrix} \vec{b}_1 \\ \vec{b}_2 \\ \vec{b}_3 \end{bmatrix} - \begin{bmatrix} \mathbf{0} & \mathbf{A}_{12} & \mathbf{A}_{13} \\ \mathbf{A}_{21} & \mathbf{0} & \mathbf{A}_{23} \\ \mathbf{A}_{31} & \mathbf{A}_{32} & \mathbf{0} \end{bmatrix} \begin{bmatrix} \vec{x}_1 \\ \vec{x}_2 \\ \vec{x}_3 \end{bmatrix}^{n} \right). \quad (3.22)$$

Likewise a Block Gauss-Seidel method would repeatedly apply

$$\downarrow \begin{cases} \vec{x}_1^{n+1} = \mathbf{A}_{11}^{-1} \left(\vec{b}_1 - \mathbf{A}_{12}\vec{x}_2^{n} - \mathbf{A}_{13}\vec{x}_3^{n} \right) \\ \vec{x}_2^{n+1} = \mathbf{A}_{22}^{-1} \left(\vec{b}_2 - \mathbf{A}_{21}\vec{x}_1^{n+1} - \mathbf{A}_{23}\vec{x}_3^{n} \right) \\ \vec{x}_3^{n+1} = \mathbf{A}_{33}^{-1} \left(\vec{b}_3 - \mathbf{A}_{31}\vec{x}_1^{n+1} - \mathbf{A}_{32}\vec{x}_2^{n+1} \right), \end{cases} \quad (3.23)$$

where each equation in Equation 3.23 is solved sequentially and thus not easily parallelized. The order in which these equations are solved is arbitrary, but must be specified. The convergence rate for Equation 3.23 should be higher than for Equation 3.22. However, the convergence rate may not be able to justify not using these methods in parallel. The main objective of a preconditioner is to provide an easily invertible approximation to the system matrix. Thus, the application of Equation 3.22 or Equation 3.23 can be limited to a small number of applications. The residual error for methods like Jacobi or Gauss-Seidel generally decreases rapidly in the first few iterations and then slows for the remainder of the iteration process. Thus when using this type of preconditioner, the number of applications will be limited to one or two.

3.2.3 Inexact Newton Methods

A way to reduce the computational resources of the nonlinear solution method is to use an inexact Newton method, which progressively reduces the linear solution tolerance as the iterative solution approaches the converged solution. In solving the linear system $\mathbf{A}\vec{x} = \vec{b}$, the relative norm of the linear residual $\vec{r} = \mathbf{A}\vec{x} - \vec{b}$ gives an estimate of how close the current solution $\vec{x}$ is to the exact solution $\vec{x}^*$. The relation given in Equation 3.17 states that if the condition number is low, the

relative residual gives a good estimate for how close the current solution is to the true solution in a relative sense. Iterative solvers repeat their iteration process until the residual is below a given tolerance. The tolerance is often compared to the readily available relative residual on the right hand side of Equation 3.17.

Choosing this tolerance wisely can improve the convergence and computation time in the simulation. A tighter tolerance requires more iterations to converge, while a looser tolerance can be reached with fewer iterations. Since the goal of the linear solver in this work is to solve the solution update for the nonlinear solver, the linear solver tolerance will depend on the precision required of the nonlinear solver. This linear tolerance relation is given by

$$\tau_k \leq \eta_k \|\vec{F}(\vec{U}_k)\|, \tag{3.24}$$

where η_k is some forcing term chosen as $0 \leq \eta_k \leq 1$ for the k-th nonlinear iteration [134–136]. Thus the tolerance for the linear solver is reduced as the solution of the nonlinear system approaches the exact solution [117]. A guard is added to the definition in Equation 3.24 for small residuals. If the nonlinear residual is already small, a larger tolerance is used to exit the linear solver faster and to avoid needless iterations. The full definition of the linear tolerance is

$$\tau_k = \begin{cases} 10\|\vec{F}(\vec{U}_k)\| & ; \|\vec{F}(\vec{U}_k)\| \in (0, \tau_{NL}] \\ 10^{-5} & ; \|\vec{F}(\vec{U}_k)\| = 0 \\ 0.1\|\vec{F}(\vec{U}_k)\| & ; \text{otherwise} \end{cases} . \tag{3.25}$$

The tolerance definition given in Equation 3.25 is a simple definition that successively tightens the linear tolerance as the nonlinear solution approaches the converged solution. More sophisticated definitions for the forcing term η_k in Equation 3.24 have been studied which compare successive nonlinear residual norms and guard against rapid decreases in η_k. However, in results from multiple test cases, the simplistic tolerance definition like that of Equation 3.25 can improve the convergence results over choosing a very small tolerance [134].

3.2.4 Jacobian-Free Newton-Krylov Method

A significant drawback to Newton's method is in having to calculate and store the Jacobian matrix of Equation 3.5. In some cases the Jacobian matrix may not be readily available if the residual formulation is constructed from an inaccessible computation routine. This section describes a variation of Newton's method that can be used when the Jacobian is either prohibitively large to store and compute or is inaccessible.

Krylov subspace linear solvers only require the result of applying the linear system matrix to a given vector. Given that the Jacobian is a matrix of first order derivatives, the Jacobian vector product can be approximated by a finite difference relation with the residual

$$\mathbf{J}\vec{v} \approx \frac{\vec{F}(\vec{U}+\varepsilon\vec{v}) - \vec{F}(\vec{U})}{\varepsilon}, \qquad [1^{\text{st}} \text{ order}] \quad (3.26)$$

$$\mathbf{J}\vec{v} \approx \frac{\vec{F}(\vec{U}+\varepsilon\vec{v}) - \vec{F}(\vec{U}-\varepsilon\vec{v})}{2\varepsilon}, \qquad [2^{\text{nd}} \text{ order}] \quad (3.27)$$

where ε is a small parameter that is optimized for truncation and round-off error [37]. The class of nonlinear solvers that use this approximation for the Jacobian inversion is called Jacobian-Free Newton-Krylov (JFNK) methods [37]. The finite difference approximation can be computed with higher order formulations which require multiple evaluations of the residual vector, but are less susceptible to numerical errors; the subtraction of two numbers that are close together in finite precision can be unstable. In this work the default finite difference relation is a centered difference scheme giving 2^{nd} order convergence in the small parameter ε. This centered difference scheme requires two evaluations of the residual for every matrix vector product, but is less susceptible to instabilities from finite precision subtraction. The small parameter ε is computed using relations found in [137]

$$\varepsilon = \frac{\sqrt{1+\|\vec{U}\|}}{\|\vec{v}\|}\bar{\varepsilon} \qquad \bar{\varepsilon} = \begin{cases} \sqrt{\varepsilon_{\text{mach}}} & ;\text{forward difference} \\ \sqrt[3]{\frac{\varepsilon_{\text{mach}}}{2}} & ;\text{centered difference} \end{cases}, \quad (3.28)$$

where $\varepsilon_{\text{mach}}$ is $\sim 2\times10^{-16}$ for double precision. The relation in Equation 3.28 is similar to the one given by Knoll & Keyes in [37], but extended to the central difference scheme [137].

The subtraction in finite difference relations, used to approximate the derivative of a function, can suffer from numerical errors in finite precision arithmetic [130]. Computers represent real numbers as a finite array of binary bits, meaning that the floating point representation of a real number introduces rounding approximations

$$\tilde{x} = x(1+\varepsilon), \quad (3.29)$$

where $\tilde{x}$ is the floating point representation of $x \in \mathbb{R}$, and ε is the rounding error bounded by machine precision ($|\varepsilon| < \varepsilon_{\text{mach}}$). This rounding error incurred by the floating point representation becomes noticeable when subtracting two numbers that are close together. The errors due to round off are sporadic and not easily predicted.

To illustrate the errors incurred when using finite precision finite differences, the function

$$f(x) = \frac{e^x}{\sqrt{\sin x}}, \quad (3.30)$$

is taken and its derivative is evaluated numerically at $x = 0.5$. Figure 3.3 shows

the absolute error between the numerical finite difference and the analytically evaluated derivative as a function of the small parameter ε. The figure shows that as ε decreases from 10^{-1}, the error in the derivative behaves as expected for the forward and central differences. The forward difference error is decreasing linearly, while the central difference error is decreasing quadratically. There is however a moment when both methods reach a minimum error, afterwhich reducing ε causes increasingly sporadic errors in the finite difference. The minima for the two finite differences correspond to an epsilon that minimizes both truncation and round off errors and is what the relation in Equation 3.28 is estimating.

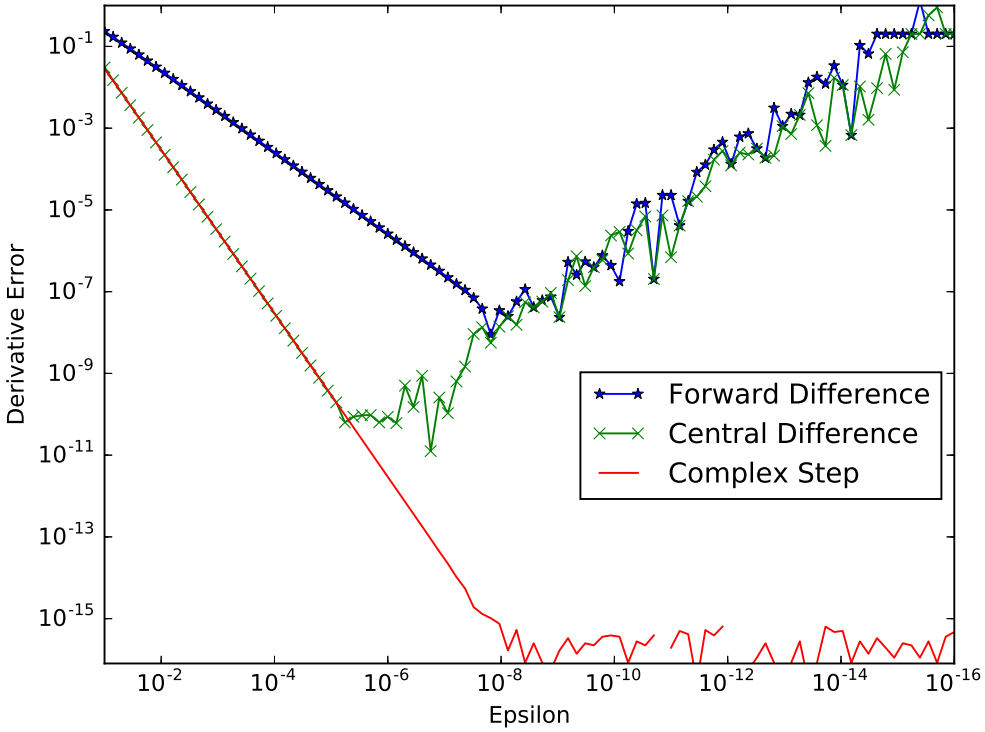

Figure 3.3. Convergence of Three Finite Difference Formulations in the Small Parameter ε

The third method shown in Figure 3.3 is a recently studied method for numerically evaluating the derivative of a function. This method, called the complex step method by Martins *et al.* [138], eliminates the round off errors by evaluating the numerical derivative in the complex plane

$$\mathbf{J}\vec{v} \approx \frac{\mathbb{I}\mathrm{m}\left\{\vec{F}(\vec{U} + i\varepsilon\vec{v})\right\}}{\varepsilon}. \tag{3.31}$$

When this method is applied to Equation 3.30, the error in Figure 3.3 experiences the same truncation error as the centered difference scheme, but never experiences the influence of round off error. The numerical error remains stable at $\varepsilon_{\text{mach}}$ as ε is decreased. This method however has a large drawback, in that if the residual

is not able to be computed in complex arithmetic, the method is not applicable. In the case of this work, the residuals from physics components are computed using external algorithms and are not readily transformed to work in complex arithmetic. Thus, the complex step method will not be used in this work, but instead focus on higher order finite differences to remedy numerical instabilities from finite precision subtraction.

Preconditioning with JFNK

The focus on Block Jacobi and Block Gauss-Seidel in Section 3.2.2 is based on the idea of using optimized physics components to invert the preconditioner. This preconditioning method can be translated to a JFNK method by partitioning the multiplying vector $\vec{v}$ to the Jacobian. For example, to compute an approximate inverse of the first block in Equation 3.22, the right hand side is modified by subtracting the off-diagonal matrix vector product

$$\mathbf{J}_{12}\vec{v}_2 + \mathbf{J}_{13}\vec{v}_3 \approx \frac{\vec{f}_1\left(\vec{U} + \varepsilon \begin{bmatrix} 0 \\ \vec{v}_2 \\ \vec{v}_3 \end{bmatrix}\right) - \vec{f}_1\left(\vec{U}\right)}{\varepsilon}, \tag{3.32}$$

where the $\mathbf{A}_{ij}$ in Equation 3.22 appears as Jacobian subblocks. The residual for the first physics component is denoted by $\vec{f}_1$ as in Equation 3.1. Likewise, the evaluation of the inverse of the block diagonal term is given by

$$\mathbf{J}_{11}\vec{v}_1 \approx \frac{\vec{f}_1\left(\vec{U} + \varepsilon \begin{bmatrix} \vec{v}_1 \\ 0 \\ 0 \end{bmatrix}\right) - \vec{f}_1\left(\vec{U}\right)}{\varepsilon}, \tag{3.33}$$

where again the subblocks of $\mathbf{A}$ appear as parts of the Jacobian matrix. The block diagonal terms can then be inverted in the same way as the full Jacobian. The Block Jacobi algorithm for a matrix-free preconditioner is given by

Algorithm 2: Apply Matrix-Free Block Jacobi Preconditioner

1 **for** each physics block i **do**
2 $\quad \vec{v} = \vec{w}_1 + \vec{w}_2$ where $\vec{w}_1 = \left[0, \ldots, 0, \vec{v}_i, 0, \ldots, 0\right]^T$ and $\vec{w}_2 = \left[\vec{v}_1, \ldots, \vec{v}_{i-1}, 0, \vec{v}_{i+1}, \ldots, \vec{v}_N\right]^T$
3 $\quad \vec{b}_i = \vec{b}_i - \frac{\vec{f}_i(\vec{U}+\varepsilon\vec{w}_2) - \vec{f}_i(\vec{U})}{\varepsilon}$
4 $\quad$ invert diagonal block using $\mathbf{J}_{ii}\vec{v}_i \approx \frac{\vec{f}_i(\vec{U}+\varepsilon\vec{w}_1) - \vec{f}_i(\vec{U})}{\varepsilon}$
5 **end**

The algorithm can be slightly modified to use a Block Gauss-Seidel method, but then a specific order to the physics components must be imposed.

The preconditioners described were tested on a 26 energy group, spatially heterogeneous problem. The identity preconditioner is equivalent to not having a preconditioner, while the physics-based Block Jacobi (PB-Jacobi) and Block Gauss-Seidel (PB-Gauss-Seidel) operate as previously described. An order must be chosen, for the Block Gauss-Seidel preconditioner, in which to solve the physics components. The solution order is chosen as Temperature, Precursor, and Flux. This order was chosen because the temperature dependence does not depend on the precursor concentration and multiplying the most recent update by a zero matrix does not improve convergence. It is desirable that the most coupled component be solved last; in this case, the Flux depends strongly on the other components. A preconditioner aims to improve the convergence rate of the inversion of the Jacobian matrix. In this light, the preconditioner should not have any effect on the number of nonlinear iterations required per time step. Figure 3.4 shows the number of nonlinear iterations required to produce a converged solution at each time step.

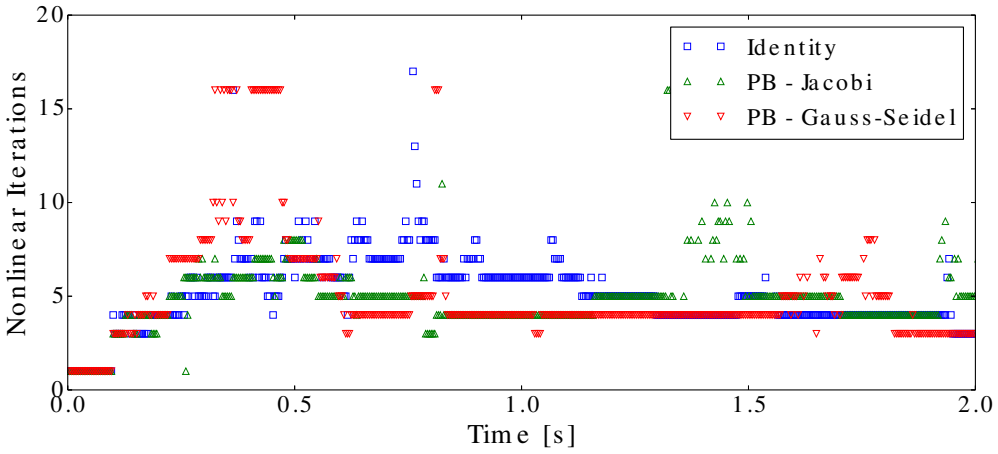

Figure 3.4. Comparison of Nonlinear Iterations to Produce Converged Solution per Time Step Required When Using an Identity or Physics-Based Preconditioner During the Simulation of Heterogeneous Problem Discussed in Section 4.4.2 with a Time Size of 0.004 s.

The figure shows that there is little difference between the three preconditioners tested. At certain points through the transient one method performs better than the others, but on average the number of nonlinear iterations is the same among preconditioners. The number of nonlinear iterations is unaffected by the preconditioner because the preconditioner only affects the solution of the local linear model in Newton's method; a preconditioner will not improve the error of the local linear model.

To really compare the efficacy of preconditioners, the number of linear iterations per nonlinear iteration must be compared. A good preconditioner will reduce the number of linear iterations needed to invert the Jacobian matrix. Figure 3.5 shows the average ratio of linear to nonlinear iterations for each time step of the same transient.

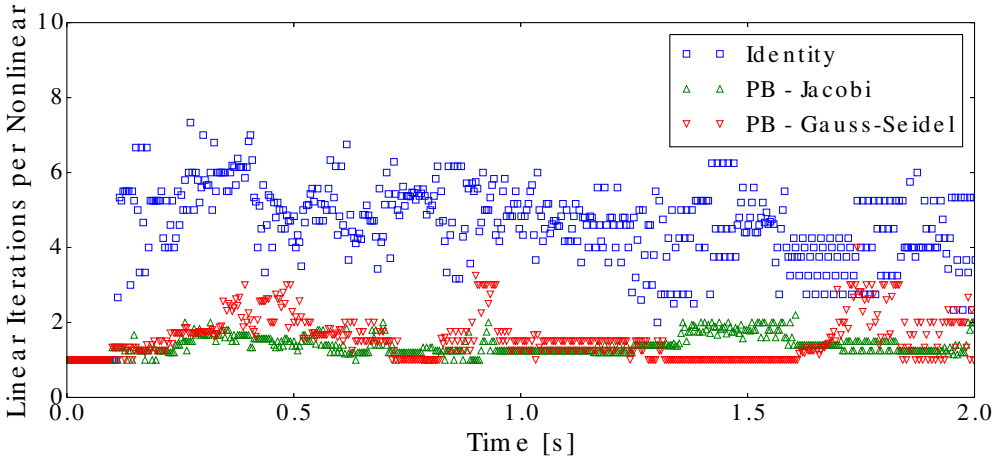

Figure 3.5. Comparison of Average Linear Iterations per Nonlinear Iteration Required per Time Step to Produce a Converged Solution When Using an Identity or Physics-Based Preconditioner During the Simulation of Heterogeneous Problem Discussed in Section 4.4.2 with a Time Size of 0.004 s.

It is clear that this ratio for the physics-based preconditioners is significantly smaller than the ratio for the identity preconditioner. The physics-based preconditioners consistently have an average ratio of about 2 for the transient, while the identity preconditioner is consistently between 3 and 7 linear iterations per nonlinear iteration. Looking closer at the physics-based preconditioners, the Block Gauss-Seidel preconditioner experiences times where the average ratio is larger than the Block Jacobi preconditioner. Based on the 26 energy group and spatially heterogeneous problem, a Block Jacobi preconditioner performs the best. There may be more optimal choices for preconditioners, but the Block Jacobi preconditioner can serve as an effective default for the multiphysics system.

3.3 Residual Formulation

The advantage of the JFNK method in storage reduction and quadratic convergence prompt the use of this method for the analysis used in this work. The superior convergence to operator splitting and tight coupling assure the accurate solution to reactor analysis problems. This section is dedicated to how the nonlinear residual for each physics component is constructed from existing computer codes developed to solve a single physics component.

The physics components most influential to reactor accident transient analysis are the transport of neutrons and the transfer of heat within the reactor. Additionally the concentration of delayed neutron precursors will be treated as a separate physics component, even if the delayed neutron precursors could be contained within the neutron transport model. Thus the global residual for the system will be

$$\vec{F}(\vec{U}) = \begin{bmatrix} \vec{f}_\phi(\vec{u}_\phi, \vec{u}_c, \vec{u}_T) \\ \vec{f}_c(\vec{u}_\phi, \vec{u}_c, \vec{u}_T) \\ \vec{f}_T(\vec{u}_\phi, \vec{u}_c, \vec{u}_T) \end{bmatrix}, \tag{3.34}$$

where ϕ denotes neutron transport, C denotes delayed neutron precursors, and T denotes heat transfer. This section will describe the process of building each physics component residual for use in the JFNK framework presented earlier.

3.3.1 Neutron Transport Residual

The transport equation from the previous chapter (Equation 2.1) after spatial, angular, and energy discretization is written in matrix form for compactness

$$\frac{1}{v}\frac{\partial \vec{\psi}}{\partial t} = -\mathbf{L}\vec{\psi} + \mathbf{H}\vec{\psi} + \mathbf{P}_\beta\vec{\psi} + \mathbf{X}_d\mathbf{\Lambda}\vec{C} + \vec{Q}, \tag{3.35}$$

where $\vec{\psi}$ is the angular, group, and spatial dependent flux. The matrix $\mathbf{L}$ accounts for the $\vec{\Omega}\cdot\vec{\nabla}$ and Σ_t terms, $\mathbf{H}$ is the discretized scattering matrix, $\mathbf{P}_\beta$ is the discretized prompt production matrix, $\mathbf{X}_d\mathbf{\Lambda}\vec{C}$ is the contribution from delayed neutron precursors, and $\vec{Q}$ accounts for a fixed source. An implicit Euler method can be applied to Equation 3.35 to discretize the time variable, where matrices operate on the solution at the next $(n+1)$ time step

$$\frac{\vec{\psi}^{n+1} - \vec{\psi}^{n}}{v\Delta t} + \mathbf{L}\vec{\psi}^{n+1} = \mathbf{H}\vec{\psi}^{n+1} + \mathbf{P}_\beta\vec{\psi}^{n+1} + \mathbf{X}_d\mathbf{\Lambda}\vec{C} + \vec{Q}. \tag{3.36}$$

The implicit formulation implies that an explicit form of the solution cannot be obtained, and an iterative method must be used to obtain the solution at the next time step. This should not be viewed as a drawback because of the need to use an iterative method for resolving the nonlinear coupling between physics components. Equation 3.36 can readily be placed into a residual form by rearranging all terms to be on one side of the equality. A complication arises when an existing transport code is to be used for constructing the residual. First order S_N or MOC transport codes do not generally apply matrices $\mathbf{L}$ and $\mathbf{H}$ directly, but only effectively apply the inverse matrix $(\mathbf{L}-\mathbf{H})^{-1}$ through sweeping and iterations on the scattering source. The algorithms in transport codes are written to produce an angular flux given a source distribution. If we are to use an existing transport code, the formulation of the transport residual must be modified to fit within an existing code.

We begin by rearranging Equation 3.36 so that the previous flux can be combined with the fixed source, and the loss and scattering matrices can be combined with the discretized time derivative operating on the current solution

$$\left(\underbrace{\frac{1}{v\Delta t}+\mathbf{L}-\mathbf{H}}_{\mathbf{B}}\right)\vec{\psi}^{n+1}=\mathbf{X}\left(1-\beta\right)\mathbf{F}\vec{\psi}^{n+1}+\mathbf{X}_d\mathbf{\Lambda}\vec{C}+\left(\underbrace{\vec{Q}+\frac{\vec{\psi}^{n}}{v\Delta t}}_{\tilde{Q}}\right). \quad (3.37)$$

Equation 3.37 groups the streaming, scattering, and time matrices into the matrix $\mathbf{B}$, and creates a new fixed source $\tilde{Q}$ which is only updated when the current time step has converged. The prompt production matrix has been split into two matrices: $\mathbf{F}$ which takes the angular flux and gives an isotropic source from fission, and $\mathbf{X}$ which maps the isotopic fission source to the angular and energy dependent source. The inverse of matrix $\mathbf{B}$ in Equation 3.37 is similar to the matrix available from existing S_N transport codes. The only modification to the existing transport code is to modify the total cross section to include the $\frac{1}{v\Delta t}$ term. This term acts as a homogeneous absorber applied to all media in the problem and is group dependent from the velocity [89]. Equation 3.37 can be readily transformed into a residual such as

$$\vec{f}_{\phi}^{*}=\vec{\psi}^{n+1}-\mathbf{B}^{-1}\left[\mathbf{X}\left(1-\beta\right)\mathbf{F}\vec{\psi}^{n+1}+\mathbf{X}_d\mathbf{\Lambda}\vec{C}+\tilde{Q}\right], \quad (3.38)$$

and can be used in the nonlinear methods discussed previously. Only having the inverse transport matrix $(\mathbf{L}-\mathbf{H})^{-1}$ available, limits the time discretization to first order. For example, trying to formulate Equation 3.35 in terms of a second order Crank-Nicolson method requires applying the matrix $(\mathbf{L}-\mathbf{H})$ to the previous angular flux, which is not available in standard S_N neutron transport codes.

A drawback to the residual formulation in Equation 3.38 is that the size of this residual equation is the size of the angular flux, which can be large; the size of $N_{\text{regions}} * N_{\text{groups}} * N_{\text{spatial components}} * N_{\text{directions}}$. This large size poses several problems in numerical simulation, one of which is the storage requirements for the Krylov linear solver. GMRes requires the storage of the basis vectors for the Krylov subspace, which would require storing several vectors at least as large as the angular flux. In fact, the size of the basis vectors would be much larger than the angular flux because of the concatenation with the precursor and temperature residuals. With these motivations in mind, an alternative form for Equation 3.38 is obtained which has a smaller size.

The fission source within the nuclear system provides a clear link between the neutron transport model, and the heat transfer model by way of the power. The fission source is also generally of a smaller size ($N_{\text{fission regions}} * N_{\text{spatial components}} * N_{\text{fissile isotopes}}$) than the angular flux. The number of fission regions is always a subset of the number of regions, and the number of fissile isotopes is very likely smaller than the product of the number of energy groups and number of directions. Even with a modest number of directions like an S_8 angular quadrature and a medium number of energy groups of 100, the number of fissile isotopes is generally limited to 50, giving a reduction by a factor larger than 1000.

Equation 3.38 can be formulated in terms of the fission source by applying

the fission matrix $\mathbf{F}$ to the residual. The residual is then

$$\vec{f}_\phi = \underbrace{\mathbf{F}\vec{\psi}^{n+1}}_{\vec{\mathfrak{f}}} - \mathbf{F}\mathbf{B}^{-1}\left[\mathbf{X}\left(1-\beta\right)\underbrace{\mathbf{F}\vec{\psi}^{n+1}}_{\vec{\mathfrak{f}}} + \mathbf{X}_d\mathbf{\Lambda}\vec{C} + \tilde{Q}\right], \tag{3.39}$$

where $\vec{\mathfrak{f}}$ is the current fission integral and is imposed for the neutron transport solver for each evaluation of the residual.

This formulation of the residual can be implemented by slightly modifying an existing S_N transport code that can solve eigenvalue or fixed source problems. The largest modification is in having to impose the current fission integral instead of it being calculated from the angular flux, and being able to apply the fission matrix $\mathbf{F}$ after the inverse matrix $\mathbf{B}^{-1}$ is applied. These modifications allow for the procedure in Algorithm 3 to be implemented for calculating the neutron transport residual.

Algorithm 3: Calculation of Neutron Transport Residual

```
/* Fixed Source and Previous Angular Flux updated externally
   when incrementing time step.                                */
```

1 Set fission integral $\mathfrak{f}$ as given by linear solver
2 Set the current precursor concentration C as given by linear solver
3 Modify cross sections based on temperature as given by linear solver
4 Invoke Transport Solver to apply $\mathbf{X}$ to $\mathfrak{f}$, invert $\mathbf{B}$, and apply $\mathbf{F}$
5 Subtract result from given $\mathfrak{f}$

The procedure in Algorithm 3 highlights that the residual construction depends on each physics component. In Steps 1-3, the current iterate for the multiphysics solution is used to modify parameters in the neutron transport code. The transport code is then called in components to apply the available operators.

3.3.2 Delayed Neutron Precursor Residual

The delayed neutron precursor evolution equation is presented in matrix form

$$\frac{\partial \vec{C}}{\partial t} = -\mathbf{\Lambda}\vec{C} + \mathcal{B}\mathbf{F}\vec{\psi}, \tag{3.40}$$

where $\vec{C}$ is the delayed neutron precursor concentration from all precursor groups, $\mathbf{F}$ is the operator which takes the angular flux and gives the isotropic fission source without the $(1-\beta)$ term, $\mathcal{B}$ takes a fission source and gives the delayed precursor production rate, and all other symbols retain their meaning from the transport residual. The time derivative is implicitly discretized to yield the residual equation

$$\vec{f}_C = \left(\frac{1}{\Delta t}\mathbf{I} + \mathbf{\Lambda}\right)\vec{C}^{n+1} - \mathcal{B}\underbrace{\mathbf{F}\vec{\psi}^{n+1}}_{\vec{\mathfrak{f}}} - \frac{1}{\Delta t}\vec{C}^{n}. \tag{3.41}$$

The term for the fission integral appears in this residual also, making its construction compatible with the form of the transport residual in Equation 3.39. The current iterate for the precursor concentration is multiplied by the factor $(\frac{1}{\Delta t} + \lambda_j)$ for the precursor group j, the fission integral $\vec{\mathfrak{f}}$ is multiplied by the delayed neutron fraction corresponding to group j, and the previous solution is normalized by the time step size and subtracted.

The residual construction presented in Algorithm 3 and the residual in Equation 3.41 were tested to have been correctly implemented by verifying the convergence rate of the solution error versus the time step size Δt. An infinite homogeneous medium was taken with one energy group and two delayed neutron precursor groups to allow an exact solution to be obtained for the kinetic problem. Temperature dependence was not accounted for in this verification exercise; accounting for temperature dependence makes obtaining an analytic solution impossible. The exact solution can be obtained by computing the eigenvalues (η_i) and eigenvectors (E_i) of the resulting matrix system $\vec{U}' = \mathbf{A}\vec{U}$, where $\mathbf{A}$ is given by

$$\begin{bmatrix} v\left(\Sigma_s - \Sigma_t + (1-\beta)\chi\nu\Sigma_f\right) & \chi_{d,1}\lambda_1 & \chi_{d,2}\lambda_2 \\ \beta_1\nu\Sigma_f & -\lambda_1 & \\ \beta_2\nu\Sigma_f & & -\lambda_2 \end{bmatrix}.$$

The exact solution to the resulting matrix system is then of the form

$$\begin{bmatrix} \phi \\ C_1 \\ C_2 \end{bmatrix}(t) = \alpha_1 E_1 e^{\eta_1 t} + \alpha_2 E_2 e^{\eta_2 t} + \alpha_3 E_3 e^{\eta_3 t}, \tag{3.42}$$

where the constants α_i can be determined by the initial condition. Comparing the error of the solution at the end of the simulation when the time step is decreased yields the convergence plot shown in Figure 3.6.

The norm of the error of the solution at the end of the simulation is expected to converge linearly as the time step size is decreased. Figure 3.6 shows that as the number of time steps increases, the error is reduced in a linear trend. The green line in Figure 3.6 indicates a linear reduction in error. As the number of time steps increases (consequently the timestep size decreases), the relative error asymptotically approaches the linear trend until a point where it begins to drift. The drift as the number of time steps increases beyond ten thousand is due to the accumulation of finite precision errors. This point corresponds to a time step size of 1.83E−5 s. From the convergence displayed in Figure 3.6, the residuals are determined to have been implemented correctly.

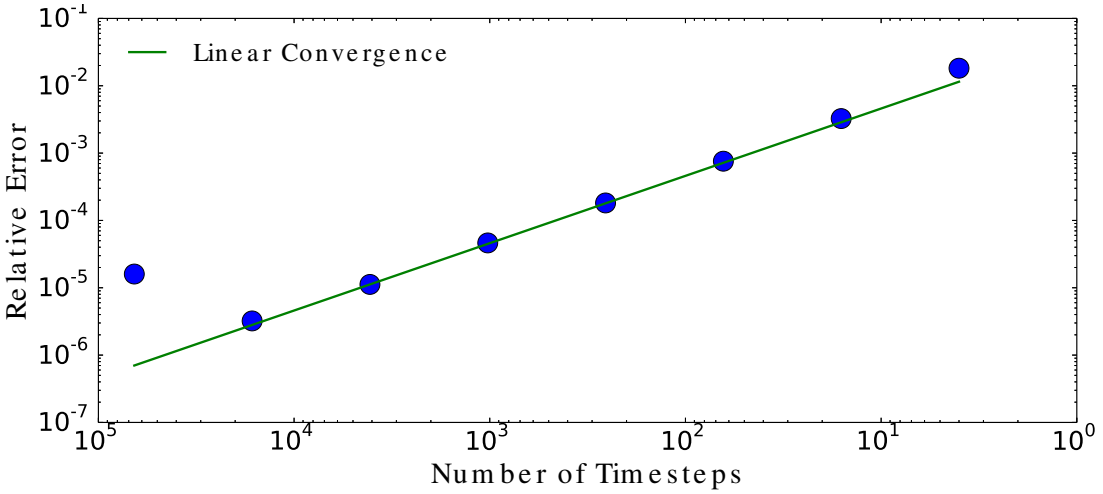

Figure 3.6. Convergence of Neutron Transport and Precursor Residuals

3.3.3 Heat Transfer Residual

There are two heat transfer models discussed in the previous chapter, a lumped capacitance model and a multichannel model. The lumped capacitance model is put into residual form in the same way that the precursor concentration is

$$\vec{f_T} = \begin{bmatrix} \frac{\alpha_f}{\Delta t} + h & -h \\ -h & \frac{\alpha_w}{\Delta t} + h \end{bmatrix} \begin{bmatrix} T_f^{n+1} \\ T_w^{n+1} \end{bmatrix} - \frac{1}{\Delta t} \begin{bmatrix} \alpha_f T_f^n \\ \alpha_w T_w^n \end{bmatrix} - \begin{bmatrix} P(t_{n+1}) \\ -\dot{Q}_{\text{out}}(t_{n+1}) \end{bmatrix}, \tag{3.43}$$

by implicitly discretizing the time derivative and moving all terms to one side of the equality.

The multichannel model discussed in Section 2.2.2 is more complicated than the lumped capacitance model and is constructed in a similar manner to the neutron transport residual. The fission integral from the transport residual is used to obtain the spatial power distribution, which is specified in the multichannel code. Additionally the material temperatures are set, and the new temperature distribution in the fuel and water is produced. The multichannel code can be conceptualized as a function

$$\begin{bmatrix} T_f^{out} \\ T_w^{out} \end{bmatrix} = G(P, T_f^{in}, T_w^{in}), \tag{3.44}$$

that accepts temperature and power distributions and returns a corresponding temperature distribution. The input temperature distribution is used to evaluate material properties throughout the domain. The residual can then be constructed

by obtaining the difference between the input and output temperature distributions. Thus the residual is

$$\vec{f}_T = \begin{bmatrix} T_f^{in} \\ T_w^{in} \end{bmatrix} - \begin{bmatrix} T_f^{out} \\ T_w^{out} \end{bmatrix} = \begin{bmatrix} T_f^{in} \\ T_w^{in} \end{bmatrix} - G(P, T_f^{in}, T_w^{in}). \tag{3.45}$$

This simple residual construction allows for minimal modifications to the existing code to construct the residual vector.

As mentioned for operator splitting, the residual construction for simultaneous systems encounters data transfer between the physics components. For the construction of residuals in this work, the data transfer is accomplished by a series of averages to connect each physics components' solution to the others' mesh.

For the transfer of the power and temperature between the multichannel and transport codes, the power is given to the multichannel code as the total power and a pin-wise fraction. Thus in the residual construction for the temperature component, the power and spatial distribution is computed by the transport code and, given a map between the two spatial meshes, is assigned in the multichannel code. The same map is used to impose the temperature for the macroscopic cross sections in the transport code.

The map between the neutron transport and thermal hydraulics models is based on user input and is different for each geometry studied. A more precise data transfer method could be prepared, but would require large modifications to the existing physics models. For example the two physics components could be discretized using the finite element method, where transfers between meshes could be accomplished through projections onto an opposing physics components' mesh [113]. This would require the spatial temperature distribution in the thermal hydraulics model to be projected onto a finite element space, which is not readily available in the current version.

The present work focuses on two dimensional transport with three dimensional thermal hydraulics. To relate the reduced dimension transport to the thermal hydraulics model, an axial profile needs to be either computed or assumed. Results involving the multichannel thermal hydraulics model either have a flat axial profile, or a profile that was computed from an initially critical three dimensional transport calculation. This axial profile is assumed constant through the simulation process.

The present chapter has discussed the numerical methods necessary to produce a multiphysics framework with the goal of obtaining accurate solutions to reactor physics problems. The numerical methods presented in this chapter are used to obtain multiphysics solutions presented in remaining chapters.

Chapter 4

Homogenization

Homogenization methods play a central role in the study of reactor analysis. The accurate generation of homogenized cross sections is of the utmost importance to reduce the introduction of model errors in reactor simulations. This chapter focuses on the traditional homogenization methods used in reactor analysis, and modifications needed to use homogenized cross sections in time dependent multiphysics simulations.

4.1 Motivation

Homogenization methods are used regularly in reactor analysis when a detailed calculation is too costly. For instance for a PWR core, there are 193 fuel assemblies 4 m tall, each containing 289 rods (264 fuel rods and 25 non-fuel rods). A moderate spatial resolution (one spatial point per rod and one point per centimeter in axial direction) would result in about 22 million spatial points. Additionally for each spatial point, an accurate resolution of the angular and energy dependence is needed to calculate the angular flux. For thermal reactors, about 300 energy groups are used to discretize the energy domain. For fast reactors, this number can be as large as 2000. The angular domain can be discretized using discrete directions, which for an S_8 quadrature in three dimensions results in 80 angular directions [139]. This leads to an angular flux with 535×10^9 unkowns, which is typically not stored for static calculations but is for transient calculations. Simply storing the angular flux in double precision would require about 4 terabytes of memory, which is not feasible on all but the highest performance super computers. This insight leads engineers and reactor physicists to develop methods which reduce the memory consumption and computation time while obtaining an accurate solution. Cross section homogenization is one of the ways to reduce the size of the problem being solved while still maintaining important characteristics of the solution. Typically reaction rates and the value of k_{eff} are the quantities of interest that are to be preserved in homogenization processes, since often engineers are interested in the power or absorption rate in a region of the reactor and the criticality state.

The procedure used for homogenization in reactor analysis involves several steps: self-shielding with pin cells, detailed flux calculation on lattice, cross section weighting, full core calculation, and a possible iteration sequence over these steps [52, 140]. Deterministic transport codes are typically employed in the self shielding and detailed lattice calculation, however Monte Carlo codes have been used as an alternative to a deterministic calculation [141]. Monte Carlo codes have only been used in validation practices since a deterministic calculation is usually faster than a Monte Carlo calculation.

An underlying assumption with homogenization methods is that the solution obtained during the detailed lattice calculation should approximate the heterogeneous solution in the larger global problem. However, recent work [28] and simple analysis shows that during transient situations, the time dependent and static solutions can be significantly different. Nonetheless, current practice is to use a static calculation in the detailed lattice calculation, even when performing time dependent calculations on the reactor problem. Given that the time dependent and static solutions are not equivalent, cross sections which are produced from a static solution may not accurately represent the time dependent solution. This chapter explores these errors and studies new homogenization methods designed to produce more accurate homogenized cross sections for time dependent calculations.

4.2 Classical Formulation

The topic of cross section homogenization covers a wide range of methods. In the simplest case, homogenization is a process of taking the weighted average of cross sections to obtain averaged values. The weighting function is typically a flux, so that the weighted average preserves reaction rates, which were defined in Section 2.1. Cross section homogenization that uses the heterogeneous solution from the global problem as the weighting function can be referred to as *equivalence theory* [42]. However using the global heterogeneous solution is of little interest because of the difficulty to obtain it. Homogenization becomes practical when using reference solutions from representative subdomains in what is referred to as *general equivalence theory* [42]. For the cases studied in this chapter, the problem domain is small enough to obtain a global solution as the reference solution. For these solutions, general equivalence theory will not be necessary.

Another class of homogenization methods is based on the asymptotic limit of an expansion of the heterogeneous angular flux. The angular flux is expanded about a small parameter of some characteristic length or energy scale. This expansion, performed at different length scales, is used to deconstruct the global heterogeneous solution into the product of local and global solutions [142–144].

Starting from the multigroup transport equation (Equation 2.15), average valued cross sections can be defined as follows

$$\sigma_x^{G,R} = \frac{\sum_{g\in G}\sum_{r\in R}\sigma_x^{g,r}\phi_{g,r}V_r}{\sum_{g\in G}\sum_{r\in R}\phi_{g,r}V_r} \tag{4.1}$$

$$\sigma_s^{G'\to G,R} = \frac{\sum_{g\in G}\sum_{g'\in G'}\sum_{r\in R}\sigma_s^{g'\to g,r}\phi_{g',r}V_r}{\sum_{g'\in G'}\sum_{r\in R}\phi_{g',r}V_r} \tag{4.2}$$

$$\chi^G = \sum_{g\in G}\chi^g, \tag{4.3}$$

where G and R refer to the group and spatial region of the homogenized problem, g and r correspond to the group and spatial region of the detailed problem, and V_r corresponds to the volume of the spatial region r. The cross section σ_x represents reactions of type x, such as the total interaction σ_t or the fission production cross section $\nu\sigma_f$. For time dependent problems, the inverse velocity can be treated as a cross section and homogenized as σ_x. The flux used as a weighting function is supposed to approximate the fine solution flux within the homogenized region. In many reactor analysis methods, this flux comes from a detailed lattice calculation with reflecting or albedo boundary conditions.

As discussed in Section 2.1.4, a more accurate definition for Equations 4.1–4.3 is to use the angular flux instead of the scalar flux. However in this case, the homogenized cross sections become dependent on direction [67]. While it has been shown that using direction dependent cross sections does reduce errors in highly heterogeneous or anisotropic media, reactor analysis generally disregards the use of direction dependent homogenized cross sections because of the added computational complexity and small gain in accuracy. The homogenized cross sections produced for the present work will use the scalar flux and conform to the current norm in reactor analysis.

The leakage term in the transport equation does not lend itself to the same homogenization rules as the interaction cross sections because of the gradient operator. Homogenization of the leakage term dictates that the net current density for a homogenized region boundary must be equivalent in both the heterogeneous and homogeneous problems. This is generally not possible with the constraint of having a continuous flux and current density at homogeneous boundaries. General equivalence theory removes the constraint of having a continuous flux at homogenized region boundaries. The amount of discontinuity can be determined in the homogenization process through the computation of discontinuity factors; possibly as a combination of contributions from different length scales [145]. The computation of discontinuity factors depends on the desired leakage model used in the homogeneous calculation. Smith [42] defined flux discontinuity factors to be used in low order diffusion calculations by the ratio of the heterogeneous and homogeneous fluxes at the homogeneous boundaries. Later, Sanchez [146] considered discontinuity factors for the current density based on the heterogeneous and homogeneous current densities at surfaces of homogeneous regions. Alternatively, discontinuity factors may be avoided by applying a *super homogenization*

routine [43]. This method involves iteratively adjusting the homogenized cross sections until the reaction rates in the homogeneous domain equal that of the reference domain. Because of the cost of performing the iterative procedure, super homogenization is typically not used in industrial calculations.

In all homogenization methods, the weighting flux is the central source of error; if the weighting flux is far from the actual flux, there can be significant errors introduced. This can be seen in many examples, one of which is the case when a homogenized region is surrounded by very different regions. In this case the reflective boundary conditions are a poor approximation for the state of the system [44]. One way to improve the solution in this situation is to estimate an albedo condition to impose on the boundaries. Another way to incorporate the effect of unlike neighbors is by taking several homogenization regions during the process to give a better representation of the flux gradients across boundaries where the material changes dramatically; this is known as the *color-set* method [147].

Homogenization methods are shown to work relatively well in most reactor analysis calculations. However this only directly applies to static calculations. Static calculations can be useful for many applications in reactor analysis, such as fuel shuffling optimization, shutdown margin calculations, or finding the point of maximum power during steady state operation. However, in the analysis of severe accidents, such as those induced by large reactivity insertions, these methods may break down.

When producing homogenized cross sections for use in reactor analysis, the cross sections are tabulated for various operating conditions (Fuel/Moderator Temperature, Boron Concentration, Burnup, etc.). During the full core calculation, this cross section table is interpolated to reflect the operating conditions of the core. The temperature of the Fuel/Moderator will influence the cross sections, especially in the resonance energy range; this dependence is accounted for through self shielding calculations performed at each tabulated statepoint. This usage of tabulated cross sections have been repeatedly applied to diffusion calculations with transport calculations during homogenization. However, the use of such tables in transport calculations with transport calculations during homogenization has yet to be shown valid. The author presumes that the use of such tabulated homogenized cross sections is valid for transport to transport calculations with no explicit verification that such tables do not introduce significant errors.

Self shielding is an operation conducted during the homogenization process to account for the influence of cross section resonances on the energy-dependent flux. Normally self shielding is performed during the construction of homogenized cross section tables to account for temperature and material composition changes. The use of self shielding in the present work differs from the norm by performing self shielding while producing a base cross section table. The base cross section table contains cross sections in the fine space and group structure. This cross section table is used to perform reference calculations and homogenization is performed on the cross section sets in the base table, without additional application of self shielding. The cross section table produced by homogenizing the reference

table is similar to what is used in current transient reactor analysis [111]. In a rigorous sense, the self shielding calculation should be performed at each change of temperature in the reference calculation. This however becomes costly, and the assumption is made that the effects of shelf shielding may be interpolated.

4.3 Transient Formulations

Recent work has shown that an insertion of reactivity causes a shift in the energy spectrum of the transport solution [28]. This shift is not captured by criticality calculations and requires special treatment. Thus if cross sections, produced by a homogenization process using a flux from a criticality calculation, are used in a transient calculation, significant errors can be introduced due to the failure to capture this shift. Two new methods are studied to obtain a more accurate weighting flux for transient calculations: the first is based on a time-integrated flux or *fluence* (Fluence method), and the second on an asymptotic flux expansion (Alpha method).

4.3.1 Fluence Method

The first method studied to reduce errors in transient calculations, involves introducing a weighted average in the time domain to the original homogenization equation (Equation 4.1), which then becomes

$$\sigma_x^{G,R,\mathcal{T}} = \frac{\sum_{g\in G}\sum_{r\in R}\sum_{t\in\mathcal{T}}\sigma_x^{g,r,t}\phi_{g,r,t}V_r\Delta t}{\sum_{g\in G}\sum_{r\in R}\sum_{t\in\mathcal{T}}\phi_{g,r,t}V_r\Delta t} \qquad \mathcal{T} = \mathcal{T}_1, \mathcal{T}_2, \ldots, \mathcal{T}_P, \tag{4.4}$$

for the cross section σ_x; the scattering cross section has a similar definition. Now, just as one is free to choose the homogeneous regions (R) and homogeneous energy structure (G), one is free to choose the homogeneous time mesh ($\mathcal{T}$) on which time dependent cross sections are constant. The time dependence of the cross sections will generally come from their temperature dependence, which will change throughout a transient simulation.

This formulation however, could become costly because of the need to perform a homogenization routine at each time step when the flux and cross sections have changed. To reduce the cost of this homogenization method, it is assumed that the cross section is constant over time intervals $\mathcal{T}_i$ [148]. This allows the integration over time to be performed independently of the behavior of the cross section. With this approximate weighted average taken into account, the method becomes

$$\sigma_x^{G,R,T} = \frac{\sum_{g\in G}\sum_{r\in R}\sigma_x^{g,r}\left(\sum_{t\in\mathcal{T}}\phi_{g,r,t}\Delta t\right)V_r}{\sum_{g\in G}\sum_{r\in R}\left(\sum_{t\in\mathcal{T}}\phi_{g,r,t}\Delta t\right)V_r} \qquad \mathcal{T} = \mathcal{T}_1, \mathcal{T}_2, \ldots, \mathcal{T}_P, \tag{4.5}$$

with the cross section being chosen at each state point in the cross section set. This adds another dimension to the existing cross section table, which produces a larger table. The number of state points in the new cross section table is the number of state points in the base table multiplied by the number of time intervals in $\mathcal{T}$. The main drawback to such a method is in the cost associated in obtaining the time dependent flux used to homogenize cross sections. One way to reduce the cost of obtaining such a solution is to perform the time dependent calculation on subdomains of the problem, which will be discussed in Section 4.4.2.

Usually, homogenization methods are focused on conserving reaction rates; here the conservation of a similar quantity is sought: the total reaction density over a time interval. Since the goal of this method is to explicitly conserve total reaction density over a time interval, it is desired to see if the approximation introduced in Equation 4.5 will affect the conservation of the total reaction density. The total reaction density will be defined as

$$TRD = \int_{t_0}^{t_1} \sigma\big(T(t)\big)\phi(t)\mathrm{d}t, \tag{4.6}$$

where the integral is introduced to represent a more accurate evaluation of the reaction rate. The time dependence of the cross section is present through its dependence on the time dependent temperature. Since the cross sections are interpolated linearly between temperature values, the cross section can be represented as a linear function of the temperature

$$TRD = \int_{t_0}^{t_1} \Big[\sigma_0 + \alpha\big(T(t) - T_0\big)\Big]\phi(t)\mathrm{d}t, \tag{4.7}$$

where α is the derivative of the cross section dependence on temperature. The α is valid between two evaluated temperature values T_0 and T_1, for which α is constant. Equation 4.7 makes the assumption that the temperature remains in the range $[T_0, T_{\max}]$ during the time interval $[t_0, t_1]$. However, if the temperature falls outside this range, the integral may be split into intervals for which a constant α is valid. Grouping constant terms

$$TRD = (\sigma_0 - \alpha T_0)\int_{t_0}^{t_1} \phi(t)\mathrm{d}t + \alpha\int_{t_0}^{t_1} T(t)\phi(t)\mathrm{d}t, \tag{4.8}$$

reveals that the temperature dependence can be bound by the temperature extremes for which α is constant. Meaning that the true reaction rate is bound as

$$
\begin{aligned}
TRD_{\min} &= (\sigma_0 - \alpha T_0) \int_{t_0}^{t_1} \phi(t)\mathrm{d}t + \alpha T_0 \int_{t_0}^{t_1} \phi(t)\mathrm{d}t = \sigma_0 \int_{t_0}^{t_1} \phi(t)\mathrm{d}t \\
TRD_{\max} &= \left[\sigma_0 + \alpha \left(T_1 - T_0\right)\right] \int_{t_0}^{t_1} \phi(t)\mathrm{d}t \\
TRD_{\min} &< TRD < TRD_{\max},
\end{aligned}
\tag{4.9}
$$

assuming that $T_1 > T_0$. This also leads to the observation that the closer the temperature evaluations are, the smaller the allowed deviation in the evaluated reaction density. There are two factors that will affect the accuracy of the computed reaction density: the size of the time interval, and the distance between statepoint temperatures. The preceding development also applies when cross sections are interpolated in the square root of temperature instead of linearly, as is often the case for thermal reactor analysis.

4.3.2 Theory of α - Eigenvalue Problem

The second method that was studied is based on an asymptotic expansion of the flux in the time domain. The time dependent neutron transport equation is shown in matrix form

$$
\begin{aligned}
\frac{\partial \vec{\psi}}{\partial t} &= \mathbf{v}\left(\mathbf{\Sigma_s} - \mathbf{\Sigma_t} - \mathbf{T} + \mathbf{P}_\beta \mathbf{M}\right)\vec{\psi} + \mathbf{v}\mathbf{X_d}\mathbf{\Lambda}\vec{C} \\
\frac{\partial \vec{C}}{\partial t} &= \mathbf{F}_\beta \mathbf{M}\vec{\psi} - \mathbf{\Lambda}\vec{C},
\end{aligned}
\tag{4.10}
$$

where $\mathbf{v}$ is the diagonal matrix of group-wise velocities, $\mathbf{\Sigma_s}$ is the group/space-wise scattering cross section, $\mathbf{\Sigma_t}$ is the group/space-wise total interaction cross section, $\mathbf{T}$ is the diagonal matrix of streaming terms, $\mathbf{P}_\beta$ is the matrix of prompt fission terms, $\mathbf{X_d}$ is a matrix containing columns of delayed neutron emission spectra, $\mathbf{\Lambda}$ is the diagonal matrix of delayed neutron precursor decay constants, $\mathbf{F}_\beta$ is the matrix of delayed neutron production terms, and $\mathbf{M}$ is the matrix which maps the angular flux to the scalar flux. If the cross sections are assumed to be constant in time, a solution can be postulated of the form

$$
\begin{bmatrix} \vec{\psi} \\ \vec{C} \end{bmatrix}(t) \sim \vec{E} e^{\alpha t},
\tag{4.11}
$$

which when inserted into Equation 4.10, yields the following eigenvalue problem

$$\underbrace{\begin{bmatrix} \mathbf{v}\left(\mathbf{\Sigma_s} - \mathbf{\Sigma_t} - \mathbf{T} + \mathbf{P}_\beta \mathbf{M}\right) & \mathbf{v}\mathbf{X_d}\mathbf{\Lambda} \\ \mathbf{F}_\beta \mathbf{M} & -\mathbf{\Lambda} \end{bmatrix}}_{\mathbf{L}} \begin{bmatrix} \vec{\psi} \\ \vec{C} \end{bmatrix} = \alpha \begin{bmatrix} \vec{\psi} \\ \vec{C} \end{bmatrix}. \tag{4.12}$$

This type of eigenvalue problem is referred to as the α-eigenvalue problem [64]. In contrast to the k-eigenvalue problem, that is usually solved to obtain the flux distribution in stationary problems, the α-eigenvalue problem takes into account the dynamic nature of reactors in off critical configurations. In addition to Dall'Osso showing that there is a spectral shift in time dependent problems [28], Cacuci *et al.* showed that the critical spectrum differs significantly from the spectrum that comes from an α-eigenvalue problem [56].

The spectral properties of the neutron transport operator have been extensively studied to gain insight into the behavior of such operators when numerical methods are applied to the solution of equations containing these operators. One early analysis of the spectrum of the operator $\mathbf{L}$ in Equation 4.12 gave several insights into the kinetic behavior of the eigenvalue spectrum [149]. Porsching's analysis showed that for the monoenergetic spatially dependent neutron diffusion equation, there were n eigenvalues that lie within the bounds of the $-\lambda$ values in Equation 4.12 (elements of -$\mathbf{\Lambda}$). The n corresponds to the number of spatial points used in the spatial discretization of the problem domain. The properties of the multigroup transport operator showed that, provided the lowest energy a neutron can possess is bound away from zero, the eigenvalue spectrum consists of point and line spectra [150]. However, if neutrons are allowed to exist at arbitrarily low speeds, the upper bound for the continuum is the negative of the minimum value of $v\Sigma_t(v)$ [151].

Normally, to approximate the time dependent solution to Equation 4.10, one would need a complete set of eigenvectors on which to project the solution. The expansion based on Equation 4.11 can be better described as

$$\vec{\phi}(t) = \sum_{i=1}^{M} a_i \vec{E}_i e^{\alpha_i t} + \vec{\zeta}(t), \tag{4.13}$$

where $\vec{\zeta}(t)$ is a residual term from the expansion. The residual term goes to zero as t approaches infinity despite the incompleteness of the expansion space because of the asymptotic behavior of the solution [151]. Additionally, if the minimum neutron velocity is bound away from zero, the eigenvalue spectrum does not include a continuum, which reduces the size of the residual term.

Obtaining all of the eigenvectors for the α-eigenvalue problem could be costly, but for the type of problems of interest, not all eigenvectors are important. The eigenvalues of Equation 4.12 are all negative, except for possibly one value, and most are more negative than the value of the minimum velocity times total cross section. These values are largely negative and will only contribute to the solution during very short times. To reduce the cost of obtaining α-eigenmodes, only the calculation of the $N_d + 1$ principal eigenmodes is considered.

In studying the behavior of the eigenvectors from the α-eigenvalue problem, it was observed that there are $N_d + 1$ eigenvectors that have a constant positive sign for the flux portion of the eigenvector, where N_d is the number of delayed neutron precursor groups. These vectors correspond to the $N_d + 1$ principal eigenvalues in the spectrum. This set of eigenvectors with a uniform flux sign seem to correspond to the clustering of inhour modes of Henry [152]. Henry showed that the eigenvalues for Equation 4.12 cluster within the bounds of the negative of delayed neutron decay constants with a single largest eigenvalue present in each bound; the largest eigenvalue in each interval is referred to as a principal eigenvalue. All other eigenvalues within the bounds of two consecutive decay constants are smaller than the principal eigenvalue but larger than the lower bound.

Alpha-eigenmodes can be computed by eliminating the precursor concentration equation of Equation 4.12 and rearranging terms [153, 154]. The resulting equation is

$$\left(\mathbf{\Sigma_t} + \alpha\mathbf{v}^{-1} + \mathbf{T}\right)\vec{\psi} = \left(\mathbf{\Sigma_s} + \left[\mathbf{P}_\beta + \mathbf{X_d}\mathbf{\Lambda}\left(\alpha\mathbf{I} + \mathbf{\Lambda}\right)^{-1}\mathbf{F}_\beta\right]\mathbf{M}\right)\vec{\psi}, \tag{4.14}$$

which is nonlinear in the eigenvalue α. When $\alpha = 0$, Equation 4.14 reduces to the criticality equation with $k = 1$. In this case, the α- and k-eigenvalue problems describe the same system and the dominant eigenvector ψ will be equivalent for both problems.

Alpha-eigenmodes can be computed using a standard criticality code by modifying the total cross section and fission spectrum for given values of α. The criticality code can then be used with a zero search routine to find values of α which produce a value of $k = 1$ [154]. Kaper also shows that the dominant values of α are bound by the precursor decay constants (-$\mathbf{\Lambda}$). Hence, an effective way to search for these α values is to partition the search space by the diagonal elements of -$\mathbf{\Lambda}$ and search for the principal eigenvalues in each interval [155].

4.3.3 Alpha - Method

The Alpha homogenization method is a novel technique to produce homogenized cross sections which can be used in time dependent calculations [148]. This method takes eigenvectors from the α-eigenvalue problem of Equation 4.12 and uses them as a replacement for the fundamental mode of the k-eigenvalue problem for static calculations. Using a flux that comes from an eigenvalue problem which takes into account the dynamic behavior of the system should produce homogenized cross sections that also account for spectral shifts observed for time dependent solutions.

The discussion of the previous section shows that there are many eigenvectors from the α-eigenvalue problem which can be used as a weighting flux. Characteristics of the nuclear system and transient will determine which eigenvectors are useful for homogenization.

When delayed neutron precursors are suppressed, there is a dominant eigenvalue whose sign is determined by the criticality of the system. All other eigenvalues are largely negative, which will cause these modes to be extinguished shortly after a transient starts. For problems where delayed neutron precursors are suppressed, only this dominant eigenvector is taken for the weight flux.

When delayed neutrons are present however, there are multiple eigenvalues which influence the time dependent solution long after the transient begins. Contrary to the case with no delayed neutron precursors, these modes are not extinguished shortly after the transient begins. When delayed neutrons are present, a combination of several modes is used to produce a weighting flux for the homogenization process.

One way to combine eigenvectors for the alpha method would be to use the expansion Equation 4.13 with the residual term ignored as the time dependent flux appearing in the Fluence method. The expansion coefficients are calculated based on the initial condition. The integral of the time dependent flux can be performed analytically as

$$\int_{t_0}^{t_1} \mathrm{d}t\ \phi(t) = \sum_{i=1}^{M} \frac{a_i(e^{\alpha_i t_1} - e^{\alpha_i t_0})}{\alpha_i} \vec{E}_i + \underbrace{\int_{t_0}^{t_1} \mathrm{d}t\ \vec{\zeta}(t)}_{\text{assumed zero}}, \tag{4.15}$$

where the residual term $\vec{\zeta}(t)$ is approximated as zero, and the value of M can be an integer between 1 and $N_d + 1$, inclusive. This combination of eigenvectors incorporates the tools of both the α-eigenvalue problem, and the Fluence method. It reduces the cost of obtaining a time dependent solution for the Fluence method, and produces time dependent cross sections which provide important eigenvectors when they are most influential during a transient.

Another way to apply the Alpha method is through constructing a linear combination of α-eigenvectors to use in the homogenization problem like

$$\vec{\phi} = \sum_{i=1}^{M} a_i \vec{\phi}_i, \tag{4.16}$$

where the a_i are coefficients determined from a minimization of the initial condition projected onto the subspace spanned by the eigenvectors. The linear combination can be constructed using all $N_d + 1$ principal eigenvectors, or a subset of these vectors. Several subsets will be used throughout the results portion of this work. A few examples include the single dominant eigenvector, the largest and smallest principal eigenvectors (extrema), and all $N_d + 1$ vectors.

Using the eigenvector associated to the single largest eigenvalue is used for cases where delayed neutron precursors are suppressed. This subset works well because the less dominant modes for the transient are extinguished quickly after the transient begins, and much of the transient is governed by the evolution of this single mode. It will be shown however, that when delayed neutrons are present this subset is inadequate in producing homogenized cross sections which reproduce characteristics of the reference transient. This behavior can be attributed

to the transient being governed by non-dominant modes for longer times after the transient begins.

The next subset which is investigated takes both the eigenvector with the largest eigenvalue, and with the smallest principal eigenvalue (extrema). This subset was investigated to incorporate two time constants of the transient simultaneously: the fast behavior of prompt fission, and longer lived delayed neutron behavior. These two eigenvectors are chosen to take into account the fast behavior present just after the transient begins as well as the behavior associated with the asymptotic mode longer after the transient begins. An important aspect of choosing these modes as a weighting flux, is the relative weight given to each mode. These weights are chosen based on the initial condition, much like how expansion coefficients would be chosen for time dependent problems. However, since the two eigenvectors will not form a complete set, a minimization is performed to obtain the expansion coefficients. In this way, the eigenvectors are weighted in a way which would best reproduce the initial condition given the set of expansion vectors. Alternatively, a solution other than the initial flux could be used to determine expansion coefficients. However, since the initial condition for the flux is specified for the calculation, this solution is chosen for obtaining the expansion coefficients.

The third subset is similar to the previous subset of the extrema of principal eigenvalues, however all principal eigenvectors are taken to produce a weighting flux for homogenization. This subset is expected to cover a wider time range than the previous subsets because of the larger number of eigenvectors present in the set. The expansion coefficients are obtained in the same way: a minimization problem with the initial condition.

In the preceding discussion, several homogenization techniques are introduced. Table 4.1 shows a summary of the homogenization methods treated in the next section.

Table 4.1. Summary of Characteristics for Homogenization Methods

Homogenization Method	**Treatment of Self Shielding**	**Weighting Flux**	**Cross Sections Used in RHP****	**Cross Sections Produced**
Critical	Pre-calculated prior to homogenization for each state point*	Fundamental k-eigenvalue for each state point*	Fixed based on state point*	Table of cross sections corresponding to state points*
Fluence	Evaluated with each change of temperature during transient or pre-calculated for each state point*	• Time-dependent flux • Result of transient calculation in RHP** and, • Integrated over time interval	Interpolated between state points* at each evaluation of solution residual (time dependent through temperature)	Table of cross sections corresponding to state points* per time interval
Alpha	Pre-calculated prior to homogenization for each state point*	• Time dependent expansion of α-eigenmodes, integrated over time intervals • Combination of α-eigenvectors, weighted based on initial condition or, • Single dominant α-eigenvector	Fixed based on state point*	Table of cross sections corresponding to state points* or state points* per time interval

*State point - A combination of state parameters for which the characteristics of the system are pre-calculated. This assumes that the system may be found exactly at a state point or in its vicinity so that characteristics may be approximated by interpolation between state points.

**RHP: Reference Homogenization Problem - Geometric subdomain (assembly or color-set, possibly with leakage model, that is representation of subdomain within core). Used to obtain weighting flux for homogenization. Flux calculation may be static or time-dependent, depending on homogenization method.

4.4 Application of Kinetic Homogenization

As was stated in the previous section, the crucial point in homogenization is to correctly predict the heterogeneous flux used to weight cross sections. This section explores several examples where the flux used to weight cross sections is not sufficiently close to the reference flux. A spatially homogeneous geometry with energy dependence is first studied to open the idea of examining homogenization techniques for time dependent problems. The second is a spatially heterogeneous geometry to introduce more complications in the homogenization process and set the stage for future work in the domain of kinetic homogenization.

4.4.1 Homogeneous Medium

The first application of kinetic homogenization focuses on a homogeneous spatial geometry of a uranium dioxide (3.4% ^{235}U) and borated water mixture, which was previously studied by the author in [148]. The nominal material concentrations for this mixture are given in Table 4.2. Macroscopic cross sections in 281 energy groups were generated by APOLLO3® [156]. APOLLO3® uses its base cross section library generated by the GALILE [157] nuclear data processing system, which is based on the CALENDF [158] and NJOY [159] packages. GALILE is managed as a separate project, external to APOLLO3®, which also produces pointwise cross section data for the Monte Carlo code TRIPOLI4® [160]. Raw microscopic cross section data used in these results is taken from the JEFF-3.1 [161] evaluated nuclear data file set.

Table 4.2. Material Concentrations for the Homogeneous UO_2 and Borated Water Mixture

Material	Nominal Conc. [$b^{-1} \cdot cm^{-1}$]
^{235}U	7.0669E−4
^{238}U	2.1811E−2
^{16}O	4.5035E−2
H_2O	2.3709E−1
^{10}B	2.2120E−5
^{11}B	8.9037E−5

Homogeneous cross sections were generated by APOLLO3®, using the solution from a representative LWR lattice as a weight function, for various temperature and boron concentration values. The temperature of the mixture is defined by the uranium and water temperatures individually. However, the cross section table is generated in such a way that the mixture temperature can be related to a single temperature; in this example, the uranium temperature is chosen as the reference temperature for the mixture. The statepoints at which cross sections are evaluated are shown in Figure 4.1, where interpolation parameters are given as the mixture temperature deviation (ΔT) and the boron concentration as a

percentage of the nominal value.

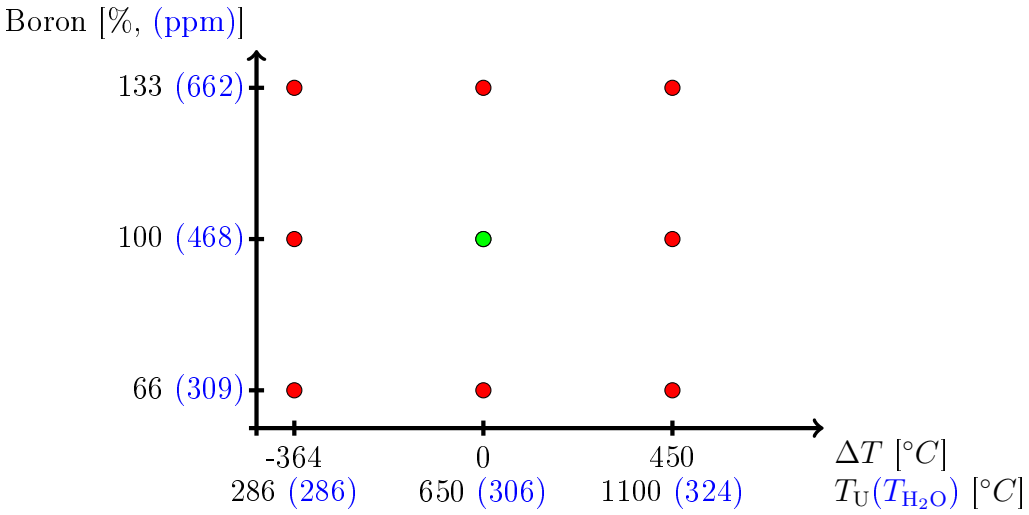

Figure 4.1. State Point Space with Interpolation Parameters: Fuel Temperature Deviation (ΔT) and Percent Boron (%). Central Point (green) Corresponds to the Nominal State. Absolute Values of Interpolation Values Included on Respective Axes.

All cross sections are generated taking into account cross section self shielding effects based on the specified state point configuration. The self shielding routine is not further conducted during the energy condensation and spatial homogenization routines studied in this chapter. Implementing the self shielding routine in the homogenization process is more straight forward for the Alpha method presented earlier because of its similarity to classical homogenization methods. The structure of the cross section table produced by the Alpha method is identical to the table produced by the Critical method; meaning any features of the critical method can be translated to the Alpha method. However, the Fluence method poses more difficulties because of the changing temperature over the time intervals. A rigorous treatment of the temperature dependence would recalculate self shielding effects at each time step where the temperature had deviated. However, to reduce the cost of this treatment, self shielding effects are computed at the state points specified in the cross section table when the base cross section table is produced. In standard reactor analysis, self shielding is accounted for during the homogenization and group condensation step to produce a cross section table that has self shielded cross sections at each state point. Here there is an intermediate step to create the reference cross section table. The reference cross section table is used in the reference calculation, afterwhich the reference cross section table is put through the homogenization and condensation routine. In all cases, whether using reference or homogenized cross section values, the table produced is similar to what is used in current reactor analyses [111].

The state points are chosen to envelop the expected temperature range for the transient. The cross sections are interpolated linearly between state points during the transient simulation. The interpolation law for each parameter is specified

in the cross section table. The choices of laws are: constant, linear, quadratic, and upstream. A constant interpolation law is a nearest neighbor interpolation, while the linear and quadratic laws use a linear or quadratic interpolation function between state points along a given axis. The upstream interpolation law is one that uses the lower bound of an interpolation interval as the result of the interpolation. This upstream law is useful for having a constant interpolation parameter during the full interval; contrary to the constant law, which will switch interpolation values at the midpoint of the interpolation interval. This upstream law is primarily used to interpolate along the time axis where cross sections are constant within the time interval. The interpolation routine was developed based on the assumption of a Cartesian grid of state points with n parameters. The n parameters form an n-dimensional interpolation space. The multidimensional interpolation is performed by recursively reducing the interpolation space along a given interpolation axis.

The initial condition for this simulation is that of a steady state critical system with a uniform temperature. The critical system is developed by performing a criticality calculation at the nominal state point; the system is made critical by normalizing the fission cross section by the value of k_{eff}. To avoid introducing a bias between state points, the fission cross section for all state points is normalized by the same value of k_{eff}. The initial uniform temperature is set at 650 °C and the scalar flux is normalized such that the power is $10\,\text{W} \cdot \text{cm}^{-3}$. The system is perturbed at 0.1 s by instantaneously changing the boron concentration by a certain percentage, where the concentration of boron remains constant. Later in the transient, at 0.2 s, the boron concentration is returned to its original value which produced a critical configuration; the system is likely to be subcritical at this point because of the temperature deviation. This reactivity insertion is driven by a step function of the boron concentration; more realistic reactivity insertions can be used such as a ramp insertion to simulate rod movement, but a step insertion is sufficient to explore the behavior of kinetic homogenization techniques.

The adiabatic temperature model (Equation 2.35), described in Section 2.2.1, is used for this homogeneous problem. The power for the homogeneous medium is explicitly given in the adiabatic model as

$$\frac{\partial T}{\partial t} = \kappa \sum_r \left(\sum_g \varepsilon_g \Sigma_{f,g,r}(t) \phi_{g,r}(t) \right) V_r - \kappa P_0, \tag{4.17}$$

where κ is a heat generation constant, ε_g is a fission energy deposition constant, $\phi_{g,r}$ is the scalar flux for group g in a region r, V_r is the volume of the region r, and P_0 is the initial power level. The time dependent heat sink of Equation 2.35 becomes the initial power times the heat generation constant to force an steady state solution when the simulation starts.

The homogeneous geometry is used in two cases where either delayed neutron precursors are enabled or suppressed to see their effect on the homogenization schemes presented.

Case Without Delayed Neutron Precursors

The simpler case with delayed neutrons suppressed is discussed presently. Delayed neutrons can be suppressed by setting the delayed neutron fraction (β) to zero, which will physically mean that all neutrons are released immediately from the fission event. The suppression of delayed neutrons affects the kinetics by removing slower evolving modes and allowing the time dependence to be governed solely by the neutron generation time. The kinetics are then governed principally by the slowest moving prompt alpha mode, and all other modes vanish much more quickly.

The subsequent power and temperature profiles, Figures 4.2 & 4.3, were generated by first performing a reference calculation with 281 energy groups. The same transient was then repeated using homogenized cross sections generated from the various methods discussed earlier. The classical homogenization method is denoted as *Critical* because of the use of a k-eigenvalue or criticality calculation to obtain the weighting flux. The new homogenization methods (*Fluence* & *Alpha*) are denoted as such in the figures.

For these transients, the time interval boundaries used in the Fluence method are $\partial\mathcal{T} = \{0.0, 0.1, 0.14, 0.16, 0.2, 0.3\}$. The initial state of the system is one of equilibrium, where the power and temperature are constant in time. This state is achieved by evaluating the k-eigenvalue of the nominal state point and normalizing the production cross section, $\nu\Sigma_f$, by this value at each state point. The normalization of all state points biases the cross sections at each state point in the same direction. Thus an equivalent reactivity insertion can be observed despite the normalization of the nominal cross section set. This normalization is also performed when using homogenized cross sections, however since the normalization is propagated through the homogenization process, this normalization is on the level of machine precision.

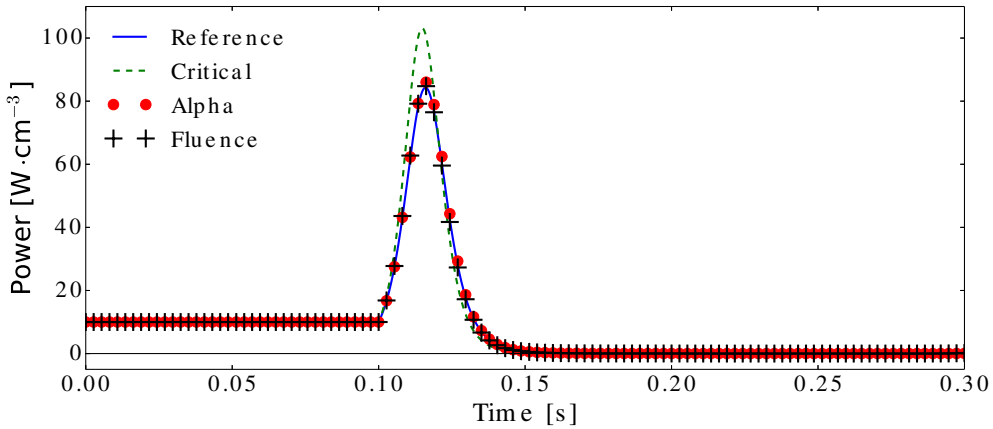

Figure 4.2. Transient Power. Spatially Homogeneous Geometry with No Delayed Neutron Precursors. Boron Concentration Reduced to 99% of Nominal Value.

Figures 4.2 & 4.3 show the power and temperature for the transient performed with three homogenization techniques. The transients in Figures 4.2 & 4.3 cor-

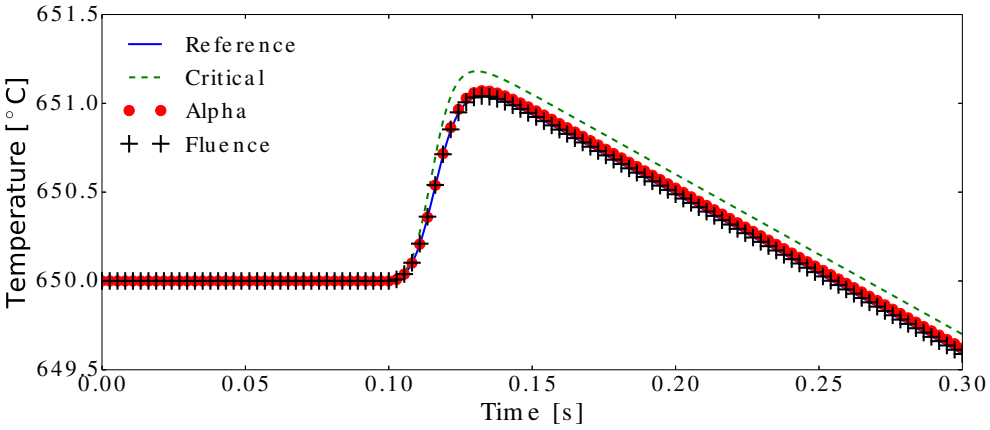

Figure 4.3. Transient Temperature. Spatially Homogeneous Geometry with No Delayed Neutron Precursors. Boron Concentration Reduced to 99% of Nominal Value.

respond to the boron concentration being reduced to 99% of the nominal value ($\rho = 110\,\text{pcm}$) at 0.1 s; transients with homogenized cross sections were performed with the 2-group structure shown in Table 4.3. Several features of these transients stand out in Figures 4.2 & 4.3. First, when the system is in a critical state initially, all homogenization methods yield exactly the correct value for the power and temperature. This supports the observation that the classical homogenization method is useful in static reactor analysis. There is also good agreement when the flux is near zero at the end of the transient, however this is due to the low value of the flux during this time. The system at the end of the transient is in a subcritical state due to the rise in temperature; since the nuclear system is not in a critical state, the flux for each method will differ slightly. However since at this point the power is nearly zero, the differences among fluxes are not noticeable.

Table 4.3. Energy Group Structure for Homogenization Routines Used in Homogeneous Medium Geometry. The Group Cutoff Refers to the Group Number of the 281 Energy Group Structure

Groups	Energy Cutoff [eV]	Group Cutoff
2	0.21	260
3	0.21	260
	0.04	272
6	951E3	22
	9.5	143
	0.21	260
	0.09	266
	0.015	276

Quantitatively it can be seen that the power transient for the case with classi-

cally homogenized cross sections does not follow the reference power very closely once the system is perturbed; this behavior is also observed in the temperature. Conversely, the Alpha & Fluence methods seem to work very well at following the power of the reference calculation. The temperature increase in this simulation is small in magnitude due to the simplified heat transfer model. The moderator will typically have a larger feedback constant than the fuel temperature in LWRs, and a small increase in the moderator temperature will have a large impact on the reactivity of the system. Since the moderator and fuel temperature are linked in this homogeneous case, a small increase of the medium temperature will cause a large reduction in the reactivity of the system.

To more quantitatively characterize the transients, several metrics are displayed in Table 4.4. Additionally, two more reactivity insertions are introduced which correspond to 98%($\rho = 220\,\text{pcm}$), and 94%($\rho = 661\,\text{pcm}$) of the nominal boron concentration. The metrics used to compare the various homogenization methods are the relative error in: maximum power, time of maximum power, total deposited energy, and the maximum temperature.

Table 4.4. Comparison of Three Homogenization Methods By Relative Error in Maximum Power, Peak Time, Total Energy, and Maximum Temperature. Homogeneous Medium Case, Collapsing Fom 281 to 2 Energy Groups Without Delayed Neutron Precursors.

		Relative Error* [%]			
Boron	**Method**	**Max Power**	**Peak Time**	**Energy**	**Max Temp.**
	Reference	$84\,\text{W}\cdot\text{cm}^{-3}$	0.116 s	2.56 J	651.1 °C
99%	Critical	22.53	1.03	4.90	2.17E−2
	Alpha	2.04	0.13	1.39	4.58E−3
	Fluence	0.66	0.13	0.08	2.61E−5
	Reference	$256.7\,\text{W}\cdot\text{cm}^{-3}$	0.112 s	3.59 J	652.1 °C
98%	Critical	27.37	0.94	7.97	4.28E−2
	Alpha	2.46	0.00	1.88	9.09E−3
	Fluence	0.77	0.13	0.05	4.98E−5
	Reference	$1.93\,\text{kW}\cdot\text{cm}^{-3}$	0.106 s	8.00 J	656.2 °C
94%	Critical	29.60	0.57	10.90	1.22E−1
	Alpha	2.78	0.00	2.42	2.65E−3
	Fluence	0.69	0.14	0.04	2.58E−4

*Relative error calculated with absolute value of difference, normalized by reference value

The error for the time of maximum power sometimes shows as zero; this is a consequence of the time discretization used for the simulation. The error of being off by a single time step is ∼0.13% which is the value shown for many of the Fluence calculations. Here, a constant time step of 1.5E−4 s is used and further refinement does not significantly influence the remaining metrics.

The results in Table 4.4 show that the Alpha and Fluence methods reduce the errors, when compared to the Critical method, for each metric significantly and for the three reactivity insertions studied. Compared to the Critical method, the Alpha method reduces the error in maximum power by about 90% and the deposited energy error is reduced by about 75% for all reactivity insertions. The reduction of the deposited energy error translates to a similar reduction in the maximum temperature error. An exception occurs for the largest reactivity insertion for which a 78% reduction in the deposited energy error results in a 98% reduction in the maximum temperature error; because of this discrepancy, it is suspected that the transient is evolving too quickly for the chosen time step size and thus there is not a great estimate of the deposited energy presented in Table 4.4. The Alpha method seems to work very well in the situation where delayed neutron precursors are suppressed. In this configuration without delayed neutron precursors, the asymptotic solution is reached very quickly due to the large negative values of the non-dominant eigenvalues of Equation 4.12. Hence, the solution to this situation is dominated by a single eigenmode for nearly the entire simulation. However, because of the temperature dependence, the spectrum is constantly changing throughout the simulation. If the solution is smoothly varying between statepoints, the interpolation between state points will not introduce large errors during the simulation.

The Fluence method also performs well in this situation. The maximum power error is reduced by 97% from the Critical method, and the deposited energy error is reduced by 99%. Again, the reduction in deposited energy error translates to a reduction in maximum temperature error. Since the Fluence method is based on the time integrated flux during a transient, the estimate for the deposited energy should be accurate. Additionally, the temperature deviation is small compared to the distance between state points: $6.2\,^{\circ}\mathrm{C} \ll 1450\,^{\circ}\mathrm{C}$. This implies that, in this case, the total reaction density estimated at a state point will accurately estimate the total reaction density during the entire simulation.

To quantify the metrics used in Table 4.4, the reference values are also included to give an idea of the size of each metric. Note that the relative errors are calculated with an absolute value of the difference from the reference value. In general, the use of the classical homogenization technique performs the worst for all cases studied. The Fluence method performs the best, especially in the total energy deposited because of this quantity's strong dependence on the integral of the time dependent flux. In such prompt transients, the energy deposition in the fuel is a close indication of the maximum temperature, which is generally the basis for many safety regulations on the fuel [162]. Hence obtaining a precise result for this parameter is important when considering the modeling of severe accident transients.

Several energy group structures are evaluated and compared to determine if there is any impact on the new homogenization methods; results from using these group structures are shown in Tables 4.5 & 4.6. Table 4.3 shows the homogenized group structures that were tested. In all group structures, the energy is bound by 19.6 MeV, and the group cut-off shown in the table refers to the group number of the 281 group structure.

Table 4.5. Comparison of Three Homogenization Methods By Relative Error in Maximum Power, Peak Time, Total Energy, and Maximum Temperature. Homogeneous Medium Case, Collapsing Fom 281 to 3 Energy Groups Without Delayed Neutron Precursors.

		Relative Error* [%]			
Boron	**Method**	**Max Power**	**Peak Time**	**Energy**	**Max Temp.**
99%	Critical	19.75	1.03	3.39	1.66E−2
	Alpha	1.01	0.00	0.69	2.29E−3
	Fluence	0.80	0.13	0.10	3.23E−5
98%	Critical	23.95	0.94	5.90	3.27E−2
	Alpha	1.23	0.00	0.94	4.54E−3
	Fluence	0.94	0.13	0.06	2.64E−6
94%	Critical	25.78	0.71	8.23	9.22E−2
	Alpha	1.39	0.00	1.21	1.32E−2
	Fluence	0.90	0.14	0.04	2.87E−4

*Relative error calculated with absolute value of difference, normalized by reference value

Table 4.6. Comparison of Three Homogenization Methods By Relative Error in Maximum Power, Peak Time, Total Energy, and Maximum Temperature. Homogeneous Medium Case, Collapsing Fom 281 to 6 Energy Groups Without Delayed Neutron Precursors.

		Relative Error* [%]			
Boron	**Method**	**Max Power**	**Peak Time**	**Energy**	**Max Temp.**
99%	Critical	5.66	0.26	1.16	5.47E−3
	Alpha	0.67	0.00	0.46	1.50E−3
	Fluence	0.51	0.13	0.06	2.04E−5
98%	Critical	6.84	0.27	1.97	1.08E−2
	Alpha	0.81	0.00	0.62	2.98E−3
	Fluence	0.59	0.13	0.04	1.98E−6
94%	Critical	7.31	0.14	2.74	3.06E−2
	Alpha	0.91	0.00	0.79	8.68E−3
	Fluence	0.54	0.00	0.03	1.94E−4

*Relative error calculated with absolute value of difference, normalized by reference value

Among all energy group structures, the effectiveness of the new homogenization methods seem to be weakly dependent on the reactivity insertion. This weak dependence on reactivity is the case for no delayed neutron precursors, because the time-dependent solution reaches the asymptotic solution very quickly after the perturbation. Similar behavior is observed when using a larger number of groups in the homogenized cross sections; the new methods outperform the Crit-

ical method. An interesting theme to note is that as the group structure for the Critical method increases, the errors are reduced. In the limiting case where the number of homogenized cross section groups is increased to 281, the weight flux would have no impact and the original reference cross sections would be recovered. However, the Critical method does not outperform the new methods, even when comparing the Critical method in 6 groups to the new methods in 2 groups. The reduction in error for the critical case when the number of groups is increased indicates that the larger group structure is able to better capture the spectral shift from the reactivity insertion, but the transient spectrum is still not well represented by a critical fundamental mode flux.

From the results studied using a very simple model (infinite homogeneous medium with no delayed neutron precursors), it is evident that using cross sections homogenized with a fundamental mode flux from a k-eigenvalue calculation introduces significant errors when used in a transient calculation. The flux during the transient is simply far from the fundamental mode flux.

Case With Delayed Neutron Precursors

Delayed neutron precursors are those isotopes which release a neutron after several beta decays of fission products, much later than neutrons emitted directly from the fission event. Their presence causes reactors to respond in much more manageable times, on the order of seconds rather than femtoseconds. Their presence also changes the spectrum of the α-eigenvalue problem operator. Instead of there being a single dominant eigenvalue, whose sign is determined by the sign of the reactivity insertion, and all other eigenvalues being orders of magnitude smaller, there are eigenvalues distributed between the negative of delayed neutron decay constants (-$\mathbf{\Lambda}$). The existence of several principal eigenmodes will alter the way the Alpha method is used. In the case of the infinite homogeneous problem, there is a single eigenvalue bound between each decay constant of $-\mathbf{\Lambda}$.

The same transient is performed as in the previous section but with delayed neutron data coming from an 8-group precursor model provided by APOLLO3®. The 8 group delayed neutron data is compiled in Table 4.7, with the 281 g delayed neutron emission spectra omitted for brevity. The β values for each isotope are calculated by taking the average over energy of the ratio $\frac{\nu_d}{\nu}$. Group dependent β values are then calculated by multiplying by a relative abundance for each precursor group.

Three reactivity insertions are studied for the case with delayed neutron precursors present: a subcritical insertion ($\rho = -1092$ pcm, -\$0.84, Boron = 110%), a supercritical insertion ($\rho = 1103$ pcm, \$0.85, Boron = 90%), and a super prompt critical insertion ($\rho = 2206$ pcm, \$1.71, Boron = 80%). A super prompt critical reactivity insertion is any insertion where $\rho \geq \beta = 1293$ pcm. The following paragraphs are a qualitative discussion of the results of these reactivity insertions.

The first subcritical transient, for which $\rho < 0$ (Figures 4.4 & 4.5), shows the power and temperature when the boron concentration is increased to 110% of the nominal value, causing the system to be in a subcritical state. The power of this insertion drops very quickly to $\sim 6\,\mathrm{W \cdot cm^{-3}}$ and then eventually starts

Table 4.7. Delayed Neutron Precursor Constants Generated by APOLLO3®. 281 group Delayed Emission Spectra Omitted for Brevity.

Group	Fraction (β)		Decay Constant (λ) [s^{-1}]
	^{235}U	^{238}U	
1	0.0002131	0.0001626	0.0124667
2	0.0010004	0.0020126	0.0282917
3	0.0005938	0.0007257	0.0425244
4	0.0012798	0.0026513	0.133042
5	0.0021502	0.0056895	0.2924672
6	0.0005866	0.0038319	0.6664877
7	0.0005275	0.0024771	1.634781
8	0.0001488	0.0018017	3.5546
	0.0065002	0.0193525	

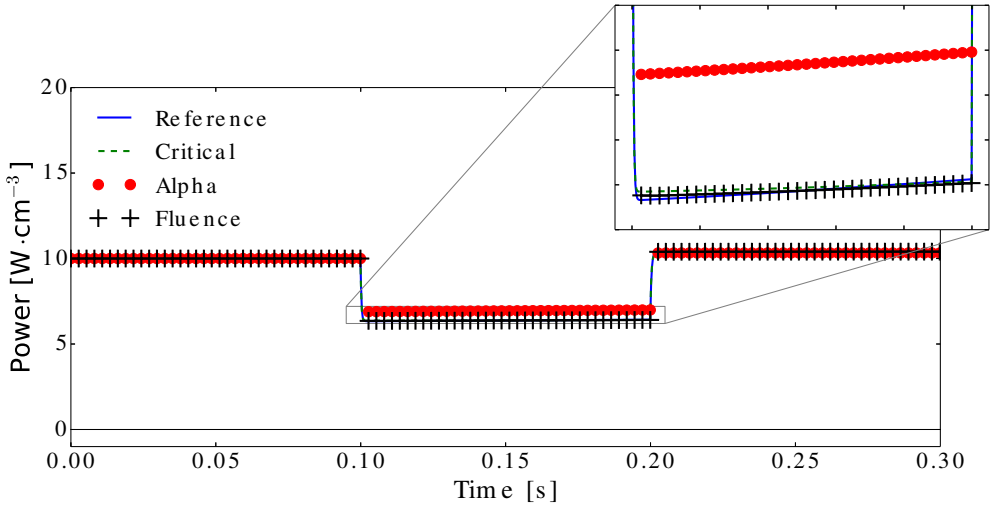

Figure 4.4. Transient Power. Spatially Homogeneous Geometry with Delayed Neutron Precursors and a Reactivity Removal.

to increase slowly until the boron concentration is returned to its original value. The slow increase in power is not visible in Figure 4.4, but is present because the decrease in temperature slowly adds reactivity to the system. In this regard, the temperature feedback shows its stabilizing properties to keep the reactor power constant. The quick reduction in power is synonymous with the prompt drop described by point reactor kinetics, but often the reactivity insertion is much larger than what the decrease in temperature can counteract.

The prompt drop (or jump) can be approximated by assuming the delayed neutron precursor concentration remains constant for times just after the instantaneous reactivity insertion and that the neutron population responds instantaneously to the reactivity insertion. By rearranging terms in Equation 4.12 after setting $\alpha = 0$, we have the relation

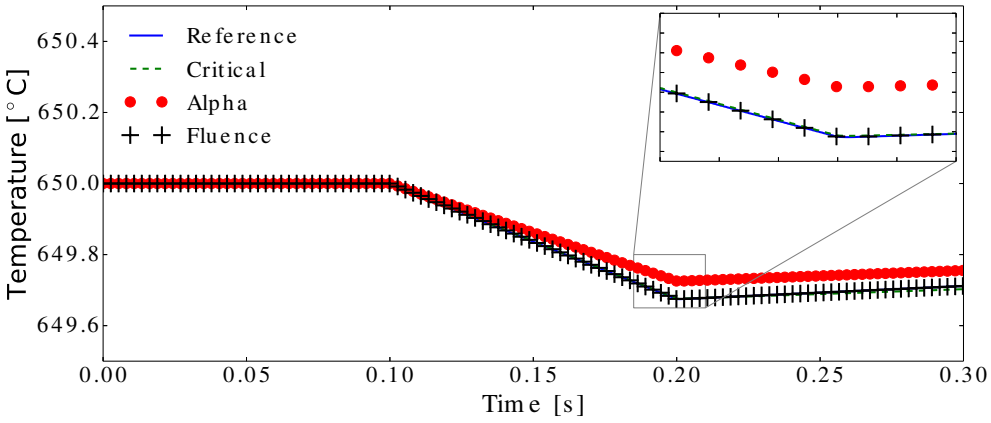

Figure 4.5. Transient Temperature. Spatially Homogeneous Geometry with Delayed Neutron Precursors and a Reactivity Removal.

$$P^{+} = \mathcal{P}\left(\mathbf{\Sigma_t} + \mathbf{T} - \mathbf{\Sigma_s} - \mathbf{P}_\beta\mathbf{M}\right)^{-1}\mathbf{X_d}\mathbf{F}_\beta\mathbf{M}\vec{\psi}_0, \tag{4.18}$$

which gives the power just after the reactivity insertion. The matrix $\mathcal{P}$ maps a flux to the integral power; note that $\vec{\psi}_0$ is normalized such that $\mathcal{P}\vec{\psi}_0$ gives the initial power. Applying Equation 4.18 to the subcritical case gives a power just after the insertion of $6.33\,\mathrm{W}\cdot\mathrm{cm}^{-3}$. This value of ∼60% of the initial power, is higher than the value that is quoted in texts referring to a system of only ^{235}U which is ∼6% [163]. However, the value quoted in texts is also for a reactivity insertion to shutdown the reactor; these insertions are typically much larger than the insertion shown here. Figure 4.4 shows that the critical homogenization method represents the power transient well in this situation. This close agreement suggests that the time dependent flux is close to the fundamental mode flux during this transient. The Alpha method however seems to drift from the reference transient and deviates significantly in Figure 4.5. In the figures presented, the single dominant eigenvector is taken for the Alpha method to show the inadequacy of the Alpha method version when delayed neutron precursors are present. This behavior suggests that the time dependent solution does not reach the asymptotic alpha solution quickly during the transient.

The second transient studied in this section is a supercritical transient for which $0 < \rho < \beta$. Figures 4.6 & 4.7 show the power and temperature, where the power increases quickly to a maximum value then decreases slowly until the boron concentration is returned to its nominal value. Figure 4.6 does not show a prompt jump followed by a slower increase in power as is expected in reactor kinetics due to the temperature feedback introduced. The slow decrease in power is characteristic of a subcritical reactor with delayed neutron precursors present. Again looking at Figures 4.6 & 4.7, the Critical method appears to perform well. This suggests that because of the delayed neutron precursors' influence on the transient, the time dependent flux is close to the fundamental mode flux. As with the subcritical case, the Alpha method does not perform very well because of the long time it takes for the time dependent solution to reach the asymptotic solution. Again, the single dominant eigenvector is taken for the Alpha method to

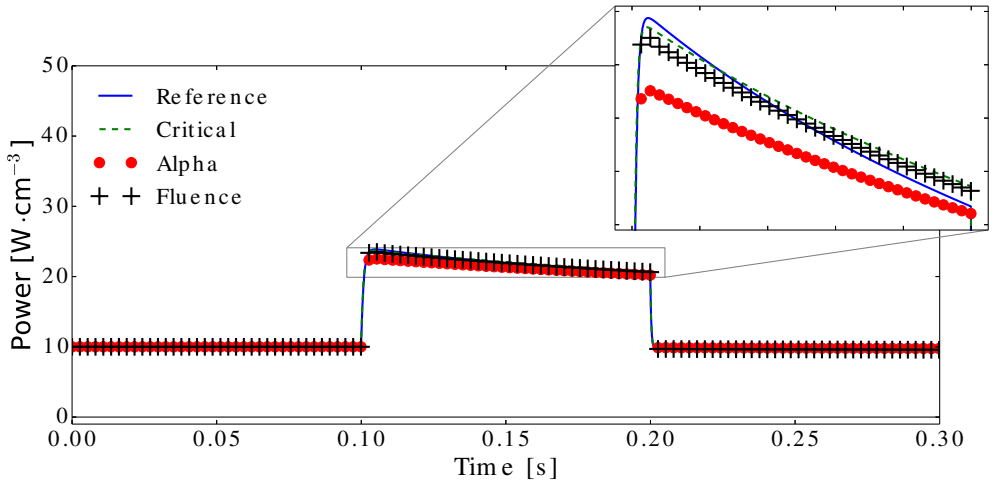

Figure 4.6. Transient Power. Spatially Homogeneous Geometry with Delayed Neutron Precursors and a Reactivity Insertion $\rho < \beta$.

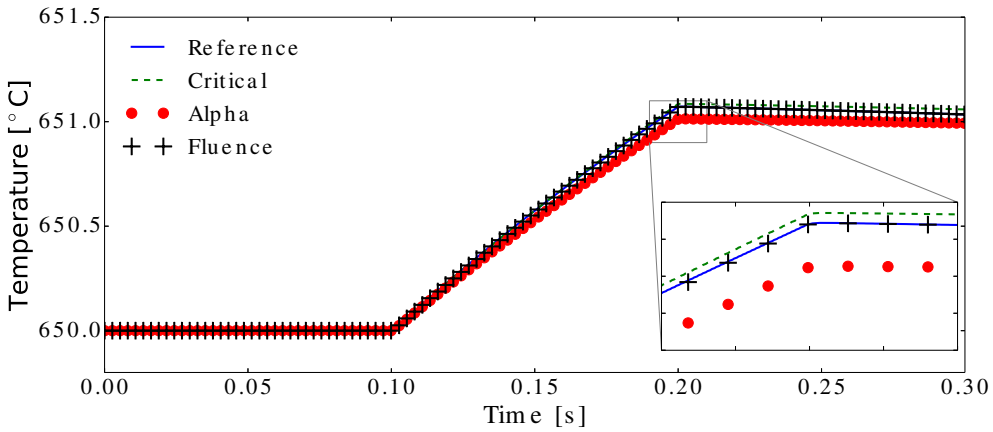

Figure 4.7. Transient Temperature. Spatially Homogeneous Geometry with Delayed Neutron Precursors and a Reactivity Insertion $\rho < \beta$.

show its inadequacy when delayed neutron precursors are present. This behavior could justify the use of critically homogenized cross sections to model operational transients, where the reactivity insertions are far from the prompt critical cutoff.

The last transient studied in this section is the super prompt critical transient, where $\rho > \beta$ and delayed neutron precursors do not influence the evolution of the reactor power. In Figure 4.8 the power increases rapidly until a maximum where the temperature increase in Figure 4.9 is sufficiently large as to counteract the reactivity insertion. The power then rapidly decreases and finishes in a long tail due to delayed neutron emission, whereafter the boron concentration is returned to its nominal value. From the figures, it is seen that the Critical method does not accurately predict the power transient, while the Fluence and Alpha methods perform well. The Alpha method performs very well, but this is because the version of the Alpha method shown in Figures 4.8 & 4.9 is not the same as in the previous reactivity insertions. The version of the Alpha method shown in Figures

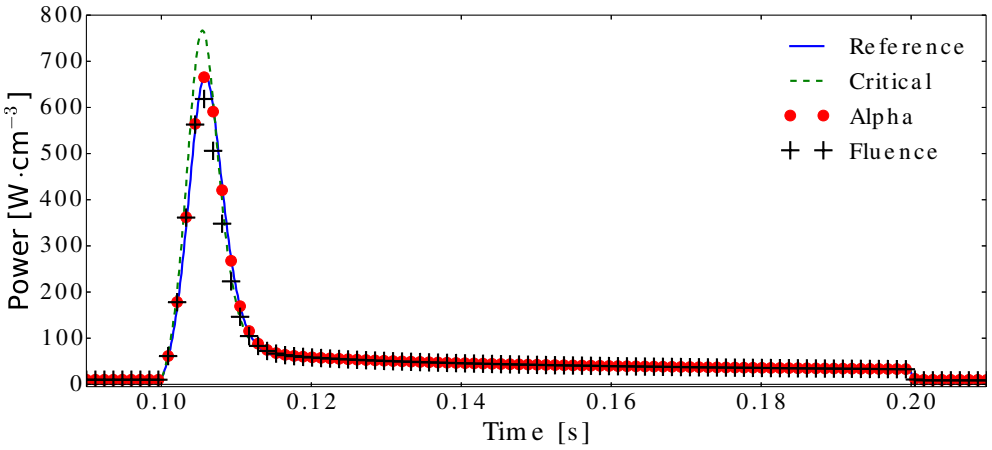

Figure 4.8. Transient Power. Spatially Homogeneous Geometry with Delayed Neutron Precursors and a Reactivity Insertion $\rho > \beta$.

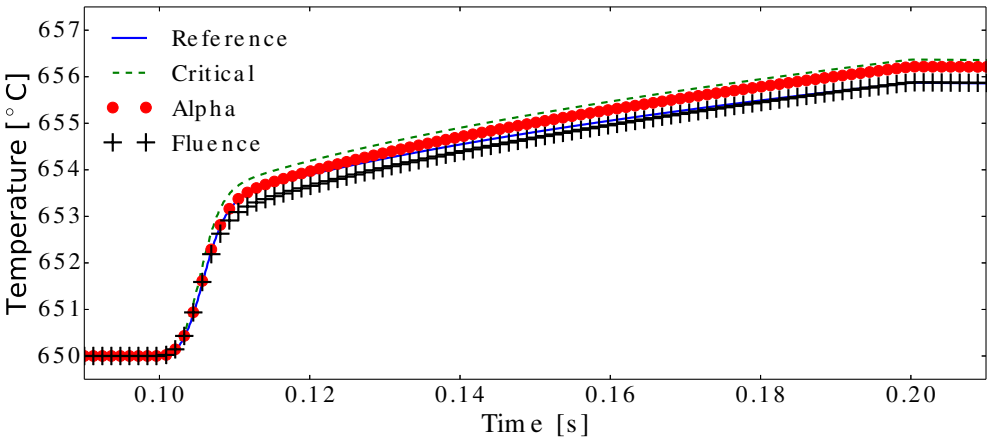

Figure 4.9. Transient Temperature. Spatially Homogeneous Geometry with Delayed Neutron Precursors and a Reactivity Insertion $\rho > \beta$.

4.8 & 4.9 takes the time dependent flux expansion and analytically evaluates the integral over time intervals (Equation 4.15) for the Fluence method. For this case, it is shown that the combination of the Fluence and Alpha methods performs much better than the two methods separately.

To better quantify the transients shown in Figures 4.4 – 4.9, Table 4.8 shows the various metrics discussed previously for the case with no delayed neutron precursors. Additionally, there are three versions of the Alpha method presented in the table; these correspond to projecting onto the space of all N_d+1 dominant vectors (N), projecting onto the space made of the extrema eigenvectors (2), and using the N_d+1 expansion as the time dependent solution in the Fluence method (F).

The subcritical transient presents a special case because the maximum power is reached after the boron concentration is returned to its nominal value. Since the temperature decreases while the boron concentration is in a perturbed state, when the boron concentration is returned to its nominal concentration, the reactor is in

Table 4.8. Comparison of Three Homogenization Methods By Relative Error in Maximum Power, Peak Time, Total Energy, and Maximum Temperature. Homogeneous Medium Case, Collapsing Fom 281 to 2 Energy Groups With Delayed Neutron Precursors. Reactivity Insertions are 110%(Removal), 90%($\rho < \beta$), and 80%($\rho > \beta$).

		Relative Error* **[%]**			
Boron	**Method**	**Max Power**	**Peak Time**	**Energy**	**Max Temp.**
	Reference	$10.40\,\mathrm{W \cdot cm^{-3}}$	0.23–0.24 s	3.57 J	650.0 °C
	Critical	1.03		0.37	
110%	Alpha (N)	0.75		1.82	
	Alpha (2)	0.77		0.38	
	Alpha (F)	0.00		0.00	
	Fluence	0.01		0.00	
	Reference	$23.9\,\mathrm{W \cdot cm^{-3}}$	0.105 s	4.16 J	651.1 °C
	Critical	0.72	0.43	0.65	2.06E−3
90%	Alpha (N)	5.65	0.43	1.13	8.98E−3
	Alpha (2)	8.70	0.43	2.50	1.69E−2
	Alpha (F)	0.16	1.72	1.15	4.69E−3
	Fluence	1.21	0.43	0.003	3.65E−5
	Reference	$668.4\,\mathrm{W \cdot cm^{-3}}$	0.106 s	9.40 J	655.9 °C
	Critical	14.73	0.28	6.30	7.59E−2
80%	Alpha (N)	18.89	0.14	1.70	1.37E−2
	Alpha (2)	9.34	0.00	3.88	4.20E−2
	Alpha (F)	0.40	0.00	5.20	5.27E−2
	Fluence	6.35	0.43	0.13	1.51E−3

*Relative error calculated with absolute value of difference, normalized by reference value

a supercritical condition. This causes the power to increase slightly after 0.2 s and reach a maximum. Additionally the time spent at this power level stretches over several time steps making a comparison unsatisfying; this is why the peak time column is empty for this reactivity insertion. Likewise the maximum temperature occurs at the beginning of the transient, so this column is also empty. A more meaningful comparison for this reactivity insertion would be the relative error of the final temperature. For the other metrics, there is reasonable agreement of the Critical method; a 1% error is larger than the other methods, but is still reasonable for many engineering calculations. The first two versions of the Alpha method produced close to the same error in maximum power, and the Alpha(F) and Fluence methods perform the best.

For the super critical transient (90% boron concentration), the Critical homogenization method performs surprisingly well. Among all the metrics, it performs consistently second best. The best is shared between the Alpha(F) and the Fluence method making it difficult to choose among the two methods. The Alpha(F)

version was proposed as an approximation to the Fluence method and performs well except in the deposited energy metric. Thus the Alpha(F) method seems to work well as an approximate Fluence method. The difference between these two methods is subtle; the Fluence method uses a flux which contains the influence of temperature feedback throughout the transient, while the Alpha method assumes the cross sections are constant through the entire transient.

In the super prompt critical case (80% boron concentration), the Critical method is largely in error and should not be used as a homogenization method during a super prompt critical transient. The Alpha method using $N_d + 1$ vectors performs as bad as the Critical method at predicting the maximum power, but significantly improves the deposited energy error. Again, the Alpha(F) and Fluence methods perform the best, as is the case for a super critical transient.

From the test with a spatially homogeneous region with and without the influence of delayed neutron precursors, several generalities can be observed. First for the case of modeling the transient due to an instantaneous insertion of reactivity above the prompt critical threshold ($\rho > \beta$), using homogenized cross sections produced using a k-eigenvalue calculation is inadequate. Their use introduces significant errors when estimating the maximum power, deposited energy, and maximum temperature. Second, using homogenized cross sections produced using a k-eigenvalue calculation can adequately predict the maximum power, deposited energy, and maximum temperature if the reactivity insertion is below the prompt critical threshold ($\rho < \beta$). This result can be used to justify the continued use of critically homogenized cross sections to model operational transients. Third, the new homogenization methods, introduced to reduce errors in predicting various transient quantities, perform well in all situations. The time integrated flux (Fluence) method performs well, but requires a potentially expensive solution. The Alpha(F) method correctly predicts the maximum power, but does not predict the deposited energy to a high accuracy.

4.4.2 Heterogeneous Medium

The previous section explored homogenization applied to a spatially homogeneous medium to introduce the concept of kinetic homogenization. The present section expands on the methods previously introduced by treating a spatially heterogeneous domain with a subchannel model to treat heat transfer.

The geometry for this heterogeneous problem is shown in Figure 4.10a, where fuel pins are in red and borated water is in blue or orange. The geometry has a heterogeneous lattice of eight square fuel pins (0.8907 cm wide) surrounding a water hole, which is denoted as Region 1 in the figure. The size of the square fuel pins was chosen to conserve the area of circular fuel pins with a diameter of 1.005 cm. This heterogeneous lattice is placed in a 3×3 array, and this 3×3 array is repeated indefinitely. Figure 4.10 shows a quarter of this geometry, where all edges have reflecting boundaries. Region 3, in orange, is at the center of this geometry. During the transient simulation, the boron concentration is partitioned into *Central Boron* (Region 3) and *Peripheral Boron* (Regions 1 & 2) where the boron concentration is perturbed by different amounts for these two partitions.

The homogenized spatial geometry is shown in Figure 4.10b, were region B (orange) corresponds to a homogenized Region 3 in Figure 4.10a. Region A corresponds to the homogenization of Regions 1 & 2.

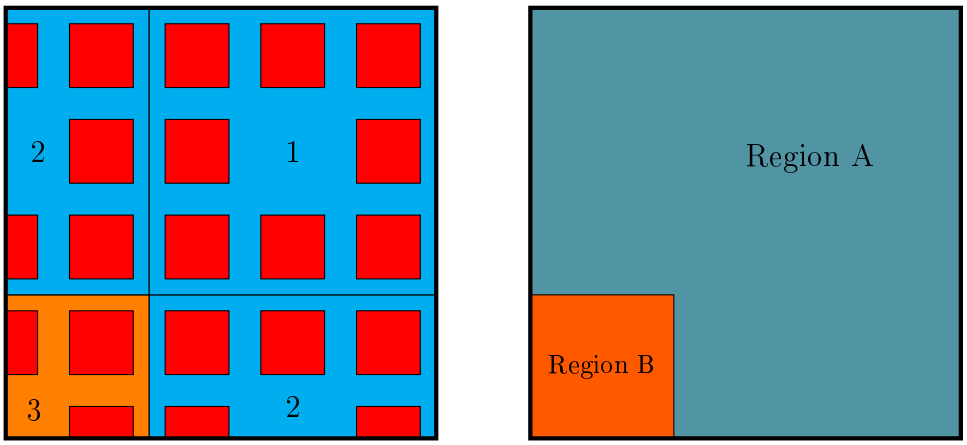

(a) Heterogeneous Pin Array. Fuel pins are red, borated water is orange or blue. Fuel is 0.8907 cm wide and the pitch is 1.295 cm.

(b) Homogeneous Regions. Region B corresponds to Region 3 in (a), while Region A corresponds to Regions 1 & 2 in (a).

Figure 4.10. Geometry and Homogenized Regions for Spatially Heterogeneous Problem [164].

The square pin cells are an artifact of the spatial geometry available in the neutron transport solver used (IDT) [82]. Modeling square pin cells allows the author to use a simplified transport solver which requires a Cartesian spatial discretization. The IDT transport solver of APOLLO3® also features an option with explicit circular pins that shares the same sweep algorithm with the Cartesian mesh option, but the time dependence in IDT was developed only with the Cartesian mesh option because of a simpler implementation of acceleration techniques. A more realistic representation of circular fuel pins can be achieved through a stair step approximation, shown in Figure 4.11, but the increased detail of the spatial mesh will increase the computational cost. It is obvious that the physical model is biased away from the real situation. From a neutronic point of view, the fuel to moderator ratio is preserved, but this alters the contact surface for the exchange of heat. However, since the same heterogeneous mesh is used for both the reference calculation and the homogenization, any physical bias in the geometry will disappear when comparing to the reference calculation.

As for the homogeneous case, reference cross section tables are produced by APOLLO3® for various statepoints. For the heterogeneous case, the fuel and water temperature can be interpolated independently, contrary to the homogeneous case of the previous section. Again a reference cross section table is generated, however for this case the reference calculation is performed with 26 energy groups. Obtaining a reference calculation, even for this relatively simple spatial geometry, with 281 energy groups is computationally intensive ($>$ 2 weeks of calculation). The reduction in energy groups brings the computation time for the reference

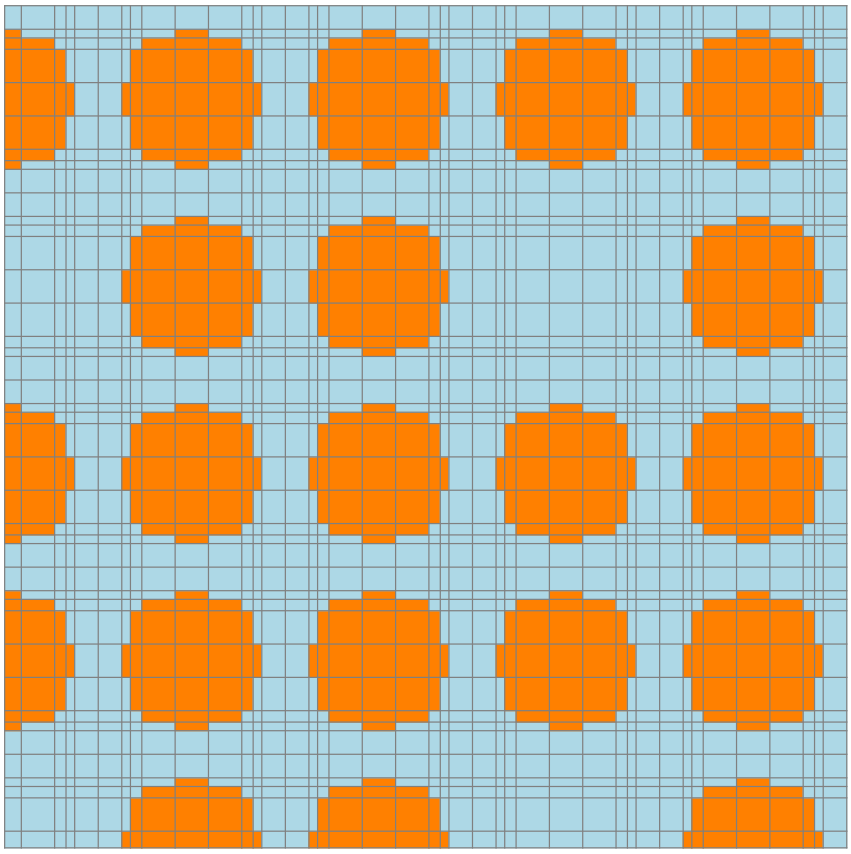

Figure 4.11. Stair Step Pin Cell Approximation for Heterogeneous Lattice Calculation.

down to ∼4 days, which is still a significant calculation, but is more tractable than with 281 energy groups.

An additional change from the previous case is the use of a multichannel code to treat the heat transfer. As discussed in Section 2.2.2, the thermal hydraulic model in the Multi-Channel Thermal Hydraulics (MCTH) code treats conduction within the fuel and forced convection in the coolant. For this case, a single average temperature per fuel pin is used to characterize the fuel temperature. Likewise, a single average temperature is used to characterize the coolant temperature for each subchannel.

The transient, shown in Figures 4.12 & 4.13, is initiated at 0.1 s as in the previous case by a reduction in the boron concentration. The reduction in the boron concentration is non-uniform, where the central assembly's boron concentration is reduced to 36% of the original value and the peripheral assemblies' boron concentration is reduced to 97% of the original value. This perturbation corresponds to a reactivity insertion of 501.1 pcm ($1.05); for this problem, $\beta =$ 479.3 pcm. The boron concentration is returned to the original values at 3.0 s, and the simulation finishes at 4.0 s. All transients are simulated with the same time step size of 0.004 s.

The reactor is initially at steady state, achieved as in the previous case by

normalizing the production cross section by k_{eff}, with a power of $10\,\text{W}\cdot\text{cm}^{-3}$. The coolant is at 1 MPa with a flow rate of $0.188\,\text{kg}\cdot\text{s}^{-1}$ and a temperature of 88.80 °C. These coolant conditions and low power produce a steady state fuel temperature that is slightly above the coolant temperature (88.81 °C). These low power conditions correspond to a cold zero power condition, where the power is low enough to not increase the temperature of the fuel [94]. Because of the low fuel temperature, the power can rise significantly before Doppler broadening of the resonances or nucleate boiling have enough time to counteract the reactivity insertion. This situation makes for a more severe accident than a reactivity insertion from full power or hot zero power [93].

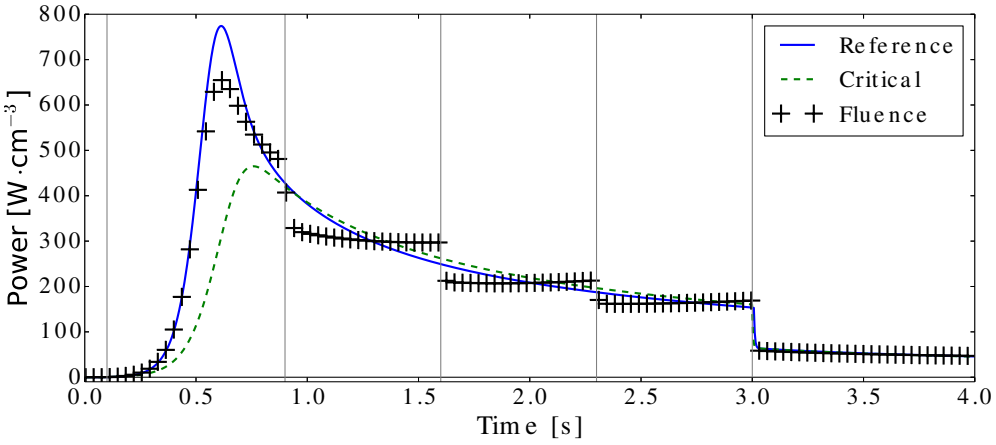

Figure 4.12. Transient Power. Spatially Heterogeneous Geometry with Delayed Neutron Precursors and a Reactivity Insertion $\rho > \beta$. Using Four Time Intervals Between 0.1 s and 3.0 s for Fluence Method.

Figure 4.12 shows the power as a function of time for the reference calculation and calculations with homogenized cross sections produced from two methods. The time discretization for the Fluence method is represented by vertical lines; there are quasi-evenly spaced intervals where the boron concentration is perturbed, between 0.1–3.0 s.

Homogenized cross sections were obtained using the heterogeneous solution from Figure 4.10a. As was mentioned earlier, homogenization methods become practical when performed on subdomains of the global problem. The results presented in this section however do no use the flux from subdomains of the problem. Instead, the solution from the entire geometry is used in the homogenization process. These two versions of homogenization (using subdomains or the entire geometry) were tested with the critically homogenized cross sections. The differences between the two versions were negligible and thus it was decided to use the entire solution for homogenization. It is suspected that because of the size of the geometry and the relative similarity between Regions 1, 2, & 3 in Figure 4.10a, the flux gradients at the interface are sufficiently small as to not affect the homogenization. This supposition was verified by performing static calculations using homogenized cross sections; for several state point configurations, the k_{eff} was the same in the heterogeneous and homogenized problems. Additionally, the same transport angular discretization is used in the reference

and homogenized calculations, which introduces less error than using a low order diffusion operator in the homogenized calculation.

To investigate the usability of the Fluence method, it was tested using subdomains to obtain the homogenized cross sections. This test is to understand if the Fluence method can be used in industrial reactor analysis problems. It was found that using the same boron concentration perturbation in the subdomain as in the reference problem resulted in a power excursion that was not representative of the reference problem. To remedy this inconsistency, the surrounding heterogeneous regions were replaced by a spatially homogeneous buffer. This modification allowed the non-uniform boron concentration perturbation to more closely resemble that of the reference problem. Once this homogeneous buffer was added, the Fluence method performed like the case when using the solution from the entire geometry for homogenization. This modification to the reference problem is similar to what is performed in the color-set method. An alternative way to possibly remove the homogeneous buffer would be to introduce a leakage model so that the reference transient is reproduced in the subdomain. This alternative however, is dependent on having a reference solution available, which is not practical for reactor analysis. Thus if subdomains are used in the homogenization process, the author will privilege using the homogeneous buffer.

Figure 4.12 shows that the critically homogenized cross sections fail to capture the first part of the reference power, but approach the reference power later in the transient. The later part of the transient is governed principally by long lived delayed neutron precursors which were distributed in a critical configuration. This again supports the observation that when delayed neutrons are dominant, critically homogenized cross sections may produce sufficiently accurate results in transient calculations. However, in the early part of the transient, when prompt neutrons and short lived delayed neutron precursors are dominant, critically homogenized cross sections perform poorly. Additionally, unlike in the previous homogeneous case, the error is not in the conservative direction. This eliminates the possibility to use critically homogenized cross sections as a *worst-case* calculation.

The Fluence method however, is better at estimating the early part of the transient, but also introduces discontinuities in the power due to the time discretization. The power in these intervals follows an average power within these regions, which is expected from the definition of fluence generated cross sections. The Fluence method seeks to conserve the total reaction density over a time interval. A way to reduce the discontinuities in this simulation could be to introduce a different interpolation law for the time variable. The law used for these results is an upstream law, which gives constant cross sections within a time interval. Using a linear interpolation law over the time interval could reduce the discontinuities introduced in this simulation.

Figure 4.13 shows the temperature of a fuel rod and a subchannel in the central assembly. The fuel temperature is shown to increase significantly until the power is lower than the cooling power of the coolant. The coolant temperature increases only slightly over the transient from 88.80 °C to 95.26 °C. The coolant temperature increases much less than the fuel temperature due to the

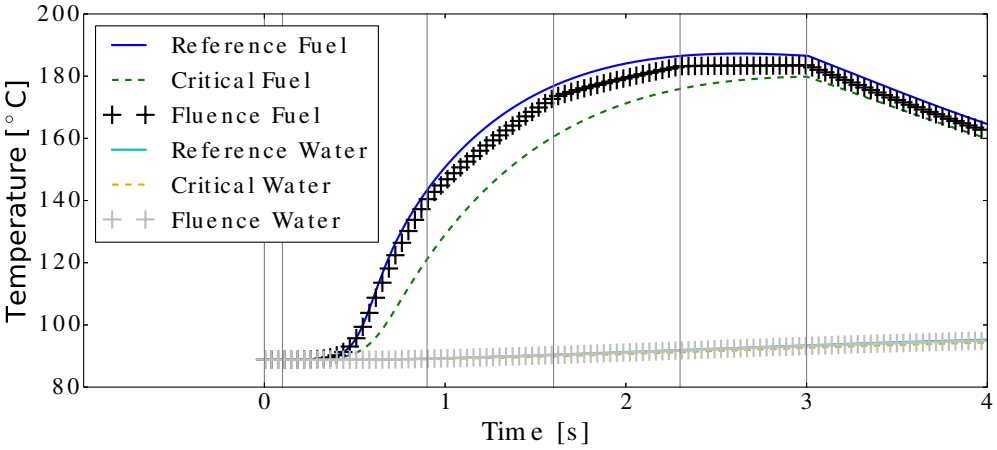

Figure 4.13. Transient Temperature. Spatially Heterogeneous Geometry with Delayed Neutron Precursors and a Reactivity Insertion $\rho > \beta$. Using Four Time Intervals Between 0.1 s and 3.0 s for Fluence Method. *Fuel* Denotes Temperature in Corner Fuel Rod of Central Lattice, *Water* Denotes Temperature in Central Water Hole.

convection of the coolant and also the higher specific heat capacity. Because of the small increase in coolant temperature, the figure shows no difference between the reference and homogenized calculations. The fuel temperature, which reacts more quickly to changes in power, shows large differences between the reference and critically homogenized transients. The Fluence method however follows the reference fuel temperature more closely.

The small geometry and reflecting boundary conditions cause the power shape to remain nearly constant through the simulation. Even with the localized perturbation in the boron concentration, the power does not experience a significant amount of tilt. This effect causes the time dependent temperature in fuel rods at the center of the geometry and on the periphery to be nearly identical.

The effect of the time discretization for the Fluence method is explored for this spatially heterogeneous case. Figures 4.14 & 4.15 show the same transient as before, but where the Fluence method uses 58 quasi-even intervals between 0.1–3.0 s, which corresponds to an interval size of 0.05 s. Because of the finer time discretization, the Fluence method more closely follows the reference calculation when compared to Figures 4.12 & 4.13.

To more quantitatively compare the transients presented, Tables 4.9, 4.10, & 4.11 show the relative errors for important metrics of the transients. Table 4.9 shows the relative errors in maximum power, time of maximum power, total energy, and the L_2 norm. With the exception of the L_2 norm, these metrics were used to analyze the previous homogeneous case. The cumulative L_p norm, defined as

$$\|\mathcal{P}_i\|_p(t) = \left(\frac{\int_{t_0}^{t} \left|\mathcal{P}_i(\tau) - \mathcal{P}_{\text{ref}}(\tau)\right|^p \mathrm{d}\tau}{\int_{t_0}^{T} \left[\mathcal{P}_{\text{ref}}(\tau)\right]^p \mathrm{d}\tau} \right)^{\frac{1}{p}}, \tag{4.19}$$

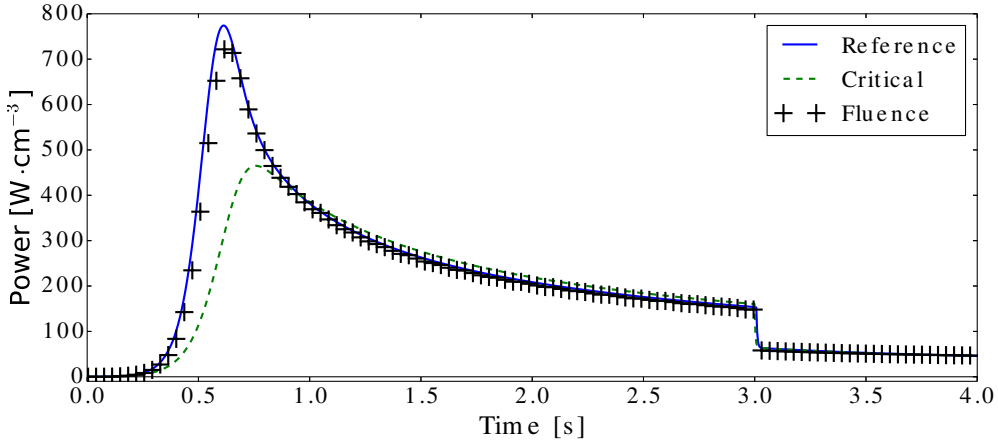

Figure 4.14. Transient Power. Spatially Heterogeneous Geometry with Delayed Neutron Precursors and a Reactivity Insertion $\rho > \beta$. Using 58 Time Intervals Between 0.1 s and 3.0 s for Fluence Method.

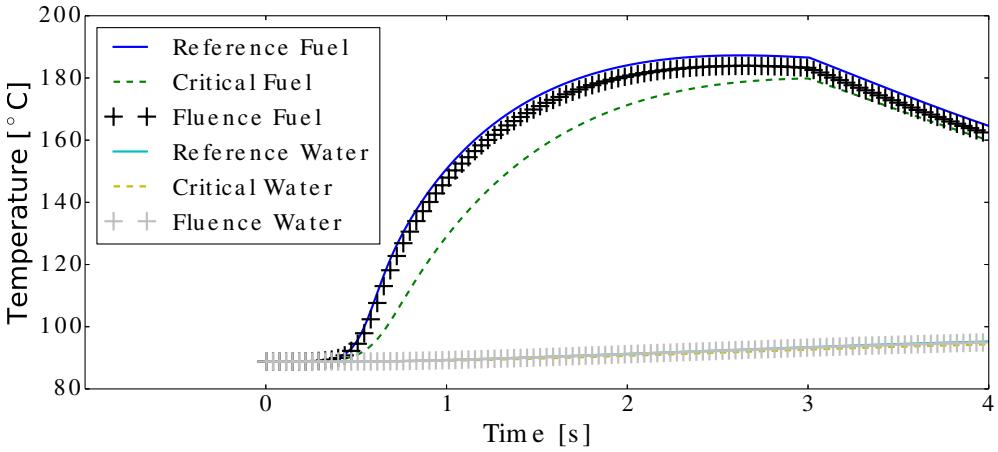

Figure 4.15. Transient Temperature. Spatially Heterogeneous Geometry with Delayed Neutron Precursors and a Reactivity Insertion $\rho > \beta$. Using 58 Time Intervals Between 0.1 s and 3.0 s for Fluence Method. *Fuel* Denotes Temperature in Corner Fuel Rod of Central Lattice, *Water* Denotes Temperature in Central Water Hole.

is introduced because the integral quantity of the total energy (corresponding to $p = 1$) can have a low value even if the transients are largely different. The L_2 norm shows how close the two transients are over the entire simulation. In Equation 4.19, p will have an integer value of either 1 or 2, and T is the maximum value for the time range. For the L_p norms presented in the following tables, the cumulative L_p norm is evaluated at the end of the simulation ($t = T$). The Fluence method is presented in Table 4.9 with the various discretizations of the time domain. The numbers correspond to the number of quasi-evenly sized time intervals between 0.1–3.0 s. Blue highlighted values correspond to the transients of Figures 4.12 & 4.13, while red highlighted values correspond to Figures 4.14 & 4.15.

Table 4.9 shows that the Fluence method performs poorly if a single time

Table 4.9. Comparison of Fluence Method to Critical Homogenization Method By Relative Error in Maximum Power, Peak Time, Total Energy, and L_2 Norm. Transient Corresponds to Reactivity Insertion $\rho > \beta$ and Various Subdivisions of Interval Between 0.1 s and 0.3 s are Compared.

	Relative Error* [%]			
Method	**Max Power**	**Peak Time**	**Total Energy**	**L_2 norm**
Reference	$774.15\,\mathrm{W}\cdot\mathrm{cm}^{-3}$	0.61 s	811.30 J	529.07
Critical	39.94	23.53	11.24	36.30
Fluence(1)	73.89	389.54	75.23	91.47
Fluence(2)	50.08	67.32	22.57	56.17
Fluence(4)	15.41	0.65	4.03	10.84
Fluence(8)	15.42	0.65	3.72	9.04
Fluence(16)	6.97	0.65	3.50	5.65
Fluence(29)	7.16	2.61	3.78	6.28
Fluence(58)	6.09	2.61	3.90	6.78

*Relative error calculated with absolute value of difference, normalized by reference value

interval during the transient range is taken (Fluence(1)); across all metrics, it performs worse than the Critical method. However with subsequent subdivisions, the errors are reduced. After 4 subdivisions, the relative errors are below those of the critical method. The reduction in error is not monotone however, which means that other sources of error become dominant, or the discretization is introducing numerical errors. For example, the total energy and L_2 norm experience a minimum error with 16 divisions, afterwhich the errors increase. Because of the increase, it is believed that the fine discretization introduces numerical errors either from the integration of the time dependent flux or the interpolation of a larger cross section table.

Table 4.10 shows the various metrics for the central fuel temperature. The total energy is replaced by the L_1 norm. In reality these metrics are equivalent, but there is no physical meaning of the time integrated temperature.

The fuel temperature in Table 4.10 shows a similar trend to the power in Table 4.9; the Fluence method outperforms the critical method only after 4 divisions. Again, for the L_1 and L_2 norms there is a minimum at 16 divisions.

The central water temperature is shown in Table 4.11, where the same metrics from Table 4.10 are compared. Because the coolant temperature responds slower to the change in power, the maximum temperature occurs at the end of the transient; all relative error values for the time of maximum temperature are thus 0.00%. However, even though the coolant temperature responds differently to the change in power, the L_1 and L_2 norms still exhibit a minimum at 16 divisions.

The preceding calculations were performed on a single core Intel(R) Xeon(R)-X5550(2.67 GHz) CPU with 8.2 MB of cache memory and 6.1 GB of random access memory. Table 4.12 shows the execution times for the Critical and Fluence methods. The timing shows the large cost associated with obtaining the reference

Table 4.10. Comparison of Fluence Method to Critical Homogenization Method By Relative Error in Maximum Temperature, Peak Time, L_1 Norm, and L_2 Norm. Transient Corresponds to Reactivity Insertion $\rho > \beta$ and Various Subdivisions of Interval Between 0.1 s and 0.3 s are Compared. Temperature Taken From Corner Fuel Rod of Central Lattice.

	Relative Error* [%]			
Method	**Max Temperature**	**Peak Time**	**L_1 norm**	**L_2 norm**
Reference	187.26 °C	2.63 s	642.01	327.76
Critical	3.97	14.00	6.51	7.56
Fluence(1)	34.91	14.31	36.71	39.76
Fluence(2)	9.04	14.00	11.86	13.05
Fluence(4)	2.00	14.00	2.05	2.24
Fluence(8)	1.68	2.74	1.80	1.91
Fluence(16)	1.63	0.30	1.65	1.74
Fluence(29)	1.75	0.61	1.79	1.88
Fluence(58)	1.80	0.61	1.86	1.94

*Relative error calculated with absolute value of difference, normalized by reference value

Table 4.11. Comparison of Fluence Method to Critical Homogenization Method By Relative Error in Maximum Temperature, Peak Time, L_1 Norm, and L_2 Norm. Transient Corresponds to Reactivity Insertion $\rho > \beta$ and Various Subdivisions of Interval Between 0.1 s and 0.3 s are Compared. Temperature Taken From Central Water Hole.

	Relative Error* [%]			
Method	**Max Temperature**	**Peak Time**	**L_1 norm**	**L_2 norm**
Reference	95.26 °C	4.00 s	365.97	183.04
Critical	0.99		0.60	0.70
Fluence(1)	5.56		2.64	3.32
Fluence(2)	1.81		1.00	1.18
Fluence(4)	0.32		0.17	0.20
Fluence(8)	0.28		0.14	0.17
Fluence(16)	0.26		0.13	0.15
Fluence(29)	0.28		0.14	0.17
Fluence(58)	0.29		0.14	0.17

*Relative error calculated with absolute value of difference, normalized by reference value

solution; this is the full multiphysics solution in 26 energy groups with full spatial heterogeneity. The solution is used to produce the homogenized cross section for the Fluence method, which is the main retractor for this method.

The generation of cross section tables takes longer for the Fluence method than for the Critical method. The Fluence method is calculating a cross section table

Table 4.12. Execution Time for Critical and Fluence Methods on 26 Energy Group, Spatially Heterogenous Problem.

Calculation	Method	Time [d - hr : min : sec]
Reference		4 - 18 : 25 : 20.39
Homogenization	Critical	10 : 55.31
	Fluence(1)	28 : 23.56
	Fluence(58)	9 : 34 : 06.25
Homogenized Transient	Critical	16 : 30.10
	Fluence(1)	16 : 24.40
	Fluence(58)	22 : 44.26

that is $n\times$ larger than the Critical cross section table, where n is the number of time intervals. For the Fluence cases shown, the number of time intervals is the number of subdivisions given in the table plus two to account for both ends of the transient. The calculation for the transient using homogenized cross sections takes close to the same time in each case. The Fluence method with 58 subdivisions takes slightly longer than the other cases because of the larger interpolation table. The algorithm used to find the enveloping state points along a larger interpolation axis has a time complexity of $\mathcal{O}(n \log n)$ because of the sort performed on state point values along each axis.

The enormous cost for computing the time dependent flux of the Fluence method warrants either the incorporation of parallel methods used to evaluate this time dependent flux, or developing an approximate solution method. A promising approximation for the Fluence method could be the use of the α-eigenvalue problem to generate a time dependent expansion. The expansion in the basis of α-eigenvectors however, does not take into account the temperature dependence throughout the transient. Since the temperature deviation in this simulation is much larger than that of the homogeneous case, this approximation may be in error.

4.5 Conclusions

This chapter explored homogenization methods applied to time dependent reactor analysis. It was shown, for both a spatially homogeneous and heterogeneous case, that using homogenized cross sections produced with a weighting flux from a criticality calculation can introduce significant errors in the transient. Two new methods for producing homogenized cross sections, appropriate for time dependent calculations, were introduced and studied: one based on an asymptotic expansion of the time dependent flux (Alpha), and another based on the time integrated flux (Fluence).

Both methods performed well when delayed neutron precursors were suppressed, but the Alpha method had to be modified when delayed neutron precursors were introduced. The Alpha method needed to include contributions from

both short and long-lived delayed neutron precursors groups. It was observed that for a reactivity insertion below the prompt critical threshold ($\rho < \beta$), the cross sections produced from using a criticality calculation performed well; the errors for the super critical transient were smaller than for the super prompt critical transient. However, the new methods still produced smaller errors than the Critical method in all cases.

When spatial heterogeneities were introduced, the Fluence method continued to perform well, but the delicate portion of this procedure will be in choosing an appropriate reference homogenization problem. To recover the behavior of non-uniform reactivity insertions, a homogeneous buffer can be added to the homogenization region of interest. It was also shown that refining the time discretization used in the Fluence method reduced the errors of various metrics until a point, where further subdivision increased the errors. It is thought that this increase in error is the result of the accumulation of numerical errors due to the larger interpolation table induced by the finer time discretization.

The time required to produce cross sections is discouraging for industrial applications, and for this method to be useful, improvements will need to be explored. One possible route for obtaining the multiphysics solution required for this method is to implement parallel algorithms throughout the models employed. The transport method used an S_8 quadrature set, and parallelizing the transport sweeps through the domain has the potential to reduce the computation time by a significant fraction. Alternatively, an approximate time dependent solution can be obtained through an expansion over α-eigenmodes. This approximation however does not take into account the effects of temperature changing over the transient, and may be considerably in error.

Chapter 5

Reduced Core Case

The present chapter discusses a reduced core problem that was studied to show how the multiphysics framework performed in accident simulations of a reactor core. The reduced core problem is made of 16 assemblies surrounding a central control blade, which is removed to simulate a Rod Drop accident in a BWR during startup. The Rod Drop accident introduces a prompt critical reactivity insertion, causing the reactor to enter into a power transient. The reduced core geometry experiences larger power gradients than the previous cases studied in Chapter 4. Studying such an accident shows that the multiphysics framework can produce coupled physics solutions, but many improvements can be made.

5.1 Reduced Core Description

5.1.1 Geometry

The reduced core is adapted from an ATRIUM-10 (10-9Q) type assembly [165]. Figure 5.1 shows the original spatial geometry from a benchmark calculation on Plutonium recycling; dimensions are given in millimeters. The material composition was changed from MOX to UOX because it was discovered that the MOX fuel composition resulted in a positive temperature feedback coefficient during startup. This positive temperature coefficient made controlling the transient simulation unattainable. With an ever increasing reactivity insertion, the power grows unbounded until an overflow error is encountered. It is possible to simulate such transients for short times, but without a stabilizing feedback mechanism, the simulated power is not bound throughout the transient. Additionally some of the structural material was removed to simplify the geometrical and thermal hydraulic modeling of this fuel assembly.

The channel boxes, which decouple the thermal hydraulics of assemblies from each other, were removed; consequently with this geometry, fluid mixing is allowed between assemblies. The interior water column separator has also been removed to facilitate thermal hydraulic modeling. The water column presents a unique type of physics to the problem. During steady state operation at full

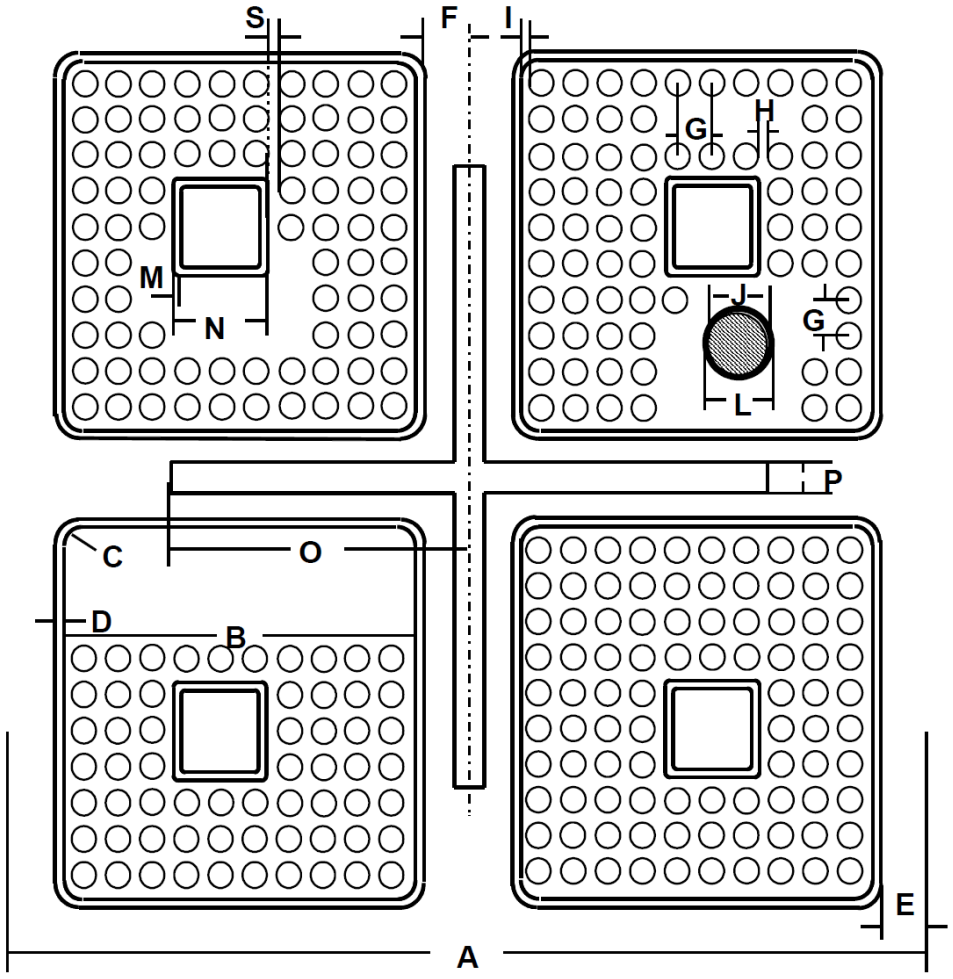

A	305.00	G	12.95	N	35.00
B	134.00	H	2.90	O	122.4
C	0.0	I	3.70	P	6.37
D	2.50	J	8.84	S	3.375
E	6.75	L	10.05		
F	6.75	M	0.725		

Note: 2S+N = 3G+H.

Figure 5.1. Original Geometry Specification for BWR Benchmark Calculation [165]

power, the coolant in the water column is at a lower temperature than the coolant surrounding fuel pins. Because of this large heat sink during steady state operation, condensation around the water column will be present. However, since the accidents studied in this work are during startup, there is not a large temperature difference between water in the column and water in contact with fuel elements. During startup, condensation on the exterior of the water column will be negligible and removing the structural material to separate the assembly from the water column will not introduce large modeling errors. Because of the startup conditions, where the fluid is largely subcooled, the intricacies of the structural

material should not impact the transient studied. Studying transients where the initial state is at Hot Zero Power (HZP), for instance, would require the modeling of such structural material.

Additionally, the circular cross sectional fuel has been transformed to square cross sectional fuel with a side length such that the cross sectional area is conserved. This approximation is introduced because of the simplified transport solver used that requires a Cartesian spatial mesh. Figure 5.2 shows the reduced core geometry adapted from the ATRIUM-10 assembly design of Figure 5.1.

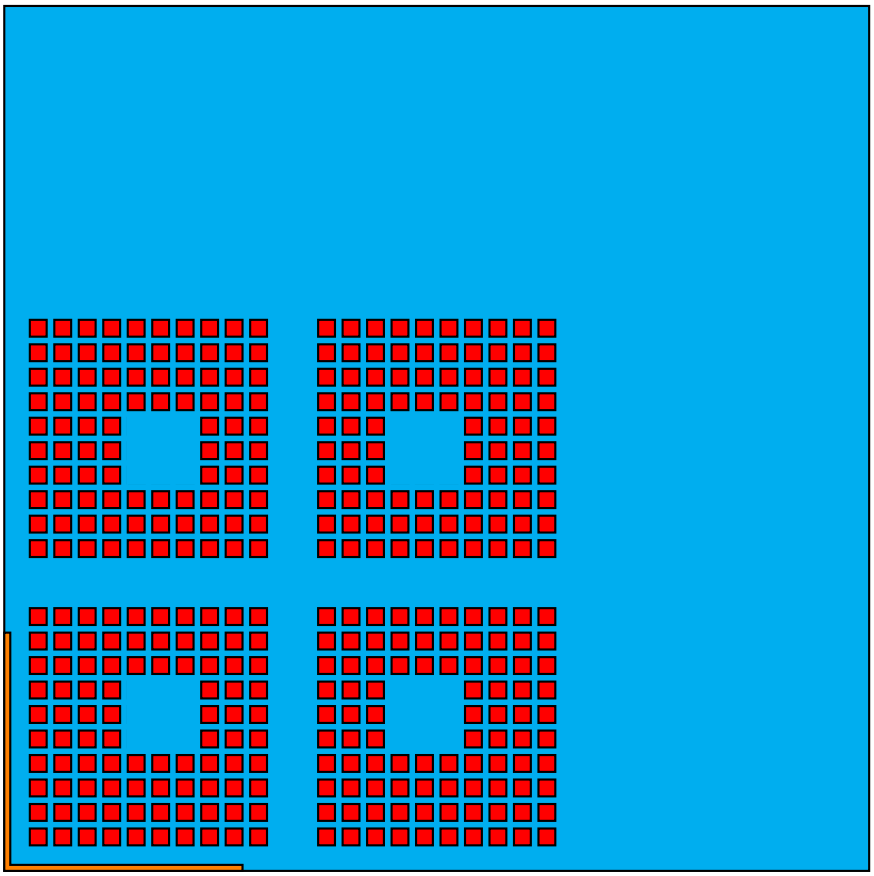

Figure 5.2. Geometry of Reduced BWR Core. Four BWR Assemblies Surrounding a Central Control Blade with Water Reflector.

The geometry presented in Figure 5.2 is one quarter of a reduced BWR core geometry. The geometry is reflected on the lower and left sides, resulting in 16 assemblies surrounding a homogeneous control blade. Vacuum boundary conditions are placed on the upper and right edges to produce a finite spatial geometry. This reduced core has a water reflector around the exterior of the 16 assemblies which has a width equal to the assembly pitch. The assembly pitch and fuel pitch are conserved from the original benchmark specification (15.25 cm and 1.295 cm respectively). The fuel, shown in red, is 0.8907 cm wide so that the cross sectional area is conserved from the circular fuel. The control blade has the same width of 0.637 cm, but the length has been increased from 12.24 cm to 12.6029 cm so that the edge of the control blade coincides with the ninth fuel pin edge. This

modification removes long slender spatial cells from the geometry that contribute to slow convergence.

The fuel material is taken to be Uranium Dioxide with enrichments ranging from 2.68% ^{235}U to 5.01% ^{235}U. The isotopic concentrations for the fuel materials of this simulation are given in Table 5.1. These isotopic concentrations are approximately what would be found in a commercial BWR-UOX assembly. The original five fuel enrichments are homogenized into an average fuel material, which is used throughout the domain. This homogenization procedure is performed before hand with APOLLO3® to produce the base cross section table for this case.

Table 5.1. Isotopic Concentrations for BWR Material

	Nominal Conc. [$\mathbf{b^{-1} \cdot cm^{-1}}$]		
Material	^{235}**U**	^{238}**U**	^{16}**O**
Fuel 1	5.9378E−4	2.1537E−2	4.4262E−2
Fuel 2	7.6282E−4	2.1371E−2	4.4266E−2
Fuel 3	9.5226E−4	2.1183E−2	4.4270E−2
Fuel 4	1.0531E−3	2.1083E−2	4.4274E−2
Fuel 5	1.1091E−3	2.1028E−2	4.4274E−2
		H_2O	
Coolant		3.3360E−2	
	^{10}**B**	^{11}**B**	**C**
Control Blade	6.1607E−2	1.5179E−2	1.9183E−2

The geometry used in the thermal hydraulics model is shown in Figure 5.3, where an eighth of the core is shown; the bottom and diagonal edges are reflected. The fuel pins and subchannel layout are delimited by solid lines. Fuel pins are shown in red, while subchannels are shown in blue. The location where temperatures are taken for interpolating temperature dependent cross sections are highlighted in yellow. The highlighted subchannel and fuel rod in the central assembly correspond to the peak power locations. The power is peaked in this location because of the influence of the water reflector and the central control blade. The highlighted subchannel and fuel rod in the peripheral assembly correspond to a median power level in the outer assemblies.

Taking more locations of the temperature for evaluating the temperature dependent cross sections can produce a more detailed effect on the spatial dependent power. However, the implementation for how temperature is accounted for in the neutron transport solver limits this number. Each material corresponds to a specific temperature interpolation; to increase the number of temperature points used, unique media must be defined causing a large increase in the size of the cross section table used. This increase in macroscopic cross section data used by the transport solver has the potential to slow the construction of the transport residual due to the increase in memory access. To limit the size of this cross

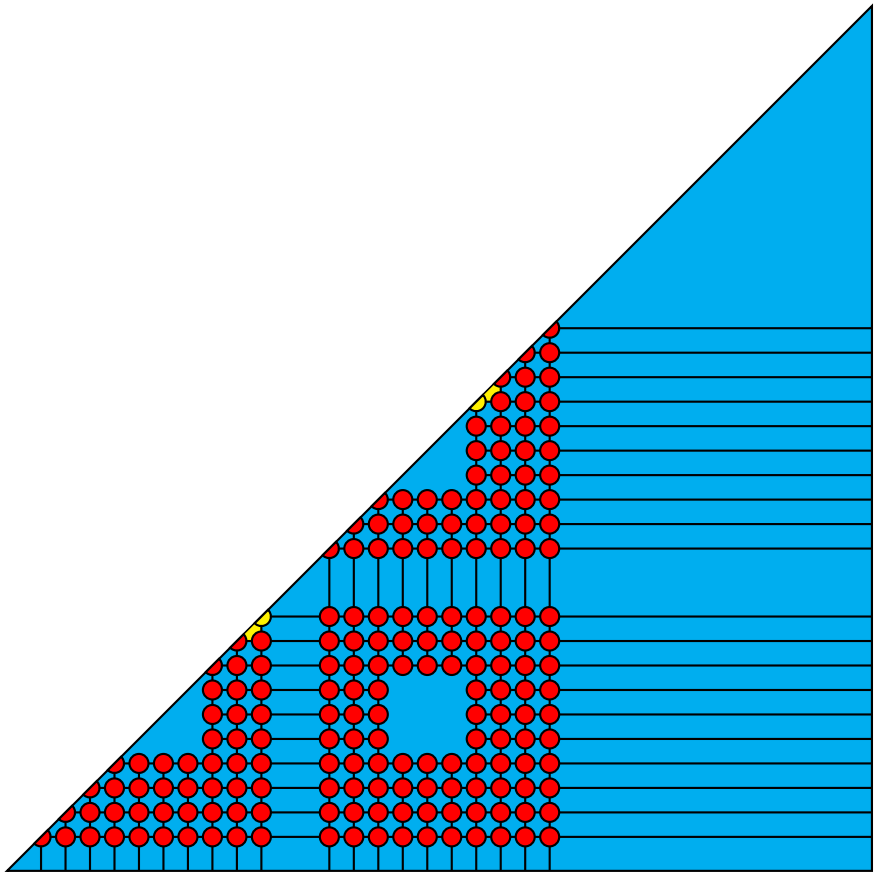

Figure 5.3. Geometry for Thermal Hydraulics. Highlighted Points Mark the Locations Where Temperature is Used to Evaluate Material Temperature for Transport Solver.

section table, only two points are taken for the fuel and water temperatures.

5.1.2 Transient Conditions

The reduced core calculation starts in a state equivalent to a Cold Zero Power (CZP) startup, with low fuel and coolant temperature. The thermal hydraulic and neutronic states are identical to that discussed in Section 4.4.2 and will be repeated here. The reactor is in a critical state with a low power of 10 W; the control blade is completely inserted. The coolant is at 1 MPa, with a flow rate of $0.188\,\mathrm{kg}\cdot\mathrm{s}^{-1}$, and a temperature of 88.80 °C. The low power and these coolant conditions produce a fuel temperature which is slightly above the coolant temperature (88.81 °C).

The transient is initiated after 0.1 s with a perturbation of the concentration of boron in the control blade. Since the neutron transport calculation is conducted in 2D, the movement of control blades through the axial direction is approximated by diluting the concentration of the neutron absorber with coolant material. The dilution is accomplished by interpolating cross sections between the fully inserted control blade and the control blade replaced with water. In the simulation presented, the final concentration of blade material is 70% of

the nominal concentration. This perturbation produces a reactivity insertion of 892.3 pcm ($1.17). The β for this reduced reactor problem is 762.1 pcm. The β for this case is computed by comparing the system reactivity with delayed neutrons present and suppressed using

$$\beta = \frac{k - k_p}{k k_p} \times 10^5, \qquad \text{[pcm]} \quad (5.1)$$

where k is the k_{eff} with delayed neutrons present, and k_p is the k_{eff} with delayed neutrons suppressed.

The movement of control rods during rod ejection transients in PWR cores is usually modeled as an instantaneous insertion of reactivity because of the parameters of the accident. A PWR rod ejection accident is defined as a mechanical failure of the control rod housing mechanism by which the control rod is moved out of the core from the motion of the coolant. The coolant in a PWR core travels from the bottom of the core to the top of the core with a speed of $\sim 7\,\text{m} \cdot \text{s}^{-1}$ [166]. The friction from the high speed of the coolant will push a control rod out of the core in $\sim 100\,\text{ms}$. The high velocity of the control rod out of the core warrants the use of an instantaneous reactivity insertion approximation.

The control blades of BWRs operate in a different way, however. The control blades enter the core from the bottom due to the steam separators and dryers being within the core vessel. A control blade drop accident in a BWR is initiated by the control blade jamming while the drive mechanism continues to withdraw. At a later time, the control blade is freed and falls to the height of the drive mechanism. Thus, for the control blade of a BWR to be ejected from the core, gravity must pull the control bade down against the flow of coolant. The control blade can take up to $\sim 4\,\text{s}$ to completely exit the core [94]. The slow rod movement in the case of BWRs suggests that a ramp insertion is more adequate for modeling the reactivity insertion. The ramp insertion for this accident consists of a linear interpolation between the initial nominal concentration of 100% and the final concentration over a period of Δt. A four second ramp insertion for the present simulation required a long simulation to be performed. To reduce the computational intensity of such a simulation, the ramp insertion is shortened to have $\Delta t = 0.4\,\text{s}$. The short reactivity insertion time is not synonymous with BWR accidents, but still provides for a slower reactivity insertion than the instantaneous insertion.

The base cross section data for this accident simulation was generated by APOLLO3® in 6 energy groups, with an averaged fuel material used throughout the domain. The generation of 6 group cross sections includes a detailed lattice calculation in 281 energy groups with critical leakage for various fuel and water temperatures and with the control blade present or replaced with water. The homogenization routine includes self shielding evaluations for each temperature state. This 6 group cross section set was then homogenized to produce a central assembly medium, a peripheral assembly medium, and a water reflector region, with 2 energy groups. The control blade material is incorporated into the central assembly medium because of the geometric overlap between the two media. Homogenization of the reflector region cannot typically be accomplished

in an isolated calculation. Because of the lack of fissile material present in the reflector, either part of the neighboring assembly must be included in the calculation or an incident flux must be used on the boundary corresponding to the flux leaving the neighboring fueled assemblies. In this homogenization process, the entire geometry is used to accurately account for the effects of neighboring assemblies, and to obtain homogenized cross sections in the reflector region. The delayed neutron precursor data contains 8 delayed neutron precursor groups, with 2 fissile isotopes.

While in Chapter 4, the Fluence method of homogenization was shown to produce more accurate cross sections for transient simulations, time constraints have warranted using the less accurate Critical method to produce homogenized cross sections. The goal of this exercise is to demonstrate that the multiphysics framework is able to produce coupled physics solutions in reactor accidents. Additionally, in studying this exercise, a cost analysis of the required execution times is performed to indicated the possibility of using this framework in industrial applications. Further studies are expected to improve the accuracy of such solutions by using cross sections generated by the Fluence method.

5.2 Results

The previously described accident was simulated using a uniform time step size of $2{\times}10^{-3}$ s. The spatial mesh for the transport calculation is discretized with a maximum mesh size of 0.5 cm. This results in 93 spatial cells in each direction, 62 of which contain fissile material with two fissile isotopes. A constant spatial dependence within each cell is used, resulting in a fission integral size of $62 \times 62 \times 2 \times 1 = 7688$. There are 8 delayed neutron precursor groups with each concentration the size of the fission integral; this produces a precurosr residual size of $8 \times 7688 = 61504$. While the thermal hydraulics model contains 198 subchannels and 189 fuel rods, with 100 axial planes. Each spatial point has a single temperature value producing a temperature residual size of $(198 + 189) \times 100 = 38700$. These discretizations produce a global residual with 107,892 entries. The details of each residual component size are given in Table 5.2.

Table 5.2. Number of Entries in Each Physics Component Residual for Reduced Core Calculation

Physics Component	**Number of Entries**
Neutron Transport	7,688
Delayed Neutron Precursor	61,504
Thermal Hydraulics	38,700
Total	107,892

The boron concentration is inserted as a ramp insertion, where the ramp portion of the insertion takes 0.4 s. The boron concentration during the simulation is shown in Figure 5.4, where the minimum boron concentration during the tran-

sient is 70% of the nominal concentration. At 1.9 s, the control blade is inserted instantaneously to simulate a SCRAM[1] event.

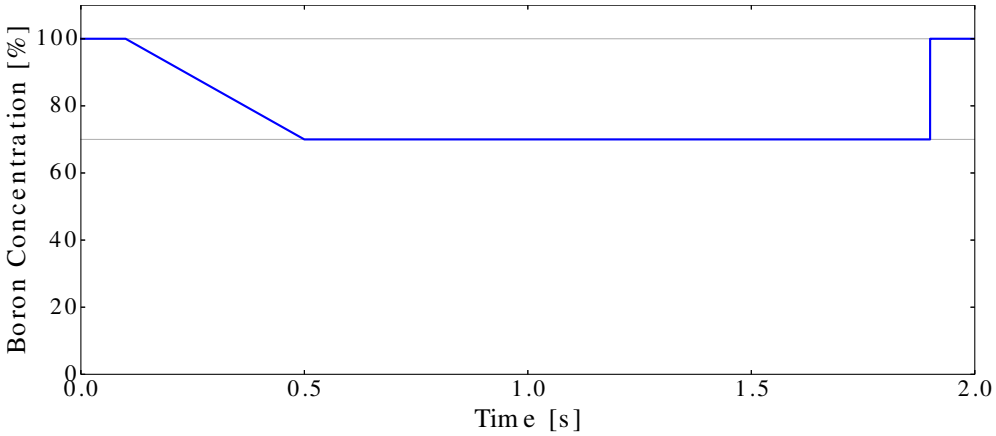

Figure 5.4. Boron Concentration During Simulation Within the Center Assembly. Minimum Concentration for Central Boron is 70%.

In the homogenization process, the control blade is homogenized with the central assembly. This, in effect, smears the boron contained in the control blade over the central assembly. A more accurate representation of reality would leave the control blade material present. However, the power tilt calculations of Figures 5.7 & 5.8 will show that the perturbation of the localized absorber used in this simulation does not largely affect the power profile. Hence the control blade smearing should not introduce significant modeling errors.

The total power of the reactor through the simulation is given in Figure 5.5. The initial power before the control blade is dropped remains constant until 0.1 s, whereafter reactivity is slowly added to the system, increasing the power. The early portion of the transient resembles a transient whose behavior is synonymous with a super critical reactivity insertion ($\rho < \beta$); there is a prompt jump followed by an exponential increase. However, after the reactivity is fully inserted, the power increases rapidly until the temperature increase is sufficient to counteract the reactivity insertion. The SCRAM event at 1.9 s is seen as the power rapidly decreases before beginning a slow exponential decrease.

The power increases from 10 W to just below 2 kW, which corresponds to an energy release of 2.13 kJ. This transient is significantly less energetic than previous transients studied. For comparison, the transient studied for the heterogeneous lattice of Chapter 4 had a maximum power of $774\,\mathrm{W}\cdot\mathrm{cm}^{-3}$ and a deposited energy of $811\,\mathrm{J}\cdot\mathrm{cm}^{-3}$. Taking into account the size of the active fuel region of this geometry produces a maximum power of 720 kW and a deposited energy of 754 kJ. The less violent transient can be attributed to the localized

[1] A SCRAM is the process of rapidly inserting neutron absorber to interrupt the fission chain reaction. The term is commonly cited as being an acronym for "Safety Control Rod Axe Man," but NRC Historian Tom Wellock concludes that the more likely origination of this word comes from an order to "scram" (run) if there was a problem during the testing of the Chicago Pile (CP-1) reactor. https://public-blog.nrc-gateway.gov/2011/05/17/putting-the-axe-to-the-scram-myth/

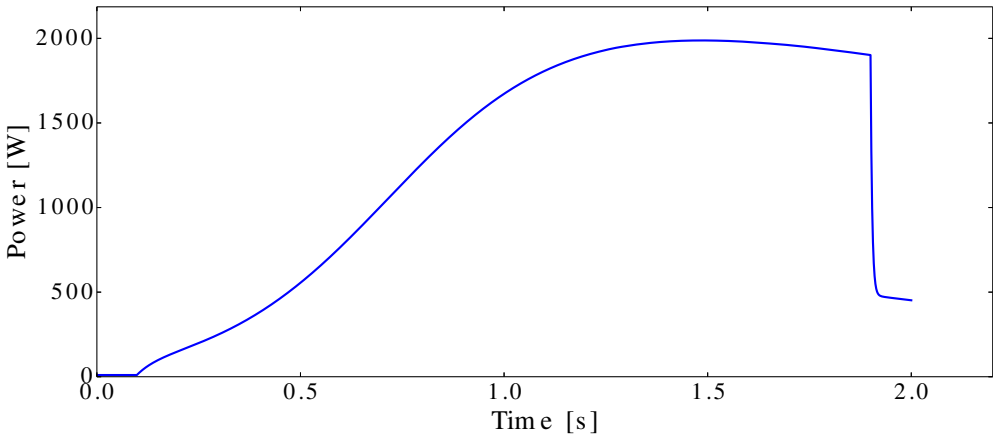

Figure 5.5. Total Power During Reduced Core Simulation.

perturbation and the significantly larger power gradients. In the heterogeneous lattice problem of Chapter 4, because of the infinitely reflected geometry, the localized perturbation is in fact repeated throughout the domain. Whereas for this transient, there is only a single control blade which is moved. Additionally, with the ramp insertion, the fuel temperature is allowed to follow the power increase more closely in the early portion of the transient. This allows negative reactivity to be slowly inserted while the control blade is being withdrawn, delaying the prompt-critical insertion point.

The fuel and water temperatures are shown in Figure 5.6. The solid lines correspond to the central assembly locations shown in Figure 5.3, while the crosses correspond to locations in the peripheral assembly. It can be noticed that there is not a significant difference between the temperatures in the central and peripheral assemblies. The removal of channel boxes around assemblies allows for the fluid to mix among assemblies, causing the fluid temperature to be more uniform than what would be present if the channel boxes remained. However, even with mixing between assemblies, the fluid temperature is not significantly changed during the transient due to the forced convection and higher heat capacity; the fluid maintains its initial uniform distribution.

The fuel temperature remaining similar through the transient can be attributed to the shape of the spatial power during the transient. Even though there is a removal of a localized absorber (the centralized control blade), the reduction in concentration does not have a significant impact on the shape of the spatial power for the perturbation needed to produce a prompt critical transient. Figure 5.7a shows the shape of the power with the control blade fully inserted, which corresponds to 100% of the nominal boron concentration. Likewise Figure 5.7b corresponds to the shape of the power when the control blade is in the dropped position, which corresponds to 70% of the nominal boron concentration. The power shown in these two figures is computed by a static k-eigenvalue calculation and normalized such that the total power is 10 W. The power shapes in these two states are very similar, which implies that there is not a significant amount of power tilt for this reactivity insertion. The perturbation of the localized absorber does affect the behavior of the reactor, but since there is still

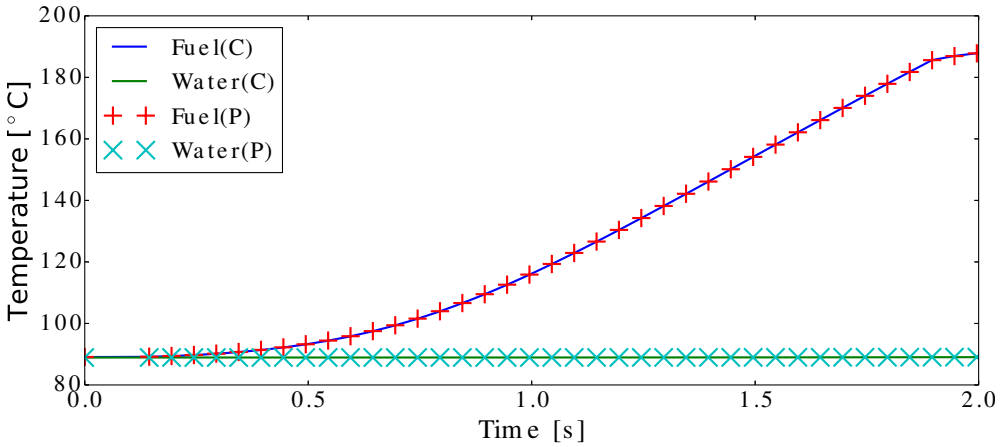

Figure 5.6. Fuel and Water Temperatures in the Central(C) and Peripheral(P) Assemblies for Reduced Core Calculation.

a significant amount of absorber present locally, the power shape only changes slightly.

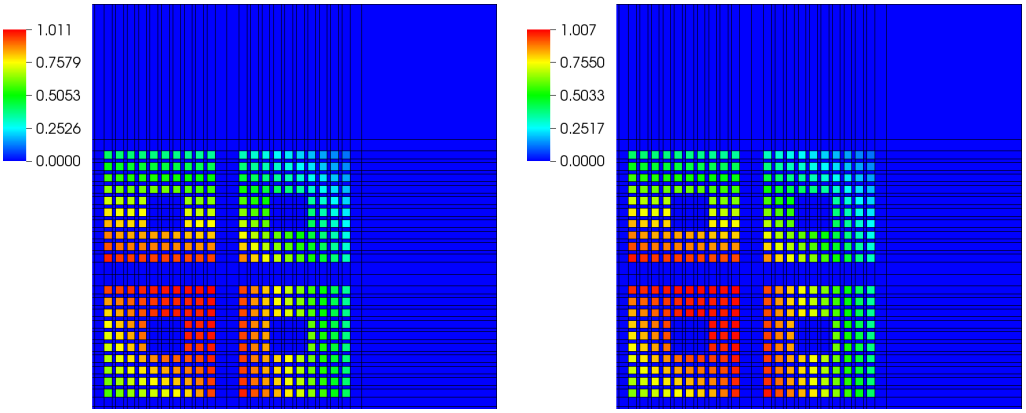

(a) Spatial Power with the Control Blade Completely Inserted. Control Blade Contains 100% Nominal Boron Concentration

(b) Spatial Power with the Control Blade Partially Removed, Corresponding to State During Transient. Control Blade Contains 70% Nominal Boron Concentration

Figure 5.7. Spatial Power for the Nominal Control Blade Position and the Perturbed Control Blade Position.

A more significant amount of power tilt can be seen in Figure 5.8, where a much lower concentration of the boron in the control blade is used. The lower boron concentration used in the control blade allows for a higher thermal flux to exist closer to the center of the geometry. This creates a shift in the location of the maximum power from the exterior of the central assembly to a more centralized location.

The spatially dependent power is shown at various times in the transient in Figures 5.9–5.13. The reflector region has a power of zero due to the absence of fissile material; this zero power level is indicated as blue in Figures 5.9–5.13.

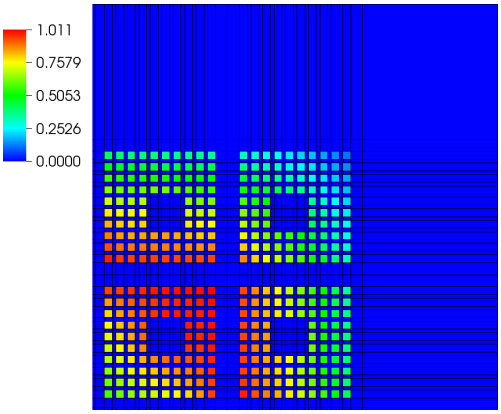

(a) Spatial Power with the Control Blade Completely Inserted. Control Blade Contains 100% Nominal Boron Concentration. Figure repeated from Figure 5.7a.

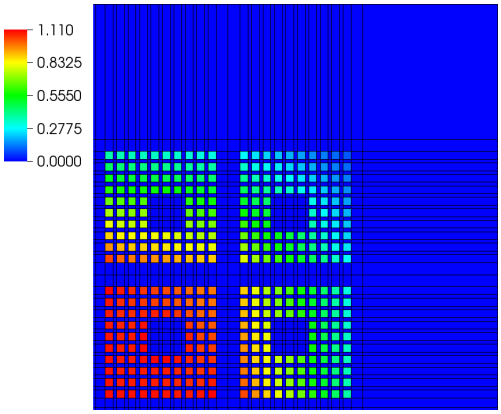

(b) Spatial Power with the Control Blade Partially Removed, Corresponding to State During Transient. Control Blade Contains 10% Nominal Boron Concentration

Figure 5.8. Spatial Power for the Nominal Control Blade Position and the Perturbed Control Blade Position. Comparing **(a)** to **(b)** shows a High Degree of Power Tilt.

The active fuel region is shown in colors ranging from light blue to red, with red denoting higher power levels. In all figures, there is diagonal symmetry from the symmetry of the problem domain. Figures 5.9 & 5.10 use a more zoomed in perspective to accentuate more details of the solution while the power is low. The remaining figures are more zoomed out due to the large increase in power. Each figure corresponds to a different time in the simulation, noted by the time bar in the lower left corner. The times correspond to the initial time, a time while the control blade is being moved, just before and after the maximum power, and at the maximum power.

The initial power distribution is shown in Figure 5.9, where the orientation of the figure puts the control blade in the top corner; this also applies to the remaining figures. Because of the presence of the control blade, the power is depressed at the center of the geometry. This central depression moves the maximum power location to the exterior of the central assembly. The maximum power is located in a band around the central assembly, which will become more apparent in subsequent figures. The total power is initially at 10 W and the maximum power is 0.8 W.

While the central control blade is being withdrawn, the power starts to increase. Figure 5.10 shows the power at 0.318 s, which is about the midpoint of the control blade withdrawal. The total power at this time is 272 W, with a maximum power of 23 W. The power increase along the exterior of the central assembly is more noticeable here and is again the result of the power depression due to the central control blade's presence. The power in the peripheral assemblies has a significant gradient due to the presence of the surrounding water reflector.

Once the control blade is fully withdrawn, the power increases quickly to a maximum. Figure 5.11 shows the power at 1.005 s, where the total power

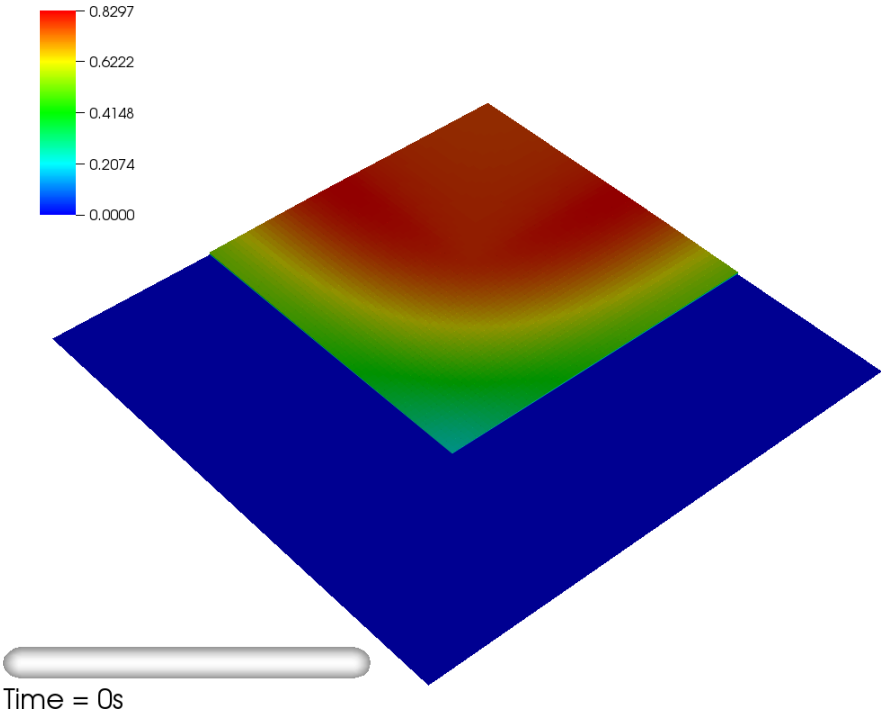

Figure 5.9. Spatially Dependent Power at Initial Time for Reduced Core Calculation. Total Power: 10 W.

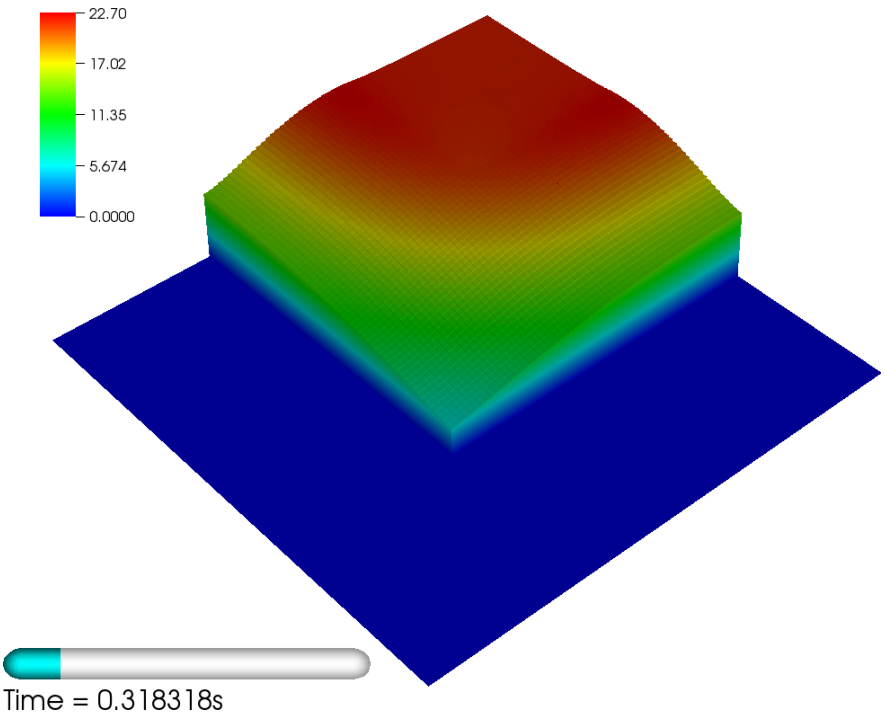

Figure 5.10. Spatially Dependent Power During Control Blade Movement. Total Power: 272 W.

is 1.68 kW and the maximum power is 140 W. The power increase along the exterior of the central assembly is clearly visible and the power gradient across

the peripheral assemblies is more pronounced.

The maximum power is reached at 1.485 s with a value of 1.99 kW. The elevated temperature in each region has not caused a significant amount of power tilt due to the small temperature gradient across the core. Hence the power shape is similar at the maximum and at lower power levels. The maximum power along the exterior of the central assembly is at 166 kW. This power increase is large enough to produce a fuel temperature which is elevated enough to counteract the effect of withdrawing the control blade. At this point the central fuel temperature is at 153.33 °C and the central subchannel temperature is at 88.96 °C. This corresponds to a temperature difference of 64.52 °C and 0.16 °C for the fuel and subchannel respectively. Since the subchannel temperature increase is small, the majority of the reactivity feedback comes from the increased fuel temperature.

After the fuel temperature has reached a sufficient amount to counteract the control blade movement, the power begins to decrease. Figure 5.13 shows the spatially dependent power at 1.730 s, where the total power is 1.95 kW, with a maximum power of 163 W. The power shape is similar to that in Figures 5.11 & 5.12, but the magnitude has decreased from that of Figure 5.12.

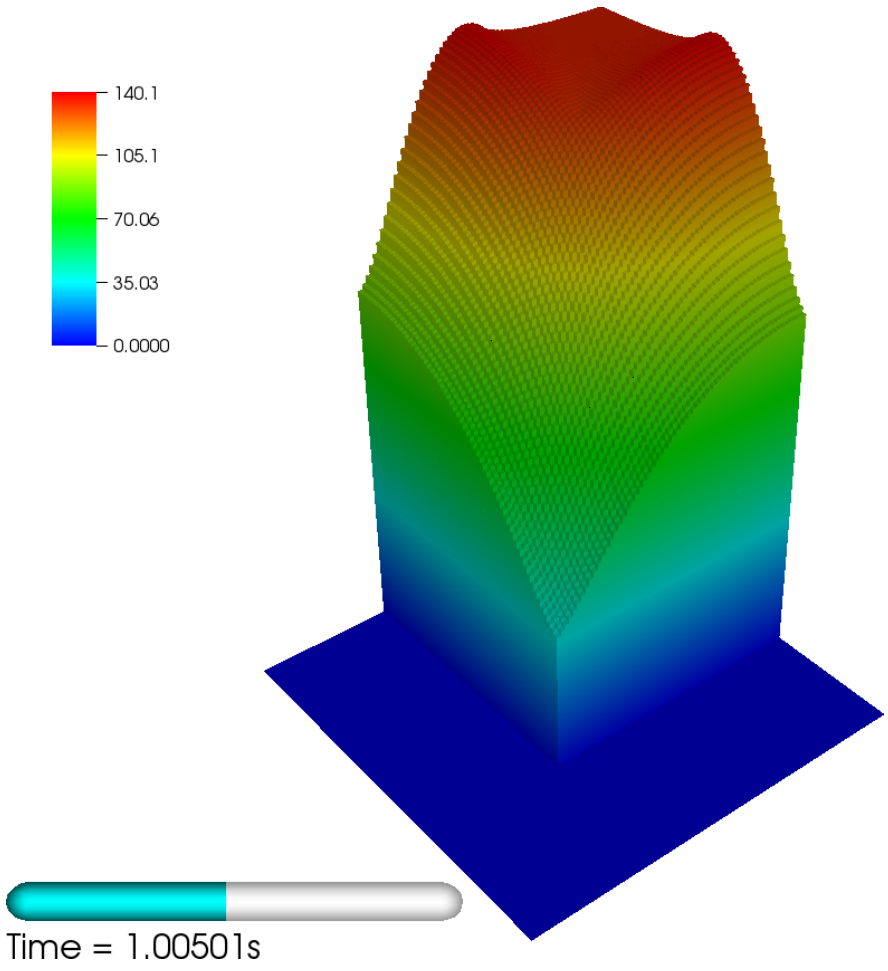

Figure 5.11. Spatially Dependent Power Before Maximum Total Power. Total Power: 1.68 kW.

Figure 5.12. Spatially Dependent Power When Total Power is at Maximum. Total Power: 1.99 kW.

Figure 5.13. Spatially Dependent Power After Maximum Total Power. Total Power: 1.95 kW.

This demonstration calculation was performed on a single processing core Intel(R) Xeon(R)-X5550(2.67 GHz) CPU with 8.2 MB of cache memory and 6.1 GB of random access memory. The entire simulation took over 3 days to complete, with detailed times shown in Figures 5.14 & 5.15. Figure 5.14 shows the cumulative time spent performing the calculation as a function of the time in the simulation. The cumulative time shows a near linear increase in computation time from 0.1 s to about 1.6 s, where the cumulative computation time rate experiences an increase. After about 1.7 s, the cumulative computation time returns to its original trend. The temporary increase in cumulative computation rate introduced an additional full day of computation time.

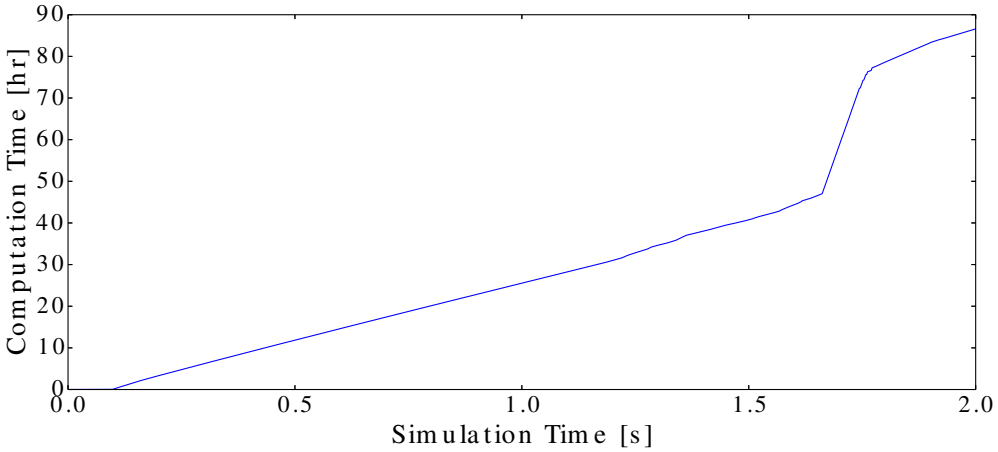

Figure 5.14. Cumulative Computation Time During Simulation in Hours for Reduced Core Calculation.

The time spent computing each time step is shown in Figure 5.15, where the computation time between 0.1 s and about 1.2 s remains nearly constant at about 3 min per time step. A large increase in the computation time per time step is seen between 1.6 s and 1.7 s, corresponding to the increase in cumulative computation time rate of Figure 5.14. Figure 5.14 is related to Figure 5.15 through a cumulative sum over the simulation time domain. This relation can be expressed as

$$F(t_i) = \sum_{j=0}^{i} f(t_j), \tag{5.2}$$

where $F(t_i)$ is the cumulative computation time for a given simulation time t_i, and $f(t_j)$ is the time required to compute the interval with an end time of t_j.

To evaluate the performance of the mulitphysics framework during the simulation, and to gain insight to the areas where improvements can be made, the number of linear and nonlinear iterations are analyzed through the simulation. The number of nonlinear iterations performed for each time step is shown in Figure 5.16. The computation time for each time step in Figure 5.15 has many of the same features as the number of nonlinear iterations per time step. The computation time is greatly increased when the number of nonlinear iterations is increased between 1.6 s and 1.7 s. A significant improvement in computation

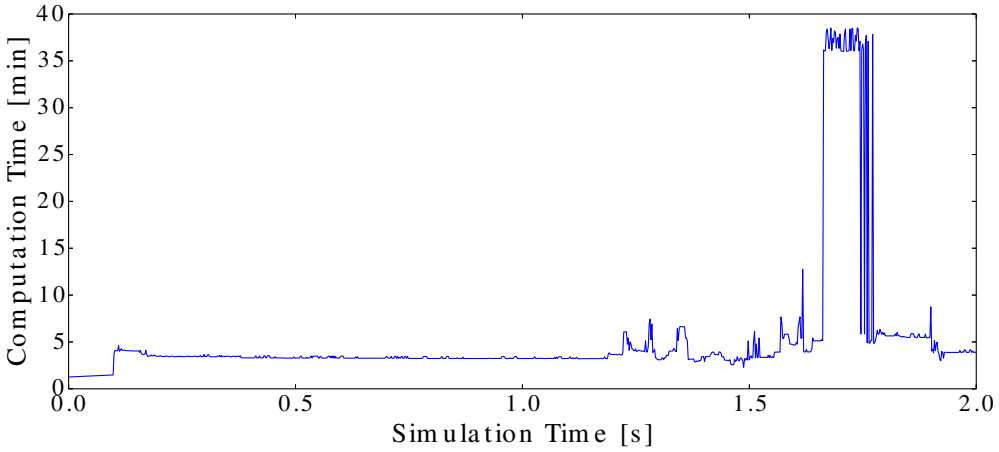

Figure 5.15. Computation for Each Time Step During Simulation in Minutes for Reduced Core Calculation.

time can be achieved by reducing the number of nonlinear iterations required to converge, especially in the interval where 15 iterations per time step are required.

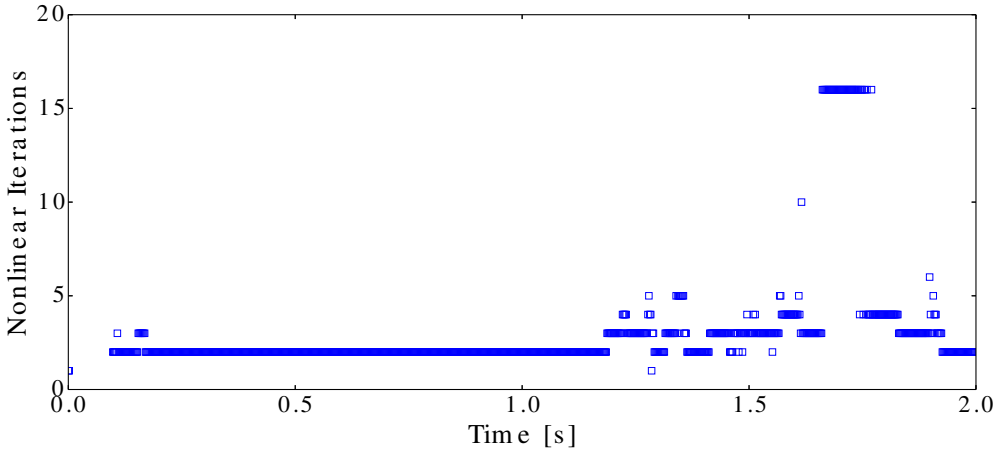

Figure 5.16. Number of Nonlinear Iterations for Each Time Step During Simulation for Reduced Core Calculation.

The average number of linear iterations per nonlinear iteration for each time step is shown in Figure 5.17. The average number of linear iterations remains relatively constant throughout the simulation at around 2 linear iterations per nonlinear iteration. This low number of linear iterations is a result of the effective physics-based preconditioner used in the simulation.

The time spent for this simulation is prohibitively expensive for industrial sized applications, and improvements will need to be made to the multiphysics framework before more detailed calculations can be conducted. The largest problem area is the increase in nonlinear iterations required to converge later in the simulation (between 1.6 s and 1.7 s). The increase from about 5 nonlinear iterations to 15 nonlinear iterations adds a full day of computation. A possible reduction in the number of nonlinear iterations could come from a reduced time step in this interval; a smaller time step means that the initial Newton iterate

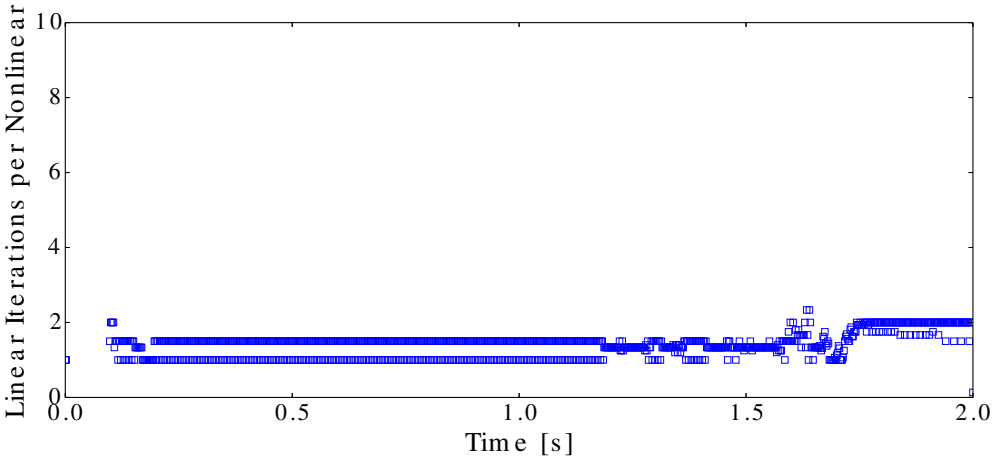

Figure 5.17. Average Number of Linear Iterations per Nonlinear Iteration for Each Time Step During Simulation for Reduced Core Calculation.

is closer to the converged solution. Conversely, an increased time step size could be used in the interval between 0.1 s and 1.2 s, given the low number of linear and nonlinear iterations required to converge. The implementation of a more sophisticated *adaptive time step* formulation would help in this regard [91].

Even outside this range of increased nonlinear iterations, where the number of nonlinear iterations is around 3 with 3 min per time step, improvements can be made. The residuals for each physics component are evaluated many times during the simulation. The average time spent computing the Transport, Precursor, and Temperature residuals is shown in Table 5.3.

Table 5.3. Average Time Spent Computing the Physics Component Residuals.

Physics Component	**Computation Time [s]**
Neutron Transport	0.5
Delayed Neutron Precursor	3.0
Thermal Hydraulics	0.05

With an average of 2 linear iterations per nonlinear iteration, each residual is evaluated 4 times per nonlinear iteration because of the centered difference formulation in the Jacobian vector product. The central difference formulation for the Jacobian vector product is repeated from Section 3.2.4

$$\mathbf{J}\vec{v} \approx \frac{\vec{F}(\vec{U}+\varepsilon\vec{v}) - \vec{F}(\vec{U}-\varepsilon\vec{v})}{2\varepsilon}. \qquad [2^{\text{nd}} \text{ order}] \quad (3.27)$$

About 73% of the computation time during a nonlinear iteration is spent inverting the physics-based preconditioner, with 70% of that time spent evaluating the precursor residual. A significant improvement in this computation could be accomplished by improving the speed of inverting the preconditioning matrix.

Since the majority of the time spent inverting the preconditioner is in evaluating the precursor residual, a substantial amount of effort should be further devoted to optimizing the precursor residual evaluation. Another option for a faster preconditioner inversion is through evaluating the inverse preconditioner in parallel; since the Jacobian is approximated as a block diagonal matrix, each diagonal block can be inverted simultaneously. Additionally, for each physics component, a coarser spatial mesh could be used to reduce the size of each physics block needing to be inverted.

The computation of the residual, which is evaluated many times during the simulation can be further optimized. The evaluation of the precursor residual is the dominant evaluation among the physics components in this simulation. The computation of the precursor residual involves the manipulation of a large vector with a size of the number of delayed neutron precursor groups times the size of the fission source; for this calculation 8 delayed neutron precursor groups are used and the fission integral contains 7,688 entries. The construction involves repeatedly scaling the fission source vector by delayed neutron constants for each precursor group; splitting this operation among several processors has the potential to bring this residual's evaluation down to the time of the transport residual evaluation. An 8× reduction in the precursor computation time could significantly reduce the overall computation time, given the large number of times this residual is evaluated.

5.3 Conclusions

The reduced core demonstration problem, computed with 2 group assembly homogenized cross sections, was completed and shows that the multiphysics solver can produce solutions to larger cases. While the framework was able to produce a solution to a larger problem, the calculation took a considerable amount of time to obtain. The reduced core problem with 2 group assembly homogenized cross sections took over 3 days to compute. This level of computation time is not suitable for use in industrial calculations.

A readily available modification to improve the computation speed could be to model an eighth core instead of a quarter core, reducing the number of spatial points the transport solver must sweep and the number of spatial points in the precursor residual evaluation. However, reducing the transport sweep time is not expected to have a large impact on the overall computation time. The evaluation of a single transport residual took an average of 0.5 s, while the evaluation of a single precursor residual took much longer, averaging 3.0 s. Reducing the cost of evaluating the precursor residual will have a larger impact on the overall computation time.

The simulations performed for this demonstration calculation were performed on a single processing core, not exploiting parallel methods. The increasing level of detail sought for multiphysics simulations in this work will inevitably require the use of parallel methods. There are several processes in this simulation which could benefit from the implementation of parallel methods; these processes constitute the class of embarrassingly parallel processes [39]. One such process is the

construction of the delayed neutron precursor residual. This evaluation involves repeated manipulations of the fission source, which are independent for each delayed neutron precursor group. The separation of this task among a number of processors has the potential to increase the evaluation speed by $8\times$. Another significant computation cost comes from the inversion of the preconditioning matrix, which can be considered an embarrassingly parallel process. While the preconditioner is effective at reducing the average number of linear iterations per nonlinear iteration, the cost of inverting this preconditioner is expensive. An immediate improvement can be made by inverting the block diagonal matrices for each physics component in parallel. Since these block inversions are independent of other physics components, each inversion can be computed in parallel. The use of parallel transport sweeps and of domain decomposition methods within the thermal hydraulics residual computations will additionally reduce the computation cost, but will have less of an immediate impact than the two previously mentioned modifications.

Several improvements to the models used to treat the case in this chapter can be made. A significant drawback to the model produced is the limited number of temperature points used to evaluate cross sections in the transport solver. There was only a single fuel and fluid temperature used for each material in the transport solver (central and peripheral assemblies). A more accurate model would take into account the spatial temperature distribution on a smaller scale. Increasing the detail of the temperature distribution within the domain has the effect of increasing the memory required to store spatially dependent macroscopic cross sections. A temperature variation in a medium will effectively increase the number of media used in the transport solver. This increased memory consumption could affect the speed of obtaining the transport solution due to the rise in memory access. For the present demonstration, the number of media could increase from three to nearly 8500.

To simulate a different type of accident, starting from HZP for example, will require a more complex thermal hydraulics model. The simulation shown in this chapter was heavily simplified thanks to the accident starting from CZP. A transient starting from HZP will require modeling the channel boxes, which decouple the thermal hydraulics between assemblies and modeling the water column present in each assembly. At HZP, there is significantly more vapor present around the fuel pins and will thus induce condensation around the heat sink provided by the water column. Additional correlations accounting for this condensation will need to be introduced to the thermal hydraulics model.

Chapter 6

Conclusions

The work discussed in this dissertation focuses on the accurate simulation of reactivity insertion accidents. The objective of this work was to show how physics component codes may be coupled together in a multiphysics framework based on JFNK and to study the impact of using homogenized cross sections in transient calculations. The methods developed in this work can be effectively applied to treat the simulation of severe accidents where the reactivity insertion is such that the nuclear system is super prompt critical. In such a case, the nuclear system is far from a fundamental mode configuration and large feedback effects are present, which drive the solution.

The homogenization methods developed in this work have been tested on smaller scale simulations to show their potential use in nuclear engineering applications. The transfer to industrial sized calculations will require a number of additional studies for these methods to be deemed useful in industrial codes. One such study should test the behavior of the methods when a neutron diffusion model is used in the homogenized calculation. In the cases treated for this work, a neutron transport model was used in both the reference calculation and the homogenized calculation. Another large advancement required for the Fluence method will be to obtain a time dependent flux in a reasonable time. This can be accomplished through parallelization or forming an appropriate approximation to the time dependent flux. The present chapter summarizes the results of this work, draws several conclusions, and gives the author's vision for the future developments of this work.

6.1 Multiphysics Coupling

One of the main goals of this work was to develop a framework in which multiple physics codes, which were not originally intended to operate in a multiphysics simulation, could be coupled. The typical way to implement such a multiphysics framework is to use an operator splitting technique where the coupling between component codes is treated through I/O. This type of coupling scheme treats only weak coupling between physics components and may experience convergence dif-

ficulties. The method of choice for this work was based on the JFNK method, where all physics components are treated in a single large system. This type of method resolves the coupling between physics components at each time step of the solution process through nonlinear iterations. A Newton method is used as the nonlinear iterator because of its superior convergence over other nonlinear methods like Fixed point and Picard.

The weak point of implementing a JFNK method to drive multiphysics simulations is in the potentially heavy modifications needed in the component codes. The JFNK method requires a solution residual be returned from each physics component, which is typically not an operation that component codes will supply. These solution residual computations must then be either implemented within the codes or computed exterior the codes by controlling operations within a component code.

Implementing the residual computation within component codes requires each component code be able to manipulate a solution from other component codes; the residual function for a single physics component depends on the solution from all physics components. Each physics component could then simply accept the entire multiphysics solution and return the solution residual for that physics component. This implementation is more robust and modular, but it requires that each time a physics component is added to the simulation, all physics component codes must be modified. At the outset of this work, it was not known if the author would have the opportunity to heavily modify component codes, so this method was not chosen.

Alternatively, computing the solution residual exterior to the component codes offers more flexibility in computing residuals. The component codes are driven through function calls, which control the various steps needed to produce a solution residual. Once these function calls are established, modifications to existing component codes are not needed if additional physics components are added to the simulation. This is the way residuals are computed within the results of this work. The delicate portion of this strategy is the correct implementation of the function calls to physics components. The code must be modified to facilitate extracting information from other solutions. Exterior to the component codes, solutions must be correctly mapped to a form that component codes are expecting.

A new formulation for the neutron transport residual was developed based on the fission source instead of the angular flux. The reduction in residual size with this formulation is significant. This new version of the neutron transport residual reduces the size of the solution by a large factor; a factor of 3120 in the heterogeneous results presented in Section 4.4.2. The residual was shown to be correctly implemented by tracking the error convergence through the refinement of the time domain. The reference solution was computed analytically from a 1 point, 1 energy group model with 2 delayed neutron precursor groups.

Two physics-based preconditioners, which only require manipulations of the solution residual, were tested. The two physics-based preconditioners (Block Jacobi and Block Gauss-Seidel) were tested against an identity preconditioner. The physics-based preconditioners were shown to reduce the average ratio of linear

to nonlinear iterations during a transient. The power behind such preconditioners, which only manipulate the solution residual, is that the underlying physics is not needed to produce an effective preconditioner. The supplier of the multiphysics framework can also supply effective physics-based preconditioners without having to know which physics components will be used within the framework.

The multiphysics framework developed for this work was tested on a reduced core BWR calculation to show the ability of the framework to produce solutions in accident simulations. The reduced core problem simulates a rod drop accident during startup from CZP. Several simplifications were introduced based on the transient starting from a CZP state, including the removal of some structural material and a low number of temperature points being used for cross section interpolation. Using 2 group assembly homogenized cross sections shows that the framework produces multiphysics solutions to the simulated accident. Additionally several improvements were suggested to more accurately and more efficiently obtain such solutions.

6.2 Homogenization

A power excursion in an infinite homogeneous medium with 281 energy groups was initially studied. It was shown that for fast transients, where a reactivity greater than β is inserted, using homogenized cross sections produced with a fundamental mode flux introduces significant errors in the time dependent power and temperature. These errors were still present, but not as significant when the reactivity insertion was below β.

Two new homogenization methods were developed to reduce the errors incurred from using a fundamental mode flux in the homogenization process. The first method (Alpha) relied on obtaining eigenvectors from an α-eigenvalue problem instead of the usual k-eigenvalue problem. The α-eigenvectors, which correspond to the $N_d + 1$ principal eigenvalues, were used in several combinations as a weighting flux in the homogenization process. The second method (Fluence) used a time integrated flux, which comes from a multiphysics solution on subdomains of the problem. The time integrated flux serves as the weighting flux in the homogenization process.

In the infinite homogeneous medium case, where spatial dependence does not appear, both new methods significantly reduced the error incurred when using critically homogenized cross sections. Initially, delayed neutrons were suppressed to explore the behavior of fast transients. Under this approximate situation, the Fluence and Alpha method performed well. The Alpha method only used the dominant eigenvector as the weighting flux. Both methods perform well because the time dependent solution reaches the asymptotic solution very quickly after the perturbation. It was also shown that the new methods are not affected by the size of the reactivity insertion or homogenized group structure.

Delayed neutrons were activated in the neutron transport model, which produce behavior that more closely resembles what is observed in reactor analysis. The addition of delayed neutrons caused the Alpha method to require more than a single eigenvector be taken as the weighting flux to capture the long term be-

havior of the transient. Several eigenvectors were combined to produce a single weight flux; three versions of this combination were explored. The version which worked the best used an integration of the time dependent solution, constructed from an expansion over the α-eigenmodes. The Fluence method was not affected by the addition of delayed neutrons. It was observed that for reactivity insertions less than β, using critically homogenized cross sections performed sufficiently well. This observation can justify the use of critical cross sections when modeling operational transients. However, when modeling super prompt critical transients, critically homogenized cross sections can introduce large errors.

A spatially heterogeneous problem was investigated to test whether such methods would perform well with a non-uniform reactivity insertion. The addition of spatial heterogeneities did not impact the performance of the new methods. The Fluence method was tested on a subdomain of the reference problem. It was observed that the Fluence method needed a homogeneous buffer to simulate the environment of the reference problem to produce effective homogenized cross sections. Without the homogeneous buffer, the same boron concentration perturbation from the reference calculation produced a much larger reactivity insertion in the isolated region calculation. The effect of the discretization of time intervals was tested for this heterogeneous problem. It was shown that errors are reduced with successive refinement of the time interval discretization until a point where interpolation errors become dominant.

The results from this work show that in certain cases, using homogenized cross sections intended for steady state calculations in transient calculations may introduce significant errors. A way to remedy the introduction of such errors is to use the new methods developed in this work which take into account the time dependent behavior of coupled physics solutions. The most effective method to apply depends on the type of transient simulated.

6.3 Future Work

Several paths are available for exploration beyond the work presented in this dissertation. The following is a discussion on the author's vision for the continued development in this area of research.

6.3.1 Multiphysics Coupling

In terms of the multiphysics simulations studied in this work, several improvements can be explored. Such improvements are both in the modeling of physical components and in the design of software used in the simulations.

The thermal hydraulic model used in these calculations uses a drift flux approximation for the velocities of steam and water. This model does not represent reality closely when applied to fast transients, where a full two species model is more appropriate. In the simulations presented for this work, the system was operating initially at CZP, where the fluid and fuel are nearly in thermal equilibrium. The rapid power transient did not raise the temperature of the fluid significantly. In performing calculations where significant steam were present,

at HFP for instance, the power excursion could significantly affect the thermal hydraulics of the steam. To study these accidents, a more complex 6-equation model should be used.

The residual formulations presented in this work were discretized in time using first order methods. In reducing the size of the transport residual by eliminating the angular flux, the residual was limited to a first order in time discretization, where higher order methods would require the manipulation of the angular flux. However, higher order methods can be advantageous when applied to stiff problems, like those of large reactivity insertion accidents. A possible way to achieve this extension is by using the Runge-Kutta methods described in Section 2.1.4. Such methods allow for a flexible way to increase the method order without significant modifications to the algorithm. An interesting study would be to observe the effect of the increased residual size on the convergence for the Krylov linear solver. The increase in residual size would be justified if the linear iterations did not significantly increase and larger time steps could be taken with the higher order Runge-Kutta method.

The BWR core calculation performed introduced several simplifying assumptions which should be addressed to produce more accurate solutions for a wider range of accidents. The reintroduction of structural material (channel boxes and assembly water columns) will require more complex thermal hydraulic modeling. The channel boxes, which decouple the thermal hydraulics of assemblies, will produce more localized effects in the fluid temperature. The water column within assemblies provides a heat sink where vapor can condense. Modeling accidents at higher powers will require incorporating condensation correlations for the influence of the central water column when more vapor is present. Modeling such accidents at higher powers could bring into question the use of a drift flux model due to the possibility of having disparate vapor and fluid velocities, at which point the thermal hydraulic model will need to be heavily modified. Additionally, a small number of temperature points are used to evaluate the temperature dependence of cross sections. Increasing the number of points used in the current implementation of the transport solver will significantly increase the number of materials present in the cross section data. This increase in cross section data storage could slow the transport solution due to the increase in memory access from the higher number of media required.

6.3.2 Software Design

During the design of the numerical framework to resolve multiphysics systems, special care was taken to provide well defined boundaries in the software. All components are programmed to well defined interfaces, making it easier to swap appropriate algorithms when necessary. For example, there are several linear solver algorithms under the "linear solver" interface; by programing to the linear solver interface, GMRes can be replaced with Gaussian elimination with minimal changes in the code. This design feature makes the software flexible and extensible; the use of external commercial numerical libraries is possible through this design. A direction the author would like to continue is in developing adapters

so that the power of these commercial numerical libraries can be used in the multiphysics framework.

Typically when solving large scale numerical simulations, significant amounts of parallelization are sought in the codes used. Parallel codes make use of the largest and fastest computers currently available. A significant weakness of the simulations presented in this work is the lack of parallel methods. A large amount of work could be devoted to adding parallel capability to the underlying physics component codes and the multiphysics framework. In the neutron transport model, a parallel sweeping algorithm could improve the size of transport problems able to be tractably solved. Domain decomposition methods can allow larger problems to be solved using large parallel machines. In the thermal hydraulic model, subchannels can be split among several processes which communicate to evaluate mixing among channels. On the level of the multiphysics framework, significant amounts of parallelization are possible. Chapter 5 demonstrated that a significant amount of time was devoted to evaluating the delayed neutron precursor residual, which involves several manipulations of the fission source. Splitting these manipulations over several processes has the potential to significantly reduce the time spent evaluating this residual. The evaluation of other residuals can also be performed in parallel, especially if the underlying physics components have parallel capabilities. The linear solvers can be made to use parallel capabilities through manipulations of matrix vector products in parallel. Furthermore, the physics-based preconditioner used in Chapter 5, which is a block diagonal matrix, can be inverted in parallel by simultaneously inverting each block diagonal matrix. Implementing such parallel methods will be essential for the continued used of the present multiphysics framework.

6.3.3 Cross Section Homogenization

The homogenization methods explored in this work have shown promise in their ability to reduce errors incurred from methods currently in practice. The development of such methods still has improvements which can be made in how the methods are applied, and to which problems these methods are applied.

When computing the weights for each eigenvector of the Alpha method, a minimization was performed with some reference flux; in the results of this work, the initial flux was chosen. This choice of reference flux was made based on the idea of finding the expansion coefficients for a time dependent solution and the availability of the initial flux. An excellent extension to the Alpha method would be to study the effect of using different reference fluxes to determine weighting coefficients. For example, if an estimate for the temperature were available, the flux could be estimated at various points through the transient and used to generate weighting coefficients for the Alpha method.

One of the most prominent advancements in homogenization methods came through the addition of extra degrees of freedom through discontinuity factors. These factors remove the assumption of a continuous flux at homogenized region interfaces to better conserve reaction rates within these regions. Adding discontinuity factors to the Fluence method can be straight forward by evaluating the

fraction of the time-integrated volume flux and of the time-integrated boundary flux. However for the Alpha method, because of the multiple eigenvectors used, there are more choices in the application of discontinuity factors. One might apply the same coefficients to the discontinuity factors, but there may be more optimal choices in how to apply these discontinuity factors. This extension is more applicable when the homogenized problem is modeled with neutron diffusion since discontinuity factors are intended to be used when applying a lower order operator in the homogenized problem.

When applying the Fluence method to spatially heterogeneous problems, a homogeneous buffer was added to the subdomain which made reactivity insertions similar in the reference problem and subdomain calculation. While this homogeneous buffer did accurately represent the surrounding assemblies, it was still required to sweep through this domain during the simulation. A less expensive option would be to approximate the surrounding media by an albedo boundary condition. If an accurate time-dependent albedo condition were available, the calculation of a time dependent solution on subdomains for the Fluence method could be performed faster.

The large drawback to the Fluence method is the cost in computing the time dependent flux used in the homogenization process. For the spatially heterogeneous case of Chapter 4, the solution took 4 days to obtain. For this method to be applied to industrial sized simulations, a reduction in the time required to obtain a time dependent flux is essential. A promising direction to pursue is in the parallelization of the calculation to obtain this solution. Parallelization of the transport sweep algorithm could provide significant speedup in this calculation.

The homogenization methods were applied to a reduced core calculation. While this application shows that these methods have the potential to be useful in transient reactor analysis, much is left to be explored. The Expert Group on Radiation Transport and Shielding (EGRTS) under the Working Party on Scientific Issues of Reactor Systems as part of the Nuclear Energy Agency is developing a time dependent benchmark problem based on the mixed oxide PWR benchmark (C5G7) [167]. Once this benchmark is available to the public, it would be desired that the new methods are applied to this case to compare the reduction in error these new methods bring.

References

[1] Clarno, K. T., Philip, B., Cochran, W. K., *et al.* "The AMP (Advanced MultiPhysics) Nuclear Fuel Performance code." *Nuclear Engineering and Design*, 252:108–120 (November 2012).

[2] Chen-Mayer, H. & Tosh, R. E. "Simulation of Radiation Dose from Diagnostic X-ray Beams." In: *COMSOL 2013 Conference* (Boston, MA (USA), 2013).

[3] Cary, J. R., Candy, J., Cobb, J., *et al.* "Concurrent, Parallel, Multiphysics Coupling in the FACETS Project." *Journal of Physics: Conference Series*, 180(012056):1–7 (2009).

[4] Mezzacappa, A. & Messer, O. E. B. "Neutrino transport in core collapse supernovae." *Journal of Computational and Applied Mathematics*, 109:281–319 (1999).

[5] Zwart, S. P., McMillan, S., Nualláin, B. O., *et al.* "A Multiphysics and Multiscale Software Environment for Modeling Astrophysical Systems." In: *International Conference on Computational Science* (Kraków (Poland), 2008).

[6] Todreas, N. E. & Kazimi, M. S. *Nuclear Systems I: Thermal Hydraulic Fundamentals* (Taylor & Francis, 1993), 2nd edition.

[7] Siegel, A., Tautges, T., Caceres, A., *et al.* "Software Design of SHARP." In: *International Topical Meeting on Mathematics & Computation and Supercomputing in Nuclear Applications (M&C + SNA 2007)* (Monterey, CA (USA), 2007).

[8] Gaston, D., Newman, C., Hansen, G., *et al.* "MOOSE: A parallel computational framework for coupled systems of nonlinear equations." *Nuclear Engineering and Design*, 239(10):1768–1778 (October 2009).

[9] Mahadevan, V. S., Ragusa, J. C., & Mousseau, V. A. "A verification exercise in multiphysics simulations for coupled reactor physics calculations." *Progress in Nuclear Energy*, 55:12–32 (March 2012).

[10] Keyes, D. E., McInnes, L. C., Woodward, C., *et al.* "Multiphysics simulations: Challenges and opportunities." *International Journal of High Performance Computing Applications*, 27:4–83 (2012).

[11] "NEAMS: The Nuclear Energy Advanced Modeling and Simulation Program." http://energy.gov/ne/downloads/nuclear-energy-advanced-modeling-and-simulation-neams-program-plan.

[12] Chauliac, C., Aragonés, J.-M., Bestion, D., *et al.* "NURESIM – A European simulation platform for nuclear reactor safety: Multi-scale and multi-physics calculations, sensitivity and uncertainty analysis." *Nuclear Engineering and Design*, 241(9):3416–3426 (September 2011).

[13] Schmidt, R. C., Belcourt, K., Clarno, K. T., *et al.* "Foundational Development of an Advanced Nuclear Reactor Integrated Safety Code." Technical report, Sandia National Lab (SAND2010-0878) (2010).

[14] Bergeaud, V. & Lefebvre, V. "SALOME: a software integration platform for multi-physics, pre-processing and visualisation." In: *International Conference on Supercomputing in Nuclear Applications and Monte Carlo (SNA + MC2010)* (Tokyo (Japan), 2010).

[15] "Salome Documentation." http://www.salome-platform.org/user-section/documentation/current-release.

[16] Ropp, D. L. & Shadid, J. N. "Stability of operator splitting methods for systems with indefinite operators: reaction-diffusion systems." *Journal of Computational Physics*, 203(2):449–466 (2005).

[17] Balay, S., Abhyankar, S., Adams, M. F., *et al.* "PETSc Users Manual." Technical Report ANL-95/11 - Revision 3.7, Argonne National Laboratory (2016).

[18] "U.S. NRC Glossary." http://www.nrc.gov/reading-rm/basic-ref/glossary.html.

[19] "Mitigation of Hydrogen Hazards in Severe Accidents in Nuclear Power Plants." Technical report, IAEA-TECDOC-1661 (2011).

[20] Studer, E., Magnaud, J., Dabbene, F., *et al.* "International standard problem on containment thermal-hydraulics ISP47 Step 1 - Results from the MISTRA exercise." *Nuclear Engineering and Design*, 237:536–551 (2007).

[21] Seiler, J. & Ganzhorn, J. "Viscosities of corium-concrete mixtures." *Nuclear Engineering and Design*, 178(3):259–268 (1997).

[22] Lee, M. & Kazimi, M. "Modeling of Corium/Concrete Interaction." Technical report, MITNE-267 (June 1985).

[23] Allelein, H.-J. & Bürger, M. "Considerations on Ex-Vessel Corium Behavior: Scenarios, MCCI and Coolability." *Nuclear Engineering and Design*, 236:2220–2236 (October 2006).

[24] Roberts, J. A. "A High-Order, Time-Dependent Response Matrix Method for Reactor Kinetics." *Nuclear Science and Engineering*, 179:333–341 (2015).

[25] Dulla, S., Mund, E. H., & Ravetto, P. "The quasi-static method revisited." *Progress in Nuclear Energy*, 50:908–920 (2008).

[26] Mika, J. "Fundamental Eigenvalues of the Linear Transport Equation." *Journal of Quantitative Spectroscopy and Radiative Transfer*, 11:879–891 (1971).

[27] Betzler, B. R., Kiedrowski, B. C., Brown, F. B., *et al.* "Calculating alpha Eigenvalues in a Continuous-Energy Infinite Medium with Monte Carlo." Technical report, Los Alamos National Lab (LA-UR-12-24472) (2012).

[28] Dall'Osso, A. "Neutron spectrum kinetics in the infinite homogeneous reactor." *Annals of Nuclear Energy*, 85:662 – 669 (November 2015).

[29] Valette, M., Pouvreau, J., Bestion, D., *et al.* "Revisiting large break LOCA with the CATHRE-3 three-field model." *Nuclear Engineering and Design*, 241:4487–4496 (2011).

[30] Fillion, P., Chanoine, A., Dellacherie, S., *et al.* "FLICA-OVAP: A new platform for core thermal-hydraulic studies." *Nuclear Engineering and Design*, 241:4348–4358 (2011).

[31] Pothukuchi, H., Patnaik, B. S. V., & Prasad, B. V. S. S. S. "Sub-channel analysis of rod bundle thermal hydraulics: Effect of eccentricity and blockage." *Nuclear Engineering and Design*, 300:475–494 (2016).

[32] Cheng, X., Batta, A., Bandini, G., *et al.* "European activities on cross-cutting thermal-hydraulic phenomena for innovative nuclear systems." *Nuclear Engineering and Design*, 290:2–12 (2015).

[33] Ober, C. C. & Shadid, J. N. "Studies on the accuracy of time-integration methods for the radiation-diffusion equations." *Journal of Computational Physics*, 195(2):743–772 (2004).

[34] Ropp, D. L., Shadid, J. N., & Ober, C. C. "Studies of the accuracy of time integration methods for reaction-diffusion equations." *Journal of Computational Physics*, 194(2):544–574 (2004).

[35] Ragusa, J. C. & Mahadevan, V. S. "Consistent and accurate schemes for coupled neutronics thermal-hydraulics reactor analysis." *Nuclear Engineering and Design*, 239:566–579 (2009).

[36] Lee, D., Downar, T. J., Ulses, A., *et al.* "Analysis of the OECD/NRC BWR Turbine Trip Transient Benchmark with the Coupled Thermal-Hydraulics and Neutronics Code TRAC-M/PARCS." *Nuclear Science and Engineering*, 148:291–305 (2004).

[37] Knoll, D. & Keyes, D. "Jacobian-free Newton-Krylov methods: a survey of approaches and applications." *Journal of Computational Physics*, 193(2):357–397 (January 2004).

[38] Heroux, M. A., Bartlett, R. A., Howle, V. E., *et al.* "An overview of the Trilinos project." *ACM Transactions on Mathematical Software*, 31(3):397–423 (2005).

[39] Foster, I. *Designing and Building Parallel Programs* (Addison-Wesley, Boston, MA (USA), 1995).

[40] Evans, T. "Denovo: A New Three-Dimensional Parallel Discrete Ordinates Code in SCALE." *Nuclear Technology*, 171(2):171–200 (August 2010).

[41] Towara, M., Schanen, M., & Naumann, U. "MPI-Parallel Discrete Adjoint OpenFOAM." *Procedia Computer Science*, 51:19–28 (2015).

[42] Smith, K. "Assembly homogenization techniques for light water reactor analysis." *Progress in Nuclear Energy*, 17(3):303–335 (January 1986).

[43] Hébert, A. & Mathonnière, G. "Development of a Third-Generation Superhomogénéisation Method for the Homogenization of a Pressurized Water Reactor Assembly." *Nuclear Science and Engineering*, 115:129–141 (1993).

[44] Clarno, K. T. & Adams, M. "Capturing the Effects of Unlike Neighbors in Single-Assembly Calculations." *Nuclear Science and Engineering*, 149(2):182–196 (February 2005).

[45] Jung, Y. S. & Joo, H. G. "Investigation of Conditional Transport Update in Method of Characteristics Base Coarse Mesh Finite Difference Transient Calculation." In: *Physics of Reactors (PHYSOR)* (Kyoto (Japan), 2014).

[46] Velarde, G., Ahnert, C., & Aragonés, J. M. "A Comparison of the Eigenvalue Equations in k, α, λ and γ in Reactor Theory. Application to Fast and Thermal Systems in Unreflected and Reflected Configurations." Technical report, Junta de Energia Nuclear (NEACRP-L-187) (1977).

[47] Gaston, D. R., Permann, C. J., Peterson, J. W., *et al.* "Physics-based multiscale coupling for full core nuclear reactor simulation." *Annals of Nuclear Energy*, 84:45–54 (October 2015).

[48] Ainscough, J. B. "Gap Conductance in Zircaloy-Clad LWR Fuel Rods." Technical report, NEA/CSNI-72 (1982).

[49] Ivanov, K. N., Beam, T. M., Baretta, A. J., *et al.* "Pressurized Water Reactor Main Steam Line Break (MSLB) Benchmark – Final Specifications." Technical report, NEA/NSC/DOC(99)8 (April 1999).

[50] Marguet, S. *La physique des réacteurs nucléaires* (Lavoisier, Paris (France), 2013).

[51] Duderstadt, J. J. & Martin, W. R. *Transport Theory* (John Wiley & Sons, New York, NY (USA), 1979).

[52] Stacey, W. M. *Nuclear Reactor Physics* (Wiley-VCH, Weinheim (Germany), 2007).

[53] Baum, E. M., Knox, H. D., & Miller, T. R. *Nuclides and Isotopes: Chart of the Nuclides* (KAPL Inc., Niskayuna, NY, 2002), 16th edition.

[54] Duderstadt, J. J. & Hamilton, L. J. *Nuclear Reactor Analysis* (John Wiley & Sons, New York, NY (USA), 1976).

[55] Spriggs, G. D., Campbell, J. M., & Piksaikin, V. M. "An 8-group Delayed Neutron Model Based on a Consistent Set of Half-lives." *Progress in Nuclear Energy*, 41:223–251 (2002).

[56] Cacuci, D., Ronen, Y., Shayer, Z., *et al.* "Eigenvalue-Dependent Neutron Energy Spectra: Definitions, Analyses, and Applications." *Nuclear Science and Engineering*, 81:432–442 (1982).

[57] Keepin, G. R. *Physics of Nuclear Kinetics* (Addison-Wesley Publishing Company, Reading, MA (USA), 1965).

[58] Brady, M. C. & England, T. R. "Delayed Neutron Data and Group Parameters for 43 Fissioning Systems." *Nuclear Science and Engineering*, 103:129–149 (October 1989).

[59] Blachot, J., Brady, M. C., Filip, A., *et al.* "Status of Delayed Neutron Data - 1990." Technical report, NEACRP-L-323 (December 1990).

[60] Parish, T. A., Charlton, W. S., Shinohara, N., *et al.* "Status of Six-Group Delayed Neutron Data and Relationships Between Delayed Neutron Parameters from the Macroscopic and Microscopic Approaches." *Nuclear Science and Engineering*, 131:208–221 (1999).

[61] Piksaikin, V., Kazakov, L., Isaev, S., *et al.* "Energy dependence of relative abundances and periods of delayed neutrons from neutron-induced fission of ^{235}U, ^{238}U, ^{239}Pu in 6- and 8-group model representation." *Progress in Nuclear Energy*, 41(1):203–222 (2002).

[62] Case, K. M. & Zweifel, P. F. *Linear Transport Theory* (Addison-Wesley Publishing Company, Reading, MA (USA), 1967).

[63] Case, K. M., de Hoffmann, F., & Placzek, G. "Introduction to the Theory of Neutron Diffusion." Technical report, Los Alamos Scientific Laboratory (June 1953).

[64] Bell, G. & Glasstone, S. *Nuclear Reactor Theory* (Van Nostrand Reinhold Company, New York, Cincinnati, Toronto, London, Melborne, 1970).

[65] Soppera, N., Bossant, M., & Dupont, E. "JANIS 4: An Improved Version of the NEA Java-based Nuclear Data Information System." *Nuclear Data Sheets*, 120:294–296 (June 2014).

[66] Reuss, P. *Précis de Neutronique* (EDP Sciences, Les Ulis (France), 2003).

[67] Won, J. H. & Cho, N. Z. "Discrete ordinates method-like transport computation with equivalent group condensation and angle-collapsing for local/global iteration." *Annals of Nuclear Energy*, 38(4):846–852 (April 2011).

[68] Yasseri, S. & Rahnema, F. "On the Consistent Spatial Homogenization Method in Neutron Transport Theory." *Journal of Computational and Theoretical Transport*, 43(1-7):240–261 (August 2014).

[69] Yasseri, S. & Rahnema, F. "Consistent Spatial Homogenization in Transport Theory." *Nuclear Science and Engineering*, 176(3):292–311 (March 2014).

[70] Cacuci, D. G. *Handbook of Nuclear Engineering* (Springer, New York, NY (USA), 2010).

[71] Adams, M. L. & Larsen, E. W. "Fast Iterative Methods for Discrete-Ordinates Particle Transport Calculations." *Progress in Nuclear Energy*, 40(1):3–159 (2002).

[72] Slaybaugh, R., Evans, T., Davidson, G., *et al.* "Multigrid in energy preconditioner for Krylov solvers." *Journal of Computational Physics*, 242:405–419 (June 2013).

[73] Wesseling, P. "Introduction to Multigrid Methods." Technical report, NASA-CR-195045 (February 1995).

[74] Janssen, B. & Kanschat, G. "Adaptive Multilevel Methods with Local Smoothing for H^1- and H^{curl}-Conforming High Order Finite Element Methods." *SIAM Journal on Scientific Computing*, 33(4):2095–2114 (2011).

[75] Palmiotti, G., Lewis, E. E., & Carrico, C. B. "VARIANT: VARIational Anisotropic Nodal Transport for Multidimensional Cartesian and Hexagonal Geometry Calculation." Technical report, Argonne National Lab (ANL-83-3) (October 1995).

[76] Lathrop, K. D. "Ray Effects in Discrete Ordinates Equations." *Nuclear Science and Engineering*, 32(3):357–369 (June 1968).

[77] Lathrop, K. D. "Remedies for Ray Effects." *Nuclear Science and Engineering*, 45(03):255–268 (September 1971).

[78] Yamamoto, A., Kitamura, Y., & Yamane, Y. "Simplified Treatments of Anisotropic Scattering in LWR Core Calculations." *Journal of Nuclear Science and Technology*, 45(3):217–229 (2008).

[79] Lathrop, K. "Spatial differencing of the transport equation: Positivity vs. accuracy." *Journal of Computational Physics*, 4(4):475–498 (December 1969).

[80] Flaherty, J. E. "Finite Element Analysis." (2000). Lecture Notes.

[81] Adams, M. L. "Discontinuous Finite Element Transport Solutions in the Thick Diffusion Limit in Cartesian Geometry." In: *ANS International Topical Meeting* (Pittsburgh, PA (USA), 1991).

[82] Zmijarevic, I. "Multidimensional Discrete Ordinates Nodal and Characteristics Method for APOLLO2 Code." In: *Mathematics and Computation (M&C)* (Madrid (Spain), 1999).

[83] Boyd, W., Shaner, S., Li, L., *et al.* "The OpenMOC Method of Characteristics Neutral Particle Transport Code." *Annals of Nuclear Energy*, 68:43–52 (2014).

[84] Santandrea, S., Jaboulay, J., Bellier, P., *et al.* "Improvements and validation of the linear surface characteristics scheme." *Annals of Nuclear Energy*, 36:46–59 (October 2009).

[85] Sanchez, R. & McCormick, N. J. "A Review of Neutron Transport Approximations." *Nuclear Science and Engineering*, 80(4):481–535 (April 1982).

[86] Baker, R. S. & Koch, K. R. "An S_n Algorithm for the Massively Parallel CM-200 Computer." *Nuclear Science and Engineering*, 128(3):312–320 (March 1998).

[87] Rosa, M., Warsa, J. S., & Chang, J. H. "Fourier Analysis of Parallel Block-Jacobi Splitting with Transport Synthetic Acceleration in Two-Dimensional Geometry." In: *Joint International Topical Meeting on Mathematics & Computation and Supercomputing in Nuclear Applications(M&C + SNA 2007)* (Monterey, CA (USA), 2007).

[88] Davidson, G., Evans, T., Jarrell, J., *et al.* "Massively Parallel, Three-Dimensional Transport Solutions for the k-Eigenvalue Problem." *Nuclear Science and Engineering*, 177(2):111–125 (June 2014).

[89] Tyobeka, B., Pautz, A., & Ivanov, K. "Application of Time-Dependent Neutron Transport Theory to High-Temperature Reactors of Pebble Bed Type." *Nuclear Science and Engineering*, 168(2):93–114 (June 2011).

[90] Lambert, J. D. *Numerical Methods for Ordinary Differential Systems* (John Wiley & Sons, New York, NY (USA), 2000).

[91] Butcher, J. C. *Numerical Methods for Ordinary Differential Equations* (John Wiley & Sons, West Sussex (England), 2008), 2nd edition.

[92] Baudron, A.-M., Lautard, J., Maday, Y., *et al.* "MINARET: Towards a time-dependent neutron transport parallel solver." In: *International Conference on Supercomputing in Nuclear Applications and Monte Carlo (SNA + MC)* (Paris (France), 2013).

[93] "Nuclear Fuel Behaviour Under Reactivity-initiated Accident (RIA) Conditions." Technical report, NEA/C-SNI/R(2010)1 (2010).

[94] Dias, A. F., Eisenhart, L. D., & Engel, R. E. "Realistic Scoping Study of Reactivity Insertion Accidents for Typical PWR and BWR Cores." *Nuclear Technology*, 121(3):346–358 (March 1998).

[95] Incropera, F. P., Dewitt, D. P., Bergman, T. L., *et al. Fundamentals of Heat and Mass Transfer* (John Wiley & Sons, Hoboken, NJ (USA), 2007), 6th edition.

[96] Sanchez, R. "UW Version of the Canal Subchannel Code." (March 1983). UWNE-83-1.

[97] Bratland, O. *Pipe Flow 2: Multi-phase Flow Assurance* (Ove Bratland, http://www.drbratland.com, 2013).

[98] Bestion, D. "From the Direct Numerical Simulation to System Codes - Perspectives for the Multi-scale Analysis of LWR Thermalhydraulics." *Nuclear Engineering and Technology*, 42(6):608–619 (2010).

[99] Robertson, E., Choudhury, V., Bhushan, S., *et al.* "Validation of OpenFOAM numerical methods and turbulence models for incompressible bluff body flows." *Computers & Fluids*, 123(21):122–145 (December 2015).

[100] Cinosi, N., Walker, S. P., Bluck, M. J., *et al.* "CFD simulation of turbulent flow in a rod bundle with spacer grids (MATIS-H) using STAR-CCM+." *Nuclear Engineering and Design*, 279:37–49 (November 2014).

[101] Bestion, D., Lucas, D., Anglart, H., *et al.* "Multiscale Thermalhydraulic Analyses Performed in NURESIM and NURISP Projects." In: *International Conference on Nuclear Engineering and the ASME 2012 Power Conference* (Anaheim, CA (USA), 2012).

[102] Bestion, D. "The physical closure laws in the CATHARE code." *Nuclear Engineering and Design*, 124(3):229–245 (December 1990).

[103] Pritchard, P. J. *Fox and McDonald's Introduction to Fluid Mechanics* (John Wiley & Sons, Hoboken, NJ, 2011), 8th edition.

[104] Marinelli, V. & Pastori, L. "Pressure Drop Calculations in BWR Rod Bundles." In: *CONF-720686-6* (1974).

[105] Jones, A. B. "Hydrodynamic Stability of a Boiling Channel." Technical report, Knolls Atomic Power Laboratory (1961). KAPL-2170.

[106] Jaregeg, K. "Development of an integrated deterministic neutronic/thermal-hydraulic model using a CFD solver." Master's thesis, Chalmers University of Technology (2012).

[107] Mahadevan, V. S., Merzari, E., Tautges, T., *et al.* "High-resolution coupled physics solvers for analysing fine-scale nuclear reactor design problems." *Philosophical Transactions of the Royal Society. Series A, Mathematical, Physical, and Engineering Sciences*, 372(2021):20130381 (August 2014).

[108] Calleja, M. "X-TREAM project: Task 1b - Survey of the state-of-the-art numerical techniques for solving coupled non-linear multi-physics equations." Technical report, Chalmers University of Technology, Göteborg (Sweden) (2014).

[109] Kotlyar, D. & Shwageraus, E. "Numerically stable Monte Carlo-burnup-thermal hydraulic coupling schemes." *Annals of Nuclear Energy*, 63:371–381 (January 2014).

[110] Kotlyar, D. & Shwageraus, E. "Monitoring and preventing numerical oscillations in 3D simulations with coupled Monte Carlo codes." *Annals of Nuclear Energy*, 71:198–205 (September 2014).

[111] Verdú, G., Miró, R., Sánchez, A. M., *et al.* "Peach Bottom Transients Analysis with TRAC/BF1-VALKIN." *Nuclear Science and Engineering*, 148(2):256–269 (October 2004).

[112] Kaya, S. & Yavuz, H. "A Nodal Kinetics and Thermohydraulics Analysis (NOKTA) Code for Analyzing Rod-Ejection Accidents and Other Transients in Nuclear Power Reactor Cores." *Nuclear Technology*, 129(1):26–35 (January 2000).

[113] Johnson, R. W., Hansen, G., & Newman, C. "The role of data transfer on the selection of a single vs. multiple mesh architecture for tightly coupled multi-physics applications." *Applied Mathematics and Computation*, 217(22):8943–8962 (July 2011).

[114] Benzi, M. "Preconditioning Techniques for Large Linear Systems: A Survey." *Journal of Computational Physics*, 182(2):418–477 (November 2002).

[115] Dugan, K. "Dynamic Adaptive Multi-mesh Refinement for Coupled Physics Equations Applicable to Nuclear Engineering." Master's thesis, Texas A&M University (August 2013).

[116] Charrier, P., Dubroca, B., Duffa, G., *et al.* "Schéma implicite pour un modèle d'hydrodynamique radiative multi-groupe 2D." Technical report, LRC-03.16 (2003). http://www.math.u-bordeaux.fr/LRC-CEA/.

[117] Kelley, C. *Iterative Methods for Linear and Nonlinear Equations* (SIAM, Philadelphia, PA (USA), 1995).

[118] Bader, Brett W. and Pawlowski, Roger P. and Kolda Tamara G. "Robust Large-Scale Parallel Nonlinear Solvers for Simulations." Technical report, Sandia National Lab (2005). SAND2005-6864.

[119] Kelley, C. T. *Solving Nonlinear Equations with Newton's Method* (Society for Industrial and Applied Mathematics, Philadelphia, PA (USA), 2003).

[120] Isaacson, E. & Keller, H. B. *Analysis of Numerical Methods* (Dover Publications, New York, NY (USA), 1966).

[121] Sorensen, D. C. "Newton's Method wih a Model Trust Region Modification." *SIAM Journal of Numerical Analysis*, 19(2):409 – 426 (April 1982).

[122] Armijo, L. "Minimization of Functions Having Lipschitz Continuous First Partial Derivatives." *Pacific Journal of Mathematics*, 16(1):1 – 3 (November 1966).

[123] Dennis, J. E. *Numerical Methods for Unconstrained Optimization in Nonlinear Equations* (Society for Industrial and Applied Mathematics, Philadelphia, PA (USA), 1996).

[124] Demmel, J. W. *Applied Numerical Linear Algebra* (Society for Industrial and Applied Mathematics, Philadelphia, PA (USA), 1997).

[125] Saad, Y. & Schultz, M. H. "GMRES: A Generalized Minimal Residual Algorithm for Solving Nonsymmetric Linear Systems." *SIAM Journal on Scientific and Statistical Computing*, 7:856–869 (July 1986).

[126] Saad, Y. *Iterative Methods for Sparse Linear Systems* (SIAM, Philadelphia, PA (USA), 2003), 2nd edition.

[127] Paige, C. C. & Saunders, M. A. "Solution of Sparse Indefinite Systems of Linear Equations." *SIAM Journal on Numerical Analysis*, 12(4):617–629 (September 1975).

[128] Embree, M. "The Tortoise and the Hare Restart GMRes." *SIAM Review*, 45:259 – 266 (2003).

[129] Arnoldi, W. E. "The principle of minimized iteration in the solution of the matrix eigenproblem." *Quarterly of Applied Mathematics*, 9:17–29 (April 1951).

[130] Trefethen, L. N. & Bau, D. *Numerical Linear Algebra* (SIAM, Philadelphia, PA (USA), 1997).

[131] Giraud, L., Langou, J., & Rozloznik, M. "The loss of orthogonality in the Gram-Schmidt orthogonalization process." *Computers & Mathematics with Applications*, 50(7):1069–1075 (October 2005).

[132] Parlett, B. *The Symmetric Eigenvalue Problem* (Society for Industrial and Applied Mathematics, Philadelphia, PA (USA), 1998).

[133] Ipsen, I. C. F. *Numerical Matrix Analysis: Linear Systems and Least Squares* (Society for Industrial and Applied Mathematics, Philadelphia, PA (USA), 2009).

[134] Eisenstat, S. C. & Walker, H. F. "Choosing the forcing terms in an inexact Newton method." *SIAM Journal on Scientific Computing*, 17(1):16 – 32 (January 1996).

[135] Ortega, J. M. & Rheinboldt, W. C. *Iterative Solution of Nonlinear Equations in Several Variables* (Society for Industrial and Applied Mathematics, Philadelphia, PA (USA), 1970).

[136] Sherman, A. H. "On Newton-Iterative Methods for the Solution of Systems of Nonlinear Equations." *SIAM Journal on Numerical Analysis*, 15(4):755 – 771 (August 1978).

[137] An, H.-B., Wen, J., & Feng, T. "On finite difference approximation of a matrix-vector product in the Jacobian-free Newton-Krylov method." *Journal of Computational and Applied Mathematics*, 236(6):1399–1409 (October 2011).

[138] Martins, J. R. R. A., Sturdza, P., & Alonso, J. J. "The complex-step derivative approximation." *ACM Transactions on Mathematical Software*, 29(3):245–262 (September 2003).

[139] Lewis, E. E. & Miller, W. F. *Computational Methods of Neutron Transport* (John Wiley & Sons, New York, NY (USA), 1984).

[140] Ade, B. J. "SCALE/TRITON Primer: A Primer for Light Water Reactor Lattice Physics Calculations." Technical report, Oak Ridge National Lab (2012). NUREG/CR-7041, ORNL/TM-2011/21.

[141] Cai, L. "Condensation et homogénéisation des sections efficaces pour les codes de transport déterministes par la méthode de Monte Carlo : Application aux réacteurs à neutron rapides de GEN IV." Ph.D. thesis, Université Paris-Sud (2014).

[142] Larsen, E. W. "Neutron Transport and Diffusion in Inhomogeneous Media. I." *Journal of Mathematical Physics*, 16(7):1421–1427 (July 1975).

[143] Larsen, E. W. "Neutron Transport and Diffusion in Inhomogeneous Media. II." *Nuclear Science and Engineering*, 60(4):357–368 (August 1976).

[144] Azmy, Y. *Nuclear Computational Science: A Century in Review* (Springer, Dordrecht Heidelberg London New York, 2010).

[145] Zhang, H., Rizwan-uddin, & Dorning, J. J. "A Multiple-Scales Systematic Theory for the Simultaneous Homogenization of Lattice Cells and Fuel Assemblies." *Transport Theory and Statistical Physics*, 26(7):765–811 (August 1997).

[146] Sanchez, R. "Assembly homogenization techniques for core calculations." *Progress in Nuclear Energy*, 51(1):14–31 (January 2009).

[147] Yamamoto, A., Kitamura, Y., & Yamane, Y. "Cell homogenization methods for pin-by-pin core calculations tested in slab geometry." *Annals of Nuclear Energy*, 31(8):825–847 (May 2004).

[148] Dugan, K., Zmijarevic, I., & Sanchez, R. "Cross-Section Homogenization for Reactivity-Induced Transient Calculations." *Journal of Computational and Theoretical Transport*, 45(6):425–441 (2016).

[149] Porsching, T. A. "On the Spectrum of a Matrix Arising from a Problem in Reactor Kinetics." *SIAM Journal on Applied Mathematics*, 16(2):301–317 (March 1968).

[150] Larsen, E. W. & Zweifel, P. F. "On the Spectrum of the Linear Transport Operator." *Journal of Mathematical Physics*, 15(11):1987–1997 (November 1974).

[151] Betzler, B. R. "Calculating Alpha Eigenvalues and Eigenfunctions with a Markov Transition Rate Matrix Monte Carlo Method." Ph.D. thesis, University of Michigan (2014).

[152] Henry, A. F. "The Application of Inhour Modes to the Description of Nonseparable Reactor Transients." *Nuclear Science and Engineering*, 20:338–351 (November 1964).

[153] Singh, K. P., Degweker, S. B., Modak, R. S., *et al.* "Iterative Method for Obtaining the Prompt and Delayed Alpha-Modes of the Diffusion Equation." *Annals of Nuclear Energy*, 38:1996–2004 (2011).

[154] Hoogenboom, J. E. "Numerical Calculation of the Delayed-α Eigenvalue Using a Standard Criticality Code." In: *Physics of Reactors (PHYSOR)* (Seoul (Korea), 2002).

[155] Kaper, H. G. "The Initial-Value Transport Problem for Monoenergetic Neutrons in an Infinite Slab with Delayed Neutron Production." *Journal of Mathematical Analysis and Applications*, 19:207–230 (1967).

[156] Schneider, D. *et al.* "APOLLO3: CEA/DEN Deterministic Multi-purpose Code for Reactor Physics Analysis." In: *Physics of Reactors (PHYSOR)* (Sun Valley, ID (USA), 2016).

[157] Coste-Delclaux, M. "GALILE: A nuclear data processing system for transport, depletion and shielding codes." In: *Physics of Reactors (PHYSOR)* (Interlaken (Switzerland), 2008).

[158] Ribon, P. "Statistical probability tables CALENDF program." In: *INIS-XN-305 (CONF-8906162)* (1989).

[159] MacFarlane, R. E. "The NJOY Nuclear Data Processing System, Version 2012." Technical report, LA-UR-12-27079 (December 2012).

[160] Brun, E., Damian, F., Dumonteil, E., *et al.* "TRIPOLI-4.8.1 version 8 User Guide." Technical report, CEA-R-6316 (February 2013).

[161] Santamarina, A., Bernard, D., & Rugama, Y. "The JEFF-3.1.1 Nuclear Data Library." Technical report, JEFF Report 22 (2009).

[162] "Nuclear Fuel Safety Criteria Technical Report." Technical report, NEA No. 7072 (2012).

[163] Lamarsh, J. R. *Introduction to Nuclear Reactor Theory* (Addison-Wesley Publishing Company, Reading, MA (USA), 1966).

[164] Dugan, K., Zmijarevic, I., & Sanchez, R. "Cross Section Homogenization Technique for Transient Calculations." In: *Physics of Reactors (PHYSOR)* (Sun Valley, ID (USA), 2016).

[165] "Physics of Plutonium Fuels: BWR MOX Benchmark Specification and Results." Technical report, NEA: 92-64-19905-5 (2003).

[166] Butterfield, M. H. *Dynamics and Control in Nuclear Power Stations* (Thomas Telford Ltd., London (England), 1992).

[167] Boyarinov, V. F., Fomicherko, P. A., Hou, J., *et al.* "Deterministic Time-Dependent Neutron Transport Benchmark without Spatial Homogenization (C5G7-TD)." (February 2016). NEA/NSC/DOC(2016).

APPENDIX A

RÉSUMÉ ÉTENDU EN FRANÇAIS

A.1 Introduction

Le domaine de l'ingénierie nucléaire englobe une vaste gamme de sujets tels que le transport de particules à travers les milieux, le transfert de chaleur dans une centrale nucléaire, et la formation d'hydrogène lors d'un accident grave. Une solution précise à ces modèles physiques permet aux scientifiques et aux ingénieurs, entre autres, de construire des stations de production d'énergie plus efficaces [1], ainsi que de prédire les effets de l'exposition aux rayonnements [2], d'étudier l'efficacité de l'utilisation de confinement magnétique pour les réacteurs de fusion [3], et de comprendre le processus d'effondrement supernovae [4, 5].

Souvent, les processus physiques étudiés par les ingénieurs nucléaires et les scientifiques sont composés de nombreux processus physiques distincts mais couplés. Ce travail porte sur le développement de stratégies de simulation qui peuvent être utilisées pour produire des solutions de haute fidélité à des problèmes de physique couplés rencontrés en génie nucléaire. L'objectif de cette thèse est de montrer comment les codes de composants physiques peuvent être adaptés pour travailler dans un cadre multiphysique basé sur une méthode de Jacobi-Free Newton-Krylov (JFNK), et de développer des procédures d'homogénéisation qui réduisent les erreurs lorsqu'elles sont appliquées à des simulations transitoires. Ce travail a commencé avec l'intention d'étudier les stratégies de couplage multiphysique applicables aux calculs industriels en génie nucléaire, mais comme cela est souvent le cas dans la recherche, on a découvert que le traitement d'homogénéisation des sections efficaces pour les calculs transitoires faisait défaut dans le développement. L'objectif de ce travail s'est ensuite tourné vers l'exploration des méthodes d'homogénéisation des sections efficaces qui sont applicables aux simulations multiphysiques transitoires.

A.1.1 Comportement des réacteurs nucléaires

Les centrales électriques nucléaires se caractérisent par leur principale source de chaleur provenant d'un processus nucléaire; actuellement elle est limitée à des événements de fission dans les centrales électriques commerciales. En fonction de la conception, une centrale nucléaire est constituée d'une boucle de refroidissement primaire et, éventuellement, plusieurs boucles de refroidissement secondaires. Le fluide de refroidissement primaire est chauffé en passant directement à travers le coeur du réacteur, qui génère de la chaleur via des réactions nucléaires. Dans les réacteurs à eau bouillante (REB), le caloporteur dans la boucle primaire passe immédiatement à travers la turbine de générateur, ce qui entraîne un cycle d'alimentation Rankine [6]. Dans les réacteurs à eau pressurisée (REP), la pression dans le circuit primaire est suffisamment élevée pour maintenir le caloporteur en dessous de la température d'évaporation. L'énergie thermique du caloporteur primaire est transférée dans une boucle secondaire à une pression inférieure, qui passe ensuite à travers une turbine de générateur.

L'intérieur d'un cœur de réacteur est un environnement riche pour les simulations physiques en raison, entre autres, de la complexité des écoulements hautement turbulent, des interactions fluide-structure et du comportement des matériaux sous irradiation. En plus de ce riche environnement de phénomènes physiques, beaucoup de ces phénomènes physiques interagissent entre eux. A titre d'exemple, la puissance du réacteur nucléaire est directement liée à la façon dont les neutrons sont distribués dans le cœur. La répartition des neutrons peut être déterminée en fonction de la géométrie du cœur, de la composition de la matière à l'intérieur du coeur, et de la répartition de la température dans le cœur. Toutefois, la répartition de la température dans le noyau peut être déterminée par la distribution de puissance dans le cœur, la géométrie du coeur et les conditions du caloporteur entrant. En outre, la géométrie du coeur est déterminée par la distribution de la température (dilatation thermique), les vibrations provoquées par l'interaction fluide-structure, et d'autres. L'interaction de ces composants physiques peut être traitée comme un système multiphysique, dont beaucoup d'efforts ont été consacrés à son étude récemment [7–10].

A.1.2 Simulations multiphysiques

La solution aux problèmes physiques couplés devient un grand intérêt dans de nombreux domaines scientifiques. Le département américain de l'énergie a commencé le programme de modélisation et simulation avancées pour le genie nucléaire (NEAMS), une collaboration internationale afin de produire une boîte à outils pour modéliser le comportement multiphysique et à différentes échelles dans les réacteurs nucléaires [11]. Ce programme soutient le groupe de travail pour la simulation avancée des réacteurs à eau légère (CASL), pôle de recherche axé sur le développement d'outils de simulation avancés pour la compréhension des phénomènes qui limitent les performances des réacteurs à eau légère. Un tel intérêt récent pour la résolution des problèmes de physique couplés a produit plusieurs logiciels disponibles à des fins spéciales: MOOSE [8], LIME [13] et SALOME [14] pour ne nommer que quelques-uns.

En fonction des contraintes d'obtention d'une solution couplée de plusieurs composantes physiques, de nombreux choix sont disponibles, mais seulement trois seront abordés: fractionnement opérateur, boîte à outils multiphysiques et JFNK. Si la contrainte principale est la réutilisation du code, une technique de fractionnement opérateur peut être utilisée [10]. Cette technique exploite les nombreuses années d'expérience qui ont contribué au développement de chaque code de composante physique. À l'heure actuelle, les solutions multiphysiques sont recherchées dans le domaine d'application où la modification lourde de codes composants devient risquée et sujette aux erreurs. Cette considération met l'accent sur la production de méthodes fractionnement opérateur stables. En outre, les codes composants sont généralement écrits sans l'extensibilité à l'esprit et l'extension de ces codes pour fonctionner dans un environnement multiphysique peut être problématique. Il est concevable que le chemin le plus facile vers une solution multiphysique est d'utiliser un programme pilote avec un fichier d'entrée/sortie (I/O) entre les codes des composants physiques. Le programme pilote devrait être basé sur une méthode de fractionnement de l'opérateur qui commande l'entrée et

la sortie entre les codes d'éléments; cette conception maximise la réutilisation du code et minimise les modifications nécessaires dans les codes de composants.

Dans la communauté de simulation commerciale, les boîtes à outils multiphysiques prennent de l'ampleur lorsque l'accent est mis sur la facilité d'utilisation au niveau de l'application. Ces outils fournissent un cadre dans lequel les simulations multiphysiques peuvent être effectuées. Généralement, ces cadres fournissent des interfaces aux codes existants qui manipulent ensuite le code existant, basé sur le schéma de calcul souhaité. Ces interfaces peuvent être soit fournies par la boîte à outils, ce qui rend uniquement utilisable dans le cadre les codes de composants physiques pris en charge, soit générées par la boîte à outils sur la base du code existant, comme cela est le cas pour SALOME [15]. Les schémas de calcul préciseront le flux de données entre les composants physiques au cours de la simulation, et généralement traiteront seulement un faible couplage entre les composantes physiques. Un ordre supérieur de discrétisation temporelle est possible, mais est sujet à des instabilités [16]. Ces types de cadres sont d'excellents choix pour les études préliminaires pour déterminer le comportement général d'un système couplé, mais échouent lorsqu'ils sont appliqués à des composants fortement couplés et à des situations qui nécessitent une discrétisation temporelle plus fine.

Plusieurs projets récents sont basés sur une méthode de JFNK, où chaque composant physique est nécessaire pour produire une solution résiduelle [8, 13, 17]. Ces méthodes traitent les composants physiques comme étant fortement couplés et fonctionnent avec des méthodes de discrétisation temporelle d'ordre élevé. Cependant, les codes de physique existants ne sont généralement pas conçus pour produire une solution résiduelle sans modification lourde. Généralement, les cadres qui fournissent le couplage par une méthode JFNK soit fourniront des codes de composants physiques distincts conçus pour fonctionner dans le cadre de couplage, soit les utilisateurs peuvent construire leurs propres codes de composantes de la physique via des bibliothèques de base fournies dans le cadre. L'adaptation des codes existants pour fonctionner dans un environnement multiphysique JFNK est généralement une tâche difficile, et sera un objectif principal de ce travail.

A.1.3 Accidents graves

Dans la conception des réacteurs nucléaires, une attention particulière est accordée à la façon dont les réacteurs se comportent dans des situations improbables mais largement préjudiciables. Ces situations constituent la classe d'accidents de base de conception (DBA) pour lesquels les réacteurs doivent être conçus pour survivre sans perte d'intégrité des systèmes, des structures et des composants nécessaires pour assurer la santé et la sécurité publique [18]. Ces accidents incluent de grandes excursions de puissance induites par l'échec de contrôle neutronique ou de perte de réfrigérant primaire, les grands tremblements de terre, les inondations et d'autres scénarios.

Une défaillance de la contrôle neutronique ou une autre perturbation de l'état du réacteur a la possibilité d'induire une grande modification de puissance. Un échec de contrôle neutronique peut provenir de la défaillance mécanique d'une

grappe de contrôle pendant la phase de démarrage, ou d'un mélange insuffisant d'absorbeur de neutrons soluble présent dans les REP. Des perturbations supplémentaires peuvent provenir de l'état du liquide de refroidissement entrant dans le coeur; un échec de turbine dans un REB entraînera une forte augmentation de la pression et provoquera une grande augmentation de puissance. Une forte augmentation de puissance peut fragiliser la gaine du combustible, qui constitue la première barrière de confinement. Il existe trois principaux niveaux de confinement conçus dans les installations nucléaires pour protéger le public contre une exposition excessive aux rayonnements; ces niveaux sont répertoriés de l'intérieur vers l'extérieur du réacteur: la gaine du combustible, la boucle du circuit primaire et l'enceinte de confinement. Les accidents les plus graves concernent les deuxième et troisième niveaux de confinement.

Au cours de ces accidents, divers phénomènes physiques peuvent apparaître à différents stades de l'accident. Une perte prolongée de refroidissement primaire peut éventuellement conduire à des risques de formation d'hydrogène par réaction chimique entre la gaine en zirconium à température élevée et le réfrigérant à base d'eau [19]. La modélisation de la distribution et de la combustion de l'hydrogène gazeux est un domaine de recherche important en raison de la possibilité d'un événement de déflagration d'hydrogène, qui peut compromettre l'intégrité de la structure de confinement [20]. Le processus de conception du réacteur consiste à traiter en toute sécurité la façon d'évacuer ou de convertir l'air riche en hydrogène pour être loin d'une concentration inflammabilité.

Si l'accident grave progresse, l'intégrité structurelle du coeur sera compromise et le Corium (coeur fondu) commencera à interagir avec la cuve et éventuellement l'enceinte de confinement en béton [21] . La modélisation de l'interaction béton-Corium (MCCI) implique de nombreux processus physiques et chimiques [22]. La prise en compte de la conception d'un tel accident est de veiller à ce que le corium fondu soit suffisamment refroidi avant de fondre à travers l'enceinte de confinement. La phase MCCI d'un accident grave peut être modélisée par un système de multiphysique avec couplage fort entre les composantes de la physique [23].

Les méthodes de calcul étudiées dans ce travail sont appliquées aux accidents de base de conception impliquant de grands modifications de puissance qui peuvent avoir un impact sur l'intégrité du combustible nucléaire en raison de leurs effets sur le premier niveau de confinement. Ce choix est basé sur la disponibilité des codes composants qui résolvent la physique sous-jacente du problème et sur l'importance d'assurer l'intégrité du premier, et sans doute le plus important niveau, de confinement. Cependant, ces méthodes de calcul peuvent également être utilisées pour étudier le comportement des accidents graves, tels que la formation d'hydrogène dans l'enceinte de confinement ou l'interaction entre le matériau de coeur fondu et le béton du plancher de confinement.

A.1.4 État de l'art en ingénierie nucléaire

L'état actuel des méthodes disponibles pour la communauté de simulation sera examinée dans cette section. L'état de l'art se concentrera sur les principaux domaines du développement dans la résolution des problèmes de physique couplés en génie nucléaire. D'abord la recherche active en neutronique et ther-

mohydraulique est discutée en mettant l'accent sur les problèmes dépendant du temps. Ensuite, deux façons de traiter les problèmes de physique couplés sont examinées. Cette section se termine avec l'application de procédés parallèles et comment les données sont traitées dans des problèmes en fonction du temps.

Neutronique et dépendance temporelle

Sans prendre en compte les contre réactions thermique, qui affectent un système nucléaire pendant un régime transitoire, il y a eu beaucoup de travail consacré à la résolution de l'équation du transport des neutrons en fonction du temps. Les méthodes dépendent du temps sont généralement liées au développement du flux en fonction du temps sur une base orthogonale [24] ou ou à la décomposition du flux temporel en un produit de deux fonctions [25]. La difficulté dans le développement sur une base orthogonale est de trouver des fonctions orthogonales appropriées qui représentent, avec précision, les caractéristiques d'une solution de transport. Habituellement, un modèle réduit en 0-D est nécessaire pour trouver une base appropriée pour le développement; les solutions au problème de α-valeur propre fournissent une telle base [26, 27]. Cette base a été utilisée pour montrer comment le spectre d'énergie est décalé par rapport à la distribution du mode fondamental pendant un transitoire [28]. La décomposition du flux en un produit d'une fonction de la forme et de l'amplitude a été appliquée à la solution de la cinétique espace-temps; cette méthode est communément appelée la méthode *quasi-statique* [25]. La fonction d'amplitude dépend uniquement du temps, et change rapidement avec le temps. Cette fonction décrit le comportement global de la solution de transport dépendant du temps. La fonction de la forme dépend de toutes les variables, mais varie lentement dans le temps. La fonction de forme est mise à jour sur des échelles de temps plus longues et est utilisée pour mettre à jour les paramètres qui entraînent l'évolution de la fonction d'amplitude.

Thermohydraulique

Le développement de modèles thermohydrauliques précises est important pour la progression continue de la conception des réacteurs à venir. Les phénomènes thermohydrauliques dans un système de réacteur nucléaire fonctionnent sur des échelles de temps et d'espace disparates, ce qui rend la résolution difficile. La tendance dans la recherche thermohydraulique est de produire des solutions toujours plus fines sur ces échelles de temps et d'espace.

Les phénomènes thermohydrauliques qui se produisent en dehors du coeur du réacteur sont généralement traités avec un modèle réuni de 1-D [29]. Ce traitement donne une perspective intégrale des phénomènes thermohydrauliques qui se produisent en dehors du coeur. A l'intérieur du coeur, des phénomènes thermohydrauliques plus complexes interviennent, ce qui nécessite des techniques de modélisation plus élaborées pour leurs résolutions. La thermohydraulique d'un assemblage de réacteur est généralement modélisée par un ensemble de canaux à 1-D couplés qui résolvent la dépendance spatiale à 3-D. Les turbulence et le mélange dans les canaux est géré par des modèles de Reynolds moyenné Navier Stokes (RANS) tels que le modèle k-ε [30]. Sur des échelles spatiales encore plus fines, davantage de détails peuvent être modélisés dans le transfert de chaleur et

l'écoulement du fluide. Cependant, pour le comportement général d'un coeur de réacteur, ces modèles détaillés deviennent trop coûteux et des modèles d'ordre inférieur sont nécessaires [31].

La modélisation thermohydraulique vise à prédire le comportement des écoulements de fluides et le transfert de chaleur dans les nouveaux modèles de réacteurs. Il existe une forte demande sur les modèles thermohydrauliques avancés pour prédire le comportement des nouveaux réacteurs de génération-IV [32]. Par exemple, l'écoulement complexe autour du combustible dans les réacteurs à lit de boulets, nécessite des méthodes robustes capables de traiter la conduction, la convection et le transfert de chaleur par rayonnement au sein de tels environnements.

Fractionnement d'opérateur

Une fois qu'un modèle dépendant du temps est produit, un moyen efficace pour obtenir des solutions physiques couplées, avec un minimum de modifications des codes actuels des composants physiques, consiste à utiliser une technique de fractionnement d'opérateur. Dans cette approche, chaque composante physique interagit avec d'autres composants physiques par les canaux I/O. Cela est généralement la première méthode utilisée pour des études de cadrage dans le comportement des systèmes couplés [33, 34]. Ces méthodes ne traitent généralement pas avec précision les termes de couplage non linéaires des problèmes multiphysiques, nécessitant un pas de temps plus petit pendant la simulation pour assurer des solutions précises [35]. Cela peut conduire à des simulations coûteuses en raison de l'augmentation du nombre d'étapes qui doivent être prises en compte pour produire une solution en fonction du temps. Certaines des erreurs rencontrées par le fractionnement d'opérateur peuvent être réduites en utilisant des méthodes d'intégration de temps d'ordre supérieur, mais cela ne converge pas non plus complètement les termes non linéaires entre les composantes physiques [9]. Pour supprimer davantage d'erreurs d'une simulation de physique couplée, une méthode fortement couplée est nécessaire. Une préoccupation supplémentaire concernant les méthodes de fractionnement d'opérateur a été l'apparition d'instabilités lorsqu'elles sont appliquées à certains problèmes de propagation [16].

Les méthodes de fractionnement d'opérateur ont été appliquées à une variété de problèmes dans le domaine de l'ingénierie nucléaire. Les équations de rayonnement-diffusion temporelles présentent des phénomènes qui sont difficiles à résoudre sans une attention particulière au contrôle de la taille de pas de temps [33]. L'efficacité de l'utilisation des méthodes de fractionnement d'opérateur dans des applications de réacteurs nucléaires a été appliquée à des problèmes de dimensions réduites [35]. Plusieurs variantes du fractionnement d'opérateur ont été appliquées pour coupler la thermohydrauliqe et la neutronique en 0-D et en 1-D. Il a été montré que, pour réduire les erreurs dues à la rigidité du système couplé, les méthodes d'intégration en temps d'ordre plus élevé doivent être utilisées. De plus, pour faire converger les non linéarités entre les composantes physiques, une itération entre les composantes physiques est nécessaire. Cependant, lors de l'analyse des accidents de réacteurs nucléaires, il est de coutume d'utiliser un modèle de diffusion de neutrons 3-D couplé à un modèle thermohydraulique 3-D afin de saisir avec précision les effets spatiaux importants pour

le transitoire [36]. L'accent mis sur l'utilisation des méthodes de fractionnement d'opérateur d'ordre élevé n'a pas encore été mis en oeuvre dans les calculs au niveau des applications.

Méthode de Jacobian-Free Newton-Krylov

Comme mentionné précédemment, un moyen efficace de résoudre un fort couplage entre les composantes physiques est d'utiliser une méthode de JFNK, avec toutes les composantes physiques pertinentes combinées dans un système numérique unique. Bien qu'il y ait eu beaucoup de travail sur la production de cadres de calcul basés sur une méthode de JFNK, les composantes physiques utilisées dans ces cadres sont limitées à celle qui sont fournies par le cadre et celles qui sont construites à l'intérieur du cadre.

Une partie importante du travail dans le développement d'une simulation efficace d'un système de multiphysique repose sur les techniques d'accélération utilisées pour converger vers une solution plus rapidement. Dans les méthodes JFNK, cette accélération est réalisée par des préconditionneurs sur le système linéaire. Il a été démontré que l'utilisation de préconditionneurs, qui sont basés sur la physique des composants sous-jacents, fonctionne très bien [37]. Ce type de préconditionneur résoudra généralement une version découplée (ou faiblement couplée) du système multiphysique.

D'autres considérations lors de la construction d'un cadre multiphysique peuvent se concentrer sur la conception de logiciels dans le cadre. La complexité des problèmes multiphysiques nécessite que beaucoup de morceaux de logiciel travaillent ensemble de façon transparente. Ce type de complexité exige une architecture modulaire pour le cadre. Une conception modulaire contient des interfaces bien définies au niveau des limites de chaque module. Des interfaces bien définies permettent également d'échanger facilement les composants modulaires. Par exemple, un module de solveur linéaire peut contenir un choix de plusieurs algorithmes de solveur linéaire. En outre, des interfaces bien définies permettent l'utilisation des bibliothèques numériques externes tels que PETSc [17] ou Trilinos [38].

Calcul parallèle

Avec la demande grandissante de solutions encore plus détaillées pour les réacteurs nucléaires, les méthodes de solution parallèles deviennent les options nécessaires et viables. Le premier niveau de calcul parallèle se compose de processus quasiment indépendants les uns des autres; de tels processus sont appelés processus parallèles *embarrassants* [39]. Un exemple de ces processus est les balayages de transport le long des directions données dans un milieu. L'évolutivité de ces parallélisation est limitée par le nombre de processus indépendants disponibles. Dans l'exemple des balayages de transport, l'évolutivité est limitée au nombre de directions utilisées pour discrétiser le flux angulaire. Des niveaux supplémentaires de parallélisation peuvent être mis en œuvre, chacun avec des exigences plus complexes en matière de communication entre les processus parallèles. Il devient évident, par rapport à la demande accrue de solutions détaillées de transport neutronique et thermohydraulique au sein des réacteurs nucléaires, que plusieurs

niveaux de parallélisme seront recherchés [40, 41].

Il existe de nombreuses bibliothèques numériques d'algèbre linéaire disponibles pour exploiter la puissance des calculs parallèles [17, 38]. Ces bibliothèques peuvent être utilisées dans le développement de simulations multiphysiques, mais le bouchon dans ces simulations provient souvent des codes de physique en série sous-jacents. Pour exploiter la puissance des calculs parallèles en simulations multiphysiques, les codes des composants physiques sous-jacents doivent également être parallèles. Le travail présenté dans cette thèse ne porte que sur l'utilisation d'algorithmes parallèles car les codes de composants physiques sous-jacents utilisés dans ce travail sont traités en tant que processus en série. La parallélisation de ces codes ne fait pas partie du cadre de cette étude. Cependant, l'utilisation de méthodes parallèles dans les simulations multiphysiques est d'une grande importance et devra être étudiée pour faire suite à ce travail.

Homogénéisation des sections efficaces

Dans l'analyse de réacteurs, le coût de calcul d'une solution détaillée est généralement rédhibitoire. L'homogénéisation des sections efficaces fournit un moyen pour prétraiter les données avant une simulation afin de réduire le nombre d'inconnues. Dans de nombreux cas, l'homogénéisation des sections efficaces consiste à produire une solution approchée qui peut être utilisée pour atteindre des valeurs des sections efficaces moyennes, typiquement sur les domaines de l'espace et d'énergie. Cette solution approchée proviendra généralement de calculs à l'état d'équilibre pour diverses configurations de température et de composition des matériaux, qui sont interpolés lors du calcul du plus grand réacteur.

L'homogénéisation des sections efficaces est optimisée pour les calculs statiques, qui représentent la majeure partie du temps de fonctionnement des réacteurs commerciaux. Pour être informatiquement avantageuse, l'homogénéisation des sections efficaces est effectuée au niveau de l'assemblage en 2-D. Les premiers travaux sur l'homogénéisation se concentrent sur la façon de conserver les taux de réaction lors de la transition entre les calculs de transport sur des assemblages à des calculs de diffusion sur le coeur. Les taux de réaction peuvent être mieux conservés en introduisant des discontinuités du flux dans les limites des régions homogénéisées [42] ou par le biais d'une procédure qui permet d'ajuster de manière itérative les sections efficaces [43].

Une grande partie des travaux récents sur les méthodes d'homogénéisation consiste à produire des sections efficaces homogénéisées où la solution globale peut être largement différente de la solution produite pour un assemblage isolé [44]. Cette situation se produit lorsque les assemblages voisins sont très différents en composition des matériaux; ce cas se produit dans des assemblages de combustible MOX. Dans ce cas, la solution approchée est loin de la solution globale, et des sections efficaces homogénéisées avec la solution approchée représenteront mal la réalité. Les méthodes qui prennent en compte les assemblages voisins doivent être utilisées, telles que la méthode *color-set*.

L'homogénéisation des sections efficaces peut être appliqué à des problèmes en fonction du temps en utilisant l'homogénéisation à la volée. Ces méthodes mettent à jour les sections efficaces homogénéisées à certaines moments dans le

transitoire lorsque les sections efficaces sont soupçonnées d'être erronées [45]. Les calculs à la volée peuvent prendre en compte les effets d'un flux en fonction du temps quand il reste proche du flux fondamental.

A.1.5 Améliorations de l'état de l'art

Le but de ce travail est d'étendre l'état de l'art des méthodes utilisées dans la communauté de la simulation numérique. Ces améliorations à l'état de l'art sont présentées dans ce paragraphe. Deux grands thèmes pour ces améliorations des méthodes de simulation actuelles seront explorés dans ce travail. Le premier est sur les méthodes de couplage qui traitent des composants physiques. Le deuxième thème porte sur la façon dont les données sont traitées au cours de la simulation des transitoires.

Méthode de Jacobian-Free Newton-Krylov

La méthode JFNK a été appliquée avec succès à des composants physiques construits dans un cadre à base de JFNK robuste. Cependant, il est souhaitable d'inclure des codes informatiques qui sont fortement optimisés pour leurs modèles spécifiques de la physique et de réutiliser les efforts importants qui ont été consacrés à leur développement. Ce travail se concentrera sur la façon dont un code numérique existant peut être adapté pour fonctionner dans un cadre de JFNK lorsque cette fonction n'a pas été dans l'intention initiale du code.

Les codes existants sont raccordés à un cadre JFNK par le calcul du résidu, qui sera spécifique à chaque composante physique. Le calcul du résidu fournira une interface transparente avec laquelle les composants de la physique peuvent interagir. Une fois qu'un résidu d'une composante physique est défini, celle-ci peut être utilisée dans une simulation. Des composants physiques supplémentaires peuvent être ajoutés à la simulation en définissant un module de calcul du résidu pour chaque composant physique supplémentaire.

Une attention particulière est consacrée à une nouvelle formulation du résidu pour le transport de neutrons. La taille de la solution de transport de neutrons peut être rédhibitoire, et la nouvelle formulation du résidu vise à réduire la taille de cette solution. La nouvelle formulation du résidu pour le transport de neutrons se révèle être correctement mise en place et réduit la taille de la solution recherchée. La réduction de la taille offre plus d'avantages que la réduction de la consommation de mémoire. Un vecteur de plus petite taille se trouve dans un espace de recherche plus petit; tout solveur Krylov qui construit des sous-espaces successifs convergera plus rapidement si le sous-espace peut approcher avec précision l'espace de recherche complet.

Un préconditionneur sans matrice, basé sur la physique, est exploré. Généralement, les préconditionneurs basés sur la physique exigent la manipulation directe du code de la physique sous-jacente. La volonté d'opérer dans un cadre modulaire et d'interagir seulement avec des codes de physique par un calcul de résidu nécessite des préconditionneurs modifiés, qui ne manipulent que le résidu. Des préconditionneurs Bloc Jacobi et Bloc Gauss-Seidel sont développés à partir de manipulations de la solution résiduelle.

Homogénéisation des sections efficaces

Comme mentionné précédemment, l'homogénéisation des sections efficaces fournit un moyen de réduire le nombre d'inconnues du système numérique dans l'analyse du réacteur. Beaucoup de progrès dans les méthodes d'homogénéisation sont orientées vers l'homogénéisation dans les calculs à l'état d'équilibre. La majorité des opérations d'un réacteur est effectuée à l'état d'équilibre, avec des variations rares qui durent peu de temps par rapport à un fonctionnement normal. L'étude de l'impact de l'application de ces méthodes d'homogénéisation lors des calculs transitoires n'a pas largement apparu dans la littérature relative à l'analyse du réacteur. Un seul rapport a été trouvé, mentionnant utilisation de différents problèmes de valeurs propres pendant l'homogénéisation pour différentes configurations [46].

Une question qui s'est posée au cours de ce travail fut, « Des sections efficaces homogénéisées, destinées aux calculs à l'état d'équilibre, peuvent-elles être utilisées pour des simulations transitoires ? ». Il a été vite découvert que lors des transitoires très rapides, où le réacteur est loin d'être critique, ces sections efficaces peuvent introduire des erreurs importantes dans la puissance en fonction du temps. Cette prise de conscience a incité l'auteur à explorer des façons de réduire l'erreur introduite par ces sections efficaces homogénéisées.

Deux méthodes, conçues pour réduire l'erreur introduite lors de l'utilisation des sections efficaces destinées à des calculs à l'état d'équilibre, sont développées et testées. L'une de ces méthodes est basée sur le développement du flux en fonction du temps sur une base qui provient d'un problème de valeur propre qui représente le comportement en fonction du temps. La méthode de développement présente la liberté de choisir la taille de la base de développement et le poids relatif entre les vecteurs de la base de développement. Ces coefficients peuvent être déterminés par une minimisation sur le sous-espace de développement et une solution choisie, typiquement la condition initiale. L'autre méthode est basée sur un flux intégré en temps sur de grands intervalles de temps de la simulation dynamique. Les intervalles de temps sont librement choisis et doivent généralement coïncider avec des changements importants de la solution: durée de la perturbation, puissance maximale, émission des neutrons retardés, etc. Cette méthode, en plus de capturer le comportement dépendant du temps de la solution, capture les effets des contre-réactions dus aux variations de température au cours de la simulation. Ces deux méthodes sont testées et comparées à des solutions de référence pour une série de phénomènes transitoires disponibles.

A.2 Simulation multiphysique

Cette section explique comment les solutions multiphysiques sont obtenues. Deux méthodes de premier plan sont disponibles: le couplage simultané et le couplage séquentiel. Les méthodes de couplage séquentiel sont celles dans lesquelles chaque composant physique est résolu indépendamment et couplé à d'autres composants physiques par des transferts de données des solutions. Les méthodes de couplage simultané traitent le système multiphysique comme un seul système numérique et obtiennent une solution à tous les composants physiques par itérations non-linéaires.

A.2.1 Système séquentiel

La méthode la plus facilement disponible pour coupler des modèles physiques indépendants est par une manière de couplage séquentiel, qui peut aussi être désigné comme *fractionnement d'opérateur*. Cette méthode implique la résolution de chaque composant physique séparément avec les solutions des autres composants physiques en données d'entrée. Il existe des variantes de cette méthode, basé sur la solution d'entrée utilisée provenant des autres composants physiques: soit la solution au pas de temps précédent, soit la solution la plus récente. Cette méthode est avantageuse quand il y a des modèles physiques distincts pour chaque composant physique qui sont optimisés pour traiter les échelles de la longueur de temps caractéristiques pour cette composante physique. Il y a généralement plusieurs années d'expérience qui se manifestent dans un code informatique pour résoudre une composante physique donnée; cette méthode se construit directement sur cette expérience.

Le fractionnement d'opérateur est généralement un processus non-itératif, ce qui signifie que, à chaque pas de temps, un seul passage à travers les modèles physiques est effectué. Cela ne converge pas les non-linéarités entre les composantes physiques, et peut être au mieux à premier ordre à la discrétisation de temps [9, 107]. Cette méthode est décrite dans la figure 3.1, où le modèle neutronique prend la température de l'étape précédente en tant que donnée d'entrée. La puissance produite par le modèle neutronique est introduite dans le modèle thermohydraulique, qui produit une nouvelle distribution de la température. Souvent, cette méthode décalée ne résoudra pas avec précision les non-linéarités produites par des sections efficaces dépendant de la température à chaque pas de temps. La convergence d'un tel processus peut être remis en question, en particulier si les composants physiques fonctionnent à des échelles de temps significativement différentes [108]. En outre, en raison de la nature explicite de ce schéma numérique, des oscillations peuvent être observées dans certains cas [109, 110].

La méthode de fractionnement d'opérateur peut être itérée jusqu'à ce que les non-linéarités entre les composantes physiques soient totalement convergées. Ce processus est décrit dans la figure 3.2 où, à chaque pas de temps, la solution la plus récente du modèle neutronique est introduite dans le modèle thermohydraulique. Ensuite, la solution la plus récente pour le modèle thermohydraulique est introduite dans le modèle neutronique. Le processus est répété jusqu'à ce qu'un niveau de convergence suffisant entre les deux modèles soit atteint. Bien que ce procédé fasse converger les non-linéarités entre chaque composant physique, la vitesse de convergence est linéaire et peut devenir coûteuse. Il est généralement nécessaire d'accélérer ce type de méthode pour avoir un temps de calcul acceptable [107]. Le processus itératif entre les composantes physiques produit une méthode numérique inconditionnellement stable, ce qui élimine les oscillations observées avec la version décalée du fractionnement d'opérateur [109, 110].

Les méthodes de couplage séquentiel sont des méthodes couramment utilisées pour coupler les codes existants en raison des faibles modifications nécessaires à la mise en œuvre de ces méthodes [89, 111, 112]. Le véritable défi que représente ces méthodes est dans la façon de transférer avec précision les solutions à d'autres modèles de composants physiques. Le transfert de solution peut être réalisé par un

certain type d'interpolation ou de projection sur le maillage d'un autre composant physique [113].

Bien que le processus de fractionnement d'opérateur puisse présenter des inconvénients pour l'obtention d'une solution multiphysique, il est utile en tant que préconditionneur pour des processus simultanés. L'utilisation de préconditionneurs *Bloc* ou *Physiquement Basé* a été montrée comme étant essentielle dans la résolution de problèmes multiphysiques simultanés [37, 114].

A.2.2 Système simultané

Un grand nombre de travaux récents ont été consacrés à l'étude d'une approche de système simultané [8, 9, 115, 116]. Le système simultané est réalisé en formant un résidu non-linéaire pour chaque composante physique et en plaçant chacun de ces résidus dans un résidu global pour le système couplé. Le problème physique non-linéaire couplé peut alors être défini comme: trouver la solution qui produit un vecteur résidu nul.

Dans ce travail, la méthode de Newton est exclusivement utilisée pour trouver la solution du système non-linéaire, qui se compose d'une linéarisation du résidu non-linéaire et un processus itératif pour trouver une solution amenant la linéarisation du résidu à zéro. La méthode de Newton est dérivée du développement de Taylor à plusieurs variables du résidu, dans lequel la perturbation linéaire contient une matrice de termes dérivés du premier ordre appelée la jacobienne.

La méthode de Newton est construite à partir de la troncature du développement Taylor après le terme linéaire et de la résolution du système linéaire qui rendra l'approximation du résidu nulle. La méthode de Newton consiste à calculer la jacobienne et le résidu pour l'itération en cours, et à inverser la matrice jacobienne pour trouver le vecteur de mise à jour approprié, qui est ajouté à la solution courante.

Ce processus est répété jusqu'à ce que le résidu ou le vecteur de mise à jour est *suffisamment petit*. Une définition couramment utilisée de *suffisamment petit* est une certaine tolérance absolue plus une fraction de la norme du résidu original [117]. Cette définition de la tolérance non-linéaire permet à la méthode de Newton de converger même si le résidu d'origine est grand; dans ce cas, une réduction significative de la taille du résidu est recherchée.

La méthode de Newton est localement q-quadratique convergente, ce qui signifie que, si l'itération initiale pour la méthode est suffisamment proche de la solution, la méthode convergera quadratiquement. L'exigence pour l'itération initiale d'être suffisamment proche de la solution convergée n'est pas aussi contraignante que ce à quoi pourrait s'attendre. Dans l'application de la méthode de Newton pour résoudre des PDEs implicitement intégrés, l'itération initiale est considérée comme la solution au pas de temps précédent [119, 120]. Si le pas de temps est suffisamment petit, la solution convergée est proche de la solution au pas de temps précédent.

Pour s'assurer que la méthode de Newton converge vers la solution correcte, même lorsque l'itération initiale est loin de la solution, une technique de globalisation doit être utilisée [119]. Il existe deux techniques principales de globalisation utilisées pour la méthode de Newton: la région de confiance et la recherche en

ligne. La méthode de la région de confiance construit un modèle quadratique local autour de l'itération actuelle et résout le modèle quadratique dans une région de confiance d'un certain rayon. La région de confiance nécessite des modifications importantes dans l'algorithme de Newton pour intégrer cette globalisation [121]. La globalisation de la recherche en ligne, quant à elle, ne nécessite que des petites modifications si l'algorithme de Newton est déjà localement convergent; par conséquent, la méthode de recherche en ligne est préférable dans ce travail.

La méthode de recherche en ligne suppose que la mise à jour de la solution est orientée dans le bon sens (c'est-à-dire une direction descendante), mais peut dépasser la solution ciblée. L'objectif de la méthode de recherche en ligne est de réduire l'ampleur de la mise à jour de la solution jusqu'au moment où la norme du résidu est suffisamment réduit. Le facteur de réduction pour la mise à jour de la solution peut être obtenu par la règle Armijo [122].

Un inconvénient important de la méthode de Newton est d'avoir à calculer et à stocker la matrice jacobienne. Dans certains cas, la matrice jacobienne peut ne pas être facilement disponible si la formulation du résidu est construite à partir d'une routine de calcul inaccessible. Ce travail utilise une variante de la méthode de Newton, qui peut être utilisée lorsque la jacobienne est soit de taille rédhibitoire pour calculer ou stocker, soit inaccessible.

Les solveurs linéaires des sous-espaces Krylov ne nécessitent que le résultat de l'application de la matrice du système linéaire à un vecteur donné. Étant donné que la jacobienne est une matrice de dérivés du premier ordre, le produit vectoriel de la jacobienne peut être approchée par une différence finie avec le résidu. La classe des solveurs non-linéaires qui utilisent cette approximation pour l'inversion de la jacobienne est appelée méthodes Jacobian-Free Newton-Krylov (JFNK) [37]. L'approximation des différences finies peut être calculée avec des formulations d'ordre supérieur qui nécessitent plusieurs évaluations du résidu, mais qui sont moins sensibles aux erreurs numériques; la soustraction de deux nombres qui sont rapprochés dans la précision finie peut être instable. Dans ce travail, la relation de différence finie par défaut est un schéma de différence centrée, qui est convergent de l'ordre 2 dans le paramètre des perturbations petites. Ce schéma de différence centrée nécessite deux évaluations du résidu pour chaque produit vectoriel de la matrice, mais est moins sensible aux instabilités de soustraction de précision finie. Le petit paramètre de perturbation est calculée en utilisant les relations trouvées dans [137]

Préconditionnement avec JFNK

Une méthode bloc de préconditionnement peut être étendue à un environnement JFNK en divisant le vecteur qui multiplie la matrice jacobienne dans le solveur Krylov. Le vecteur de multiplication est remis à zéro pour les indices qui ne correspondent pas au bloc étant inversé. Cela permet uniquement au vecteur de multiplication d'agir sur le bloc qui doit être inversé. Cette méthode de préconditionnement est testée sur un problème spatialement hétérogène avec 26 groupes d'énergie. Les préconditionneurs n'affectent pas le nombre d'itérations non-linéaires nécessaires pour produire une solution convergée. Ce comportement est attendu car les préconditionneurs agissent uniquement sur le modèle linéaire

local de la méthode de Newton. Il est montré que les préconditionneurs basés sur la physique amènent le nombre moyen d'itérations linéaires par itération non-linéaire à deux, tandis que le préconditionneur identité comprend toujours entre 3 et 7 itérations linéaires par itération non-linéaire.

D'après le problème spatialement hétérogène avec 26 groupes d'énergie, un préconditionneur bloc Jacobi présente le meilleur résultat. Il peut y avoir des choix plus optimaux pour le préconditionnement, mais le préconditionneur bloc Jacobi peut servir de préconditionneur efficaces par défaut pour un système multiphysique.

A.2.3 Formulation des résidus

L'avantage de la méthode JFNK par la réduction de stockage et de la convergence quadratique invite l'utilisation de cette méthode pour l'analyse étudiée dans ce travail. La convergence supérieure par rapport au fractionnement d'opérateur et au couplage fort assure une solution plus exacte aux problèmes d'analyse de réacteurs. Cette section est dédiée à une nouvelle formulation du résidu du transport de neutrons qui utilise un code de transport de neutrons existant et réduit la taille du résidu par un facteur important.

Résidu du transport des neutrons

L'équation de transport (Equation 2.1), après discrétisation temporelle, spatiale, angulaire, et énergétique, écrite sous forme de matrice pour la compacité, est montrée dans l'équation 3.36.

La formulation implicite de l'équation 3.36 implique qu'une forme explicite de la solution ne peut pas être obtenue, et une méthode itérative doit être utilisée pour obtenir la solution à l'étape suivante. Cela ne doit pas être considéré comme un inconvénient en raison de la nécessité d'utiliser une méthode itérative pour résoudre le couplage non-linéaire entre les composantes physiques. L'équation 3.36 peut être facilement réécrite sous forme de résidu en déplaçant tous les termes d'un côté de l'égalité. Une complication survient lorsqu'un code de transport existant doit être utilisé pour la construction du résidu. Les codes de transport de premier ordre (S_N ou MOC) n'utilisent généralement pas les matrices $\mathbf{L}$ et $\mathbf{H}$ directement, mais utilisent uniquement de manière efficace la matrice inverse $(\mathbf{L}-\mathbf{H})^{-1}$ par balayage et itération sur la source de diffusion. Les algorithmes dans les codes de transport sont écrits pour produire un flux angulaire à partir d'une distribution de source donnée. La formulation est modifiée en combinant d'une part le terme de temps inversé avec l'opérateur de perte et d'autre part, le flux précédent avec le terme de source fixe. La modification de l'opérateur de perte permet au nouvel opérateur de perte d'être inversé en utilisant une méthode de balayage de transport classique.

Un inconvénient d'une telle formulation du résidu est que la taille de cette équation correspond à celle du flux angulaire, qui peut être importante (la taille de $N_{\text{régions}} * N_{\text{groupes}} * N_{\text{composants spatiaux}} * N_{\text{directions}}$). Cette grande taille pose plusieurs problèmes dans la simulation numérique, dont l'un est l'exigence de stockage pour le solveur linéaire Krylov. GMRes nécessite le stockage des vecteurs de base pour le sous-espace Krylov, ce qui nécessiterait de stocker plusieurs vecteurs au moins

aussi grands que le flux angulaire. En effet, la taille des vecteurs de base serait beaucoup plus grande que celle du flux angulaire en raison de l'enchaînement avec les résidus de la température et des précurseurs de neutrons retardés. Avec ces motivations à l'esprit, une forme alternative de taille plus petite est obtenue.

La source de fission au sein du système nucléaire fournit un lien clair entre le modèle de transport de neutrons, et le modèle de transfert de chaleur par l'intermédiaire de la puissance. La source de fission est aussi généralement de taille plus petite ($N_{\text{régions fissiles}} * N_{\text{composants spatiaux}} * N_{\text{isotopes fissiles}}$) que le flux angulaire. Le nombre de régions de fission est toujours un sous-ensemble du nombre de régions, et le nombre d'isotopes fissiles est très probablement plus petit que le produit du nombre de groupes d'énergie et du nombre de directions. Même avec un petit nombre de directions comme une quadrature angulaire S_8 et un nombre moyen de groupes d'énergie de 100, le nombre d'isotopes fissiles est généralement limité à 50, donnant une réduction d'un facteur de plus de 1000.

Le résidu du transport peut être formulé en termes de la source de fission en intégrant sur toutes les directions et en multipliant par la section efficace de fission. Cette formulation du résidu peut être réalisée en modifiant légèrement le code de transport S_N existant, qui peut résoudre les problèmes de sources fixes ou de valeurs propres. La plus grande modification est d'avoir à imposer l'intégrale de fission présente au lieu qu'elle soit calculée à partir du flux angulaire, et d'appliquer la matrice de fission après l'inversion de la matrice de transport par le balayage.

A.3 Homogénéisation transitoire

Les méthodes d'homogénéisation jouent un rôle central dans l'étude de l'analyse du réacteur. La génération précise des sections homogénéisées est de la plus haute importance pour réduire l'introduction d'erreurs de modèle dans les simulations de réacteurs. Cette section se concentre sur les méthodes d'homogénéisation traditionnelles utilisées dans l'analyse du réacteur, et sur les modifications nécessaires pour utiliser des sections efficaces homogénéisées dans des simulations multiphysiques dépendant du temps.

A.3.1 Motivation

Les méthodes d'homogénéisation sont régulièrement utilisées dans l'analyse du réacteur lorsqu'un calcul détaillé est trop coûteux. Par exemple, pour un coeur de REP, il y a 193 assemblages combustibles de 4 m de haut, contenant chacun 289 crayons (264 crayons combustibles et 25 crayons non combustibles). Une résolution spatiale modérée (un point spatial par crayon et un point par centimètre dans le sens axial) se traduirait par environ 22 millions points spatiaux. En outre, pour chaque point de l'espace, une résolution précise de la dépendance angulaire et énergétique est nécessaire pour calculer le flux angulaire. Pour les réacteurs thermiques, environ 300 groupes d'énergie sont utilisés pour discrétiser le domaine de l'énergie. Pour les réacteurs rapides, ce nombre peut monté jusqu'à 2000. Le domaine angulaire peut être discrétisé en utilisant des directions distinctes, ce qui, pour une quadrature S_8 en trois dimensions correspond à 80 directions angulaires [139]. Cela conduit à un flux angulaire avec 535×10^9 in-

connues, qui n'est généralement pas stocké pour les calculs statiques, mais qui l'est pour les calculs transitoires. Simplement stocker le flux angulaire en double précision, nécessiterait environ 4 téraoctets de mémoire, ce qui est impossible sur tous les ordinateurs à part sur les super-ordinateurs de haute performance. Cette idée conduit les ingénieurs et les physiciens des réacteurs à développer des méthodes qui réduisent la consommation de mémoire et le temps de calcul, tout en obtenant une solution précise. L'homogénéisation des sections efficaces est l'une des façons de réduire la taille du problème, tout en conservant les caractéristiques importantes de la solution. Typiquement, les taux de réaction et la valeur de k_{eff} sont les quantités d'intérêt qui doivent être conservées dans les procédés d'homogénéisation, car, souvent, les ingénieurs sont intéressés par la puissance ou le taux d'absorption dans une région du réacteur et par l'état de critique du réacteur.

La procédure utilisée pour l'homogénéisation dans l'analyse du réacteur comporte plusieurs étapes: l'auto-protection avec des cellules de crayons, le calcul de flux détaillé sur réseau, la pondération des sections efficaces, le calcul au niveau du coeur, et une potentielle séquence d'itération sur ces étapes [52, 140]. Les codes de transport déterministes sont généralement employés dans le calcul d'auto-protection et du flux détaillé de réseau. Cependant les codes Monte Carlo ont été utilisés comme alternative à un calcul déterministe [141]. Les codes Monte Carlo ont été utilisés uniquement dans les pratiques de validation puisqu'un calcul déterministe est généralement plus rapide que le calcul de Monte Carlo.

Une hypothèse sous-jacente avec des méthodes d'homogénéisation est que la solution obtenue lors du calcul du réseau se rapproche de la solution hétérogène dans le problème global plus large. Cependant, des travaux récents [28] et une analyse simple montrent que, lors de situations transitoires, les solutions dépendant du temps et statiques peuvent être sensiblement différentes. Néanmoins, la pratique actuelle est d'utiliser un calcul statique dans le calcul du réseau, même lorsque les calculs en fonction du temps sont effectués sur un problème de réacteur. Étant donné que les solutions dépendant du temps et statique ne sont pas équivalentes, les sections efficaces produites à partir d'une solution statique peuvent ne pas représenter exactement la solution en fonction du temps. Cette section explore ces erreurs et introduit de nouvelles méthodes d'homogénéisation conçues pour produire des sections efficaces homogénéisées plus précises pour les calculs en fonction du temps.

A.3.2 Formulation classique

Le thème de l'homogénéisation des sections efficaces couvre un large éventail de méthodes. Dans le cas le plus simple, l'homogénéisation est un procédé considérant la moyenne pondérée des sections efficaces pour obtenir des valeurs moyennes. La fonction de pondération est typiquement un flux, de sorte que la moyenne pondérée conserve les taux de réaction, qui sont définies au paragraphe 2.1. L'homogénéisation des sections efficaces qui utilise la solution hétérogène du problème complet comme fonction de pondération peut être appelée *théorie d'équivalence* [42]. Cependant, l'utilisation de la solution hétérogène globale présente peu d'intérêt en raison de la difficulté pour l'obtenir. L'ho-

mogénéisation devient pratique lors de l'utilisation des solutions de référence de sous-domaines représentatifs dans ce qui est appelé *théorie générale de l'équivalence* [42].

Un autre type de méthodes d'homogénéisation est basée sur la limite asymptotique d'une développement du flux angulaire hétérogène. Le flux angulaire est développé autour d'un petit paramètre d'une certaine échelle de longueur ou de l'énergie caractéristique. Cette développement, réalisée à différentes échelles de longueur, est utilisée pour décomposer la solution hétérogène globale en un produit de solutions locales et globales [142–144].

Dans tous les procédés d'homogénéisation, le flux de pondération est la principale source d'erreur; si le flux de pondération est loin du flux réel, des erreurs importantes peuvent être introduites. Ceci peut être constaté dans de nombreux exemples, dont l'un est le cas où une région homogénéisée est entourée par des régions très différentes. Dans ce cas, les conditions limites réfléchissantes sont une mauvaise approximation de l'état du système [44]. Une façon d'améliorer la solution dans cette situation est d'estimer une condition d'albédo à imposer aux frontières. Une autre façon d'intégrer l'effet d'un environnement différent est en prenant plusieurs régions d'homogénéisation au cours du processus pour donner une meilleure représentation des gradients de flux à travers les frontières où les matériaux changent de façon important; ceci est connu sous le nom de méthode *color-set* [147].

Il est montré que les méthodes d'homogénéisation fonctionnent relativement bien dans la plupart des calculs d'analyse du réacteur. Cependant cela ne vaut directement que pour des calculs statiques. Les calculs statiques peuvent être utiles pour de nombreuses applications dans l'analyse du réacteur, telles que l'optimisation du réarrangement combustibles, le calcul de la marge d'arrêt, ou pour trouver le point de puissance maximale pendant le fonctionnement en régime permanent. Cependant, dans l'analyse des accidents graves, tels que ceux induits par les changements importantes de réactivité, ces méthodes peuvent échouer.

Lors de la production des sections efficaces homogénéisées pour une utilisation dans l'analyse du réacteur, les sections efficaces tabulées pour différentes conditions de fonctionnement (température combustible/modérateur, concentration en bore, taux de combustion, etc.). Lors du calcul au niveau du coeur, cette table de sections efficaces est interpolée pour refléter les conditions de fonctionnement du coeur. La température du mélange combustible/modérateur aura une influence sur les sections efficaces, notamment dans la gamme d'énergie de résonance; cette dépendance est prise en compte grâce à des calculs d'auto-protection réalisés à chaque point tabulé. Cette utilisation des sections efficaces tabulées a été appliquée de façon répétée à des calculs de diffusion avec des calculs de transport pendant l'homogénéisation. Cependant, l'utilisation de ces tables dans les calculs de transport avec des calculs de transport pendant l'homogénéisation n'a pas encore été montrée valide. L'auteur suppose que l'utilisation de ces sections efficaces homogénéisées tabulées est valable pour les calculs de transport à transport, sans vérification explicite que ces tableaux n'introduisent pas d'erreur significative.

L'auto-protection est une opération effectuée au cours du processus d'homogénéisation pour tenir compte de l'influence des résonances des sections efficaces

sur le flux dépendant de l'énergie. Normalement, l'auto-protection est réalisé lors de la construction de tables de sections efficaces homogénéisées pour tenir compte des changements de température et de composition des matériaux. L'utilisation de l'auto-protection dans le présent travail diffère de la norme en effectuant l'auto-protection tout en produisant une table de sections efficaces de base. La table de sections efficaces de base contient des sections efficaces dans la structure de l'espace et groupe fine. Cette table de sections efficaces est utilisé pour effectuer des calculs de référence et l'homogénéisation est effectuée sur l'ensemble des sections efficaces dans la table de base, sans application supplémentaire de l'auto-protection. La table de sections efficaces produite en homogénéisant la table de référence est similaire à ce qui est utilisé dans les analyses transitoires actuelles du réacteur [111]. De façon rigoureuse, le calcul d'auto-protection devrait être effectué à chaque changement de température dans le calcul de référence. Cela devient cependant coûteux, et on fait l'hypothèse que les effets d'auto-protection peuvent être interpolés.

A.3.3 Formulations transitoires

Des travaux récents ont montré qu'un changement de réactivité provoque un décalage dans le spectre d'énergie de la solution de transport [28]. Ce décalage n'est pas visible lors de calculs de criticité et nécessite un traitement spécial. Ainsi, si des sections efficaces, produites par un procédé d'homogénéisation utilisant un flux provenant d'un calcul de criticité, sont utilisés dans un calcul transitoire, des erreurs significatives peuvent être introduites en raison de l'échec à capturer ce décalage. Deux nouvelles méthodes sont étudiées pour obtenir un flux de pondération plus précis pour les calculs transitoires: le premier est basé sur un flux intégré dans le temps ou *fluence* (méthode fluence), et le second sur une développement de flux asymptotique (méthode alpha).

Méthode fluence

La première méthode étudiée pour réduire les erreurs dans les calculs transitoires, consiste à introduire une moyenne pondérée dans le domaine temporel dans l'équation d'homogénéisation d'origine. A ce stade, tout comme les régions homogènes et la structure énergétique homogène peuvent être librement choisies, le maillage de temps homogène sur lequel les sections efficaces dépendant du temps sont constantes peut être librement choisi. La dépendance temporelle des sections efficaces proviendra généralement de leur dépendance à la température, ce qui changera au cours d'une simulation transitoire.

Cette formulation peut cependant être coûteuse en raison de la nécessité d'exécuter un calcul d'homogénéisation à chaque intervalle de temps lorsque les sections efficaces et le flux ont changé. Pour réduire le coût de ce procédé d'homogénéisation, on suppose que la section efficace est constante sur des grands intervalles de temps [148]. Ceci permet d'exécuter l'intégration dans le temps indépendamment du comportement de la section efficaces. Cette moyenne ajoute une autre dimension à la table des sections efficaces existante, ce qui produit une table plus grande. Le nombre de points dans la nouvelle table de sections efficaces correspond au nombre de points dans la table de base multiplié par le nombre

d'intervalles de temps dans le domaine d'intervalle de temps macro. Le principal inconvénient de cette méthode est le coût associé à l'obtention du flux en fonction du temps utilisé pour homogénéiser les sections efficaces. Une façon de réduire le coût d'obtention d'une telle solution consiste à effectuer le calcul en fonction du temps sur des sous-domaines du problème.

Habituellement, les méthodes d'homogénéisation sont axées sur la conservation des taux de réaction; ici, la conservation d'une quantité similaire est recherchée: la densité totale de réaction pendant un intervalle de temps.

Méthode alpha

La méthode d'homogénéisation alpha est une nouvelle technique pour produire des sections efficaces homogénéisées qui peuvent être utilisées dans les calculs dépendant du temps [148]. Cette méthode considère des vecteurs propres du problème-α et les utilise comme remplacement pour le mode fondamental du problème k-valeur propre pour les calculs statiques. L'utilisation d'un flux qui provient d'un problème de valeur propre prenant en compte le comportement dynamique du système devrait produire des sections efficaces homogénéisées qui représentent également les décalages spectraux observés pour les solutions en fonction du temps.

Il existe de nombreux vecteurs propres problème α-valeur propre qui peuvent être utilisés comme flux de pondération. Les caractéristiques du système nucléaire et transitoire permettront de déterminer quelles vecteurs propres sont utiles pour l'homogénéisation.

Lors que les précurseurs de neutrons retardés sont supprimés, il y a une seule valeur propre dominante dont le signe est déterminé par le caractère critique du système. Toutes les autres valeurs propres sont largement négatives, ce qui provoquera l'extinction de ces modes peu après le début du transitoire. Pour des problèmes où les précurseurs de neutrons retardés sont supprimés, seul ce vecteur propre dominant est considéré comme flux de pondération.

Cependant, lorsque les neutrons retardés sont présents, il existe plusieurs valeurs propres qui influencent la solution dépendant du temps après le début du transitoire. Contrairement au cas sans précurseur de neutrons retardés, ces modes ne sont pas disparus peu après le début du transitoire. Quand les neutrons retardés sont présents, une combinaison de plusieurs modes est utilisée pour produire un flux de pondération pour le processus d'homogénéisation.

Une façon de combiner les vecteurs propres pour la méthode alpha serait d'utiliser un développement. Les coefficients de développement sont calculés en fonction de la condition initiale. L'intégrale du flux dépendant du temps peut être effectuée de manière analytique.

Cette combinaison de vecteurs propres inclut à la fois les outils du problème α-valeur propre, et ceux du procédé de fluence. Elle réduit le coût de l'obtention d'une solution en fonction du temps pour la méthode de fluence, et produit des sections efficaces dépendant du temps qui fournissent des vecteurs propres importants quand ils sont le plus influents lors d'un transitoire.

Une autre façon d'appliquer la méthode alpha consiste à construire une combinaison linéaire de valeurs propres α à utiliser dans le problème de l'homogé-

néisation, où les coefficients de développement sont déterminés à partir d'une minimisation de la condition initiale, projetée sur le sous-espace engendré par les vecteurs propres. La combinaison linéaire peut être construite en utilisant tous les $N_d + 1$ principaux vecteurs propres, ou un sous-ensemble de ces vecteurs. Ici, N_d est le nombre de groupes de précurseurs de neutrons retardés. Plusieurs sous-ensembles sont utilisés dans la partie de ce travail présentant les résultats, par exemple: le vecteur propre dominant seul, le plus grand et le plus petit des vecteurs propres principaux (extrema), et l'ensemble des $N_d + 1$ vecteurs.

L'association du vecteur propre et de la plus grande valeur propre est utilisée pour les cas où les précurseurs de neutrons retardés sont supprimés. Ce sous-ensemble fonctionne bien car les modes moins dominants sont disparus rapidement après le déclenchement du transitoire, et une grande partie du transitoire est gérée par l'évolution de ce mode unique. Il sera montré cependant que, lorsque les neutrons retardés sont présents, ce sous-ensemble est insuffisant pour produire des sections efficaces homogénéisées qui reproduisent les caractéristiques du transitoire de référence. Ce comportement peut être attribué au fait que le transitoire est géré par des modes non-dominants bien après le début du transitoire.

Le prochain sous-ensemble étudié considère à la fois le vecteur propre avec la plus grande valeur propre, et les plus petites valeurs propres principales (extrema). Ce sous-ensemble a été étudié pour incorporer simultanément deux constantes de temps du transitoire: le comportement rapide de la fission prompte, et le comportement plus lent de l'émission des neutrons retardés. Ces deux vecteurs propres sont choisis pour prendre en compte le comportement rapide présent juste après le début du transitoire ainsi que le comportement associé au mode asymptotique bien après le début du transitoire. Un aspect important de choisir ces modes comme flux de pondération, est le poids relatif accordé à chaque mode. Ces poids sont choisis en fonction de l'état initial, tout comme la façon dont les coefficients de développement seraient choisis pour des problèmes dépendant du temps. Cependant, étant donné que les deux vecteurs propres ne forment pas un ensemble complet, une minimisation est effectuée pour obtenir les coefficients de développement. De cette façon, les vecteurs propres sont pondérés d'une manière qui reproduirait le mieux la condition initiale, étant donné l'ensemble des vecteurs de développement. En variante, une solution autre que le flux initial pourrait être utilisée pour déterminer des coefficients de développement. Cependant, étant donné que l'état initial pour le flux est spécifié pour le calcul, cette solution est choisie pour l'obtention des coefficients de développement.

Le troisième sous-ensemble est similaire au sous-ensemble précédent des extrema des valeurs propres principales, mais tous les vecteurs propres principaux sont considérés pour produire un flux de pondération pour l'homogénéisation. Ce sous-ensemble est pris pour couvrir une plage de temps plus large que les sous-ensembles précédents en raison du plus grand nombre de vecteurs propres présents dans l'ensemble. Les coefficients de développement sont obtenus de la même façon: un problème de minimisation avec la condition initiale.

Les méthodes décrites dans cette section ont été appliquées à plusieurs transitoires, à la fois dans les milieux homogènes et hétérogènes. Il a été montré, à la fois pour un cas spatialement homogène et pour un cas spatialement hétérogène,

que des sections efficaces homogénéisées produites avec un flux de pondération provenant d'un calcul critique peuvent introduire des erreurs importantes dans le transitoire.

Les deux méthodes produisent de bons résultats lorsque les précurseurs de neutrons retardés ont été supprimés, mais la méthode alpha a dû être modifiée lorsque les précurseurs de neutrons retardés ont été introduits. La méthode alpha a besoin d'inclure les contributions des précurseurs de neutrons retardés à vie court et à vie longue. Il a été observé que pour une insertion de réactivité au-dessous du seuil prompt critique ($\rho < \beta$), les sections efficaces produites à partir d'un calcule critique fonctionnent bien; les erreurs pour le transitoire supercritique étaient plus petites que pour le transitoire super prompt critique. Cependant, les nouvelles méthodes ont toujours produit des erreurs plus petites que la méthode critique dans tous les cas.

Lorsque des hétérogénéités spatiales ont été introduites, la méthode fluence a continué à bien fonctionner, mais la partie délicate de cette procédure sera dans le choix d'un problème d'homogénéisation de référence approprié. Pour récupérer le comportement des insertions de réactivité non uniformes, un tampon homogène peut être ajouté à la zone d'homogénéisation d'intérêt. Il a également été démontré que le raffinage de la discrétisation de temps utilisée dans le procédé de fluence réduit les erreurs de divers paramètres jusqu'à un point où plus de subdivisions ont augmenté les erreurs. Cette augmentation de l'erreur peut être le résultat de l'accumulation d'erreurs numériques en raison de la plus grande table d'interpolation induite par la discrétisation temporelle plus fine.

Le temps nécessaire pour produire des sections efficaces est décourageant pour les applications industrielles, et pour que cette méthode soit utile, des améliorations devront être explorées. Une voie possible pour obtenir la solution multiphysique requise pour cette méthode consiste à mettre en œuvre des algorithmes parallèles dans l'ensemble des modèles utilisés. La méthode de transport utilisé une quadrature S_8, et la parallélisation des balayages de transport à travers le domaine a le potentiel de réduire le temps de calcul par une fraction significative. Alternativement, une solution en fonction du temps approximative peut être obtenue par un développement sur des modes propres α. Cependant, cette approximation ne prend pas en compte les effets du changement de la température pendant le transitoire et peut être considérablement dans l'erreur.

A.4 Conclusions

Les travaux discutés dans cette thèse se concentrent sur la simulation précise des accidents d'insertion de réactivité. L'objectif de ce travail est de montrer comment les codes de composants physiques peuvent être couplés dans un cadre multiphysique basé sur JFNK et d'étudier l'impact de l'utilisation des sections efficaces homogénéisées dans les calculs transitoires. Les méthodes développées dans ce travail peuvent être efficacement appliquées pour traiter la simulation des accidents graves où l'insertion de réactivité est telle que le système nucléaire est super prompt critique. Dans un tel cas, le système nucléaire est loin d'une configuration en mode fondamental et de grands effets de contre réactions qui poussent la solution sont présents.

Les méthodes d'homogénéisation développées dans ce travail ont été testées sur des simulations de petite échelle pour montrer leur utilisation potentielle dans des applications de génie nucléaire. Le transfert à des calculs de taille industrielle nécessitera un certain nombre d'études supplémentaires pour que ces méthodes soient jugées utiles dans les codes industriels. Une telle étude devra tester le comportement des méthodes lorsqu'un modèle de diffusion de neutrons est utilisé dans le calcul homogénéisé. Dans les cas traités dans ce travail, un modèle de transport de neutrons a été utilisé à la fois dans le calcul de référence et dans le calcul homogénéisé. Un autre grand progrès requis pour la méthode fluence sera d'obtenir un flux en fonction du temps dans un délai raisonnable. Ceci peut être accompli grâce à la parallélisation ou la formation d'une approximation appropriée au flux dépendant du temps. La présente section résume les résultats de ce travail, tire plusieurs conclusions, et donne la vision de l'auteur pour les futurs développements de ce travail.

A.4.1 Couplage multiphysique

L'un des principaux objectifs de ce travail était de développer un cadre dans lequel plusieurs codes physiques, qui ne sont pas prévus à l'origine pour fonctionner dans une simulation multiphysique, pourraient être couplés. La façon typique de mettre en œuvre un tel cadre multiphysique est d'utiliser une technique de fractionnement d'opérateur où le couplage entre les codes des composants est traité par le biais d'I/O. Ce type de schéma de couplage ne traite que le couplage faible entre les composants physiques et peut éprouver des difficultés de convergence. La méthode de choix pour ce travail a été basée sur la méthode JFNK, où toutes les composantes physiques sont traitées dans un seul grand système. Ce type de méthode résout le couplage entre les composantes physiques à chaque pas de temps du processus de solution par des itérations non-linéaires. Une méthode de Newton est utilisée comme itérateur non linéaire en raison de sa convergence supérieure par rapport aux autres méthodes non linéaires, comme le point fixe et Picard.

Le point faible de mettre en œuvre une méthode de JFNK pour conduire des simulations multiphysiques est dans les modifications potentiellement lourdes nécessaires dans les codes de composants. Le procédé JFNK nécessite qu'une solution résiduelle soit renvoyée par chaque composant physique, ce qui n'est généralement pas une opération que les codes composants fourniront. Ces calculs de résidus doivent être soit mis en œuvre dans les codes soit calculés à l'extérieur des codes en contrôlant les opérations dans un code de composant.

La mise en œuvre du calcul résiduel dans les codes de composants nécessite que chaque code de composant soit capable de manipuler une solution provenant d'autres codes de composants; la fonction résiduelle pour un seul composant physique dépend de la solution de tous les composants physiques. Chaque composant physique pourrait alors simplement accepter la solution multiphysique complète et retourner la solution résiduelle pour ce composant physique. Ce mode de réalisation est plus robuste et modulaire, mais il exige qu'à chaque fois qu'un élément physique est ajouté à la simulation, tous les codes de composant physique soient modifiés.

En variante, le calcul de la solution résiduelle à l'extérieur des codes composants offre une plus grande souplesse dans le calcul de résidus. Les codes de composants sont gérés par des appels de fonctions, qui contrôlent les différentes étapes nécessaires pour produire une solution résiduelle. Une fois que ces appels de fonction sont établis, les modifications des codes composants existants ne sont pas nécessaires si les composants physiques supplémentaires sont ajoutés à la simulation. Ceci est la façon dont les résidus sont calculés dans les résultats de ce travail. La partie délicate de cette stratégie est la mise en œuvre correcte des appels de fonction à des composants physiques. Le code doit être modifié pour faciliter l'extraction d'informations provenant d'autres solutions. A l'extérieur des codes de composants, les solutions doivent avoir la forme que les codes composants attendent.

Une nouvelle formulation pour le résidu du transport de neutrons résiduel a été développée sur la base de la source de fission au lieu du flux angulaire. La réduction de la taille du résidu avec cette formulation est importante. Cette nouvelle version du résiduel du transport des neutrons réduit la taille de la solution par un facteur important; un facteur de 3120 dans les résultats hétérogènes présentés au paragraphe 4.4.2. Il a été montré que le résidu est correctement mis en œuvre en suivant la convergence de l'erreur par le raffinement du domaine temporel. La solution de référence a été calculée analytiquement à partir d'un modèle 1 point, 1 groupe d'énergie avec 2 groupes de précurseurs de neutrons retardés.

Deux Préconditionneurs basés sur la physique, qui ne nécessitent que des manipulations de la solution résiduelle, ont été testés. Les deux préconditionneurs basés sur la physique (Bloc Jacobi et Bloc Gauss-Seidel) ont été testés et comparés au préconditionneur d'identité. Il a été montré que les préconditionneurs basés sur la physique réduisent le rapport moyen du nombre d'itérations linéaires d'itérations non-linéaires lors d'un transitoire. La puissance derrière ces préconditionneurs, qui ne manipulent que la solution résiduelle, est que la physique sous-jacente n'est pas nécessaire pour produire un préconditionneur efficace. Le fournisseur du cadre multiphysique peut également fournir des préconditionneurs efficaces basés sur la physique sans avoir à connaître les composants physiques qui seront utilisés dans le cadre.

A.4.2 Homogénéisation

Un changement de puissance dans un milieu infini homogène avec 281 groupes d'énergie a été étudié initialement. Il a été montré que, pour les transitoires rapides où une réactivité supérieure à β est insérée, l'utilisation de sections efficaces homogénéisées produites avec un flux du mode fondamental introduit des erreurs significatives dans la puissance et de la température en fonction du temps. Ces erreurs étaient toujours présentes, mais pas aussi importantes lorsque l'insertion de réactivité était inférieure à β.

Deux nouvelles méthodes d'homogénéisation ont été développées pour réduire les erreurs liées à l'utilisation d'un flux de mode fondamental dans le processus d'homogénéisation. La première méthode (Alpha) fondée sur l'obtention de vecteurs propres d'un problème de α-valeur propre au lieu du problème habituel

de k-valeur propre. Les α-valeurs propres, qui correspondent aux $N_d + 1$ valeurs propres principales, ont été utilisés dans différentes combinaisons comme flux de pondération dans le processus d'homogénéisation. La deuxième méthode (fluence) utilise un flux intégré en temps, qui provient d'une solution multiphysique sur les sous-domaines du problème. Le flux temporel intégré sert de flux de pondération dans le processus d'homogénéisation.

Dans le cas d'un milieu infini homogène, où la dépendance spatiale n'existe pas, les deux nouvelles méthodes ont considérablement réduit l'erreur induite lors de l'utilisation des sections efficaces homogénéisées critiques. Dans un premier temps, les neutrons retardés ont été supprimés pour explorer le comportement des transitoires rapides. Dans cette situation approximative, la méthode fluence et la méthode alpha fonctionnent bien. La méthode alpha a utilisé uniquement le vecteur propre dominant comme flux de pondération. Les deux méthodes fonctionnent bien car la solution en fonction du temps atteint la solution asymptotique très rapidement après la perturbation. Il a également été montré que les nouvelles méthodes ne sont pas affectées par la taille de l'insertion de réactivité ou par la structure du groupe homogénéisé.

Les neutrons retardés ont été activés dans le modèle de transport des neutrons, ce qui produit un comportement qui ressemble plus à ce qui est observé dans l'analyse du réacteur. L'addition de neutrons retardés a entraîné pour la méthode alpha la nécessité de considérer plus d'un vecteur propre comme flux de pondération, pour saisir le comportement à long terme du transitoire. Plusieurs vecteurs propres ont été combinés pour produire un seul flux de pondération; trois versions de cette combinaison ont été explorées. La version qui fonctionne le mieux utilise une intégration de la solution en fonction du temps, construite à partir d'un développement sur des α-modes propres. La méthode fluence n'a pas été affectée par l'addition de neutrons retardés. Il a été observé que, pour les insertions de réactivité inférieurs à β, l'utilisation des sections efficaces homogénéisées critiques fonctionne suffisamment bien. Cette observation peut justifier l'utilisation de sections efficaces critiques lors de la modélisation des transitoires de fonctionnement. Cependant, lors de la modélisation des transitoires super prompt critiques, les sections efficaces homogénéisées critiques peuvent introduire des erreurs importantes.

Un problème spatialement hétérogène a été étudié afin de déterminer si de tels procédés fonctionneraient bien avec une insertion de réactivité non-uniforme. L'ajout d'hétérogénéités spatiales n'a pas d'incidence sur la performance des nouvelles méthodes. Le procédé de fluence a été testé sur un sous-domaine du problème de référence. Il a été observé que la méthode de fluence a besoin d'un tampon homogène pour simuler l'environnement du problème de référence pour produire de bonnes sections efficaces homogénéisées. Sans le tampon homogène, la même perturbation de la concentration de bore dans le calcul de référence produit une insertion de réactivité beaucoup plus grande dans le calcul de la région isolée. L'effet de la discrétisation des intervalles de temps a été testé pour ce problème hétérogène. Il a été montré que les erreurs sont réduites par affinages successifs de l'intervalle de temps jusqu'au point où les erreurs d'interpolation deviennent dominantes.

Les résultats de ce travail montrent que dans certains cas, l'utilisation des sections efficaces homogénéisées destinées à des calculs d'équilibre dans des calculs transitoires peut introduire des erreurs importantes. Un moyen de remédier à l'introduction de ces erreurs est d'utiliser les nouvelles méthodes développées dans ce travail, qui prennent en compte le comportement dépendant du temps des solutions physiques couplées. La méthode la plus efficace à appliquer dépend du type de transitoire simulé.

A.4.3 Travaux à venir

Plusieurs directions sont disponibles pour l'exploration au-delà du travail présenté dans cette thèse. Ce qui suit est une discussion sur la vision de l'auteur pour la poursuite du développement dans ce domaine de recherche.

Couplage multiphysique

En termes de simulations multiphysiques étudiées dans ce travail, plusieurs améliorations peuvent être explorées. Ces améliorations portent à la fois sur la modélisation des composants physiques et sur la conception des logiciels utilisés dans les simulations.

Le modèle thermohydraulique utilisé dans ces calculs utilise une approximation du flux flotté pour les vitesses de vapeur et d'eau. Ce modèle ne représente fidèlement pas la réalité lorsqu'il est appliqué aux transitoires rapides, où un modèle complet de deux état est plus approprié. Dans les simulations présentées dans ce travail, le système fonctionne initialement au CZP, où le fluide et le combustible sont presque en équilibre thermique. Le changement rapide de puissance n'a pas élevé la température du fluide de manière significative. En effectuant des calculs où la vapeur était présente de manière importante, à HFP par exemple, le changement de puissance pourrait affecter de manière significative la thermohydraulique de la vapeur. Pour étudier ces accidents, un modèle plus complexe à 6 équations doit être utilisé.

Les formulations du résidu présentées dans ce travail ont été discrétisées dans le temps en utilisant des méthodes de premier ordre. En réduisant la taille du résidu de transport en éliminant le flux angulaire, le résidu a été limité à un premier ordre dans la discrétisation du temps, où les méthodes d'ordre supérieur nécessiteraient la manipulation du flux angulaire. Cependant, les méthodes d'ordre supérieur peuvent être avantageuse lorsqu'elles sont appliquées à des problèmes raides, comme ceux des accidents de grande insertion de réactivité. Une voie possible pour réaliser cette extension est à l'aide des méthodes de Runge-Kutta décrites au paragraphe 2.1.4. Ces méthodes permettent de manière souple d'augmenter l'ordre de la méthode sans modification importante de l'algorithme. Une étude intéressante serait d'observer l'effet de la plus grande taille du résidu sur la convergence pour le solveur linéaire Krylov. L'augmentation de la taille du résidu serait justifiée si les itérations linéaires n'augmentient pas de manière significative et de plus grands pas de temps pourraient être pris avec la méthode d'ordre supérieur de Runge-Kutta.

Conception de logiciel

Lors de la conception du cadre numérique pour résoudre les systèmes multiphysiques, un soin particulier a été pris pour fournir des limites bien définies dans le logiciel. Tous les composants sont programmés pour des interfaces bien définies, ce qui rend plus facile d'échanger des algorithmes appropriés, si nécessaire. Par exemple, il existe plusieurs algorithmes de solveur linéaire sous l'interface «solveur linéaire»; en programmant vers l'interface solveur linéaire, GMRes peut être remplacé par l'élimination de Gauss avec des changements minimes dans le code. Cette caractéristique de conception rend le logiciel flexible et extensible; l'utilisation des bibliothèques numériques commerciales extérieures est possible grâce à cette conception. Une direction que l'auteur souhaite poursuivre est dans le développement des adaptateurs afin que la puissance de ces bibliothèques numériques commerciales puisse être utilisée dans le cadre multiphysique.

En général, lorsque la résolution de simulations numériques à grande échelle, des quantités importantes de parallélisation sont recherchées dans les codes utilisés. Les codes parallèles utilisent les calculateurs actuellement disponibles les plus puissants et les plus rapides. Une faiblesse importante des simulations présentées dans ce travail est le manque de méthodes parallèles. Un travail important pourrait être consacré à l'ajout d'une capacité de parallélisation aux codes des composants physiques sous-jacents et au cadre multiphysique. Dans le modèle de transport de neutrons, un algorithme de balayage parallèle pourrait améliorer la taille des problèmes de transport, rendant leur résolution plus abordable. Les méthodes de décomposition du domaine peuvent permettre la résolution de plus grands problèmes en utilisant de grandes machines parallèles. Dans le modèle thermohydraulique, des sous-canaux peuvent être répartis entre plusieurs processus qui communiquent pour évaluer le mélange entre les canaux. Au niveau du cadre multiphysique, des quantités importantes de parallélisation sont possibles. Le chapitre 5 a montré que beaucoup de temps a été consacré à l'évaluation du résidu de précurseur de neutrons retardés, ce qui implique plusieurs manipulations de la source de fission. Le fractionnement de ces manipulations sur plusieurs processus a le potentiel de réduire considérablement le temps passé à évaluer ce résidu. L'évaluation des autres résidus peut également être effectués en parallèle, en particulier si les composants physiques sous-jacents ont des capacités de parallélisation. Les solveurs linéaires peuvent être faits pour utiliser les capacités de parallélisation à travers des manipulations de produits de matrices et de vecteurs en parallèle. En outre, le préconditionneur basé sur la physique utilisé dans le chapitre 5, qui est une matrice diagonale par bloc, peut être inversé en parallèle en inversant simultanément chaque matrice diagonale par bloc. La mise en œuvre de telles méthodes parallèles sera essentielle pour l'utilisation future du cadre multiphysique présent.

Homogénéisation des sections efficaces

Les méthodes d'homogénéisation explorées dans ce travail ont montré des résultats prometteurs dans leur capacité à réduire les erreurs provenant de méthodes actuellement utilisées. Le développement de ces méthodes a encore des améliorations qui peuvent être apportées sur la façon dont les méthodes sont appliquées,

et à quels problèmes ces méthodes sont appliquées.

Lors du calcul des poids pour chaque vecteur propre de la méthode alpha, une minimisation a été réalisée avec un certain flux de référence; dans les résultats de ce travail, le flux initial a été choisi. Ce choix de flux de référence a été fait sur la base de l'idée de trouver les coefficients de développement d'une solution en fonction du temps et de la disponibilité du flux initial. Une excellente extension de la méthode alpha serait d'étudier l'effet de l'utilisation de différents flux de référence pour déterminer les coefficients de pondération. Par exemple, si une estimation de la température était disponible, le flux pourrait être estimé à différents points au transitoire et être utilisé pour générer des coefficients de pondération pour la méthode alpha.

L'un des progrès les plus importants dans les méthodes d'homogénéisation a été par l'ajout de degrés de liberté supplémentaires grâce à des facteurs de discontinuité. Ces facteurs éliminent l'hypothèse d'un flux continu au niveau des interfaces des régions homogénéisées afin de mieux conserver les taux de réaction à l'intérieur de ces régions. L'ajout de facteurs de discontinuité à la méthode de fluence peut être simple en évaluant la fraction du flux intégré dans le temps dans la région su le flux intégré dans le temps aux limites de la région. Toutefois, pour la méthode alpha, en raison des multiples vecteurs propres utilisés, il y a plus de choix dans l'application de facteurs de discontinuité. On pourrait appliquer les mêmes coefficients pour les facteurs de discontinuité, mais il peut y avoir des choix plus optimaux dans la façon d'appliquer ces facteurs de discontinuité. Cette extension est plus applicable lorsque le problème homogénéisé est modélisé par diffusion de neutrons étant donné que les facteurs de discontinuité sont destinés à être utilisés lors de l'application d'un opérateur d'ordre inférieur dans le problème homogénéisé.

Lors de l'application de la méthode de fluence à des problèmes spatialement hétérogènes, un tampon homogène a été ajouté au sous-domaine, ce qui rend les insertions de réactivité similaires dans le problème de référence et dans le calcul du sous-domaine. Bien que ce tampon homogène représentait avec précision les assemblages environnants, il était encore nécessaire de balayer ce domaine au cours de la simulation. Une option moins coûteuse serait d'approcher les milieux environnants par une condition aux limites de l'albédo. Si une condition d'albédo exacte dépendant du temps état disponible, le calcul d'une solution en fonction du temps sur les sous-domaines par la méthode de fluence pourrait être réalisé plus rapidement.

Le grand inconvénient de la méthode de fluence est le coût dans le calcul du flux en fonction du temps, utilisé dans le processus d'homogénéisation. Pour le cas spatialement hétérogène du chapitre 4, la solution a pris 4 jours pour être obtenue. Pour que cette méthode soit appliquée à des simulations de taille industrielle, une réduction du temps nécessaire pour obtenir un flux dépendant du temps est essentielle. Une voie prometteuse à poursuivre est la parallélisation du calcul pour obtenir cette solution. La parallélisation de l'algorithme de balayage de transport pourrait fournir une accélération significative dans ce calcul.

Les procédés d'homogénéisation ont été appliqués à un calcul de coeur réduit. Bien que cette application montre que ces méthodes ont le potentiel d'être

utile dans l'analyse du réacteur à l'état transitoire, il reste beaucoup à explorer. Le Groupe d'Experts sur le Transport de Rayonnements et la Radioprotection (EGRTS), dans le cadre du groupe de travail sur les questions scientifiques des systèmes de réacteurs pour l'Agence pour l'Energie Nucléaire, développe un problème de référence en fonction du temps sur la base du problème de référence REP MOX (C5G7) [167]. Une fois que ce problème de référence sera à disposition du public, il serait souhaitable que les nouvelles méthodes soient appliquées à ce cas afin de comparer la réduction de l'erreur que ces nouvelles méthodes apportent.

APPENDIX B

SELECTED ALGORITHMS OF MULTIPHYSICS FRAMEWORK

The following is a selection of important algorithms used within the multiphysics framework developed for this work. The selected algorithms are: Newton Iterations with line search globalization, GMRes, and QR.

B.1 Newton Iterations

Newton iterations consist of consecutive linearizations of the nonlinear residual around the current approximate solution. This method is detailed in Algorithm 4. Newton's method is given a function that computes the solution residual associated to a solution and the initial solution iterate. The initial solution residual is then computed from the residual function and the initial solution. The convergence tolerance is determined by the sum of an absolute tolerance and some fraction of the original residual size.

If the solution is sufficiently close to the exact solution, as estimated by the norm of the residual function, the current solution is returned. Newton's method repeatedly calculates an solution update by applying the inverse Jacobian to the current residual vector. A damping parameter α is computed which ensures a sufficient reduction to the norm of the residual. The damping parameter is applied when updating the current solution. Newton's method is repeated until the residual norm is below the convergence tolerance, or when the maximum number of iterations have been reached.

The Jacobian inversion shown in Algorithm 4 is accomplished by applying a linear solver with the Jacobian matrix evaluated at the current iterate $\vec{U}$.

The globalization method used in this work is a line search method, presented in Algorithm 5. This method used, is an implementation of the Armijo rule, where the parameter α is repeatedly reduced by a factor of 2 if the size of the residual is not sufficiently reduced.

The combination of Newton's iterations and a line search globalization produces a stable nonlinear solver which can be applied to time dependent multiphysics simulations.

B.2 Linear Solvers

The principle linear solver used in this work to invert the Jacobian in Newton's Method is the GMRes solver. The algorithm for this method is outlined in Algorithm 6, which is repeated from Section 3.2.2. GMRes successively builds approximations to the solution space through a Gram-Schmidt orthogonalization process. The featured algorithm includes a re-orthogonalization step, which helps to ensure that the basis vectors are in fact orthogonal to each other [131].

In the minimization problems performed for the Alpha method, a QR algorithm is used to solve the system of equations. A minimization problem occurs when the right hand side vector is not contained within the column space of the matrix. This happens when a matrix is rectangular, with more rows than columns. The minimization finds the solution when the right hand side vector is

Algorithm 4: Nonlinear Newton Iteration

Input : Residual Function $\vec{F}(\vec{U})$, initial solution $\vec{U}_0$
Output: Converged Solution $\vec{U}$

$\vec{f}_0 = \vec{F}(\vec{U}_0)$ // Compute Initial Residual
$\vec{U} = \vec{U}_0, \quad \vec{f} = \vec{f}_0$ // Set Current solution and residual to initial vectors
$\tau = \tau_a + \tau_r \|\vec{f}_0\|$ // Compute convergence tolerance
if $\|\vec{f}\| < \tau$ **then**
  return $\vec{U}$ // return current solution
end
for $k = 1, 2, \ldots,$ nMaxIterations **do**
  $\mathrm{d}\vec{U} = -\mathbf{J}^{-1}\vec{f}$ // Invert Jacobian
  $\alpha = \text{lineSearch}\left(\vec{F}(\vec{U}), \vec{U}, \mathrm{d}\vec{U}, \|\vec{f}\|\right)$ // Calculate damping coefficient
  $\vec{U} = \vec{U} + \alpha * \mathrm{d}\vec{U}$ // Update solution
  $\vec{f} = \vec{F}(\vec{U})$ // Compute new residual
  if $\|\vec{f}\| < \tau \;\&\; \|\mathrm{d}\vec{U}\| < \tau$ **then**
    return $\vec{U}$ // Return solution if converged
  end
end
return $\vec{U}$ // If Newton's method does not converge, throw a warning and return the best estimate for solution

projected onto the column space of the matrix.

An effective algorithm at solving minimization problems is the QR algorithm, which successively applies orthogonal matrices to the matrix and the right hand side to produce an upper triangular matrix. The resulting upper triangular matrix can then be inverted with backward substitution.

Algorithm 5: Line Search Method for Newton Iterations

Input : Residual Function $\vec{F}(\vec{U})$, Solution $\vec{U}$, Solution Update $\mathrm{d}\vec{U}$, Residual Norm $\|\vec{f}\|$
Output: Damping Coefficient α

$\alpha = 1.0, \quad \beta = 1 \times 10^{-4}$ // Initialize parameters
for $k = 1, 2, \ldots,$ nMaxIterations **do**
  $\eta = (1 - \alpha\beta)\|\vec{f}\|$ // Calculate sufficient reduction criteria [Armijo Rule]
  $\vec{U}' = \vec{U} + \alpha \mathrm{d}\vec{U}$ // Calculate solution update
  $\vec{f}' = \vec{F}(\vec{U}')$ // Calculate residual vector
  if $\|\vec{f}'\| < \eta$ **then**
    return α // If residual sufficiently reduced, return coefficient
  else
    $\alpha = \frac{\alpha}{2}$ // Else, reduce coefficient
  end
end
return α // If not sufficiently converged, return smallest factor

Algorithm 6: Right Preconditioned GMRes with Reorthogonalization in Arnoldi

Input : Linear System Matrix $\mathbf{A}$, right-hand side $\vec{b}$, initial iterate $\vec{x}_0$
Output: Converged Solution $\vec{x}$

$\vec{r}_0 = \mathbf{M}_L^{-1}\left(\vec{b} - \mathbf{A}\vec{x}_0\right), \quad \beta = \|\vec{r}_0\|, \quad \vec{v}_1 = \frac{\vec{r}_0}{\beta}, \quad \mathbf{V}_1 = \vec{v}_1$ // Init first basis vector
for $k = 1, 2, \ldots$ **do**
  $\vec{z} = \mathbf{M}_R^{-1}\vec{v}_k$ // Apply Preconditioner
  $\vec{w} = \mathbf{M}_L^{-1}\mathbf{A}\vec{z}$ // Action of matrix
  $\vec{h}' = \mathbf{V}_k^{\mathrm{T}}\vec{w}$ // Calculate projection coefficients
  $\vec{v}' = \vec{w} - \mathbf{V}_k\vec{h}'$ // First orthogonalization
  $\vec{h}'' = \mathbf{V}_k^{\mathrm{T}}\vec{v}'$ // Recalculate projection coefficients
  $\vec{h} = \vec{h}' + \vec{h}''$ // Combine projection coefficients
  $\hat{v}_{k+1} = \vec{v}' - \mathbf{V}_k\vec{h}''$ // Reorthogonalization
  $\vec{v}_{k+1} = \frac{\hat{v}_{k+1}}{\|\hat{v}_{k+1}\|}$ // Normalization of basis vector
  $\mathbf{H}_k = \begin{bmatrix} \mathbf{H}_{k-1} & \vec{h} \\ 0 & \|\hat{v}_{k+1}\| \end{bmatrix}$ // Augmentation of Hessenberg Matrix
  $\min_y \|\beta\vec{e}_1 - \mathbf{H}_k\vec{y}_k\|$ // Solve minimization problem
  if $\|\beta\vec{e}_1 - \mathbf{H}_k\vec{y}_k\| <$ tolerance **then**
    exit // If converged, exit "for" loop
  else
    $\mathbf{V}_{k+1} = \left[\mathbf{V}_k \mid \vec{v}_{k+1}\right]$ // otherwise, augment basis matrix
  end
end
$\vec{x} = \vec{x}_0 + \mathbf{M}_R^{-1}\mathbf{V}_k\vec{y}$ // Return converged solution

Algorithm 7: QR Orthogonal Triangularization

Input : Rectangular Matrix $\mathbf{A}$, Right Hand Side $\vec{b}$
Output: Solution $\vec{x}$

// Orthogonal Triangularization
for $k = 1, 2, \ldots,$ nColumns **do**
  $\vec{z} = \mathbf{A}(k : \text{end}, k)$ // Extract column of $\mathbf{A}$ below diagonal
  $\vec{z}(1) = \vec{z}(1) + \text{sign}(\vec{z}(1))\|\vec{z}\|$ // Compute Householder reflector
  $\vec{z} = \vec{z}/\|\vec{z}\|$ // Normalize $\vec{z}$
  for $j = k, k+1, \ldots,$ nColumns **do**
    $w = \vec{z}^{\mathrm{T}}\mathbf{A}(k : \text{end}, j)$ // Scalar product of $\vec{z}$ with j-th column of $\mathbf{A}$
    for $i = k, k+1, \ldots,$ nRows **do**
      $\mathbf{A}(i, j) = \mathbf{A}(i, j) - 2w\vec{z}(i - k + 1)$ // Apply Householder reflector to j-th column of $\mathbf{A}$
    end
  end
  $w = \vec{z}^{\mathrm{T}}\vec{b}(k : \text{end})$ // Scalar product of $\vec{z}$ with right hand side $\vec{b}$
  for $i = k, k+1, \ldots,$ nRows **do**
    $\vec{b}(i) = \vec{b}(i) - 2w\vec{z}(i - k + 1)$ // Apply Householder reflector to right hand side
  end
end
// Backward Substitution
for $i =$ nColumns, nColumns $- 1, \ldots, 1$ **do**
  $s = \vec{b}(i)$
  for $j = i + 1, i + 2, \ldots, nColumns$ **do**
    $s = s - \vec{x}(j) * \mathbf{A}(i, j)$
  end
  $\vec{x}(i) = s/\mathbf{A}(i, i)$
end
return $\vec{x}$

université PARIS-SACLAY | ÉCOLE DOCTORALE PHENIICS

Titre: Développement d'un solveur multiphysique dans le code APOLLO3® et applications à l'homogénéisation des sections efficaces

Mots clés: multi-physique, homogénéisation, transport des neutrons, thermo-hydraulique

Résumé: Le comportement des réacteurs nucléaires dépend sur plusieurs composants physiques qui s'interagissent fortement. La solution aux problèmes d'analyses réacteurs doit prendre en compte ses interactions pour produire des estimations encore plus précises. Ces travaux concernent un méthode pour obtenir des solutions de haute précision à des simulations multiphsyiques pour le comportement des réacteurs nucléaires aux situations accidentelles.
En plus d'étudiant des méthodes numériques à la solution aux systèmes physiques fortement couplées, le traitement des données utilisées aux simulations a été étudié. Il est montré que les sections efficaces peuvent introduire des erreurs importantes en fonction du transitoire simulé. En utilisant des section efficaces homogénéisées avec un méthode traditionnel, optimisé pour des calculs statiques, des erreurs importantes sont introduits quand l'insertion de réactivité est au-dessus de prompte critique. Deux méthodes sont étudiés pour réduire telles erreurs dans un cas homogène. Un méthode est basé sur l'integration du flux en temps, et le seconde est basé sur une expansion asymptotique en temps. Les deux méthodes sont montrés à réduire les erreurs introduits avec les sections efficaces générées avec un flux fondamentale. Le méthode avec le flux intégré est appliqué à un cas hétérogène, où des modèles plus complexes sont utilisées. L'effet de raffinement du domaine d'intégration en temps est montré de réduire des erreurs jusqu'à un moment où d'autres erreurs deviennent dominantes. Le solveur multiphysique est aussi montré d'être capable de obtenir des solution aux problèmes de grand taille en traitant un accident de chute de grappe d'un REB au démarrage.

Title: Developing a Multiphysics Solver in APOLLO3® and Applications to Cross Section Homogenization

Keywords: multiphysics, homogenization, neutron transport, thermal hydraulics

Abstract: The behavior of nuclear reactors depends on many physical processes which interact and strongly affect one another. The solution to problems in reactor analysis should take into account these interactions to produce increasingly accurate estimates of reactor behavior. This work studies a method to obtain high fidelity solutions to strongly coupled physics components in solutions to the behavior of nuclear reactors in accident transient situations.
In addition to studying the numerical methods used to resolve such strongly coupled physics systems, the treatment of data used in such simulations is studied. It is discovered that homogenized cross sections used in transient simulations may introduce significant errors depending on the transient being simulated. Using a traditional homogenization method which is intended for static calculations is shown to introduce significant errors in a simulation when the reactivity insertion is above the prompt-critical threshold. Two methods are explored to reduce such errors in a spatially homogeneous case. One method is based on the time integrated flux, while the other is based on an asymptotic expansion of the flux in the time domain. Both methods are shown to reduce the errors introduced through using cross sections generated with a fundamental mode flux.
The time integrated flux method is further tested on a spatially heterogeneous geometry, where more complex physical models are utilized. The impact of refinement of the time integration domain is shown to reduce simulation errors until a point where other errors become dominant. The multiphysics simulation framework is also shown to be capable of obtaining solutions to larger problems, more suited to reactor analysis by treating a Rod Drop accident in a BWR during startup.

Université Paris-Saclay
Espace Technologique / Immeuble Discovery
Route de l'Orme aux Merisiers RD 128
91190 Saint-Aubin, France